

# **A New Generation of Isoform Selective Hsp90 Inhibitors: Targeting the Cytosolic Hsp90 Isoforms**

By  
Sanket J. Mishra

Submitted to the graduate degree program in Medicinal Chemistry and the graduate faculty of  
The University of Kansas in partial fulfillment of the requirements for the degree of Doctor of  
Philosophy

Committee:

---

Brian S. J. Blagg, Ph.D  
Committee Chair

---

Apurba Dutta, Ph.D  
Co-Chair

---

Paul Hanson, Ph.D

---

Michael F. Rafferty, Ph.D

---

Jeff P. Krise, Ph.D

Date defended: 03/23/2018

The Dissertation Committee for Sanket J. Mishra certifies that this is the approved version of the following dissertation:

**A New Generation of Isoform Selective Hsp90 Inhibitors:  
Targeting the Cytosolic Hsp90 Isoforms**

---

Brian S. J. Blagg, Ph.D  
Committee Chair

Date approved: 03/23/2018

## Abstract

Heat shock protein 90 kDa (Hsp90) is a member of the molecular chaperone family of proteins that processes newly synthesized polypeptides into their three-dimensional and biologically active form. In addition, Hsp90 assists in the stabilization, trafficking and refolding of denatured proteins. Many Hsp90-dependent proteins are critical to the pathogenesis of cancer, neurodegeneration and/or viral infection. As a result, Hsp90 has garnered attention as a chemotherapeutic target and has resulted in the development of more than 17 Hsp90 inhibitors that have been evaluated in clinical trials. However, these inhibitors exhibit *pan*-inhibitory activity against all four Hsp90 isoforms: Hsp90 $\alpha$ , Hsp90 $\beta$ , Grp94 and Trap1, which results in various side effects, including, hepatotoxicity, cardiotoxicity, and renal toxicity. Therefore, the development of isoform-selective Hsp90 inhibitors has been proposed to delineate the contribution of each Hsp90 isoform towards these toxicities.

The cytosolic Hsp90 isoforms,  $\alpha$  and  $\beta$ , modulate the activity of numerous Hsp90-dependent proteins that regulate cancer progression. Hydrolysis of ATP by the N-terminal nucleoside-binding site provides the energy required for the maturation of client protein substrates, and all four Hsp90 isoforms share >85% identity within this region. Between cytosolic Hsp90 isoforms ( $\alpha$  and  $\beta$ ), the N-terminal ATP-binding site exhibits >95 % identity. As a result, the design of inhibitors that selectively target individual cytosolic Hsp90 isoforms has been challenging. Described herein is the development of Hsp90 $\beta$ - and Hsp90 $\alpha$ -selective inhibitors using a structure-based approach that has produced compounds that exhibit both high selectivity and affinity. The efficacy of these inhibitors has been evaluated against an array of cancer cell lines and revealed an Hsp90 isoform-dependent cancer profile.

## **Acknowledgment**

Graduate school has been a long and arduous journey, but support and guidance from everyone around me provided the motivation to get through. First, i would like to thank my advisor Dr. Brian Blagg for providing me the opportunity to work under his supervision. Through his mentoring, Brian inculcated independent thinking and creative approach in me that proved helpful in resolving problems that manifested during my research. Brian's enthusiasm for science was infectious, keeping the lab environment brimming with excitement, and lab members inspired and motivated.

I owe a great debt to my family who have been a constant source of support during the entire time course of this training. Specifically, during the times of crisis, which were plenty. Without their constant motivation this journey would have been unimaginably harder. In particular, my parents who were a pillar of support and motivation by continuously believing in me. I am grateful to my brothers Prasun, Pravin and my sister Prarthana who were always available to offer support and kept me sane by engaging me in discussions over the phone.

I would also like to thank my fellow lab members both past and present, who made my lab work a pleasant experience. I must give a special thanks to late Dr. Anuj Khandelwal, who was my teammate on all of my projects and was an excellent resource of scientific as well as general discussions. Anuj's contributions to sciences and his impact on the lives of people around him will always be remembered. Other members of that deserve special thanks are Gaurav Garg, Leah Forsberg, Vincent Crowley, Rachel Davis, and Caitlin Kent, who were instrumental in my development as a scientist and as a person, making my experience at KU enjoyable. Outside of the Blagg laboratory, I am thankful to department faculty members and graduate students who influenced my career. Specifically, members from Dr. Ryan Altman's, Dr. Paul Hanson's and Dr. Jon Tunge's lab for providing resources and chemicals.

I must thank the Department of Medicinal Chemistry at The University of Kansas for the extensive training I have received during my graduate career. Norma Henley and Jane Buppenhoff deserve special thanks for coordinating the administrative work and simplifying the stay of the graduate students in the department. I would also like to thank Dr. Apurba Dutta, Dr. Paul Hanson, Dr. Michael Rafferty, and Dr. Jeff Krise for serving on my committee and providing their valuable time and thoughtful suggestions.

## Abbreviations:

17-AAG: 17-allylamino-17-demethoxygeldanamycin  
17-DMAG :17-dimethylamino-17-demethoxygeldanamycin  
3D: three dimensional  
ADP: Adenosine diphosphate  
Aha1: Hsp90 co-chaperone (ATPase activator)  
Akt: Protein kinase B  
Ala: Alanine  
ALK: Anaplastic lymphoma kinase  
Apaf-1: Apoptotic peptidase activating factor 1  
ARNT: Aryl hydrocarbon receptor nuclear translocator  
Asn: Asparagine  
Asp: Aspartate  
ATM: Ataxia-telangiectasia-mutated kinase  
ATP: Adenosine triphosphate  
BBB: Blood brain barrier  
BBr<sub>3</sub>: Boron tribromide  
Bcl-2: B-cell lymphoma 2 gene that regulates apoptosis  
Bcr-Abl: Bcr-Abl fusion protein with tyrosine-kinase activity  
BCSC: breast cancer stem cell  
BF<sub>3</sub>.etherate: Boron trifluoride diethyl etherate  
BMI1: B lymphoma Mo-MLV insertion region 1 homolog  
BRAF: B-Raf proto-oncogene  
CDK4: Cyclin-dependent kinase 4  
CDK6: Cyclin-dependent kinase 6  
CHIP: Carboxy terminus of Hsc70 interacting protein  
c-IAP1: Cellular Inhibitor of Apoptosis Protein 1  
CL: Charged linker  
c-MET: tyrosine-protein kinase Met  
CTD: C-terminal domain  
CXCR4: C-X-C chemokine receptor type 4  
DCM: Dichloromethane  
DIPEA: *N,N*-diisopropylethylamine  
DMF: *N,N*-dimethylformamide  
DMSO: Dimethyl sulfoxide  
DNA: Deoxyribonucleic acid  
EDCI: 1-ethyl-3-(3-dimethylaminopropyl) carbodiimide  
EEVD: A domain that recognizes the tetratricopeptide-containing repeat (TPR) domain  
EGCG: Epigallocatechin gallate  
eHsp90 $\alpha$ : Extracellular heat shock protein 90 kDa alpha isoform

ER: Endoplasmic reticulum  
ErbB2/ Her2: Receptor tyrosine-protein kinase erbB-2  
EZH2: Enhancer of zeste homolog 2  
FAK: Focal adhesion kinase  
FANCA: Fanconi anemia core complex-associated protein 20  
FGFR3: Fibroblast growth factor receptor 3  
FKBP51 and FKBP52: Immunophilins that bind to FK506 protein  
FKBP8: FK506-binding protein 8  
Flt-3: fms like tyrosine kinase 3  
FP: Fluorescence Polarization  
GALAXY 1 and 2: Clinical trial studies conducted on patients with advanced non-small cell lung cancer  
GDA: Geldanamycin  
GHKL: Family of ATPases consisting of DNA Gyrase, Hsp90, Histidine Kinase, and Mut L  
GI<sub>50</sub>: 50 % growth inhibitory concentration  
GIST: Gastrointestinal Stromal Tumor  
Grp94: Glucose regulated protein 94  
HCT116: Colorectal carcinoma cell line  
hERG: Human ether-a-go-go-related gene potassium channels  
HIF-1: Hypoxia-inducible factor 1  
HIP: Hsp70 interacting protein  
HIV: human immunodeficiency virus  
HMG1: 3-hydroxy-3-methylglutaryl-coenzyme A reductase 1  
HOBt·H<sub>2</sub>O: Hydroxybenzotriazole hydrate  
HOP: Hsp90-Hsp70 organizing protein  
HSF-1: Heat shock factor-1  
Hsp: Heat shock protein  
HSR: Heat shock response  
h-Tert: Human telomerase  
HTS: High throughput screen  
IGF: Insulin-m growth factor  
IL-6: Interleukin 6  
IL-8: Interleukin 8  
Ile: Isoleucine  
IRAK: Interleukin-1 receptor-associated kinase  
K<sub>d</sub>: Dissociation constant  
kDa: Kilo daltons  
Leu: Leucine  
Lys: Lysine  
MAFG: Transcription factor MafG  
MCF-7: Estrogen receptor negative breast cancer cell line

*m*CPBA: *meta*-chloroperoxybenzoic acid  
MD: Middle domain  
MDA-MB-231: Human breast adenocarcinoma cell line  
MEK: Mitogen-activated protein kinase kinase  
MeOH: Methanol  
MG63: bone osteosarcoma cells  
MMP 1-3: Matrix metalloproteinase-1, 2- and -3  
MutL: DNA mismatch repair protein  
MYC1: Transcription factor MYC1  
Myt1: Myelin transcription factor 1  
NaN<sub>3</sub>: Sodium azide  
NaOH: Sodium hydroxide  
NCI: National cancer institute  
NECA: N-ethyl-carboximido adenosine  
NEK: Serine/threonine-protein kinase Nek  
NF-κB: Nuclear factor kappa-light-chain-enhancer of activated B cells  
NMR: Nuclear magnetic resonance  
NSCLC: Non-small cell lung cancer  
NTD: N-terminal domain  
p53: Tumor protein p53  
PD: Pharmacodynamic  
PDB: Protein data bank  
Phe: Phenyl alanine  
PK: Pharmacokinetic  
Plk: Polo like kinase  
RAF-1: RAF proto-oncogene serine/threonine-protein kinase  
RDA: Radamide  
RDC: Radicicol  
RIP: Receptor-interacting protein kinase  
SAR: Structure-activity relationship  
Ser: Serine  
SkBr3: Estrogen receptor positive breast cancer cell line  
SREBF1: Sterol regulatory element-binding protein 1  
STAT3: Signal transducer and activator of transcription 3  
TBAF: Tetrabutyl ammonium fluoride  
TCF 12: Transcription Factor 12  
TGF-β: Transforming growth factor beta  
THF: Tetrahydrofuran  
Thr: Threonine  
TMSCF<sub>3</sub>: Trifluoromethyltrimethylsilane  
TMSCN: Trimethylsilyl cyanide  
TPR: Tetratricopeptide-containing repeat



Trap-1: TNF receptor associated protein 1

Trp: Tryptophan

Tyr: Tyrosine

VEGFR: Vascular endothelial growth factor receptor

Wee1: Wee1 like protein kinase

# Table of Contents

## List of Sections:

### CHAPTER I

#### Introduction to Hsp90 Function, Structure and Regulation

I.1 Introduction-----	1
I.2 Hsp90 structure-----	2
2-I.3 Hsp90 chaperone cycle-----	3
I.4 Therapeutic disruption of Hsp90 chaperone cycle-----	5
I.5 Hsp90 inhibitors-----	7
I.5.1 Natural products as Hsp90 N-terminal inhibitors-----	7
I.5.2 Small molecule inhibitors of the Hsp90 N-terminus-----	10
I.5.3 Induction of the Heat Shock Response (HSR)-----	15
I.5.4 Isoform-selective Hsp90 inhibitors-----	16
I.5.4.1 Grp94-selective inhibitors-----	17
I.5.4.2 Trap1-selective inhibitors-----	19
I.5.4.3 Hsp90 $\alpha$ / $\beta$ -selective dual inhibitors-----	20
I.5.4.4 Hsp90 $\alpha$ -selective compounds-----	21
I.5.4.5 Hsp90 $\beta$ -selective compounds-----	22
I.6 Conclusions and future directions-----	22
I.7 References-----	24

## CHAPTER II

### Development of a Novel Series of Compounds for Hsp90 $\beta$ -Selective Inhibition

II.1 Hsp90 $\beta$ and cancer-----	34
II.2 Overlay studies with the Hsp90 isoform N-terminal ATP-binding sites-----	37
II.3 Modeling of the resorcinol-based Hsp90 $\beta$ -selective inhibitor, KUNB31-----	40
II.4 Design of a benzamide-based Hsp90 $\beta$ -selective inhibitor-----	41
II.4.1 Proposal of the Isoquinolin-1(2H)-one based Hsp90 $\beta$ -selective series-----	43
II.4.2 Synthesis of the Isoquinolin-1(2H)-one series-----	44
II.4.3 Determination of binding affinities for 4a-j-----	46
II.4.4 Replacement of the <i>trans</i> -4-aminocyclohexanol in 4d-----	49
II.4.5 Evaluation of binding affinities for 5a-g-----	51
II.5 Cellular studies-----	52
II.5.1 Determination of growth-inhibitory effects on cancer cells-----	52
II.5.2 Determination of the growth-inhibition and client protein degradation in urological cancer cells-----	55
II.5.3 HER2-dependency on Hsp90 isoforms-----	57
II.6 Conclusions and future directions-----	59
II.7 Method and experiments-----	60
II.8 References-----	84

## Chapter III

### Development of Hsp90 $\alpha$ -Selective Inhibitors

III.1 Hsp90 $\alpha$ and its significance in cancer-----	89
III.2 Variations in the N-terminal ATP-binding site in the Hsp90 isoforms-----	91
III.3 Binding of the small molecule inhibitors to the N-terminal ATP-binding site of Hsp90 $\alpha$ -----	92
III.4 The discovery of the monophenol-based Hsp90 $\alpha$ -selective inhibitor-----	94
III.5 Optimization studies of <b>7</b> and its 5-position substituents-----	97
III.5.1 Exploration of alternative 4-phenol scaffolds-----	97
III.5.2 Investigation of 4-phenol replacements-----	98
III.5.3 Modifications to the tertiary alcohol-----	99
III.5.4 Modifications to the gem-dimethyl-----	101
III.5.5 Installation of appendages onto the tertiary alcohol-----	104
III.5.6 Substitutions to probe the Hsp90 $\alpha$ open conformation-----	106
III.6 Cellular studies-----	111
III.7 Conclusions -----	111
III.8 Methods and experiments -----	112
III.9 References-----	150

## Chapter IV

### Optimization of the Hsp90 $\alpha$ -selective Compounds

IV.1 Benzenethiols containing Hsp90 $\alpha$ -selective inhibitors-----	153
IV.2 Chimeric Hsp90 $\alpha$ -selective compounds -----	156

IV.3 Structure-activity relationship studies on the benzenethiol ring-----	160
IV.4 Selectivity of the Hsp90 $\alpha$ -selective compounds against Grp94 and Trap1-----	164
IV.5 Analysis of the co-crystal structures of 58 and 61g with Hsp90 $\alpha$ -----	166
IV.6 Discovery of the aminophenol-containing Hsp90 $\alpha$ -selective scaffold-----	167
IV.7 Biological studies-----	169
IV.7.1 Antiproliferative effect on cancer cells-----	169
IV.8 Conclusions and future directions-----	174
IV.9 Methods and Experiments-----	174
IV.10 References -----	200

**List of Figures:**

**CHAPTER I**

**Introduction to Hsp90 Function, Structure and Regulation**

Figure 1.1. The Crystal structure of Hsp90-----	2
Figure 1.2. The Hsp90-chaperone cycle-----	3
Figure 1.3 Proposed mechanism of Hsp90 inhibition for cancer treatment-----	5
Figure 1.4: Geldanamycin and its derivatives-----	7
Figure 1.5: Radicol and its derivatives-----	9
Figure 1.6: Purine based Hsp90 N-terminal Inhibitors-----	10
Figure 1.7: Resorcinol containing Hsp90 inhibitors-----	12
Figure 1.8: Benzamide based Hsp90 inhibitors-----	14

Figure 1.9: Proposed mechanism of induction of heat shock response with Hsp90 N-terminal inhibitors-----	15
Figure 1.10: Structures of Grp94-selective compounds-----	17
Figure 1.11: Subpockets in Grp94 N-terminal ATP-binding site-----	18
Figure 1.12: Compounds for selective Trap-1 inhibition-----	19
Figure 1.13: Hsp90 $\alpha/\beta$ -selective compounds-----	20
Figure 1.14: Hsp90 $\alpha$ -selective compounds-----	21
Figure 1.15: Hsp90 $\beta$ -selective compound KUNB31-----	22

## CHAPTER II

### Development of a Novel Series of Compounds for Hsp90 $\beta$ -Selective Inhibition

Figure 2.1: Sequence alignment of Hsp90 isoforms-----	37
Figure 2.2: Modeling of Radicol into the N-terminal ATP binding site of Hsp90 isoforms-----	38
Figure 2.3: Modeling of 2.1 into the Hsp90 $\alpha$ and Hsp90 $\beta$ -----	40
Figure 2.4: Apparent $K_{ds}$ of KUNB31 and its binding mode in Hsp90 $\beta$ -----	41
Figure 2.5: Structures and binding $K_d$ of the benzamide based Hsp90-----	41
Figure 2.6: Compound 31 modeled into the N-terminal ATP-binding pocket-----	42
Figure 2.7: Overlay of proposed unsaturated compound with the compound 31-----	43
Figure 2.8: Compound 4d modeled in Hsp90 $\alpha$ and Hsp90 $\beta$ ATP binding pocket -----	48
Figure 2.9: Overlay of the proposed binding modes of 4d and 5a in the Hsp90 $\beta$ binding site-----	49

Figure 2.10: Modeled picture of 5a and Apparent $K_d$ values of 5a-g-----	51
Figure 2.11: NCI-60 single dose screening results for 4d-----	53
Figure 2.12: NCI-60 five dose $GI_{50}$ determination screening results for 4d-----	54
Figure 2.13: Western blot analysis of client proteins with 4d in UM-UC-3 cells-----	56
Figure 2.14: Western blot analysis with 5b to study client protein degradation in SkBr3 cells----	57
Figure 2.15: Effect of 5b on viability of MDA-MB-231-----	58

### **Chapter III**

#### **Development of Hsp90 $\alpha$ -Selective Inhibitors**

Figure 3.1: Binding of Radicicol to Hsp90 $\alpha$ and Hsp90 $\beta$ -----	91
Figure 3.2: The closed conformation of Hsp90 $\alpha$ -----	92
Figure 3.3: Structure and Hsp90 $\alpha$ binding interactions of each Hsp90 inhibitor chemotypes-----	93
Figure 3.4: Binding affinities for the monophenols 6 and 7 and their proposed binding models-	95
Figure 3.5: The 5-position modifications onto 7 and their proposed binding models-----	96
Figure 3.6: Compound 8 modeled into Hsp90 $\alpha$ ATP-binding pocket-----	96
Figure 3.7: Evaluation of compounds 12 and 13-----	97
Figure 3.8: Proposed phenol group replacements-----	98
Figure 3.9: Replacement and modifications of the tertiary alcohol group in 10-----	99
Figure 3.10: Proposed model of 10 binding to closed form of Hsp90 $\alpha$ -----	102
Figure 3.11: Proposed binding mode of 36d-----	107

Figure 3.12: Proposed compounds with conformational restraint-----109

## Chapter IV

### Optimization of the Hsp90 $\alpha$ -selective Compounds

Figure 4.1: Compound 11 modeled into the open conformation of Hsp90 $\alpha$ -----153

Figure 4.2: Binding modes of PU-H71 and SNX 2112 in the Hsp90 $\alpha$  ATP-binding site-----154

Figure 4.3: An overlay of observed binding mode of PU-H71 and 11-----154

Figure 4.4: Structures and K<sub>d</sub> values of the proposed compounds 44 and 45-----155

Figure 4.5: Methylenedioxyphenyl containing phenols 46-50-----156

Figure 4.6: Binding pose of 49 modeled in the HSp90 $\alpha$  ATP-binding site-----158

Figure 4.7: Structures of proposed compounds 54-58-----158

Figure 4.8: Determination of K<sub>d</sub> of the selected Hsp90 $\alpha$ -selective analogs against Grp94 and Trap1-----165

Figure 4.9: Co-crystal structure of 58 and 61g with Hsp90 $\alpha$ -----166

Figure 4.10: Investigation of selectivity of resorcinol and aminophenol cores in the presence of bromine at the 5-position-----168

Figure 4.11: Modeling of binding poses of 62 and 64 in Hsp90 $\alpha$ -----168

Figure 4.12: NCI-60 cancer cell screening results from the single dose experiment of 35b-----171

Figure 4.13: NCI-60 cancer cell screening results from the single dose experiment of 36d-----172

Figure 4.14: NCI-60 cancer cell screening results from the single dose experiment of 61g-----173



**List of Tables:**

**CHAPTER I**

**Introduction to Hsp90 Function, Structure and Regulation**

Table 1.1: Co-chaperones and co-activators that regulate Hsp90 chaperone cycle-----4

Table 1.2: Hallmarks of cancer and the associated Hsp90 client proteins-----6

**Chapter II**

**Development of a Novel Series of Compounds for Hsp90 $\beta$ -Selective Inhibition**

Table 2.1: Apparent  $K_d$  values of compounds 4a-k-----47

Table 2.2:  $GI_{50}$  values of 4d against urological cancer cells-----55

**Chapter III**

**Development of Hsp90 $\alpha$ -Selective Inhibitors**

Table 3.1:  $K_d$  values of phenolic replacement compounds-----99

Table 3.2:  $K_d$  values for 19-23-----101

Table 3.3:  $K_d$  values for 24-28-----104

Table 3.4:  $K_d$  values for 35a-k-----105

Table 3.5:  $K_d$  values for 36a-e-----106

Table 3.6:  $K_d$  values for 39a-i-----108

Table 3.7:  $K_d$  values for 40-43-----111

## Chapter IV

### Optimization of the Hsp90 $\alpha$ -selective Compounds

Table 4.1: K <sub>d</sub> determination of 46-50-----	157
Table 4.2: K <sub>d</sub> determination of 54-58-----	159
Table 4.3: Binding affinities of 61a-k-----	161
Table 4.4: Binding affinities of 61l-t-----	163

#### List of Schemes:

## Chapter II

### Development of a Novel Series of Compounds for Hsp90 $\beta$ -Selective Inhibition

Scheme 2.1: Synthesis of 4a-i-----	44
Scheme 2.2: Synthesis of 4j-----	45
Scheme 2.3: Synthesis of 4k-----	45
Scheme 2.4: Synthesis of 5a-g-----	50

## Chapter III

### Development of Hsp90 $\alpha$ -Selective Inhibitors

Scheme 3.1: Synthesis of phenolic replacement compounds 14,15 and 16-----	98
Scheme 3.2: Synthesis of 19-23-----	100
Scheme 3.3: Synthesis of 24, 25 and 28-----	103
Scheme 3.4: Synthesis of 26 and 27-----	103
Scheme 3.5: Synthesis of 35a-k-----	105

Scheme 3.6: Preparation of compounds 36a-e-----	107
Scheme 3.7: Synthesis of the compounds 39a-i-----	108
Scheme 3.8: Synthesis of 40-43-----	110

## Chapter IV

### Optimization of the Hsp90 $\alpha$ -selective Compounds

Scheme 4.1: Synthesis of 44 and 45-----	155
Scheme 4.2: Synthesis of 46-48-----	156
Scheme 4.3: Synthesis of 49 and 50-----	157
Scheme 4.4: Synthesis of 54-58-----	159
Scheme 4.5: Synthesis of 61a-c and 61d-t-----	160
Scheme 4.6: Synthesis of 64-----	169

## CHAPTER I

### Introduction to Hsp90 Function, Structure and Regulation

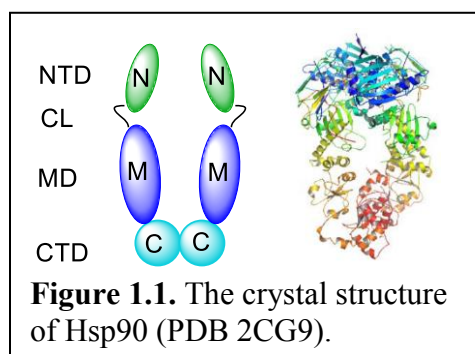
#### I.1 Introduction

Molecular chaperones are a class of protein that regulate proteostasis by assisting in the conformational maturation of nascent polypeptides (referred to as client proteins) and the refolding of denatured proteins. The heat shock proteins (Hsps) belong to the ubiquitously expressed molecular chaperone family that are highly conserved in eukaryotes. The 90kDa Heat shock protein (Hsp90) is one of the most abundant Hsps and represents ~1-2% of the total cellular protein in unstressed cells and ~4-6% in stressed cells, including malignancy.<sup>1-2</sup> Hsp90 is responsible for the maturation of more than 300 protein substrates, wherein numerous client proteins (e.g., ErbB2, B-Raf, Akt, steroid hormone receptors, mutant p53, HIF-1, survivin, telomerase, etc.) are the key regulators of oncogenic transformation, growth, and metastasis.<sup>3-6</sup> Inhibition of the Hsp90 protein folding machinery results in client protein ubiquitination and subsequent degradation by the proteasome, resulting in cell death.<sup>7-8</sup> Hsp90-dependent clients are associated with 10 hallmarks of cancer, thus, Hsp90 inhibition provides a therapeutic opportunity to treat cancer via simultaneous disruption of multiple cellular pathways involved in cancer.<sup>9</sup> While inhibition of Hsp90 is being pursued for the treatment cancer, the induction of Hsp levels has been proposed as a novel approach towards the treatment of diseases such as Parkinson's, Alzheimer's, Huntington's, and those caused by the aggregation of prion-related proteins.<sup>3, 10</sup> Hsp90 inhibitors can also be used as anti-infective agents due to the importance of Hsp90 in pathogenic growth.<sup>11</sup> As a result, many Hsp90 inhibitors have undergone or are undergoing clinical evaluations.<sup>12-13</sup> There are four human isoforms of Hsp90; Hsp90 $\alpha$  (inducible) and Hsp90 $\beta$  (constitutively expressed) are present in cytosol, whereas the endoplasmic reticulum (ER) residing glucose

regulated protein 94 (Grp94/gp96/endoplasmic) and mitochondrial isoform, tumor necrosis factor associated protein (Trap-1/Hsp75) are present in distinct organelles.<sup>14</sup>

## I.2 Hsp90 Structure

Hsp90 exists as a homodimer and each monomer comprises three structural domains: a highly conserved 25kDa N-terminal ATP-binding domain (NTD), a 35kDa flexible middle domain (MD), and a 12 kDa C-terminal dimerization domain (CTD) (Figure 1.1).<sup>3</sup> Hsp90 is a



member of the GHKL (Gyrase, Hsp90, Histidine Kinase and MutL) subgroup of ATPases, which contain a conserved Bergerat fold in the N-terminal ATP-binding site.<sup>15</sup> ATP binds the NTD ATP-binding site of the GHKL superfamily in a unique bent conformation, as opposed to an extended ATP conformation.<sup>16</sup> The Bergerat fold present in the NTD comprises four  $\beta$ -sheets and three  $\alpha$ -helices with an ATP-binding pocket located in the middle.<sup>17-18</sup> Additionally, in the NTD, conserved residues of the Bergerat fold form an “ATP lid” which closes upon ATP binding, but switches to the open conformation in the ADP bound state.<sup>14</sup> The NTD is the major site of ATP hydrolysis in Hsp90 and represents the most druggable binding pocket in Hsp90, as all but one of the Hsp90 inhibitors in clinical trials target this binding site. The MD is connected to the NTD by a flexible and highly charged linker (CL) that is required for interactions with co-chaperones and client proteins (e.g. Aha1, CHIP).<sup>19</sup> This domain also regulates ATP hydrolysis at the NTD via interactions with the  $\gamma$ -phosphate of ATP.<sup>20</sup>

The CTD is responsible for the homodimerization in Hsp90,<sup>21</sup> and contains an EEVD motif that recognizes the tetratricopeptide-containing repeat (TPR) domain found in various co-

chaperones and immunophilins. In eukaryotic Hsp90, opening of the CTD is anticorrelated to closing of the NTD.<sup>21</sup> The CTD has an additional nucleotide-binding site that allosterically regulates NTD ATPase activity.<sup>22</sup> Natural products such as Novobiocin and EGCG bind to the CTD and modulate the Hsp90 protein folding process.<sup>23-25</sup>

### I.3 Hsp90 Chaperone Cycle

Client protein maturation, refolding, and aggregation by Hsp90 are achieved via the formation of a heteroprotein complex. Although the Hsp90-mediated protein folding mechanism has not been completely elucidated, we now know that it involves various co-chaperones, immunophilins, and partner proteins.<sup>26</sup> The chaperone cycle begins with the association of nascent polypeptides with molecular chaperones, Hsp70 and Hsp40 in conjunction with ATP **(1)** (Figure 1.2). Subsequently, bound ATP is hydrolyzed to ADP, which prevents the aggregation of polypeptides. The resulting complex is further stabilized by binding to Hsp70 interacting protein (HIP) **(2)**.<sup>27</sup> Hsp90-Hsp70

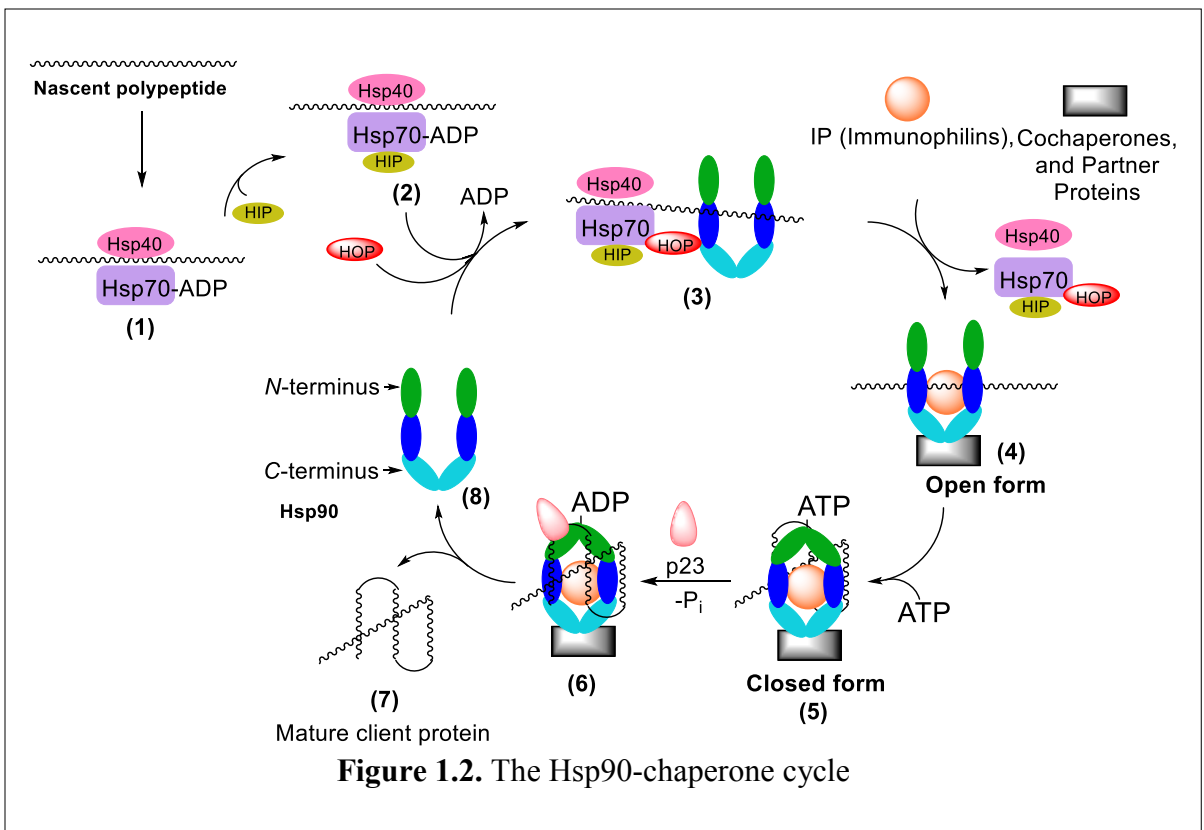


**Figure 1.2.** The Hsp90-chaperone cycle

organizing protein (HOP), which contains a tetratricopeptide repeat (TPR) domain, recognized by both, Hsp90 and Hsp70, coordinates the transfer of the unfolded protein from Hsp70 to the Hsp90 (3).<sup>28</sup> In the following step, immunophilins (FKBP51, FKBP52), co-chaperones and partner proteins bind the Hsp90 homodimer to form an activated multiprotein complex (4) with simultaneous release of Hsp70, Hip and HOP.<sup>28</sup> ATP

<b>Co-chaperone or Co-activator</b>	<b>Function</b>
Aha1	Stimulates ATPase activity
Cdc37	Mediates activation of protein kinase substrates
CHIP	Involved in degradation of unfolded client proteins
Cyclophilin-40	Peptidyl propyl isomerase
FKBP51 and 52	Peptidyl propyl isomerase
Hop	Mediates interaction between Hsp90 and Hsp70
Hsp40	Stabilizes and delivers client proteins to Hsp90 complex
Hsp70	Stabilizes and delivers client proteins to Hsp90 complex
p23	Stabilizes closed, clamped substrate bound conformation
HIP PP5	Inhibits ATPase activity of Hsp70 Protein phosphatase 5
Sgt1	Client adaptor, involved in client recruitment
Tom70	Facilitates translocation of pre-proteins into mitochondrial matrix
WISp39	Regulates p21 stability

**Table 1.1:** Co-chaperones and co-activators that regulate Hsp90 chaperone cycle.

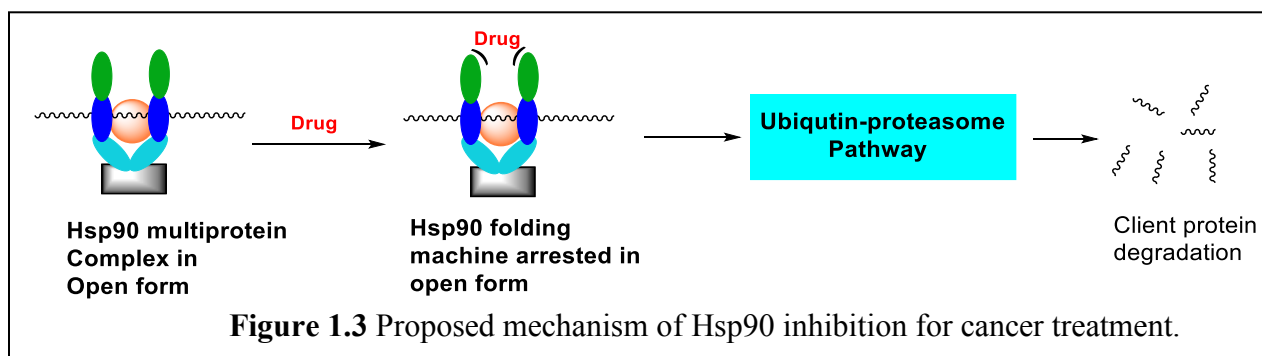
then binds to the open NTD

and promotes formation of the closed conformation of Hsp90 (5) that clamps around the bound client protein.<sup>29</sup> Small molecules compete with ATP for binding to the NTD, and subsequently prevent formation of the closed form (5) which leads to client protein degradation via the ubiquitin-proteasome pathway.<sup>29</sup> However, in the presence of ATP, the co-chaperone p23 is recruited to further stabilize the closed Hsp90 complex and subsequent ATP hydrolysis provides the energy required for client protein folding (6).<sup>29</sup> The mature protein (7) is then released from the complex

and the heteroprotein complex disassembles. The Hsp90 chaperone cycle is regulated by a number of post-translational modifications, such as, acetylation, phosphorylation, S-nitrosylation, methylation and by co-chaperones that modulate affinity for client proteins, ATPase activity, and stability of the heteroprotein complex (Table 1.1).<sup>27, 30, 31-33</sup>

#### I.4 Therapeutic Disruption of Hsp90 Chaperone Cycle

Indirect disruption of Hsp90 client maturation via Hsp90 inhibition represents a unique therapeutic approach for the treatment of various diseases, as these client proteins carry out a wide range of cellular functions that are critical in multiple diseases. Rapidly growing cancer cells require oncoproteins at increased levels to sustain all 10 hallmarks of cancer, many of which are Hsp90-



dependent clients (Table 1.2).<sup>34</sup> For example, Hsp90-dependent tyrosine kinases and steroid hormones receptors drive the progression of various cancers by amplifying growth signals.<sup>35</sup> Therefore, inhibition of Hsp90 provides an alternate approach to traditional chemotherapy for the treatment of cancer. Hsp90 inhibition provides combinatorial disruption of multiple client proteins, producing effects on multiple pathways simultaneously with a single agent. Figure 1.3 explains the mechanism by which client proteins are directed towards their degradation upon Hsp90 inhibition. When inhibitors bind the Hsp90 multiprotein complex and prevent formation of the closed form needed for the maturation of client proteins, the complex is directed toward the



ubiquitin-proteasome pathway, which leads to degradation of the clients. While reduced levels of Hsp90 via inhibition is desired for the treatment of cancer, induction of the pro-survival heat shock response leads to increased levels of various heat shock proteins and is beneficial for the treatment of neurodegenerative disorders that manifest their pathology through accumulation of misfolded proteins. An overall increase in Hsp's leads to solubilization of neurotoxic protein aggregates.<sup>36</sup> Hence, drugs that induce Hsp90 at non-toxic levels can serve as valuable and novel treatment option for neurodegenerative disorders. In addition to cancer and neurodegeneration, inhibitors of Hsp90 are being sought for the treatment infectious diseases.<sup>37</sup>

Due to an abundance of Hsp90 in cells, concerns have arisen regarding selectivity of Hsp90 inhibitors against normal tissue. It was subsequently discovered that Hsp90 inhibitors accumulate predominantly in tumor cells rather than in normal cells, and thus result in a large therapeutic window.<sup>38-39</sup> Kamal and co-workers proposed that the accumulation of Hsp90 inhibitors in tumor cells

Hallmarks of Cancer	Hsp90 Client Protein(s)
1. Self-sufficiency in growth signals	Raf-1, AKT, Her2, MEK, Bcr-Abl
2. Insensitivity to anti-growth signals	Plk, Wee1, Myc1, CDK4, CDK6, Myt1
3. Evasion of apoptosis	RIP, AKT, p53, C-MET, Apaf-1, Survivin
4. Limitless replicative potential	Telomerase (h-Tert)
5. Sustained angiogenesis	FAK, AKT, Hif-1 $\alpha$ , VEGFR, Flt-3
6. Tissue invasion and Metastasis	C-MET
7. Deregulated cellular energetics	ARNT, HIF-1 $\alpha$ , HMG1, SREBF1
8. Avoiding immune destruction	IRAK3
9. Tumor-promoting inflammation	IL-6, IL-8, IRAK1, IRAK2, IRAK3
10. Genome instability and mutation	FANCA, MAFG, NEK8, NEK9, NEK11

**Table 1.2:** Hallmarks of cancer and the associated Hsp90 client proteins

results from the activated Hsp90 heteroprotein complex that resides in cancer cells. During the

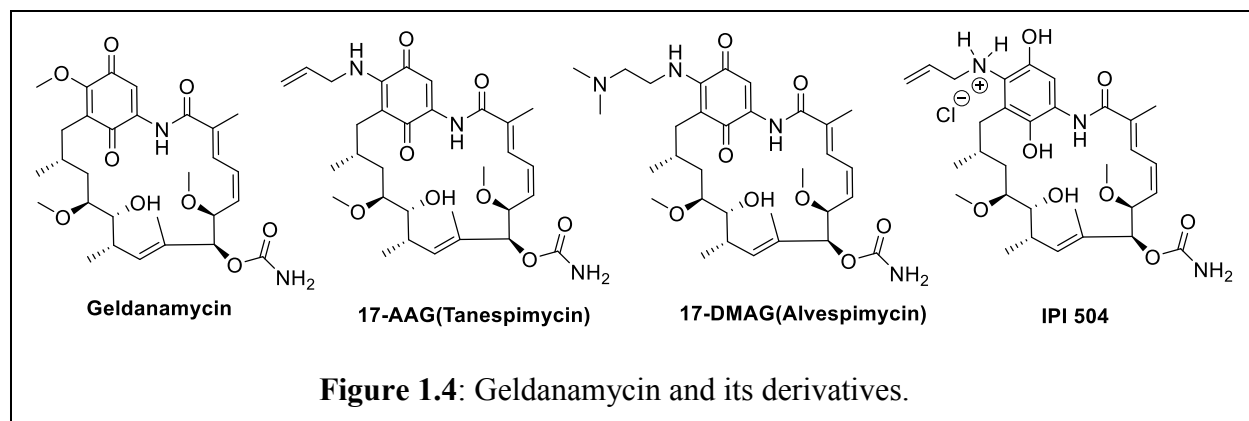
studies, it was shown that the heteroprotein complex manifests enhanced affinity for ATP or inhibitors, whereas in normal cells, Hsp90 exists as a homodimer that exhibits lower affinity for ligands.<sup>40</sup> Clinical trials with the Hsp90 inhibitor, 17-AAG, have produced promising results in phase I and II studies in patients with HER2 over-expressing breast cancer, which, served as proof-of-concept for Hsp90 inhibition.<sup>41</sup> In addition, Hsp90 inhibitors have been investigated for the selective delivery of cytotoxic compounds to the cancer cells by taking advantage of the enhanced affinity of the heteroprotein complex in tumors.<sup>42</sup>

## **1.5 Hsp90 Inhibitors**

The complexity of the Hsp90 chaperone cycle represents multiple opportunities to modulate Hsp90's activity. Broadly, Hsp90 inhibitors can be divided into three classes based on their binding modes; (1) Hsp90 N-terminal inhibitors; (2) Hsp90 C-terminal inhibitors, and (3) disrupters of Hsp90/co-chaperone interactions.<sup>43</sup> At present, only N-terminal inhibitors have undergone clinical evaluations as anti-cancer agents. Historically, N-terminal inhibition has been the most widely explored and sought-after approach, however, alternative modes of Hsp90 inhibition are emerging as promising strategies.<sup>44-47</sup>

### **1.5.1 Natural products as Hsp90 N-terminal inhibitors**

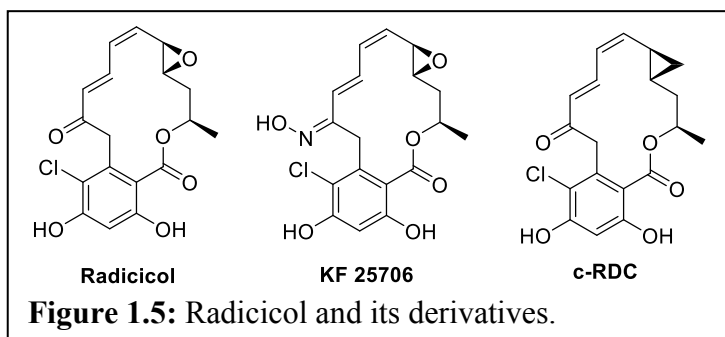
The ansamycin antibiotic natural product, geldanamycin (GDA), was the first Hsp90 inhibitor identified (Figure 1.4), which was originally isolated from the fermentation broth of *Streptomyces hygroscopicus* in 1970.<sup>48</sup> GDA was found to reverse the phenotype of *v-src* transformed cells, which led to hypothesis that GDA manifested its effect via functional inhibition of *v-src*.<sup>49</sup> In an



effort to characterize the mechanism of action manifested by GDA, Whitesell and Neckers utilized an immobilized GDA derivative that affinity purified with Hsp90, establishing it as major biological target of GDA.<sup>22</sup> Ultimately, GDA was co-crystallized with Hsp90, which revealed GDA to bind to N-terminal ATP-binding site. As evaluated in the co-crystal structures, GDA restrains Hsp90 in its closed form **(5)** (Figure 1.2), and disrupts the chaperone cycle.<sup>50-51</sup> Although GDA exhibited promising anticancer activities against various cell lines *in vitro*, it failed as a clinical candidate due to its poor solubility, lack of *in vivo* stability, and hepatotoxicity.<sup>23</sup> However, it has been useful as a chemical probe to elucidate Hsp90-dependent client proteins and to study the mechanism of Hsp90 during malignant transformation. Subsequent structure-activity relationship studies with semisynthetic derivatives led to the development of 17-(allylamino)-17-demethoxygeldanamycin (17-AAG) and 17-(2-dimethylaminoethylamino)-17-desmethoxygeldanamycin (17-DMAG), which manifested improved toxicity profile and led to the clinical investigation.<sup>41, 52</sup> 17-AAG is prone to cytochrome P450 3A4-mediated oxidation of the alpha methylene on the 17-amino substituent which results in subsequent hydrolysis of the C-N bond to produce the amino analogue, IPI-493. IPI-493 manifests growth inhibitory activity against breast cancer cells (SKBr3) at 33 nM, which is similar to that of 17-AAG.<sup>53</sup> Infinity Pharmaceuticals developed another water soluble GDA analogue, IPI-504 after it was determined

that the hydroquinone of IPI-504 was the active component and more water-soluble than the quinone. Subsequent studies with IPI-504 led to its clinical evaluation.<sup>54-55</sup> Current efforts on GDA research has focused on reduction of the toxicities associated with the redox-active benzoquinone moiety, as well as the use of GDA analogues in combination with other therapies.

Radicicol (RDC) is a macrocyclic lactone that was first isolated from the fungi, *Monocillium nordinii* and *Monosporium bonorden*, and identified as an antifungal agent in

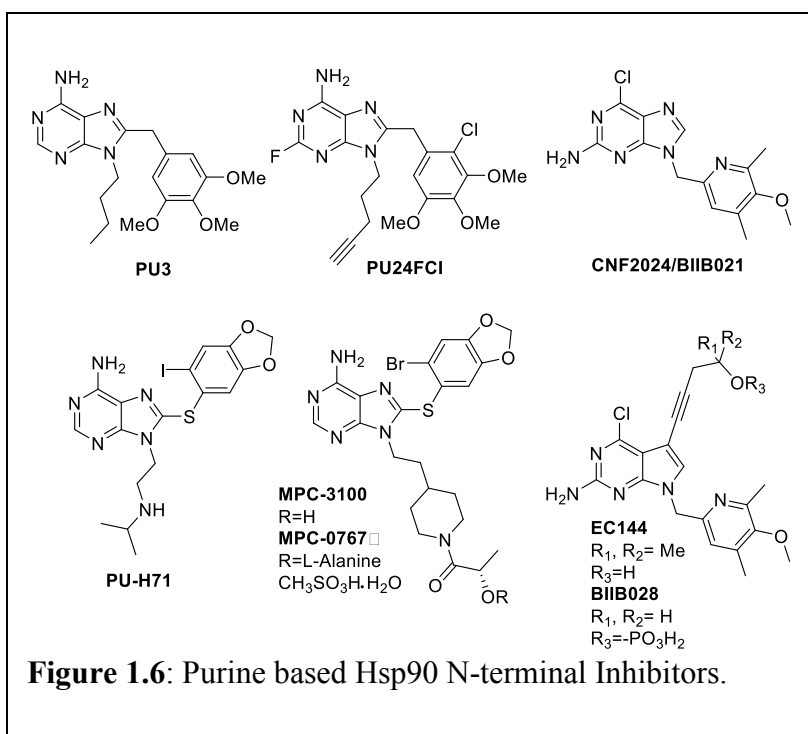


1953(Figure 1.5).<sup>56</sup> RDC was believed to be a tyrosine kinase inhibitor, but later confirmed that it acts via Hsp90 inhibition of the N-terminus ( $K_d= 14\text{nM}$ ).<sup>57</sup> RDC exhibits promising anticancer activity *in vitro*, but not *in vivo*, likely due to the  $\alpha,\beta,\gamma,\delta$ -unsaturated ketone and epoxide, which make it prone to rapid metabolism.<sup>58</sup> Therefore, SAR studies have focused on the identification of analogues that elicit improved *in vivo* stability. Modifications such as the oxime in KF 25706, have led to the development of derivatives that manifest improved inhibitory activity *in vitro* as well as in tumor xenograft models.<sup>23</sup> Furthermore, replacement of the labile allylic epoxide with a cyclopropyl ring (cycloproparadicicol, c-RDC) was shown to manifest similar activity as the natural product.<sup>59</sup> Due to these detriments, RDC has served only as a chemical probe to study Hsp90 biology. However, structural modifications to RDC have led to related small molecule inhibitors that incorporated the resorcinol pharmacophore.

**I.5.2 Small Molecule Inhibitors of the Hsp90 N-terminus.** Limited availability, metabolic liabilities and structural complexity have driven the development of small molecule Hsp90

inhibitors that maintain the key interactions manifested by the natural products with the N-terminal ATP binding site. These compounds can be classified into three categories; 1) purine-, 2) resorcinol-, and 3) benzamide-derived. Initially, the endogenous ligand for the N-terminal binding site, ATP, served as a template for the design of small molecule inhibitors. In 2001, Chiosis and co-workers used X-ray

crystallographic analysis and molecular modeling to design PU3, which contained a purine moiety linked to an aryl ring that mimicked the unique shape adopted by ATP when bound to the N-terminal binding pocket (Figure 1.6). PU3 was the first rationally designed Hsp90 inhibitor that manifested low



micromolar affinity ( $K_d = 15\text{-}20 \mu\text{M}$ ) with moderate anti-proliferative activity ( $IC_{50} = 50 \mu\text{M}$ ) against MCF-7 breast cancer cells.<sup>60</sup> Optimization of PU3 led to the more potent compound, PU24FCI, which manifested improved anti-proliferative activity against breast, lung, colon, and prostate cancer cell lines, and induced the degradation of Hsp90-dependent client proteins including HER2, Akt, Raf-1 and mutant p53. Evaluation of PU24FCI *in vivo* revealed its tumor specificity over normal tissue.<sup>61-62</sup> CNF2024/BIIB021 is an optimized and purine-based inhibitor that contains a pyridylmethylene group that was disclosed in 2005 and represented the first purine-based inhibitor to enter clinical trials (evaluated in Phase I trials for gastrointestinal stromal tumor

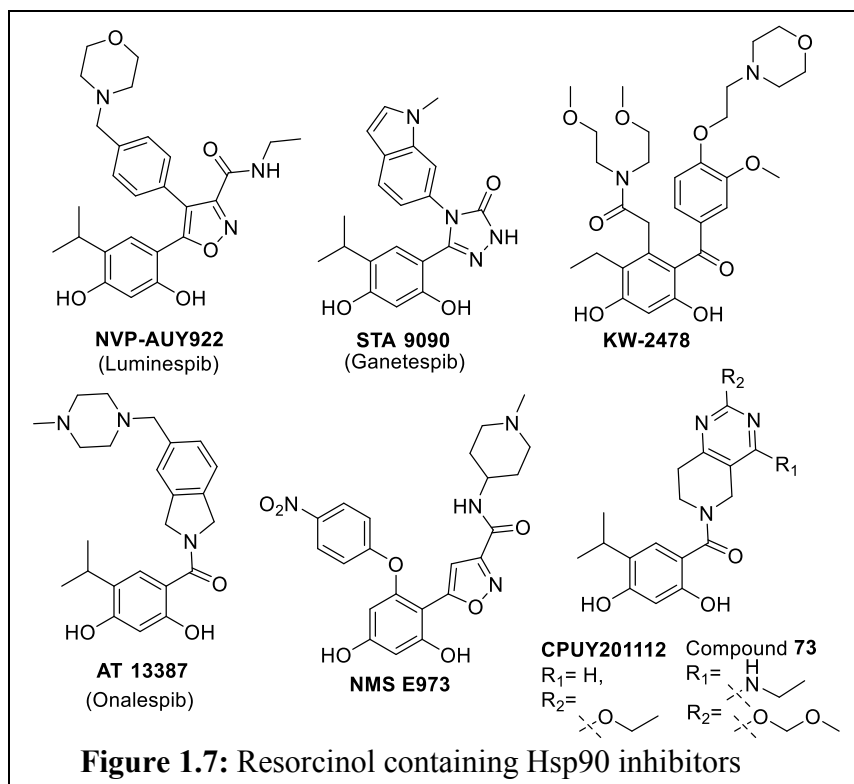
and chronic lymphocytic leukemia).<sup>63-64</sup>

Subsequent studies focused on improving the low bioavailability associated with the purine analogues and eventually led to the incorporation of an alkylamino group which manifested increased solubility (Figure 1.6, PU-H71).<sup>63</sup> PU-H71 contained a 3-isopropylamino-propyl side chain that exhibited ~16 nM binding affinity for Hsp90 with an  $IC_{50}$  of ~50 nM in HER2 degradation assays.<sup>65</sup> This analog showed significant efficacy *in vivo* and advanced into clinical trials for the treatment of patients with low-grade non-Hodgkins lymphoma, as well as patients with advanced malignancies. Results from the clinical evaluations of PU-H71 are encouraging as tumor regression has been observed.<sup>66</sup> MPC-3100 is another purine based compound developed by Myrexix Inc. that underwent Phase I trials for recurrent and refractory tumors along with a safe and tolerable dosing profile and manageable adverse effects.<sup>67</sup> Unfortunately, further development of MPC-3100 has been halted due to poor solubility and formulation issues. To alleviate these concerns, pro-drugs were incorporated into the molecule and resulted in the identification of L-alanine mesylate ester (Figure 1.6, MPC-0767), which exhibited improved pharmacokinetic (PK) and pharmacodynamic (PD) profiles.<sup>68</sup> EC144 (Figure 1.6) is an alkyne-containing purine analog that is based on the BIIB021 structure, and exhibits improved *in vitro* ( $IC_{50}$ =1.1 Vs 5.1 nM) and *in vivo* (~20-fold efficacy improvement in mice) activity when compared to BIIB021.<sup>69</sup> BIIB028 is a phosphate ester prodrug of the homopropargylic alcohol of EC144 sans the dimethyl group, which exhibits improved solubility and is currently under phase I clinical evaluation for patients with solid tumors.<sup>70</sup>

Since the resorcinol ring of Radicicol maintains key interactions with the Hsp90 N-terminal binding pocket, it has served as a template for the development of inhibitors, many of which have entered clinical trials (Figure 1.7). NVP-AUY 922 (Luminespib) is an optimized hit

obtained from a high throughput screen (HTS) by Vernalis. After acquisition, Novartis advanced the compound into both Phase I and II clinical trials, as a single agent therapy and in combination with other drugs including a kinase inhibitor (Erlotinib) and/or a proteasome inhibitor (bortezomib).<sup>12, 71-73</sup> However, a limited response was observed during these trials that discouraged further evaluation of NVPAUY922. Sigma-Tau Research has explored variants of NVPAUY922

via replacement of the isoxazole ring with a triazole.<sup>74</sup> SST0116CL1 represents a compound developed by Sigma Tau that contains an amide linker between the morpholine and isoxazole and maintains binding affinity.<sup>75</sup> STA9090 (Ganetespib) is a potent



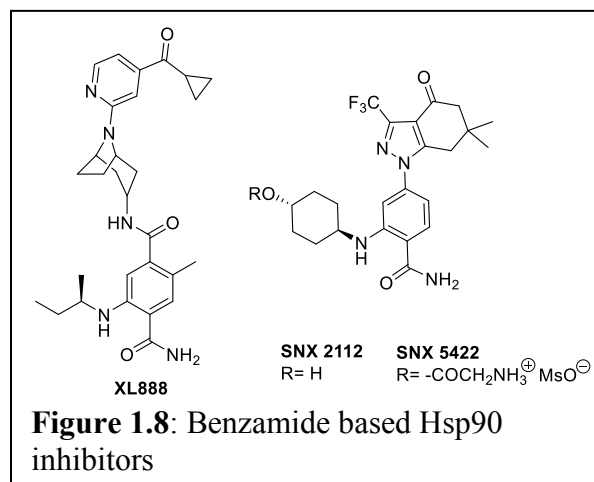
Hsp90 inhibitor developed by Synta Pharmaceuticals. In the clinic, STA9090 was shown to be well tolerated and without the notable toxicities associated with the GDA analogs. STA9090 has shown promise as a single agent in trials for patients with non-small cell lung cancer (NSCLC) and HER2-positive metastatic breast cancer. In particular, it manifested single-agent activity against NSCLC, in patients with anaplastic lymphoma kinase (ALK)-positive disease. STA9090 was the first rationally designed compound to progress into Phase III studies. In combination with docetaxel during II GALAXY-1 studies, STA9090 improved patient outcomes in overall and

progression-free survival as comparison to docetaxel alone in patients with advanced lung adenocarcinoma.<sup>76</sup> Based on encouraging data from the Phase II study, a subgroup of patients were chosen for a Phase III GALAXY-2 evaluations, unfortunately, the overall response rate of ganetespib and docetaxel was 13.7% as compared to 16% with docetaxel alone. Additionally, the disease stability was slightly higher in the combination arm (56%) as compared to the docetaxel arm (50%).<sup>77</sup> Many Phase I/II, clinical trials are being conducted in combination with other agents that may potentiate the effects and range of STA9090 for the treatment of other cancers.<sup>24, 78-79</sup>

KW-2478 was developed by Kyowa Hakko Kirin Pharma through a combinatorial of drug development strategies that included lead optimization, microbial screening, X-ray crystallography, cell-based assays and *in vivo* evaluations.<sup>80</sup> Due to low nM binding affinity and anti-proliferative activity, KW-2478 was shown to be well tolerated in Phase I studies for multiple myeloma, chronic lymphocytic leukemia and B-cell non-Hodgkin's lymphoma along with no dose-limiting toxicity at doses up to 99 mg/m<sup>2</sup>.<sup>81</sup> In combination with bortezomib, KW-2478 was well tolerated and produced an overall response rate of 39% during Phase I/II studies that investigated relapsed/refractory multiple myeloma patients.<sup>82</sup> Astex pharmaceuticals developed AT13387 (Onalespib), a small molecule inhibitor that manifests subnanomolar Hsp90 binding affinity and low nanomolar cellular activity. AT13387 resulted from a unique fragment-based screening approach that utilized a combination of NMR and high throughput X-ray crystallography.<sup>83</sup> This compound entered Phase I studies for investigation against solid tumors and advanced to Phase II studies for GIST (alone and in combination with imatinib),<sup>84</sup> Phase II for prostate cancer (alone or in combination with abiraterone), and Phase I/II for NSCLC (alone or in combination with crizotinib).<sup>85</sup> AT13387 has also shown promise against malignant gliomas (alone and in combination with temozolomide).<sup>86</sup> AT13387 is one of the most recent compounds to enter clinical



evaluations and six studies are currently in the recruitment phase, which will further investigate the Hsp90 inhibition as therapeutic target for various cancers. In contrast with other resorcinol-containing inhibitors, NMS-E973 is phloroglucinol-derived compound, wherein the additional phenol has been substituted with a p-nitrophenyl ring.<sup>87</sup> NMS-E973 can cross the blood brain barrier (BBB), and induce the tumor shrinkage of different human tumor xenografts with increased efficacy against tumors resistant to kinase inhibition. Furthermore, NMS-E973 was evaluated in an intracranially implanted melanoma model.<sup>88</sup> Recent work on the resorcinol scaffold resulted in the development of CPUY201112, a tetrahydropyridopyrimidine-containing molecule that exhibits antiproliferative activity in a wild type p53 dependent cells, as well as efficacy against MCF-7 cells in xenograft models.<sup>89-90</sup> Modifications to CPUY201112 led to compound 73, which exhibits improved pharmacokinetic properties and growth inhibitory efficacy against HCT116 and MCF-7 cells alongside reduced ocular toxicities as compared to NVPAUY922 in *in vivo* models.<sup>91</sup>



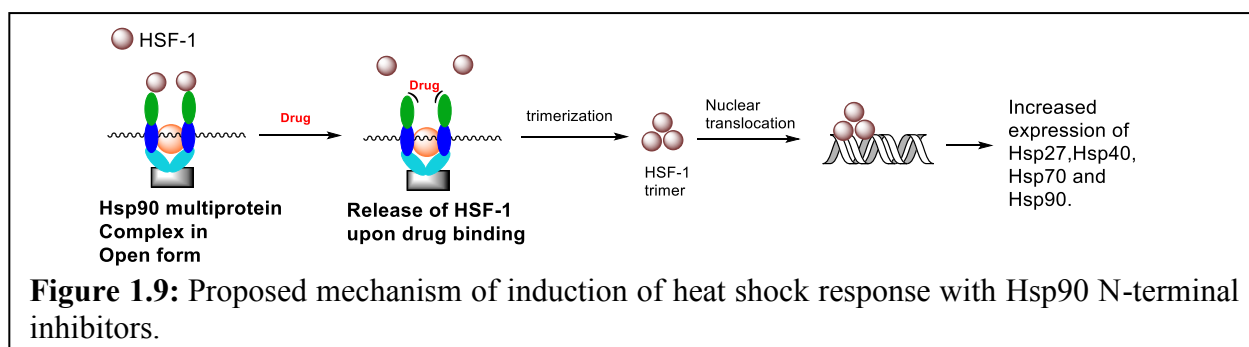
XL888 and SNX5422 belong to the benzamide-containing class of Hsp90 inhibitors. XL888 is a tropane containing compound that resulted from HTS of ~4.1 million compounds from Exelixis.<sup>92</sup> XL888 was found to reduce the proliferation of vemurafenib resistant melanoma cell lines in 3D cell culture as well as mouse

xenograft models.<sup>93</sup> Clinical studies continue for XL888 in combination with vemurafenib and cobimetinib to treat unresectable BRAF mutated stage III/IV melanoma. Serenex discovered SNX 2112 via an affinity-based chromatography screen for ligands that could displace Hsp90 proteins from a purine-based resin.<sup>94-95</sup> SNX 5422 is a mesylate salt of the parent drug which provides

improved solubility and oral administration. Due to concerns arising from ocular toxicities during clinical evaluations, subsequent studies with SNX 5422 as a clinical candidate were discontinued. Recently, this compound was acquired by Esanex, and is sponsoring a Phase I study for the treatment of neuroendocrine tumors in combination with everolimus. In addition, a recent patent disclosure by Esanex has proposed the use of SNX 5422 and related benzamide analogs for the treatment of HIV via the modulation of viral DNA integration into the host genome.<sup>96</sup>

### I.5.3 Induction of the Heat Shock Response (HSR)

The progress of Hsp90 N-terminal inhibitors as clinical candidates has been fraught with many challenges. One of the major drawbacks is the induction of pro-survival heat-shock response (HSR),<sup>97-98</sup> which leads to increased expression of various Hsp's including Hsp90, Hsp70, Hsp27, and Hsp42. This pro-survival response is mediated by heat shock factor-1 (HSF-1), an Hsp90 bound transcription factor that remains inactive in unstressed/normal cells due to its association with Hsp90.<sup>99-100</sup> However, during cellular stress or the administration of an Hsp90 N-terminal inhibitor, HSF-1 is dissociated from Hsp90.<sup>101</sup> When unbound to Hsp90, HSF-1 trimerizes in cytosol, becomes hyperphosphorylated, and then translocates into the nucleus, wherein it



upregulates the transcription of Hsp's upon binding to heat shock element (Figure 1.9).<sup>102-103</sup> Due to the increased levels of Hsp90 following the treatment with the inhibitor, subsequent dosing and scheduling issues emerge, which leads to the exacerbation of adverse effects and higher doses. As

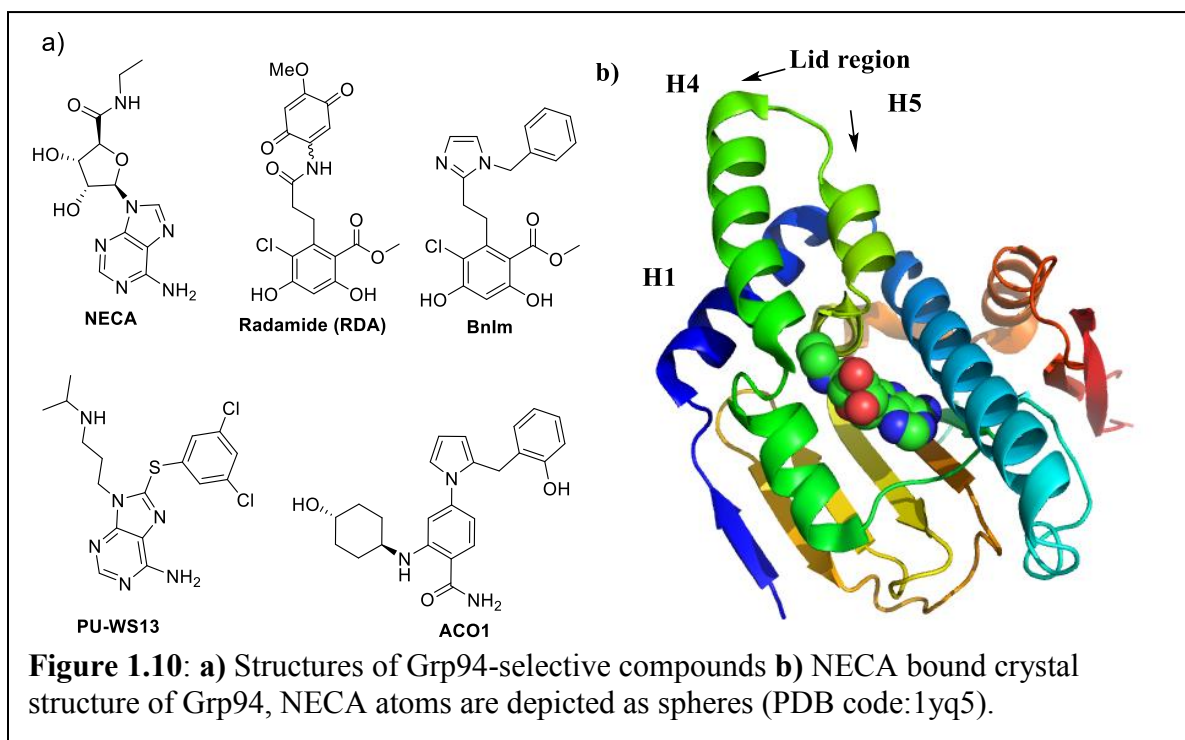
a result, alternative methods to modulate Hsp90 function have been sought, which led to C-terminal inhibitors, HS90/co-chaperone disruptors, allosteric modulators and the development of isoform-selective Hsp90 inhibitor.<sup>6, 25</sup>

#### **I.5.4 Isoform-selective Hsp90 Inhibitors**

Hsp90 inhibitors undergoing clinical evaluation are known to target all four Hsp90 paralogs, which is termed as pan-inhibition. Collectively, Hsp90's are involved in the folding and maturation of over more than 300 client protein substrate.<sup>104</sup> As a consequence of pan-inhibition, the endogenous functions of all Hsp90-dependent client proteins are affected, and collateral disruption of these clients is believed to result in adverse effects. Targeting a specific Hsp90 isoform may enable the treatment of diseases that are driven by an isoform-dependent client population without manifesting the undesired on target effects that are observed with pan-inhibitors. Toxicities observed with the pan-inhibitors include hepatotoxicity, ocular toxicity, hyponatremia, hypoglycemia, renal failure and induction of the heat shock response.<sup>4</sup>

The rational design of isoform-selective Hsp90 inhibitors has been a challenging task, due to the highly conserved and structurally identical nature of the Hsp90 isoforms. Overlay of the N-terminal ATP-binding site residues of all four isoforms reveals >85% identity, whereas, within the cytosolic isoforms Hsp90 $\alpha$  and Hsp90 $\beta$ , the sequence identity is >95%.<sup>105</sup> Grp94 shares the least homology between among the four isoforms, which results from a 5-amino acid insertion that causes a conformational change within the ATP-binding pocket and produces distinct subpockets that have been exploited for the development of Grp94-selective inhibitors.

### I.5.4.1 Grp94-Selective Inhibitors

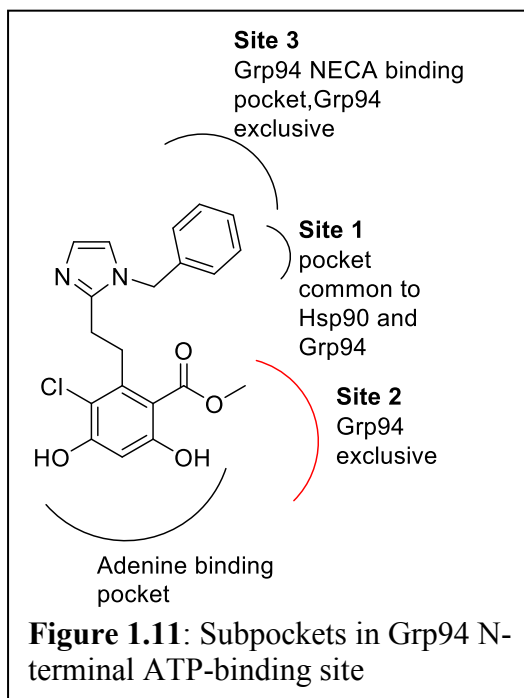


N-ethyl-carboximido adenosine (NECA) (Figure 1.12), an agonist at the adenosine receptors was the first compound to exhibit selective inhibition of Grp94, as it was found to bind Grp94 with 200 nM  $K_d$ , but not Hsp90.<sup>106</sup> The co-crystal structure of NECA bound to the N-terminus of Grp94 revealed the ethyl amide to project into a subpocket that does not exist in other isoforms (Figure 1.10 and 1.11).<sup>107</sup> Due to an unfavorable PK profile and its affinity for the adenosine A2 receptor, NECA does not represent a scaffold that is amenable to further development. The chimeric Hsp90 inhibitor, Radamide (RDA), upon crystallization with Grp94 was found to project its quinone ring into the same subpocket as NECA. However, only the *cis*-amide conformation of the amide was able to project the quinone ring into this subpocket, as the *trans*-amide projected the quinone into solvent and negated Grp94-selectivity.<sup>108</sup> In subsequent studies, the inclusion of an imidazole ring that served as a *cis*-amide isostere resulted in the first rationally designed Grp94-selective compound, Bnlm.<sup>109</sup> Bnlm exhibited a  $K_d$  of  $\sim 1.1 \mu\text{M}$  and  $\sim 12$ -fold selectivity against Hsp90 $\alpha$ .

Optimization of BnIm has led to inhibitors that exhibit improved affinity and selectivity for Grp94 ( $K_d \sim 200$  nM and  $\sim 41$ -fold selectivity).<sup>110</sup> Furthermore, replacement of the imidazole with a phenyl ring in BnIm led to improved potency and selectivity ( $K_d \sim 540$  nM and  $\sim 73$ -fold selectivity).<sup>111</sup> A screen of purine-based Hsp90 inhibitors resulted in the discovery of PU-WS13, a highly selective Grp94 inhibitor that bound Grp94 in a previously unseen conformation.<sup>112</sup> An overview of the N-terminal binding pocket of Grp94 is provided in Figure 1.11 with BnIm as a reference ligand. Interestingly, the thioether of the PU-WS13 was found to orient the 3, 5-dichlorophenyl moiety into Site 2, a pocket that was not observed in the NECA-Grp94 Complex. Occupation of this unique Grp94 subpocket provided PU-WS13  $\sim 140$ -fold selectivity over Hsp90 $\alpha$ . The benzamide based compound, SNX 2112 (Figure 1.8) is distinct from other scaffolds, in that it binds Grp94 with  $\sim 100$ -fold weaker affinity than it does to cytosolic

Hsp90. Based on the molecular modeling studies, the structural features preventing SNX2112 binding to Grp94 were determined and then modified to reverse the selectivity of SNX2112 to develop a Grp94-selective compound, ACO1. ACO1 manifested a  $K_d$  of  $\sim 440$  nM and  $>200$  fold selectivity against Hsp90 $\alpha$ .<sup>113</sup> Functionally, Grp94 is responsible for the maturation of secreted client proteins such as, Toll-like receptors (1, 2, 4, and 9), IGF-I, IGF-II, integrins, and HER2.

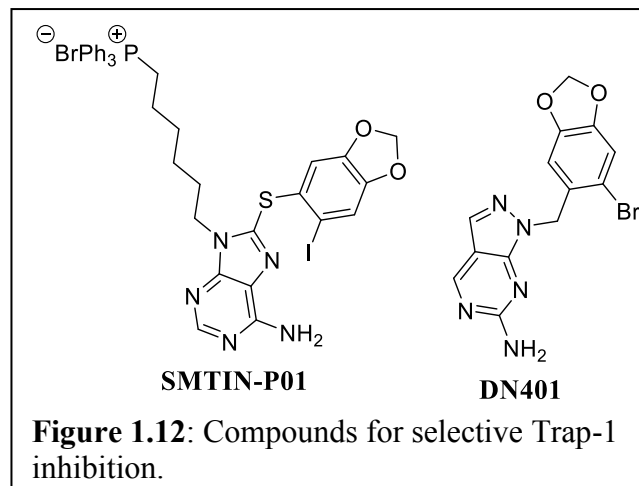
Therefore, Grp94-selective inhibitors are under investigation for the treatment of various diseases,



including liver cancer, multiple myeloma, rheumatoid arthritis and glaucoma.<sup>114-116</sup> Selective inhibition of Grp94 does not induce Hsp90 nor Hsp70, and therefore represents a significant advantage over pan-inhibitors.

#### 1.5.4.2 Trap1-selective Inhibitors

TNF receptor associated protein 1 (Trap1), the mitochondrial Hsp90 isoform is less investigated than other isoforms. Recent studies suggest that Trap-1 exhibits high similarity to both Grp94 and Hsp90. Like Grp94, Trap1 contains a 2-amino acid

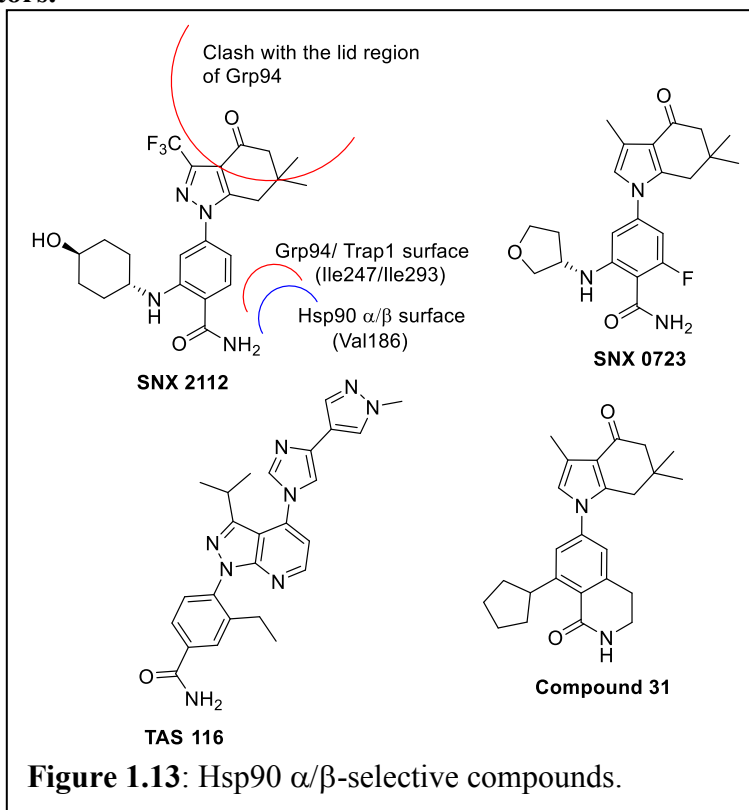


insertion (Ala191, Glu192) between helices 4 and 5 of the lid region, however, helix 4 of Trap1 is highly similar to that of Hsp90.<sup>117</sup> Due to the lack of well-defined structural differences that could guide the rational design of selective Trap1 inhibitors, initial efforts to target Trap1 focused on organelle-specific drug delivery. As an example, triphenylphosphonium was conjugated to a purine based Hsp90 inhibitor, PU-H71, to produce SMTIN-P01. SMTIN-P01 (Figure 1.12) exhibited ~100-fold increased accumulation in the mitochondria and also induced mitochondrial membrane depolarization in Hela cells.<sup>118</sup> In addition, SMTIN-P01 did not increase the levels of Hsp70, indicating a minimum effect on cytosolic chaperones. The crystal structure of human Trap1 in complex with the pan-Hsp90 inhibitors, PU-H71 and BIIB-021, have been solved (PDB codes 4ZIF, 4Z1G),<sup>118</sup> which has shed light onto the structural disorder of the lid in Trap1 upon occupation by a ligand. To exploit the difference in the Trap1 lid rearrangement, BIIB021 was modified to contain a pyrazolopyrimidine ring that produced a ~9-fold Trap1-selective compound, DN401 ( $K_d$  for Trap1= 79 nM). This compound manifests efficacy against multiple cancer cell

lines and was evaluated in a PC3 xenograft model.<sup>119</sup> Due to high similarity with other isoforms, selectivity of ligand binding will depend upon an increased understanding of Trap1 binding site and conformational changes within.

#### 1.5.4.3 Hsp90 $\alpha/\beta$ -selective dual inhibitors.

The benzamide series of Hsp90 inhibitors have shown an inherent selectivity for the cytosolic isoforms, Hsp90 $\alpha/\beta$ , versus Grp94 and Trap1. This is exemplified by, SNX 2112, which shows >100-fold decreased affinity for both Grp94 and Trap1. Two key differences between the cytosolic Hsp90's and Grp94/Trap1 is closure of the lid upon ligand binding,<sup>113</sup> as well as presence of Ile247 in Grp94 (PDB

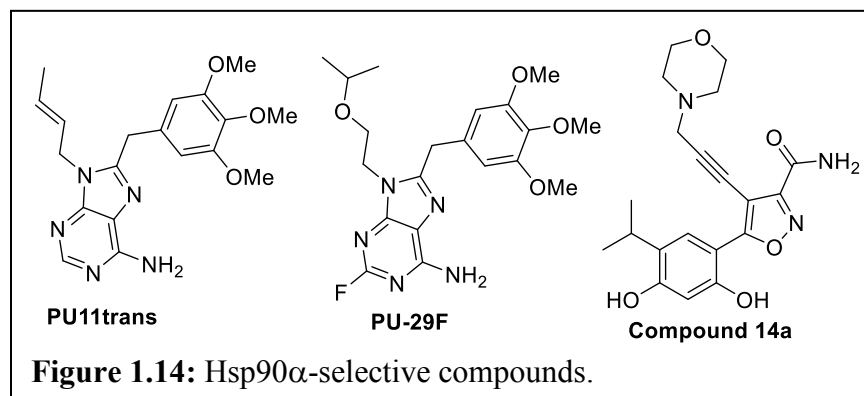


code: 4NH9) and Ile253 in Trap1(PDB code: 4Z1F) which serve *in lieu* of Val186 in both  $\alpha/\beta$  (Hsp90 $\alpha$  PDB code: 2XAB, Hsp90 $\beta$  PDB code: 1UYM), that present a steric clash with the benzamide compounds (Figure 1.13). Increased selectivity for the cytosolic isoforms was achieved with SNX0723 by incorporation of a fluorine atom onto the benzamide ring and exacerbating a steric clash with Trap1, which led to enhanced selectivity over Trap1 (~400 fold). TAS-116 is another benzamide containing compound that manifested  $\alpha/\beta$ -selectivity. Interestingly, TAS-116 manifests potent activity against NCI-H1975 non-small cell lung carcinoma tumors, with minimal accumulation in retinal tissue as compared to NVPAUY922. The difference in distribution of

TAS116 has been hypothesized to produce minimal ocular toxicity.<sup>120</sup> In 2014, a cyclic benzamide series was prepared resulting in compound 31 (Figure 1.13), which exhibited >1000 fold selectivity against Grp94 and Trap1 while binding to Hsp90 $\alpha/\beta$  with ~5 nM  $K_d$ .<sup>121</sup> Compound 31 was found to be equipotent to pan-HSP90 inhibitors in its ability to promote the clearance of mutant huntingtin protein (mHtt) in vitro, while exhibiting an improved tolerability profile.<sup>121</sup> Furthermore, EC144 (Figure 1.6), a purine based compound, manifests 300- and 1200-fold weaker binding affinity to Grp94 and Trap1, respectively, presumably, due to unfavorable interactions between the lid region and the substituted pyridine ring (Figure 1.6).<sup>69</sup>

#### 1.5.4.4 Hsp90 $\alpha$ -selective compounds

The inducible isoform Hsp90 $\alpha$  and the constitutively expressed isoform, Hsp90 $\beta$ , both reside in the cytosol and share the highest identity among the four isoforms, consequently, >95% amino acids within the N-terminal ATP binding site are identical. In fact, only two amino acids differ within NTD between Hsp90 $\alpha$  and Hsp90 $\beta$  (Ser52/Ala52 and Ile91/Leu91 differ between



Hsp90 $\alpha/\beta$ , Hsp90 $\alpha$  PDB code: 2XAB, Hsp90 $\beta$  PDB code: 1UYM). Therefore, the rational design of Hsp90 $\alpha$  or  $\beta$ -selective

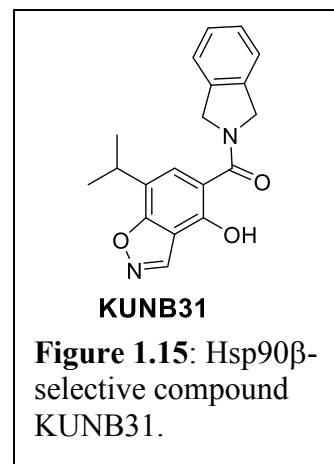
compounds has been a daunting task. Not surprisingly, little progress has been made toward the development of Hsp90 $\alpha$ -selective compounds. However, researchers have serendipitously discovered compounds that exhibit Hsp90 $\alpha$  selectivity, which include PU-11trans and PU-29F (Figure 1.14), both of which bind Hsp90 $\alpha$  with  $K_d$  of ~5 and ~18  $\mu$ M, respectively and exhibit ~4



fold selectivity versus Hsp90 $\beta$ .<sup>112</sup> In a separate study, resorcinol-based compound 14a, was found to manifest ~9 fold selectivity for Hsp90 $\alpha$  over Hsp90 $\beta$ .<sup>122</sup>

#### 1.5.4.5 Hsp90 $\beta$ -selective compounds

As discussed previously, both cytosolic isoforms are highly identical. Therefore, discovery efforts for Hsp90 $\beta$ -selective inhibitors, much like Hsp90 $\alpha$ , have been discouraging. Overlay studies performed with the Hsp90 isoforms suggest that Hsp90 $\beta$  ATP binding site is slightly more hydrophobic than Hsp90 $\alpha$ .<sup>112</sup> However, in a ground-breaking study, Khandelwal and coworkers discovered the first rationally designed Hsp90 $\beta$ -selective compound, KUNB31. With the



aid of modeling studies and a series of modifications to the resorcinolic scaffold, an isoxazole ring was incorporated into the clinical candidate AT13387 (Figure 1.7) to yield KUNB31, which binds selectively to Hsp90 $\beta$  N-terminal binding site with ~180 nM  $K_d$  and ~45-fold selectivity versus Hsp90 $\alpha$ .<sup>123</sup> KUNB31 showed degradation of Hsp90 $\beta$ -dependent client proteins such as c-IAP1, CXCR4, and CDK6 with minimum induction of Hsp70 and Hsp90, alluding to Hsp90 $\beta$ -selective inhibition as a safer alternative to pan-Hsp90 inhibition.<sup>123</sup>

## 1.6 Conclusions and Future Directions

The excitement surrounding the discovery of Hsp90 as the master regulator of >300 client proteins responsible for disease progression has led to extensive efforts toward the discovery of Hsp90 inhibitors. As a consequence, more than 17 clinical candidates entered trials, but the enthusiasm soon passed after a series of disappointments resulting from clinical trials were reported. The failures of these initial inhibitors, which were mostly natural product derived, were attributed to the structural liabilities and poor pharmacokinetic profiles. Subsequent modification and

pharmacophoric dissection of the natural products led to the second-generation inhibitors with smaller molecular structures. The wave of second-generation inhibitors that entered clinical trials included PU-H71, NVPAUY922, STA9090, SNX5422, and AT13387, which also suffered some setbacks. However, AT13387 has shown promise. Despite their high affinities, two major concerns plaguing current Hsp90 inhibitors in clinical trials are toxicities (ocular-, cardio-, hepato-toxicities) and the induction of heat shock response, these concerns have resulted in the termination of many trials, suggesting a need for alternate strategies to Hsp90 inhibition. Adverse reactions or lack of efficacy may be attributed to indiscriminate inhibition of all Hsp90 isoforms that results in reduced accumulation of the drug at the site of action. During the early stages of Hsp90 inhibitor development, rational design of isoform selective inhibitors was considered a tedious task. However, discovery of Grp94-selective inhibitor proved that the achievement of selectivity was within reach with the aid of rational design to modulate ligand binding and exploit conformational flexibility of Hsp90 binding sites. The cytosolic isoforms Hsp90 $\alpha$  and  $\beta$ , offer very little binding site differences in contrast to Grp94, which exhibits significant conformational changes. As a result, various scaffolds such as BnIm, PU-WS13 and ACO1 have been developed for Grp94-selective inhibition. Grp94 inhibitors have shown promise in the treatment of disease such as cancers, glaucoma, and current research is ongoing to improve potency and PK properties such that these inhibitors can be translated into successful therapies. Trap1 has remained a relatively unexplored isoform, however, recent studies have revealed peculiarities about its ligand bound conformation which have been exploited to discover compound such as DN401. Despite structural homology amongst Hsp90 $\alpha$  and Hsp90 $\beta$ , the minimal differences in the binding site have been carefully exploited to discriminate binding of ligand. A remarkable example being KUNB31, that has uncovered that Hsp90 $\beta$ -selective inhibition can be a viable approach to develop agent with

reduced heat shock response induction, leading to potentially safer Hsp90 inhibitors. Comparatively, Hsp90 $\alpha$  presents greater challenges towards the design of isoform selective inhibitor as it lacks spatial subpockets that can be occupied by the ligand. However, selectivity has been observed with compounds such as PU-29F and compound 14a, that bind to the N-terminal of Hsp90 $\alpha$  with slightly higher affinities versus Hsp90 $\beta$ . The design of the Hsp90 $\alpha$ -selective inhibitors with high potency and selectivity is still an unexplored avenue and future designs may take advantage of the thermodynamic differences in binding of ligand between the isoforms. With the rapid advancement of structural and biological understanding of Hsp90 and its isoforms, the future of Hsp90 inhibitors appears hopeful for the treatment of not only cancer but a range of diseases with lesser adverse effects and safer therapeutic dosing profile.

## **I.7 References.**

1. Taipale, M.; Jarosz, D. F.; Lindquist, S. HSP90 at the hub of protein homeostasis: emerging mechanistic insights. *Nature reviews. Molecular cell biology* **2010**, *11*, 515-28.
2. Li, J.; Buchner, J. Structure, function and regulation of the hsp90 machinery. *Biomed J* **2013**, *36*, 106-17.
3. Powers, M. V.; Workman, P. Inhibitors of the heat shock response: biology and pharmacology. *FEBS letters* **2007**, *581*, 3758-69.
4. Neckers, L.; Workman, P. Hsp90 molecular chaperone inhibitors: are we there yet? *Clin. Cancer. Res.* **2012**, *18*, 64-76.
5. da Silva, V. C.; Ramos, C. H. The network interaction of the human cytosolic 90 kDa heat shock protein Hsp90: A target for cancer therapeutics. *J. Proteomics* **2012**, *75*, 2790-802.
6. Holzbeierlein, J. M.; Windsperger, A.; Vielhauer, G. Hsp90: a drug target? *Current oncology reports* **2010**, *12*, 95-101.
7. Ebrahimi-Fakhari, D.; Saidi, L. J.; Wahlster, L. Molecular chaperones and protein folding as therapeutic targets in Parkinson's disease and other synucleinopathies. *Acta Neuropathol Commun* **2013**, *1*, 79.
8. Stancato, L. F.; Chow, Y. H.; Hutchison, K. A.; Perdew, G. H.; Jove, R.; Pratt, W. B. Raf exists in a native heterocomplex with hsp90 and p50 that can be reconstituted in a cell-free system. *J. Biol. Chem.* **1993**, *268*, 21711-6.
9. Hanahan, D.; Weinberg, R. A. Hallmarks of cancer: the next generation. *Cell* **2011**, *144*, 646-74.

10. Macario, A. J.; Conway de Macario, E. Sick chaperones, cellular stress, and disease. *N. Engl. J. Med.* **2005**, *353*, 1489-501.
11. Rochani, A. K.; Singh, M.; Tatu, U. Heat shock protein 90 inhibitors as broad spectrum anti-infectives. *Curr. Pharm. Des.* **2013**, *19*, 377-86.
12. Jhaveri, K.; Taldone, T.; Modi, S.; Chiosis, G. Advances in the clinical development of heat shock protein 90 (Hsp90) inhibitors in cancers. *Biochim. Biophys. Acta* **2012**, *1823*, 742-55.
13. Jhaveri, K.; Ochiana, S. O.; Dunphy, M. P.; Gerecitano, J. F.; Corben, A. D.; Peter, R. I.; Janjigian, Y. Y.; Gomes-DaGama, E. M.; Koren, J., 3rd; Modi, S.; Chiosis, G. Heat shock protein 90 inhibitors in the treatment of cancer: current status and future directions. *Expert Opin Investig Drugs* **2014**, *23*, 611-28.
14. Subbarao Sreedhar, A.; Kalmár, É.; Csermely, P.; Shen, Y.-F. Hsp90 isoforms: functions, expression and clinical importance. *FEBS Lett.* **2004**, *562*, 11-15.
15. Taipale, M.; Krykbaeva, I.; Koeva, M.; Kayatekin, C.; Westover, K. D.; Karras, G. I.; Lindquist, S. Quantitative analysis of HSP90-client interactions reveals principles of substrate recognition. *Cell* **2012**, *150*, 987-1001.
16. Dutta, R.; Inouye, M. GHKL, an emergent ATPase/kinase superfamily. *Trends Biochem. Sci* **2000**, *25*, 24-8.
17. Grenert, J. P.; Sullivan, W. P.; Fadden, P.; Haystead, T. A.; Clark, J.; Mimnaugh, E.; Krutzsch, H.; Ochel, H. J.; Schulte, T. W.; Sausville, E.; Neckers, L. M.; Toft, D. O. The amino-terminal domain of heat shock protein 90 (hsp90) that binds geldanamycin is an ATP/ADP switch domain that regulates hsp90 conformation. *The Journal of biological chemistry* **1997**, *272*, 23843-50.
18. Roe, S. M.; Prodromou, C.; O'Brien, R.; Ladbury, J. E.; Piper, P. W.; Pearl, L. H. Structural basis for inhibition of the Hsp90 molecular chaperone by the antitumor antibiotics radicicol and geldanamycin. *J. Med. Chem.* **1999**, *42*, 260-6.
19. Pearl, L. H.; Prodromou, C. Structure and in vivo function of Hsp90. *Curr. Opin. Struct. Biol.* **2000**, *10*, 46-51.
20. Prodromou, C.; Pearl, L. H. Structure and functional relationships of Hsp90. *Curr. Cancer Drug Targets* **2003**, *3*, 301-23.
21. Donnelly, A. C.; Mays, J. R.; Burlison, J. A.; Nelson, J. T.; Vielhauer, G.; Holzbeierlein, J.; Blagg, B. S. The design, synthesis, and evaluation of coumarin ring derivatives of the novobiocin scaffold that exhibit antiproliferative activity. *The Journal of organic chemistry* **2008**, *73*, 8901-20.
22. Whitesell, L.; Mimnaugh, E. G.; De Costa, B.; Myers, C. E.; Neckers, L. M. Inhibition of heat shock protein HSP90-pp60v-src heteroprotein complex formation by benzoquinone ansamycins: essential role for stress proteins in oncogenic transformation. *Proceedings of the National Academy of Sciences of the United States of America* **1994**, *91*, 8324-8.
23. Messaoudi, S.; Peyrat, J. F.; Brion, J. D.; Alami, M. Recent advances in Hsp90 inhibitors as antitumor agents. *Anti-cancer agents in medicinal chemistry* **2008**, *8*, 761-82.
24. Kim, Y. S.; Alarcon, S. V.; Lee, S.; Lee, M. J.; Giaccone, G.; Neckers, L.; Trepel, J. B. Update on Hsp90 inhibitors in clinical trial. *Curr. Top. Med. Chem.* **2009**, *9*, 1479-92.
25. Biamonte, M. A.; Van de Water, R.; Arndt, J. W.; Scannevin, R. H.; Perret, D.; Lee, W. C. Heat shock protein 90: inhibitors in clinical trials. *J. Med. Chem.* **2010**, *53*, 3-17.

26. Li, Z.; Srivastava, P. K. Tumor rejection antigen gp96/grp94 is an ATPase: implications for protein folding and antigen presentation. *EMBO J.* **1993**, *12*, 3143-51.
27. Prodromou, C. The 'active life' of Hsp90 complexes. *Biochimica et biophysica acta* **2012**, *1823*, 614-23.
28. Rohl, A.; Rohrberg, J.; Buchner, J. The chaperone Hsp90: changing partners for demanding clients. *Trends Biochem. Sci* **2013**, *38*, 253-62.
29. Li, J.; Richter, K.; Reinstein, J.; Buchner, J. Integration of the accelerator Aha1 in the Hsp90 co-chaperone cycle. *Nat. Struct. Mol. Biol.* **2013**, *20*, 326-31.
30. Connell, P.; Ballinger, C. A.; Jiang, J.; Wu, Y.; Thompson, L. J.; Hohfeld, J.; Patterson, C. The co-chaperone CHIP regulates protein triage decisions mediated by heat-shock proteins. *Nat. Cell Biol.* **2001**, *3*, 93-6.
31. Mollapour, M.; Bourbouli, D.; Beebe, K.; Woodford, M. R.; Polier, S.; Hoang, A.; Chelluri, R.; Li, Y.; Guo, A.; Lee, M. J.; Fotooh-Abadi, E.; Khan, S.; Prince, T.; Miyajima, N.; Yoshida, S.; Tsutsumi, S.; Xu, W.; Panaretou, B.; Stetler-Stevenson, W. G.; Bratslavsky, G.; Trepel, J. B.; Prodromou, C.; Neckers, L. Asymmetric Hsp90 N domain SUMOylation recruits Aha1 and ATP-competitive inhibitors. *Mol. Cell* **2014**, *53*, 317-29.
32. Mollapour, M.; Neckers, L. Post-translational modifications of Hsp90 and their contributions to chaperone regulation. *Biochim. Biophys. Acta* **2012**, *1823*, 648-55.
33. Walton-Diaz, A.; Khan, S.; Bourbouli, D.; Trepel, J. B.; Neckers, L.; Mollapour, M. Contributions of co-chaperones and post-translational modifications towards Hsp90 drug sensitivity. *Future Med. Chem.* **2013**, *5*, 1059-71.
34. Hanahan, D.; Weinberg, Robert A. Hallmarks of Cancer: The Next Generation. *Cell* **144**, 646-674.
35. Miyata, Y.; Nakamoto, H.; Neckers, L. The therapeutic target Hsp90 and cancer hallmarks. *Curr. Pharm. Des.* **2013**, *19*, 347-65.
36. Paul, S.; Mahanta, S. Association of heat-shock proteins in various neurodegenerative disorders: is it a master key to open the therapeutic door? *Mol. Cell. Biochem.* **2014**, *386*, 45-61.
37. Solit, D. B.; Chiosis, G. Development and application of Hsp90 inhibitors. *Drug Discov. Today* **2008**, *13*, 38-43.
38. Neckers, L. Heat shock protein 90: the cancer chaperone. *J. Biosci.* **2007**, *32*, 517-30.
39. Chiosis, G.; Neckers, L. Tumor selectivity of Hsp90 inhibitors: the explanation remains elusive. *ACS Chem. Biol.* **2006**, *1*, 279-84.
40. Kamal, A.; Thao, L.; Sensintaffar, J.; Zhang, L.; Boehm, M. F.; Fritz, L. C.; Burrows, F. J. A high-affinity conformation of Hsp90 confers tumour selectivity on Hsp90 inhibitors. *Nature* **2003**, *425*, 407-10.
41. Sidera, K.; Patsavoudi, E. HSP90 inhibitors: current development and potential in cancer therapy. *Recent patents on anti-cancer drug discovery* **2014**, *9*, 1-20.
42. Bobrov, E.; Skobeleva, N.; Restifo, D.; Beglyarova, N.; Cai, K. Q.; Handorf, E.; Campbell, K.; Proia, D. A.; Khazak, V.; Golemis, E. A.; Astsaturov, I. Targeted delivery of chemotherapy using HSP90 inhibitor drug conjugates is highly active against pancreatic cancer models. *Oncotarget* **2017**, *8*, 4399-4409.
43. Brandt, G. E.; Blagg, B. S. Alternate strategies of Hsp90 modulation for the treatment of cancer and other diseases. *Curr. Top. Med. Chem.* **2009**, *9*, 1447-61.

44. Hall, J. A.; Kusuma, B. R.; Brandt, G. E.; Blagg, B. S. Cruentaren A binds F1F0 ATP synthase to modulate the Hsp90 protein folding machinery. *ACS Chem. Biol.* **2014**, *9*, 976-85.
45. Hall, J. A.; Forsberg, L. K.; Blagg, B. S. Alternative approaches to Hsp90 modulation for the treatment of cancer. *Future Med. Chem.* **2014**, *6*, 1587-605.
46. Zhao, H.; Brandt, G. E.; Galam, L.; Matts, R. L.; Blagg, B. S. Identification and initial SAR of silybin: an Hsp90 inhibitor. *Bioorg. Med. Chem. Lett.* **2011**, *21*, 2659-64.
47. Brandt, G. E.; Schmidt, M. D.; Prisinzano, T. E.; Blagg, B. S. Gedunin, a novel hsp90 inhibitor: semisynthesis of derivatives and preliminary structure-activity relationships. *J. Med. Chem.* **2008**, *51*, 6495-502.
48. DeBoer, C.; Meulman, P. A.; Wnuk, R. J.; Peterson, D. H. Geldanamycin, a new antibiotic. *J. Antibiot. (Tokyo)* **1970**, *23*, 442-7.
49. Jove, R.; Hanafusa, H. Cell transformation by the viral src oncogene. *Annu. Rev. Cell Biol.* **1987**, *3*, 31-56.
50. Mimnaugh, E. G.; Chavany, C.; Neckers, L. Polyubiquitination and proteasomal degradation of the p185c-erbB-2 receptor protein-tyrosine kinase induced by geldanamycin. *J. Biol. Chem.* **1996**, *271*, 22796-801.
51. Stebbins, C. E.; Russo, A. A.; Schneider, C.; Rosen, N.; Hartl, F. U.; Pavletich, N. P. Crystal structure of an Hsp90-geldanamycin complex: targeting of a protein chaperone by an antitumor agent. *Cell* **1997**, *89*, 239-50.
52. Ramanathan, R. K.; Egorin, M. J.; Erlichman, C.; Remick, S. C.; Ramalingam, S. S.; Naret, C.; Holleran, J. L.; TenEyck, C. J.; Ivy, S. P.; Belani, C. P. Phase I pharmacokinetic and pharmacodynamic study of 17-dimethylaminoethylamino-17-demethoxygeldanamycin, an inhibitor of heat-shock protein 90, in patients with advanced solid tumors. *Journal of clinical oncology : official journal of the American Society of Clinical Oncology* **2010**, *28*, 1520-6.
53. Egorin, M. J.; Rosen, D. M.; Wolff, J. H.; Callery, P. S.; Musser, S. M.; Eiseman, J. L. Metabolism of 17-(allylamino)-17-demethoxygeldanamycin (NSC 330507) by murine and human hepatic preparations. *Cancer Res.* **1998**, *58*, 2385-96.
54. Floris, G.; Debiec-Rychter, M.; Wozniak, A.; Stefan, C.; Normant, E.; Faa, G.; Machiels, K.; Vanleeuw, U.; Sciot, R.; Schoffski, P. The heat shock protein 90 inhibitor IPI-504 induces KIT degradation, tumor shrinkage, and cell proliferation arrest in xenograft models of gastrointestinal stromal tumors. *Mol. Cancer Ther.* **2011**, *10*, 1897-908.
55. Siegel, D.; Jagannath, S.; Vesole, D. H.; Borello, I.; Mazumder, A.; Mitsiades, C.; Goddard, J.; Dunbar, J.; Normant, E.; Adams, J.; Grayzel, D.; Anderson, K. C.; Richardson, P. A phase 1 study of IPI-504 (retaspimycin hydrochloride) in patients with relapsed or relapsed and refractory multiple myeloma. *Leukemia & lymphoma* **2011**, *52*, 2308-15.
56. Delmotte, P.; Delmotte-Plaque, J. A new antifungal substance of fungal origin. *Nature* **1953**, *171*, 344.
57. Soga, S.; Shiotsu, Y.; Akinaga, S.; Sharma, S. V. Development of radicicol analogues. *Curr. Cancer Drug Targets* **2003**, *3*, 359-69.
58. Geng, X.; Yang, Z.-Q.; Danishefsky, S. J. Synthetic Development of Radicicol and Cycloproparadicicol: Highly Promising Anticancer Agents Targeting Hsp90. *Synlett* **2004**, *2004*, 1325-1333.

59. Yang, Z. Q.; Geng, X.; Solit, D.; Pratilas, C. A.; Rosen, N.; Danishefsky, S. J. New efficient synthesis of resorcinyllic macrolides via ynolides: establishment of cycloproparadicicol as synthetically feasible preclinical anticancer agent based on Hsp90 as the target. *J. Am. Chem. Soc.* **2004**, *126*, 7881-9.
60. Chiosis, G.; Timaul, M. N.; Lucas, B.; Munster, P. N.; Zheng, F. F.; Sepp-Lorenzino, L.; Rosen, N. A small molecule designed to bind to the adenine nucleotide pocket of Hsp90 causes Her2 degradation and the growth arrest and differentiation of breast cancer cells. *Chem. Biol.* **2001**, *8*, 289-99.
61. Llauger, L.; He, H.; Kim, J.; Aguirre, J.; Rosen, N.; Peters, U.; Davies, P.; Chiosis, G. Evaluation of 8-arylsulfanyl, 8-arylsulfoxyl, and 8-arylsulfonyl adenine derivatives as inhibitors of the heat shock protein 90. *Journal of medicinal chemistry* **2005**, *48*, 2892-905.
62. Vilenchik, M.; Solit, D.; Basso, A.; Huezo, H.; Lucas, B.; He, H.; Rosen, N.; Spampinato, C.; Modrich, P.; Chiosis, G. Targeting wide-range oncogenic transformation via PU24FCl, a specific inhibitor of tumor Hsp90. *Chem. Biol.* **2004**, *11*, 787-97.
63. Kasibhatla, S. R.; Hong, K.; Biamonte, M. A.; Busch, D. J.; Karjian, P. L.; Sensintaffar, J. L.; Kamal, A.; Lough, R. E.; Brekken, J.; Lundgren, K.; Grecko, R.; Timony, G. A.; Ran, Y.; Mansfield, R.; Fritz, L. C.; Ulm, E.; Burrows, F. J.; Boehm, M. F. Rationally designed high-affinity 2-amino-6-halopurine heat shock protein 90 inhibitors that exhibit potent antitumor activity. *Journal of medicinal chemistry* **2007**, *50*, 2767-78.
64. Jhaveri, K.; Taldone, T.; Modi, S.; Chiosis, G. Advances in the clinical development of heat shock protein 90 (HSP90) inhibitors in cancers. *Biochim Biophys Acta.* **2012**, *1823*.
65. He, H.; Zatorska, D.; Kim, J.; Aguirre, J.; Llauger, L.; She, Y.; Wu, N.; Immormino, R. M.; Gewirth, D. T.; Chiosis, G. Identification of potent water soluble purine-scaffold inhibitors of the heat shock protein 90. *Journal of medicinal chemistry* **2006**, *49*, 381-90.
66. Gerecitano, J. F.; Modi, S.; Rampal, R.; Drilon, A. E.; Fury, M. G.; Gounder, M. M.; Harding, J. J.; Hyman, D. M.; Varghese, A. M.; Voss, M. H.; France, F. O.; Taldone, T.; Gomes DaGama, E.; Uddin, M.; Chiosis, G.; Lewis, J. S.; Lyashchenko, S. K.; Larson, S. M.; Pressl, C.; Dunphy, M. Phase I trial of the HSP-90 inhibitor PU-H71. *J. Clin. Oncol.* **2015**, *33*, 2537-2537.
67. Kim, S.-H.; Bajji, A.; Tangallapally, R.; Markovitz, B.; Trovato, R.; Shenderovich, M.; Baichwal, V.; Bartel, P.; Cimbora, D.; McKinnon, R.; Robinson, R.; Papac, D.; Wettstein, D.; Carlson, R.; Yager, K. M. Discovery of (2S)-1-[4-(2-{6-Amino-8-[(6-bromo-1,3-benzodioxol-5-yl)sulfanyl]-9H-purin-9-yl}ethyl)piperidin-1-yl]-2-hydroxypropan-1-one (MPC-3100), a Purine-Based Hsp90 Inhibitor. *J. Med. Chem.* **2012**, *55*, 7480-7501.
68. Kim, S.-H.; Tangallapally, R.; Kim, I. C.; Trovato, R.; Parker, D.; Patton, J. S.; Reeves, L.; Bradford, C.; Wettstein, D.; Baichwal, V.; Papac, D.; Bajji, A.; Carlson, R.; Yager, K. M. Discovery of an l-alanine ester prodrug of the Hsp90 inhibitor, MPC-3100. *Bioorg. Med. Chem. Lett.* **2015**, *25*, 5254-5257.
69. Shi, J.; Van de Water, R.; Hong, K.; Lamer, R. B.; Weichert, K. W.; Sandoval, C. M.; Kasibhatla, S. R.; Boehm, M. F.; Chao, J.; Lundgren, K.; Timple, N.; Lough, R.; Ibanez, G.; Boykin, C.; Burrows, F. J.; Kehry, M. R.; Yun, T. J.; Harning, E. K.; Ambrose, C.; Thompson, J.; Bixler, S. A.; Dunah, A.; Snodgrass-Belt, P.; Arndt, J.; Enyedy, I. J.; Li, P.; Hong, V. S.; McKenzie, A.; Biamonte, M. A. EC144 Is a Potent Inhibitor of the Heat Shock Protein 90. *J. Med. Chem.* **2012**, *55*, 7786-7795.

70. Hong, D.; Said, R.; Falchook, G.; Naing, A.; Moulder, S.; Tsimberidou, A. M.; Galluppi, G.; Dakappagari, N.; Storgard, C.; Kurzrock, R.; Rosen, L. S. Phase I study of BIIB028, a selective heat shock protein 90 inhibitor, in patients with refractory metastatic or locally advanced solid tumors. *Clin. Cancer. Res.* **2013**, *19*, 4824-31.
71. Johnson, M. L.; Yu, H. A.; Hart, E. M.; Weitner, B. B.; Rademaker, A. W.; Patel, J. D.; Kris, M. G.; Riely, G. J. Phase I/II Study of HSP90 Inhibitor AUY922 and Erlotinib for EGFR-Mutant Lung Cancer With Acquired Resistance to Epidermal Growth Factor Receptor Tyrosine Kinase Inhibitors. *J. Clin. Oncol.* **2015**, *33*, 1666-1673.
72. Garcia-Carbonero, R. C., A.; Paz-Ares, L. Inhibition of Hsp90 molecular chaperones: moving into the clinic. *Lancet. Oncol.* **2013**, *14*, e358-e369.
73. Jhaveri, K.; Ochiana, S. O.; Dunphy, M. P.; Gerecitano, J. F.; Corben, A. D.; Peter, R. I. Heat shock protein 90 inhibitors in the treatment of cancer: current status and future directions. *Expert Opin Investig Drugs.* **2014**, *23*.
74. Taddei, M.; Ferrini, S.; Giannotti, L.; Corsi, M.; Manetti, F.; Giannini, G.; Vesci, L.; Milazzo, F. M.; Alloatti, D.; Guglielmi, M. B.; Castorina, M.; Cervoni, M. L.; Barbarino, M.; Foderà, R.; Carollo, V.; Pisano, C.; Armaroli, S.; Cabri, W. Synthesis and Evaluation of New Hsp90 Inhibitors Based on a 1,4,5-Trisubstituted 1,2,3-Triazole Scaffold. *Journal of medicinal chemistry* **2014**, *57*, 2258-2274.
75. Vesci, L.; Milazzo, F. M.; Carollo, V.; Pace, S.; Giannini, G. Preclinical antitumor activity of SST0116CL1: a novel heat shock protein 90 inhibitor. *Int. J. Oncol.* **2014**, *45*, 1421-9.
76. Ramalingam, S.; Goss, G.; Rosell, R.; Schmid-Bindert, G.; Zaric, B.; Andric, Z.; Bondarenko, I.; Komov, D.; Ceric, T.; Khuri, F.; Samarzija, M.; Filip, E.; Ciuleanu, T.; Hirsh, V.; Wehler, T.; Spicer, J.; Salgia, R.; Shapiro, G.; Sheldon, E.; Teofilovici, F.; Vukovic, V.; Fennell, D. A randomized phase II study of ganetespib, a heat shock protein 90 inhibitor, in combination with docetaxel in second-line therapy of advanced non-small cell lung cancer (GALAXY-1). *Ann. Oncol.* **2015**, *26*, 1741-8.
77. Solit, D. B.; Basso, A. D.; Olshen, A. B.; Scher, H. I.; Rosen, N. Inhibition of heat shock protein 90 function down-regulates Akt kinase and sensitizes tumors to Taxol. *Cancer Res.* **2003**, *63*.
78. Jhaveri, K.; Modi, S. Ganetespib: research and clinical development. *Onco Targets Ther.* **2015**, *8*, 1849-1858.
79. Jhaveri, K.; Wang, R.; Teplinsky, E.; Chandarlapaty, S.; Solit, D.; Cadoo, K.; Speyer, J.; D'Andrea, G.; Adams, S.; Patil, S.; Haque, S.; O'Neill, T.; Friedman, K.; Esteva, F. J.; Hudis, C.; Modi, S. A phase I trial of ganetespib in combination with paclitaxel and trastuzumab in patients with human epidermal growth factor receptor-2 (HER2)-positive metastatic breast cancer. *Breast Cancer Research* **2017**, *19*, 89.
80. Nakashima, T.; Ishii, T.; Tagaya, H.; Seike, T.; Nakagawa, H.; Kanda, Y.; Akinaga, S.; Soga, S.; Shiotsu, Y. New molecular and biological mechanism of antitumor activities of KW-2478, a novel nonansamycin heat shock protein 90 inhibitor, in multiple myeloma cells. *Clin. Cancer. Res.* **2010**, *16*, 2792-802.
81. Yong, K.; Cavet, J.; Johnson, P.; Morgan, G.; Williams, C.; Nakashima, D.; Akinaga, S.; Oakervee, H.; Cavenagh, J. Phase I study of KW-2478, a novel Hsp90 inhibitor, in patients with B-cell malignancies. *Br. J. Cancer* **2016**, *114*, 7-13.
82. Cavenagh, J.; Oakervee, H.; Baetiong-Caguioa, P.; Davies, F.; Gharibo, M.; Rabin, N.; Kurman, M.; Novak, B.; Shiraiishi, N.; Nakashima, D.; Akinaga, S.; Yong, K. A phase



- I/II study of KW-2478, an Hsp90 inhibitor, in combination with bortezomib in patients with relapsed/refractory multiple myeloma. *Br. J. Cancer* **2017**, *117*, 1295-1302.
83. Murray, C. W.; Carr, M. G.; Callaghan, O.; Chessari, G.; Congreve, M.; Cowan, S.; Coyle, J. E.; Downham, R.; Figueroa, E.; Frederickson, M.; Graham, B.; McMenemy, R.; O'Brien, M. A.; Patel, S.; Phillips, T. R.; Williams, G.; Woodhead, A. J.; Woolford, A. J. A. Fragment-Based Drug Discovery Applied to Hsp90. Discovery of Two Lead Series with High Ligand Efficiency. *J. Med. Chem.* **2010**, *53*, 5942-5955.
  84. Wagner, A. J.; Agulnik, M.; Heinrich, M. C.; Mahadevan, D.; Riedel, R. F.; von Mehren, M.; Trent, J.; Demetri, G. D.; Corless, C. L.; Yule, M.; Lyons, J. F.; Oganessian, A.; Keer, H. Dose-escalation study of a second-generation non-ansamycin HSP90 inhibitor, onalespib (AT13387), in combination with imatinib in patients with metastatic gastrointestinal stromal tumour. *Eur. J. Cancer* **2016**, *61*, 94-101.
  85. Lee, J.-S.; Han, J.-Y.; Ahn, M.-J.; Oh, I.-J.; Kim, H.; Lee, D. H.; Bertino, E. M.; Viteri Ramirez, S.; Pennell, N. A.; Wozniak, A. J.; Schiller, J. H.; Lin, C.; Keer, H. N.; Azab, M.; Besse, B.; Camidge, D. R. Addition of HSP90 inhibitor onalespib to crizotinib prior to progression in patients with ALK-pos NSCLC: Results of a randomized phase 2 study. *J. Clin. Oncol.* **2016**, *34*, 9059-9059.
  86. Canella, A.; Welker, A. M.; Yoo, J. Y.; Xu, J.; Abas, F. S.; Kesanakurti, D.; Nagarajan, P.; Beattie, C. E.; Sulman, E. P.; Liu, J.; Gumin, J.; Lang, F. F.; Gurcan, M. N.; Kaur, B.; Sampath, D.; Puduvalli, V. K. Efficacy of Onalespib, a Long-Acting Second-Generation HSP90 Inhibitor, as a Single Agent and in Combination with Temozolomide against Malignant Gliomas. *Clin. Cancer. Res.* **2017**, *23*, 6215.
  87. Brasca, M. G.; Mantegani, S.; Amboldi, N.; Bindi, S.; Caronni, D.; Casale, E.; Ceccarelli, W.; Colombo, N.; De Ponti, A.; Donati, D.; Ermoli, A.; Fachin, G.; Felder, E. R.; Ferguson, R. D.; Fiorelli, C.; Guanci, M.; Isacchi, A.; Pesenti, E.; Polucci, P.; Riceputi, L.; Sola, F.; Visco, C.; Zuccotto, F.; Fogliatto, G. Discovery of NMS-E973 as novel, selective and potent inhibitor of heat shock protein 90 (Hsp90). *Biorg. Med. Chem.* **2013**, *21*, 7047-7063.
  88. Fogliatto, G.; Gianellini, L.; Brasca, M. G.; Casale, E.; Ballinari, D.; Ciomei, M.; Degrassi, A.; De Ponti, A.; Germani, M.; Guanci, M.; Paolucci, M.; Polucci, P.; Russo, M.; Sola, F.; Valsasina, B.; Visco, C.; Zuccotto, F.; Donati, D.; Felder, E.; Pesenti, E.; Galvani, A.; Mantegani, S.; Isacchi, A. NMS-E973, a novel synthetic inhibitor of Hsp90 with activity against multiple models of drug resistance to targeted agents, including intracranial metastases. *Clinical cancer research : an official journal of the American Association for Cancer Research* **2013**, *19*, 3520-32.
  89. Sun, H.-P.; Jia, J.-M.; Jiang, F.; Xu, X.-L.; Liu, F.; Guo, X.-K.; Cherfaoui, B.; Huang, H.-Z.; Pan, Y.; You, Q.-D. Identification and optimization of novel Hsp90 inhibitors with tetrahydropyrido[4,3-d]pyrimidines core through shape-based screening. *Eur. J. Med. Chem.* **2014**, *79*, 399-412.
  90. Xu, X.-L.; Bao, Q.-c.; Jia, J.-M.; Liu, F.; Guo, X.-K.; Zhang, M.-y.; Wei, J.-l.; Lu, M.-c.; Xu, L.-l.; Zhang, X.-J.; You, Q.-D.; Sun, H.-P. CPUY201112, a novel synthetic small-molecule compound and inhibitor of heat shock protein Hsp90, induces p53-mediated apoptosis in MCF-7 cells. *Sci. Rep.* **2016**, *6*, 19004.
  91. Jiang, F.; Wang, H.-J.; Jin, Y.-H.; Zhang, Q.; Wang, Z.-H.; Jia, J.-M.; Liu, F.; Wang, L.; Bao, Q.-C.; Li, D.-D.; You, Q.-D.; Xu, X.-L. Novel Tetrahydropyrido[4,3-d]pyrimidines

- as Potent Inhibitors of Chaperone Heat Shock Protein 90. *Journal of medicinal chemistry* **2016**, *59*, 10498-10519.
92. Bussenius, J.; Blazey, C. M.; Aay, N.; Anand, N. K.; Arcalas, A.; Baik, T. Discovery of XL888: a novel tropane-derived small molecule inhibitor of HSP90. *Bioorg Med Chem Lett.* **2012**, *22*.
  93. Paraiso, K. H. T.; Haarberg, H. E.; Wood, E.; Rebecca, V. W.; Chen, Y. A.; Xiang, Y.; Ribas, A.; Lo, R. S.; Weber, J. S.; Sondak, V. K.; John, J. K.; Sarnaik, A. A.; Koomen, J. M.; Smalley, K. S. M. The heat shock protein-90 inhibitor XL888 overcomes BRAF inhibitor resistance mediated through diverse mechanisms. *Clin. Cancer. Res.* **2012**, *18*, 2502-2514.
  94. Chandralapaty, S.; Sawai, A.; Ye, Q.; Scott, A.; Silinski, M.; Huang, K.; Fadden, P.; Partridge, J.; Hall, S.; Steed, P.; Norton, L.; Rosen, N.; Solit, D. B. SNX2112, a Synthetic Heat Shock Protein 90 Inhibitor, Has Potent Antitumor Activity against HER Kinase-Dependent Cancers. *Clinical cancer research : an official journal of the American Association for Cancer Research* **2008**, *14*, 240-248.
  95. Huang, K. H.; Veal, J. M.; Fadden, R. P.; Rice, J. W.; Eaves, J.; Strachan, J. P.; Barabasz, A. F.; Foley, B. E.; Barta, T. E.; Ma, W.; Silinski, M. A.; Hu, M.; Partridge, J. M.; Scott, A.; DuBois, L. G.; Freed, T.; Steed, P. M.; Ommen, A. J.; Smith, E. D.; Hughes, P. F.; Woodward, A. R.; Hanson, G. J.; McCall, W. S.; Markworth, C. J.; Hinkley, L.; Jenks, M.; Geng, L.; Lewis, M.; Otto, J.; Pronk, B.; Verleysen, K.; Hall, S. E. Discovery of novel 2-aminobenzamide inhibitors of heat shock protein 90 as potent, selective and orally active antitumor agents. *Journal of medicinal chemistry* **2009**, *52*, 4288-305.
  96. ORLEMANS, E. O. M.; Haynes, B. F.; FERRARI, G.; Haystead, T.; KWIEK, J. J. Use of hsp90 inhibitors for the treatment of hiv infections and aids. Google Patents: **2016**.
  97. Conde, R.; Belak, Z. R.; Nair, M.; O'Carroll, R. F.; Ovsenek, N. Modulation of Hsf1 activity by novobiocin and geldanamycin. *Biochem. Cell Biol.* **2009**, *87*, 845-51.
  98. McCollum, A. K.; TenEyck, C. J.; Stensgard, B.; Morlan, B. W.; Ballman, K. V.; Jenkins, R. B.; Toft, D. O.; Erlichman, C. P-Glycoprotein-mediated resistance to Hsp90-directed therapy is eclipsed by the heat shock response. *Cancer Res.* **2008**, *68*, 7419-27.
  99. Zou, J.; Guo, Y.; Guettouche, T.; Smith, D. F.; Voellmy, R. Repression of heat shock transcription factor HSF1 activation by HSP90 (HSP90 complex) that forms a stress-sensitive complex with HSF1. *Cell* **1998**, *94*, 471-80.
  100. Shi, Y.; Mosser, D. D.; Morimoto, R. I. Molecular chaperones as HSF1-specific transcriptional repressors. *Genes Dev.* **1998**, *12*, 654-66.
  101. Bagatell, R.; Paine-Murrieta, G. D.; Taylor, C. W.; Pulcini, E. J.; Akinaga, S.; Benjamin, I. J.; Whitesell, L. Induction of a heat shock factor 1-dependent stress response alters the cytotoxic activity of hsp90-binding agents. *Clin. Cancer. Res.* **2000**, *6*, 3312-8.
  102. Zuo, J.; Rungger, D.; Voellmy, R. Multiple layers of regulation of human heat shock transcription factor 1. *Mol. Cell. Biol.* **1995**, *15*, 4319-30.
  103. Xia, W.; Voellmy, R. Hyperphosphorylation of heat shock transcription factor 1 is correlated with transcriptional competence and slow dissociation of active factor trimers. *J. Biol. Chem.* **1997**, *272*, 4094-102.
  104. Li, J.; Soroka, J.; Buchner, J. The Hsp90 chaperone machinery: Conformational dynamics and regulation by co-chaperones. *Biochimica et Biophysica Acta (BBA) - Molecular Cell Research* **2012**, *1823*, 624-635.

105. Chen, B. P., W. H.; Gui, L.; Bruford, E.; Monteiro, A. The HSP90 family of genes in the human genome: insights into their divergence and evolution. *Genomics* 2005, 86, 627-637.
106. Rosser, M. F.; Nicchitta, C. V. Ligand interactions in the adenosine nucleotide-binding domain of the Hsp90 chaperone, GRP94. I. Evidence for allosteric regulation of ligand binding. *J. Biol. Chem.* **2000**, 275, 22798-805.
107. Soldano, K. L.; Jivan, A.; Nicchitta, C. V.; Gewirth, D. T. Structure of the N-terminal domain of GRP94. Basis for ligand specificity and regulation. *J. Biol. Chem.* **2003**, 278, 48330-8.
108. Immormino, R. M.; Metzger, L. E. t.; Reardon, P. N.; Dollins, D. E.; Blagg, B. S.; Gewirth, D. T. Different poses for ligand and chaperone in inhibitor-bound Hsp90 and GRP94: implications for paralog-specific drug design. *J. Mol. Biol.* **2009**, 388, 1033-42.
109. Duerfeldt, A. S.; Peterson, L. B.; Maynard, J. C.; Ng, C. L.; Eletto, D.; Ostrovsky, O.; Shinogle, H. E.; Moore, D. S.; Argon, Y.; Nicchitta, C. V.; Blagg, B. S. J. Development of a Grp94 inhibitor. *J. Am. Chem. Soc.* **2012**, 134, 9796-9804.
110. Crowley, V. M.; Khandelwal, A.; Mishra, S.; Stothert, A. R.; Huard, D. J. E.; Zhao, J.; Muth, A.; Duerfeldt, A. S.; Kizziah, J. L.; Lieberman, R. L.; Dickey, C. A.; Blagg, B. S. J. Development of Glucose Regulated Protein 94-Selective Inhibitors Based on the BnIm and Radamide Scaffold. *J. Med. Chem.* **2016**, 59, 3471-3488.
111. Crowley, V. M.; Huard, D. J. E.; Lieberman, R. L.; Blagg, B. S. J. Second Generation Grp94-Selective Inhibitors Provide Opportunities for the Inhibition of Metastatic Cancer. *Chemistry (Easton)* **2017**, 23, 15775-15782.
112. Patel, P. D.; Yan, P.; Seidler, P. M.; Patel, H. J.; Sun, W.; Yang, C.; Que, N. S.; Taldone, T.; Finotti, P.; Stephani, R. A.; Gewirth, D. T.; Chiosis, G. Paralog-selective Hsp90 inhibitors define tumor-specific regulation of HER2. *Nat. Chem. Biol.* **2013**, 9, 677-84.
113. Mishra, S. J.; Ghosh, S.; Stothert, A. R.; Dickey, C. A.; Blagg, B. S. Transformation of the Non-Selective Aminocyclohexanol-Based Hsp90 Inhibitor into a Grp94-Selective Scaffold. *ACS Chem. Biol.* **2017**, 12, 244-253.
114. Suntharalingam, A.; Abisambra, J. F.; O'Leary, J. C.; Koren, J.; Zhang, B.; Joe, M. K.; Blair, L. J.; Hill, S. E.; Jinwal, U. K.; Cockman, M.; Duerfeldt, A. S.; Tomarev, S.; Blagg, B. S. J.; Lieberman, R. L.; Dickey, C. A. Glucose-regulated Protein 94 Triage of Mutant Myocilin through Endoplasmic Reticulum-associated Degradation Subverts a More Efficient Autophagic Clearance Mechanism. *The Journal of Biological Chemistry* **2012**, 287, 40661-40669.
115. Huang, Q.-Q.; Sobkoviak, R.; Jockheck-Clark, A.; Shi, B.; Mandelin, A. M.; Tak, P. P.; Haines, G. K.; Nicchitta, C. V.; Pope, R. M. Heat Shock Protein 96 is Elevated in Rheumatoid Arthritis and Activates Macrophages primarily via TLR2 Signaling. *Journal of immunology (Baltimore, Md. : 1950)* **2009**, 182, 4965.
116. Hua, Y.; White-Gilbertson, S.; Kellner, J.; Rachidi, S.; Usmani, S. Z.; Chiosis, G.; DePinho, R.; Li, Z.; Liu, B. Molecular Chaperone gp96 Is a Novel Therapeutic Target of Multiple Myeloma. *Clin. Cancer. Res.* **2013**, 19, 6242.
117. Lavery, L. A.; Partridge, J. R.; Ramelot, T. A.; Elnatan, D.; Kennedy, M. A.; Agard, D. A. Structural asymmetry in the closed state of mitochondrial Hsp90 (TRAP1) supports a two-step ATP hydrolysis mechanism. *Mol. Cell* **2014**, 53, 330-43.
118. Lee, C.; Park, H. K.; Jeong, H.; Lim, J.; Lee, A. J.; Cheon, K. Y.; Kim, C. S.; Thomas, A. P.; Bae, B.; Kim, N. D.; Kim, S. H.; Suh, P. G.; Ryu, J. H.; Kang, B. H. Development

- of a mitochondria-targeted Hsp90 inhibitor based on the crystal structures of human TRAP1. *J. Am. Chem. Soc.* **2015**, *137*, 4358-67.
119. Park, H.-K.; Jeong, H.; Ko, E.; Lee, G.; Lee, J.-E.; Lee, S. K.; Lee, A.-J.; Im, J. Y.; Hu, S.; Kim, S. H.; Lee, J. H.; Lee, C.; Kang, S.; Kang, B. H. Paralog Specificity Determines Subcellular Distribution, Action Mechanism, and Anticancer Activity of TRAP1 Inhibitors. *Journal of medicinal chemistry* **2017**, *60*, 7569-7578.
120. Ohkubo, S.; Kodama, Y.; Muraoka, H.; Hitotsumachi, H.; Yoshimura, C.; Kitade, M.; Hashimoto, A.; Ito, K.; Gomori, A.; Takahashi, K.; Shibata, Y.; Kanoh, A.; Yonekura, K. TAS-116, a highly selective inhibitor of heat shock protein 90alpha and beta, demonstrates potent antitumor activity and minimal ocular toxicity in preclinical models. *Molecular cancer therapeutics* **2015**, *14*, 14-22.
121. Ernst, J. T.; Neubert, T.; Liu, M.; Sperry, S.; Zuccola, H.; Turnbull, A.; Fleck, B.; Kargo, W.; Woody, L.; Chiang, P.; Tran, D.; Chen, W.; Snyder, P.; Alcacio, T.; Nezami, A.; Reynolds, J.; Alvi, K.; Goulet, L.; Stamos, D. Identification of novel HSP90alpha/beta isoform selective inhibitors using structure-based drug design. demonstration of potential utility in treating CNS disorders such as Huntington's disease. *J. Med. Chem.* **2014**, *57*, 3382-400.
122. Sun, J.; Lin, C.; Qin, X.; Dong, X.; Tu, Z.; Tang, F.; Chen, C.; Zhang, J. Synthesis and biological evaluation of 3,5-disubstituted-4-alkynylisoxozales as a novel class of HSP90 inhibitors. *Bioorganic & medicinal chemistry letters* **2015**, *25*, 3129-3134.
123. Khandelwal, A. Unfolding the Hsp90 Foldasome: Structure-Activity Relationship Studies on EGCG and Development of Isoform-Selective Inhibitors, Ph.D Dissertation, The University of Kansas. **2016**.

## Chapter II

### Development of a Novel Series of Compounds for Hsp90 $\beta$ -Selective Inhibition

Hsp90 inhibitors evaluated in clinical investigations bind to the N-terminal nucleotide-binding pocket and manifest pan-inhibition of all four Hsp90 isoforms; Hsp90 $\alpha$  (cytosolic and inducible), Hsp90 $\beta$  (cytosolic and constitutively expressed), Grp94 (endoplasmic reticulum residing) and TRAP1 (mitochondrial).<sup>1-2</sup> Pan-inhibition leads to non-specific functional disruption of the entire Hsp90 client population (>300 substrates), which may not be desired for the treatment cancer and/or other diseases. Some cancers, depending on their nature of origin or stage of progression, express varying needs for certain oncogenic pathways. In such cases, the disruption of only the upregulated sub-population of Hsp90 clients is desired, thereby, sparing the remaining substrates and minimizing undesired and on-target effects. For this purpose, Hsp90 isoform-selective inhibition has emerged as a promising and new approach to target the diseases regulated by both clients and co-chaperones that exhibit Hsp90 isoform-dependency.<sup>3-10</sup>

#### II.1 Hsp90 $\beta$ and Cancer

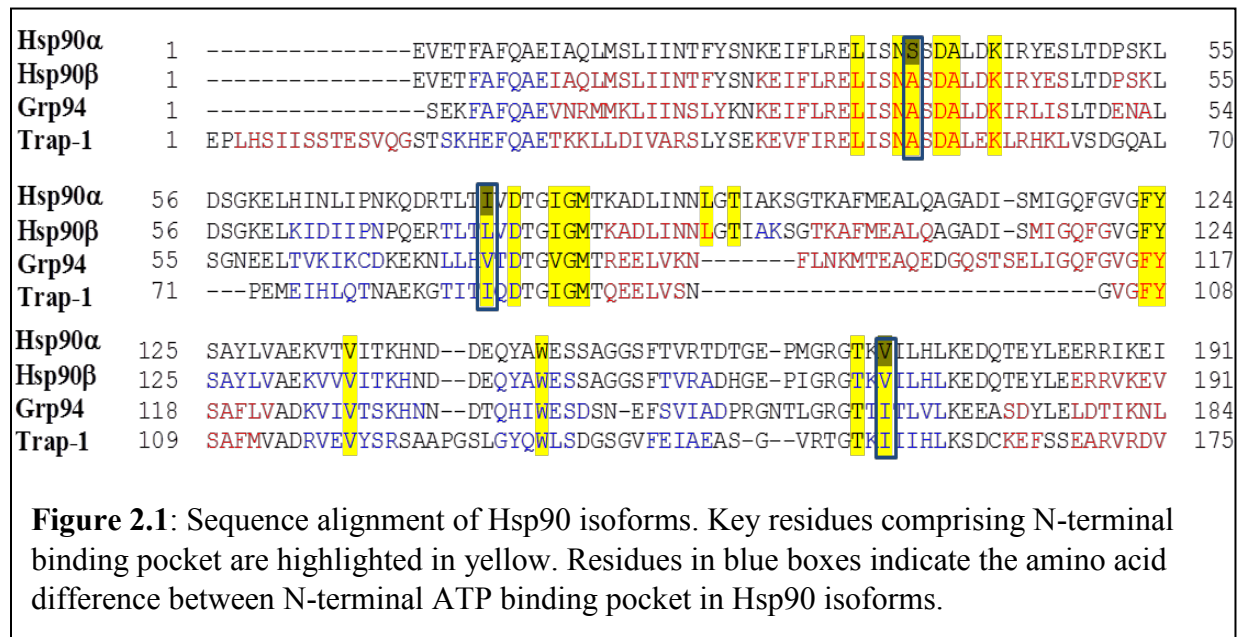
The cytosolic isoforms, Hsp90 $\alpha$  and Hsp90 $\beta$ , are responsible for the proper folding of many oncogenic proteins that are critical for cancer sustenance.<sup>11</sup> Hsp90 $\beta$  represents the constitutively expressed isoform, while Hsp90 $\alpha$  can be induced during stress or malignant transformation.<sup>1-2</sup>

Until recently, it was believed that the cytosolic isoforms share overlapping chaperone function for the majority of clients, and that each isoform could compensate for the loss of other. However, recent studies have identified clients that exhibit isoform-dependency. For example, survivin, c-Raf, and the hERG channel depend solely on Hsp90 $\alpha$ , whereas, c-IAP1, CDK6 and CXCR4 rely upon Hsp90 $\beta$  for their maturation.<sup>10, 12-13</sup> The Hsp90 $\beta$ -isoform has been shown to play a key role in early embryonic development, germ cell maturation, cytoskeleton stabilization, cellular transformation, and long term cellular adaptation.<sup>14-19</sup> In contrast, Hsp90 $\alpha$  is required for the promotion of growth, cell cycle regulation, and stress-induced cytoprotection.<sup>20-21</sup> Along with client proteins, co-chaperones also interact differently with each cytosolic isoform. For example, co-chaperone FKBP8 and GCUNC45 have been found to interact preferentially with Hsp90 $\beta$ .<sup>22-</sup>  
<sup>23</sup> Furthermore, Hsp90 $\beta$  interacts with P-glycoproteins, therefore, its expression is associated with drug-resistance.<sup>24</sup> Isoform specific phosphorylation of Hsp90 $\beta$  has been found to be important for activation of the glucocorticoid receptor.<sup>25</sup> Hsp90 $\beta$  also associates with focal adhesion kinase (FAK), and promotes the migration and invasion of breast cancer cells.<sup>26</sup> In addition, Hsp90 $\beta$  forms a complex with Bcl-2 and facilitates the survival of laryngeal carcinoma.<sup>27</sup> Recently, Hsp90 $\beta$  was shown to promote angiogenesis in hepatocellular carcinoma via increased expression of vascular endothelial growth factor receptors (VEGFRs).<sup>28</sup> Extracellular functions of Hsp90, when referenced, usually refer to Hsp90 $\alpha$ , however, few studies have uncovered that

extracellular Hsp90 $\beta$  can also exist and negatively regulate latent TGF- $\beta$  activation in MG63 osteosarcoma cells, which inhibits proliferation. In contrast, Hsp90 $\beta$  and TGF- $\beta$ 1 act synergistically to stimulate the migratory aptitude of colon cancer cells, in response to activation of  $\alpha$ v $\beta$ 6 integrin as opposed to the canonical TGF- $\beta$ 1 pathway.<sup>29</sup> Interestingly, extracellular Hsp90 $\beta$  associates with matrix metalloproteinase-3 (MMP-3) to facilitate breast cancer invasion.<sup>30</sup> Recently, Neckers and co-workers developed conformational mutants of Hsp90 to discriminate binding affinities of clients and inhibitors. Their study concluded that Hsp90 $\alpha$  binds to clients with a greater affinity relative to Hsp90 $\beta$ , whereas, small molecule inhibitors, such as ganetespib, bind Hsp90 $\beta$  with slightly greater affinity than Hsp90 $\alpha$ .<sup>9</sup> The presence of Hsp90 $\beta$  in serum and bronchoalveolar lavage fluid has been proposed to represent a biomarker for lung cancer.<sup>31-32</sup> These studies establish that clients depend upon both cytosolic isoforms despite the high degree of functional and structural overlap, supporting the hypothesis that isoform-selective inhibition represents an innovative approach to improve upon the therapeutic potential of Hsp90 inhibitors. Hsp90 $\beta$ -selective inhibition may avoid some of the detriments associated with pan-inhibitors. For example, Hsp90 $\beta$ -selective inhibition may avoid disruption and maturation of the hERG channel, which is critical for normal cardiac rhythm, thus, reducing cardiotoxicity. In addition, Hsp90 $\beta$ -specific inhibitors can serve as a chemical probe to identify additional clients that may be dependent on Hsp90 $\beta$  as well as cancers that are driven by Hsp90 $\beta$ -dependent pathways.

Collectively, these studies establish Hsp90 $\beta$  to contribute to disease pathology and that Hsp90 $\beta$ -selective inhibition represents a promising and new therapeutic alternative to pan Hsp90 inhibition.

## II.2 Overlay Studies with the Hsp90 Isoform N-Terminal ATP-Binding Sites.



Sequence alignment of the four Hsp90 isoforms was performed, which despite high similarity and identity, revealed structural differences that could be used to guide the design of isoform selective inhibitors (Figure 2.1). The differences in the primary sequences between these isoforms were correlated with a change in the overall three-dimensional structure of the binding pockets. Due to a 5-amino acid insertion in the primary sequence, Grp94 exhibits a structural change that is most significant as compared to the other isoforms. In fact, a new binding pocket in Grp94 was observed and has been exploited for the development of Grp94-selective inhibitors.<sup>33-35</sup> In contrast, Trap-1 contains a 2 amino acid insertion in its primary sequence and exhibits a conformation that



resembles the cytosolic Hsp90s as well as Grp94.<sup>36</sup> The cytosolic Hsp90 isoforms,  $\alpha$  and  $\beta$ , exhibit the highest homology (>95% identical within the N-terminal ATP-binding site), suggesting that the design of selective inhibitors for Hsp90 $\alpha$  and Hsp90 $\beta$  would be a challenge. In the N-terminal ATP-binding site, Hsp90 $\alpha$  and Hsp90 $\beta$  vary only by two amino acids, i.e. Hsp90 $\beta$  contains Ala52

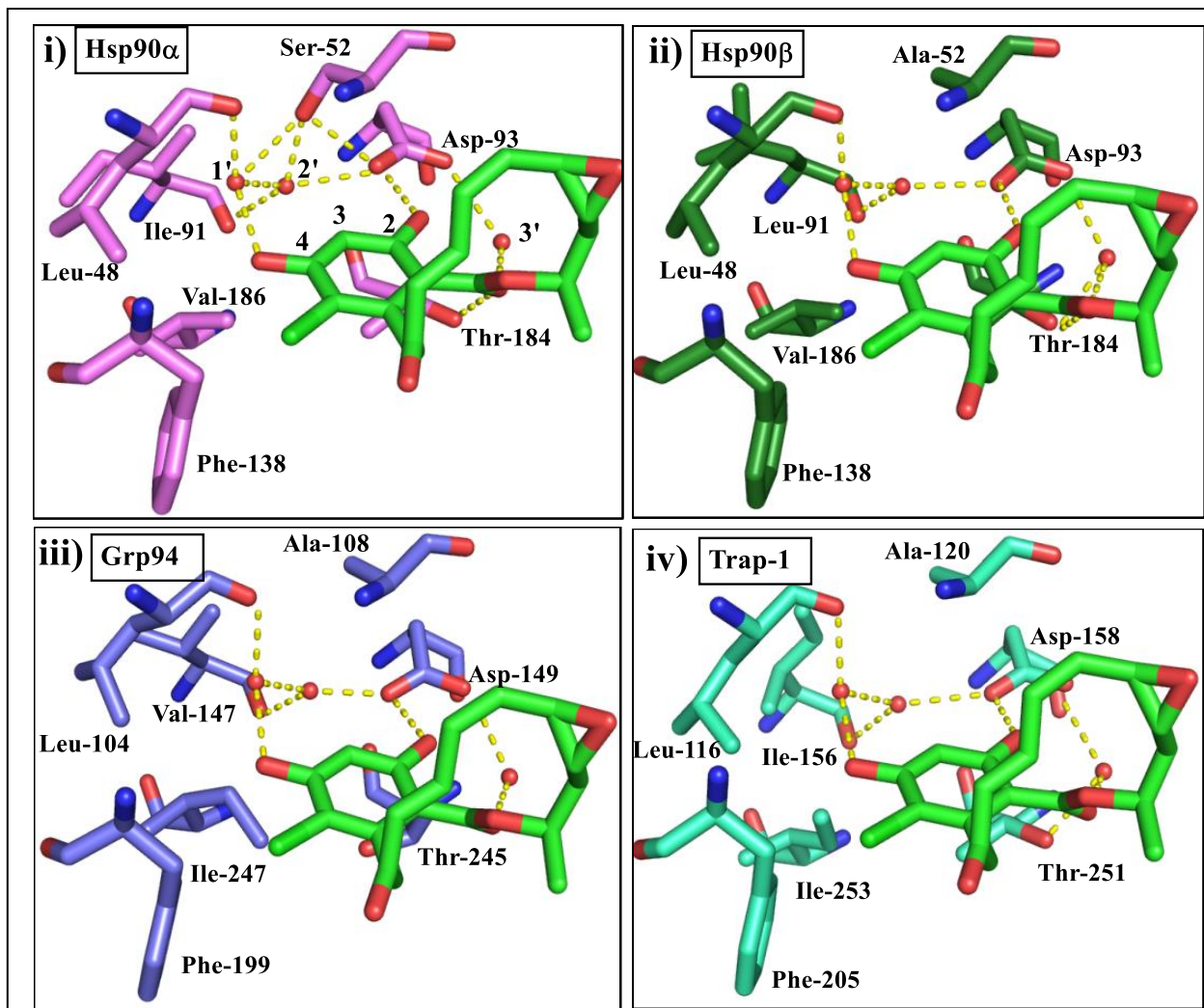


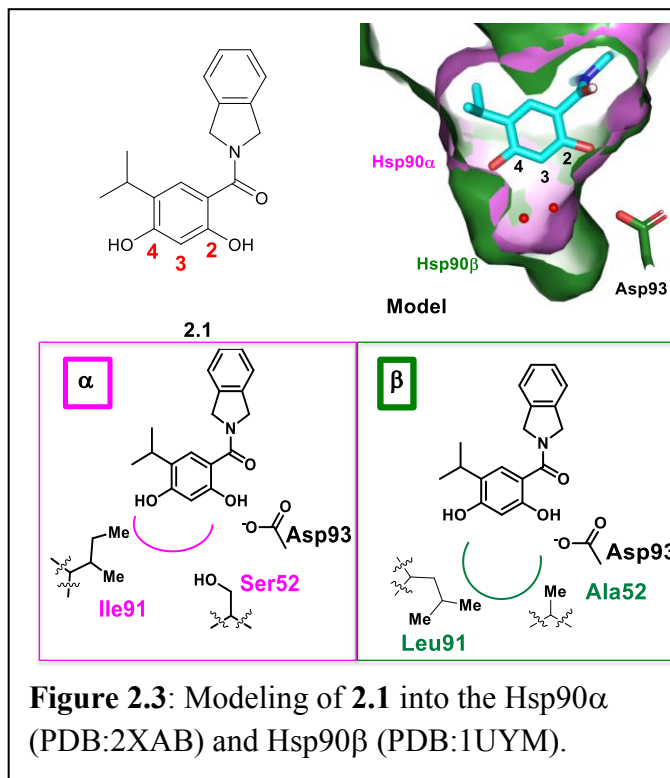
**Figure 2.2:** Modeling of Radicicol into the N-terminal ATP binding site of Hsp90 isoforms: **i)** Hsp90 $\alpha$  (PDB code: 2XAB) **ii)** Hsp90 $\beta$  (PDB code: 1UYM) **iii)** Grp94 (PDB code: 4NH9) **iv)** Trap-1 (PDB code: 4Z1F) isoforms. Water molecules are depicted as red spheres and hydrogen bonds are represented as yellow dashed lines. Radicicol is depicted as green colored sticks in all isoforms.

and Leu91, *in lieu* of Ser52 and Ile91, which are present in Hsp90 $\alpha$  (Figure 2.1). For comparison, radicicol, a resorcinol containing natural product and Hsp90 pan-inhibitor was modeled into the N-terminal ATP-binding pocket of each isoform.

As shown in Figure 2.2, a network of water mediated hydrogen bonds are present in the adenine-binding region of the ATP-binding pocket that surrounds the resorcinol of radicicol. The carbonyl and 2-phenol of radicicol interact with Thr184 and Asp93 via hydrogen bonds (Figure 2.2i) through conserved water molecules labeled as 1' and 2' (Figure 2.2i). Residues Leu48, Lys58, Asp93, Ile96, Gly97, Met98, Leu107, Thr109, Phe138, Tyr139, Trp162, and Thr184 (numbered for Hsp90 $\beta$ ) represent the amino acids that comprise the N-terminal ATP-binding pocket that are conserved amongst the four isoforms. The Grp94 and Trap1 binding pockets contain Val147 and Ile156 in place of Leu91, whereas, Val186 in Hsp90 $\alpha$  is replaced with Ile247 in Grp94 and Ile253 in Trap-1. Therefore, Grp94 and Trap-1 may produce a steric clash between ligand and Ile247 and Ile253 respectively, which may affect ligand binding and reduce inhibitor affinity.

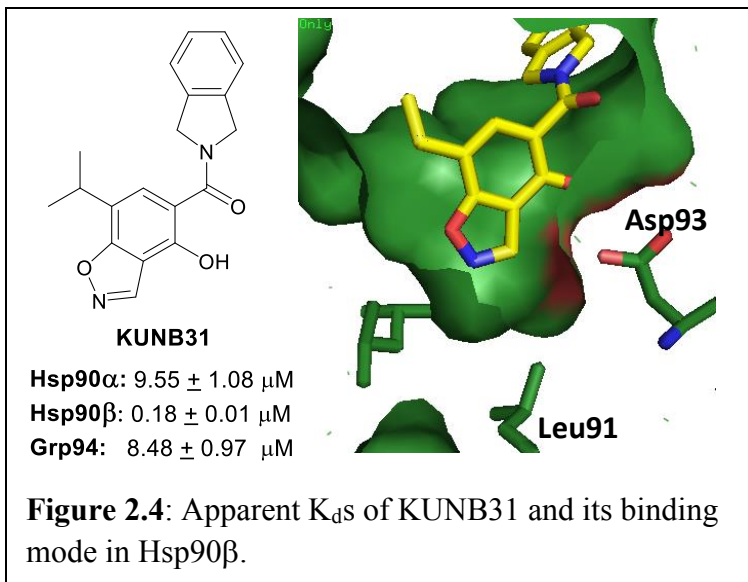
### II.3 Modeling of the Resorcinol-based Hsp90 $\beta$ -selective Inhibitor, KUNB31.

Recently, our lab developed the first Hsp90 $\beta$ -selective inhibitors via a structure-based approach. For this purpose, a resorcinol containing compound, **2.1**, a simplified version of AT13387 developed by Astex Therapeutics, was chosen as a starting



point due to its simplistic preparation and high affinity. Our model was developed using the co-crystal structures of Hsp90 $\alpha$  bound to **2.1** (PDB code:2XAB) and Hsp90 $\beta$  (bound to purine-based ligand, PDB code: 1UYM) to study the structural differences between these isoforms. It was observed that Leu91 and Ala52 in Hsp90 $\beta$  leads to an extended hydrophobic subpocket *in lieu* of a smaller and polar subpocket that's present in Hsp90 $\alpha$  (Figure 2.3). As discussed previously, the subpocket of each isoform is occupied by two water molecules that serve to coordinate a hydrogen bonding network and are present in most Hsp90 crystal structures. Careful modification to the 3- and 4-position of compound **2.1** led to **KUNB31**, an isoxazole containing compound that occupies the Hsp90 $\beta$  extended subpocket by displacing the two conserved water molecules. Co-

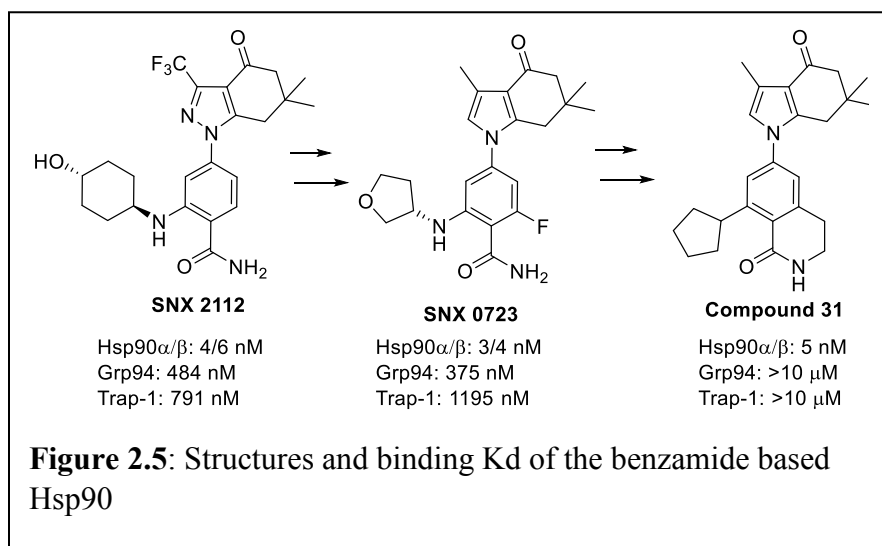
crystallization of **KUNB31** with Hsp90 $\beta$  revealed that the isoxazole ring occupied the Hsp90 $\beta$  subpocket as hypothesized, leading to selectivity against Hsp90 $\alpha$  and Grp94 (Grp94 presents a steric clash with isoxazole and Ile 247).



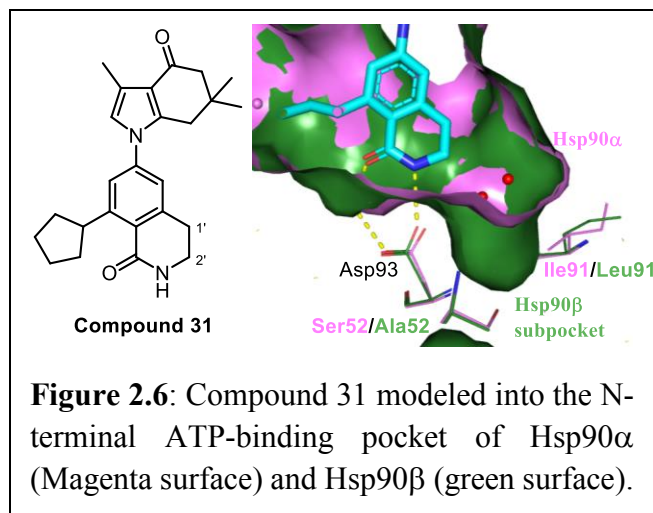
However, the size of the Hsp90 $\beta$  hydrophobic subpocket was smaller as compared to the purine co-crystal (PDB:1UYM), as the Leu91 rotamer was pointing toward the Asp93, whereas in the purine bound Hsp90 $\beta$  crystal structure, Leu91 rotates away from Asp93, creating a larger and more flexible pocket (Figure 2.3 and 2.4). Therefore, new scaffolds were designed that could induce opening of this Hsp90 $\beta$ -specific hydrophobic subpocket.

#### II.4 Design of a Benzamide Based Hsp90 $\beta$ -selective Inhibitor.

SNX 2112, a unique benzamide



containing Hsp90 inhibitor developed by Serenex Inc., exhibits a binding profile to Hsp90 isoforms that differs from the resorcinol and purine containing compounds, as it binds equipotently to Hsp90 $\alpha$  and Hsp90 $\beta$ , but manifests >100-fold reduced affinity for both Grp94 and Trap-1 (Figure 2.5).<sup>11</sup> SNX 0723 is a variant of SNX 2112, which contains of a fluorine atom ortho to the amide group.<sup>11</sup> By taking advantage of prior binding studies with SNX 0723 that suggested additional space about benzamide, Vertex pharmaceuticals developed a ring constrained benzamide analog, **Compound 31**, as a Hsp90 $\alpha/\beta$ -selective compound that exhibited no affinity for Grp94 and Trap1. Additionally, the co-crystal structure of **Compound 31** bound to Hsp90 $\alpha$  was obtained and revealed the presence of a bulky group such as a cyclopentyl ring facing the



solvent phase could reduce the dielectric constant within the binding pocket and improve potency. During our modeling studies, the co-crystal structure of **31** (PDB code: 4O0B) with Hsp90 $\alpha$  was overlaid with the Hsp90 $\beta$  co-crystal structure (PDB code:

1UYM). These studies suggested that **31** does not interfere with the conserved water molecules that are present in the Hsp90 $\alpha/\beta$  subpockets (depicted as red spheres in Figure 2.6, labeled as 1' and 2' in Figure 2.2i). Prior Studies that include the development of **KUNB31** suggest that these

conserved water molecules can be displaced, without a significant loss in affinity.<sup>37</sup> **Compound 31** contains ring-constrained benzamide group, which appears to lock the amide group into a conformation that is favored for interacting with Asp93 and appears to represent a key interaction

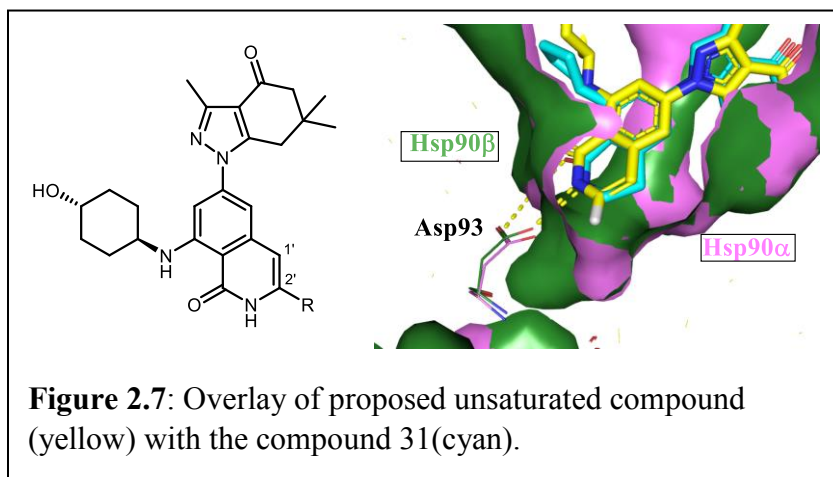
between the ligand and the

Hsp90 ATP-binding pocket.<sup>38</sup>

As observed in **KUNB31**,

Hsp90 $\beta$ -selective inhibitors

require modification of the 4-



phenol (Figure 2.2 and 2.4). However, modeling studies performed with **31** suggest that modification to the 2'-position (Figure 2.6) with substituents could displace the conserved water molecules and extend into the Hsp90 $\beta$  subpocket; leading to Hsp90 $\beta$ -selective inhibitors.

#### II.4.1 Proposal of the Isoquinolin-1(2H)-one Based Hsp90 $\beta$ -Selective Series

The cyclopentyl group was replaced with a trans-4-cyclohexanolamine in order to simplify **31**.

The tetrahydroindazolone fragment was incorporated in lieu of the pyrazolone present in **31**, as it does not affect affinity for Hsp90. Incorporation of unsaturated alkene was used to rapidly explore the special constraints of the Hsp90 $\beta$ -subpocket, as modeling supported that its introduction would maintain the benzamide interactions with Asp93 and Thr184 (Figure 2.2 and 2.6). Orientation of the 2'-position was hypothesized to project substituents into the Hsp90 $\beta$  subpocket as depicted in

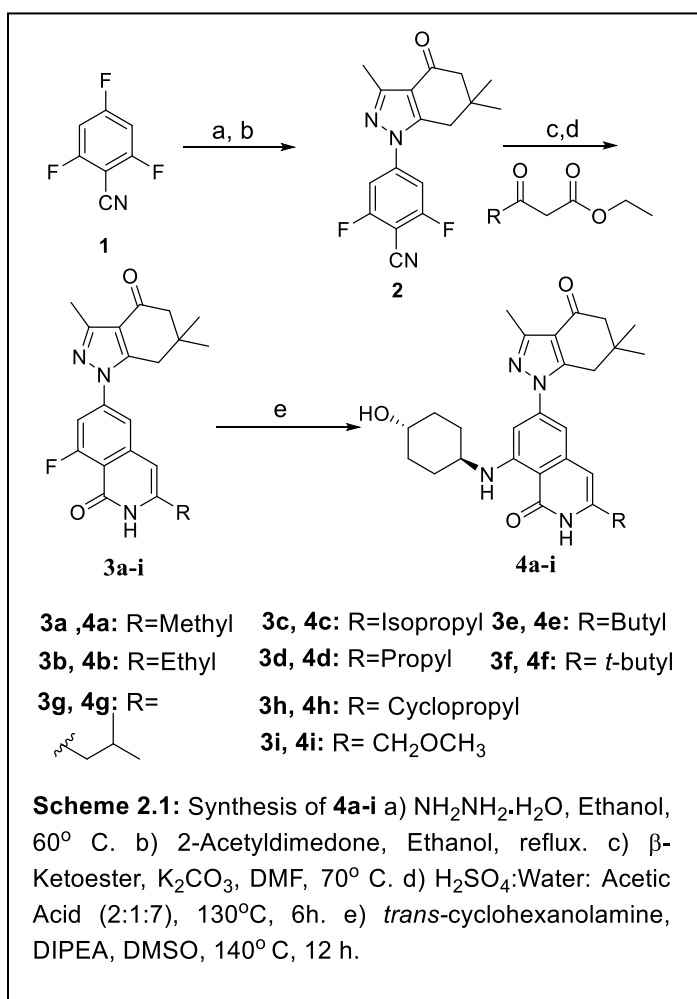
Figure 2.7. After taking the hydrophobic nature of the Hsp90 $\beta$  subpocket into consideration, linear aliphatic chains were attached to the 2'-position to develop the initial analogs. Additionally, methoxy and methylene alcohol groups were incorporated at the 2'-position to investigate potential interactions with Leu-48 (in both  $\alpha$  and  $\beta$ ) and Ser-52 in Hsp90 $\alpha$  and to determine whether there was an effect on selectivity and/or potency.

#### II.4.2 Synthesis of the Isoquinolin-1(2H)-one Series.

Synthesis commenced via installation of the saturated indazolone ring in intermediate **2** (Scheme

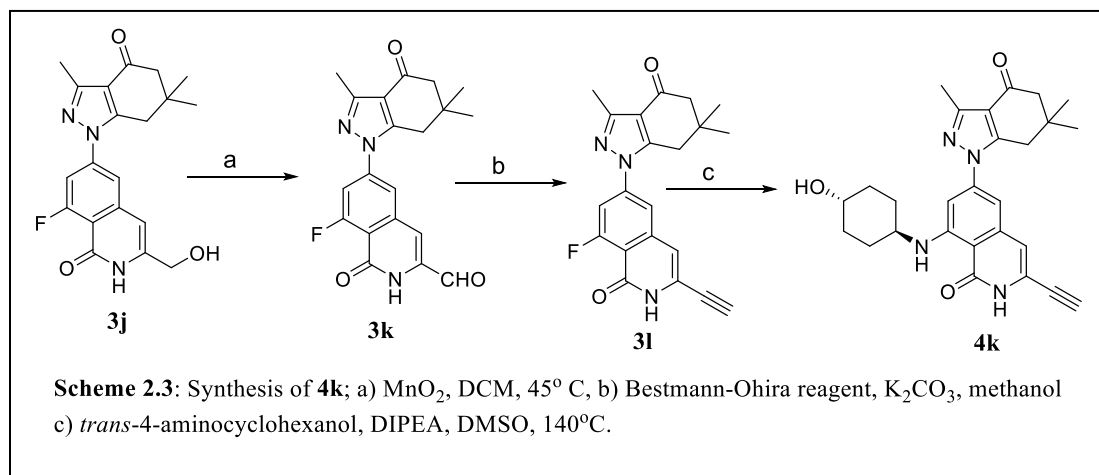
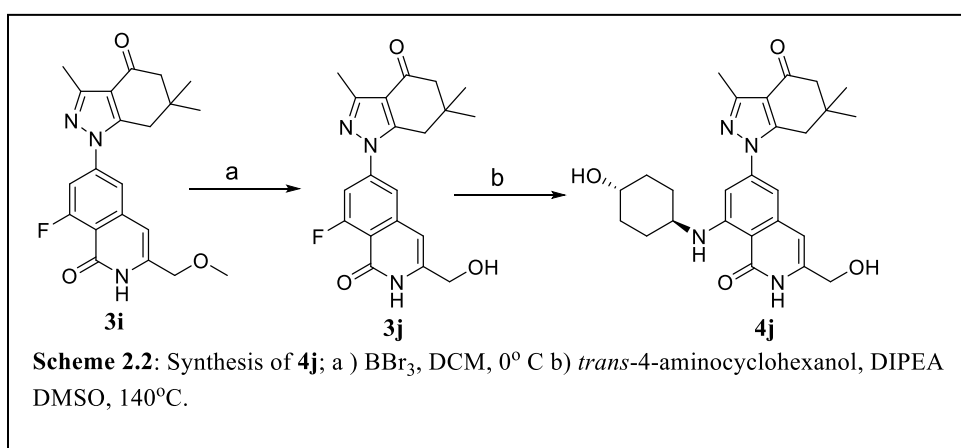
2.2). For this purpose, 2,4,6-trifluorobenzonitrile, **1**, was treated with hydrazine hydrate and 2-acetyl dimedone.<sup>39</sup> This reaction mixture resulted in the formation of the indazolone substituted intermediate, **2**.

Upon purification, **2** was reacted with the  $\beta$ -ketoester that contains the desired R-group in the presence of potassium carbonate to yield the corresponding  $\beta$ -ketoester substituted benzonitrile



intermediate. The resulting amide was used as a crude mixture in the subsequent condensation and cyclization reaction to yield intermediates **3a-i**. In the final  $S_NAr$  reaction, the *trans*-4-aminocyclohexanol was installed in the presence of DIPEA to furnish the final products, **4a-i**. Additionally, the demethylated version of compound **4i** was prepared via the treatment of **3i** with boron tribromide and subsequent installation of the amine to yield **4j** (Scheme 2.2). Intermediate **3j** provided access to the alkyne via oxidation with manganese oxide to produce the corresponding

aldehyde **3k**, which upon treatment with the Bestmann-Ohira reagent and in the presence of



potassium carbonate yielded the alkyne, **3l**. **3l** was then reacted with the *trans*-4-aminocyclohexanol to yield **4k**.

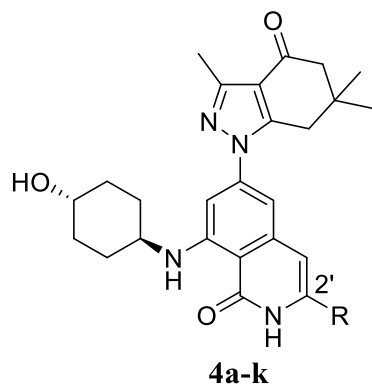


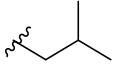
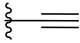
#### II.4.3 Determination of Binding Affinities for 4a-j using a Fluorescence Polarization Assay.

Once prepared, the compounds were evaluated for their binding affinities against the cytosolic isoforms, Hsp90 $\alpha$  and Hsp90 $\beta$ , by measuring their ability to competitively displace FITC conjugated GDA in a fluorescence polarization assay. The first compound in the series, **4a**, contained a methyl group at the 2'-carbon and exhibited a 3-fold selectivity for Hsp90 $\beta$ , establishing that further modification could validate the proposed hypothesis. Homologation to an ethyl resulted in **4b**, which exhibited enhanced affinity for both Hsp90 $\beta$  and Hsp90 $\alpha$ , and results from occupation of the subpockets found in both isoforms. To further probe the subpockets, an isopropyl group was installed onto **4c**, which maintained the affinity and selectivity manifested by **4b**, establishing that a branched chain can also be accommodated within the subpockets. Moreover, increasing the chain length to propyl, led to an improvement in both affinity and selectivity, as **4d** manifested ~40nM  $K_d$  for Hsp90 $\beta$  and ~21-fold selectivity over Hsp90 $\alpha$ . Additionally, **4d** exhibited lower binding affinities towards Trap-1 and Grp94 (>5 $\mu$ M for both isoforms). Encouraged with the results obtained from compound **4d**, a butyl chain was incorporated to probe the depth of the Hsp90 $\beta$  subpocket. As hypothesized, the compound containing a *n*-butyl chain exhibited excellent selectivity for Hsp90 $\beta$  (>300-fold versus Hsp90 $\alpha$ ),

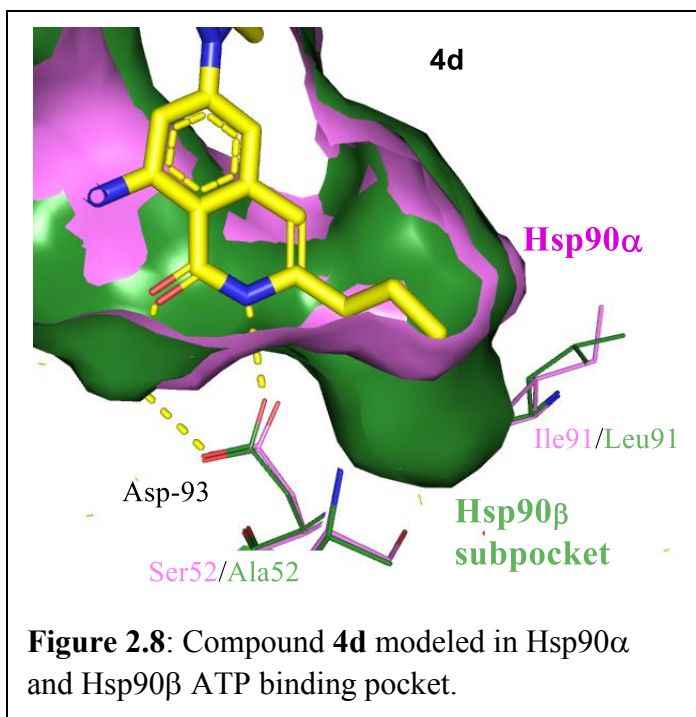
but ~4-fold loss in affinity was observed. Recalling that the isopropyl group was accommodated

**Table 2.1:** Apparent  $K_d$  values of compounds **4a-k** against Hsp90 $\alpha$  and Hsp90 $\beta$  determined using fluorescence polarization (FP) assay.



Compound	R group	Hsp90 $\alpha$ $K_d$ ( $\mu$ M)	Hsp90 $\beta$ $K_d$ ( $\mu$ M)
<b>4a</b>	Methyl	0.294 $\pm$ 0.023	0.101 $\pm$ 0.003
<b>4b</b>	Ethyl	0.180 $\pm$ 0.036	0.068 $\pm$ 0.008
<b>4c</b>	Isopropyl	0.173 $\pm$ 0.036	0.051 $\pm$ 0.008
<b>4d</b>	<i>n</i> -Propyl	0.886 $\pm$ 0.040	0.040 $\pm$ 0.003
<b>4e</b>	<i>n</i> -Butyl	>50	0.156 $\pm$ 0.018
<b>4f</b>	<i>t</i> -butyl	>50	>50
<b>4g</b>		>50	0.264 $\pm$ 0.030
<b>4h</b>	Cyclopropyl	1.88 $\pm$ 0.28	0.946 $\pm$ 0.038
<b>4i</b>	-CH <sub>2</sub> OCH <sub>3</sub>	0.306 $\pm$ 0.023	0.159 $\pm$ 0.003
<b>4j</b>	-CH <sub>2</sub> OH	0.824 $\pm$ 0.104	0.233 $\pm$ 0.018
<b>4k</b>		0.381 $\pm$ 0.003	0.337 $\pm$ 0.015

in both Hsp90 $\alpha$  and Hsp90 $\beta$ , a *t*-butyl group was incorporated as demonstrated by **4f** to determine whether the pockets could expand and accommodate spherical bulk. Not surprisingly, **4f** did not bind either isoform, which was consistent with the modeling study and suggested a steric clash between the *t*-

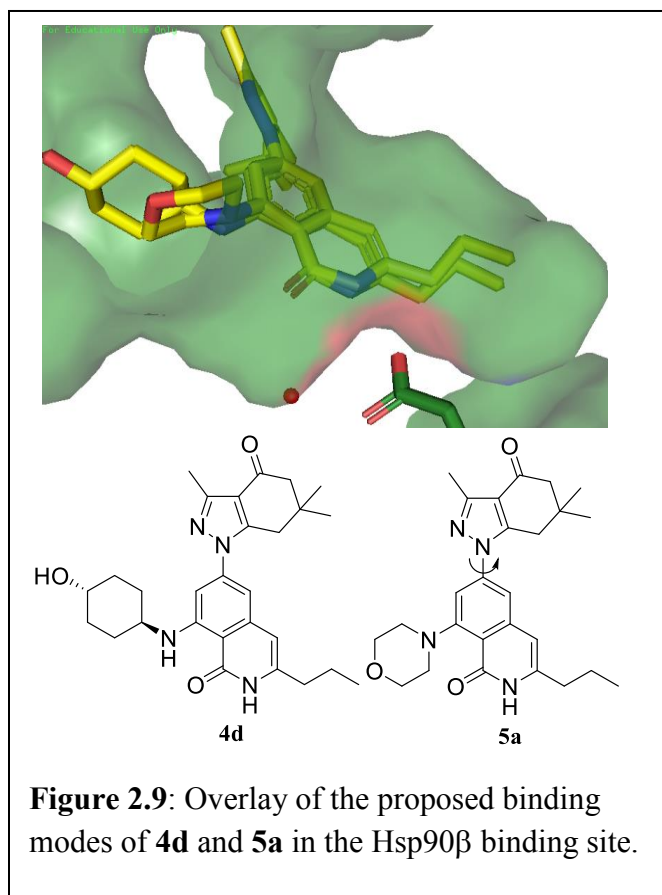


butyl group and the protein surface. Compound **4g** was then synthesized to contain an isobutyl group, which maintained selectivity, but lost affinity. A cyclopropyl group was evaluated in **4h** to determine whether such geometry would have any effect on ligand binding to either isoform. Unfortunately, loss of potency was observed with **4h** when compared to **4c**. Compounds **4i** and **4j** were synthesized to determine whether the methoxy or the corresponding alcohol could affect affinity or selectivity via interactions with Ser52 in Hsp90 $\alpha$  or Leu48 in both Hsp90 $\alpha/\beta$ . Surprisingly, these compounds still displayed a slight preference for Hsp90 $\beta$  binding, despite the presence of polar appendages, which may be attributed to the methoxy and the methylene alcohol being accommodated in the slightly larger Hsp90 $\beta$  subpocket. An acetylene group was incorporated as shown with **4k** to probe whether a linear projection into the Hsp90 $\beta$  subpocket

could impact selectivity. Disappointingly, the acetylene group occupies both Hsp90 isoform subpockets without discrimination, resulting in a loss of selectivity.

#### II.4.4 Replacement of the *trans*-4-aminocyclohexanol in **4d**.

Compound **4d** established that a propyl chain at the 2'-position produced good affinity and moderate selectivity for Hsp90 $\beta$ . Further modeling performed on **4d** suggested that modifications of the *trans*-4-aminocyclohexanol could also lead to a change in conformation within the binding site (Figure 2.9), which might result in increased potency and selectivity. Structure-activity relationship studies with **31** (Figure

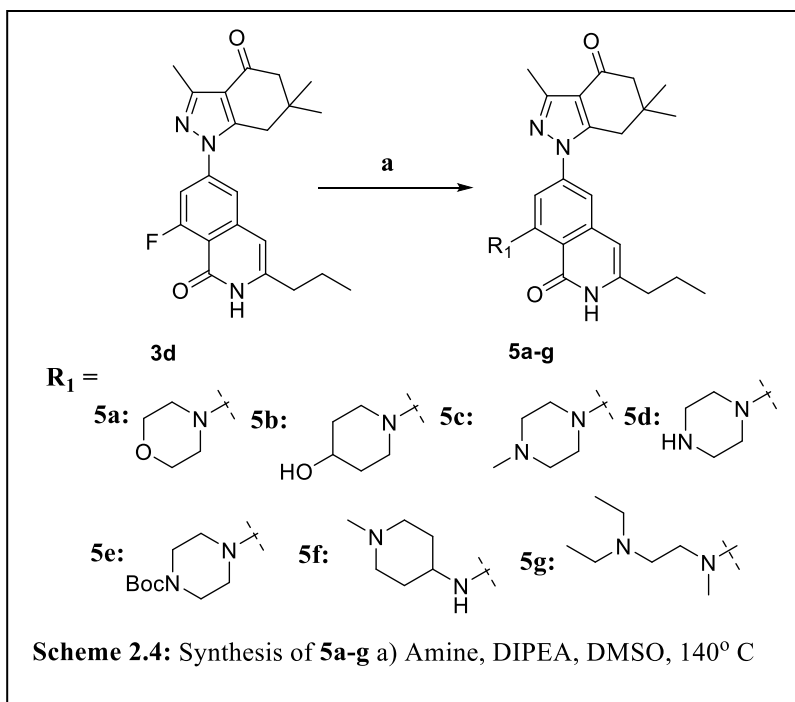


2.6) and analogs established that the *trans*-4-aminocyclohexanol could be replaced with spherical and aliphatic bulk, such as *t*-butyl or cyclopentane. Replacement of the amine with an aliphatic group does not affect selectivity for the compounds against Hsp90 $\alpha$  or Hsp90 $\beta$  (Figure 2.6).<sup>40</sup> The conformational change that appears to result from introduction of the tertiary amine is depicted in Figure 2.9. The proposed binding modes of both **4d** and the morpholine containing analog **5a**, are

presented and reflect a slight variation in binding of the isoquinolin-1(2H)-one ring, which may result from a clash between the morpholine ring and the protein surface. The change in conformation was hypothesized to produce an increase in selectivity and potentially, affinity for Hsp90 $\beta$ . Another reason for seeking replacements of the *trans*-4-aminocyclohexanol to disrupt planarity of the benzamide ring, in particular between the amine and carbonyl groups (**4d**, Figure

2.9), which may decrease solubility. For this purpose, amine replacements were investigated that included various functional groups, such as ionizable tertiary amines to improve solubility.<sup>41</sup>

Compounds **5a-g** were prepared



utilizing **3d** as an intermediate and the reaction conditions detailed in scheme 2.2.

## II.4.5 Evaluation of Binding

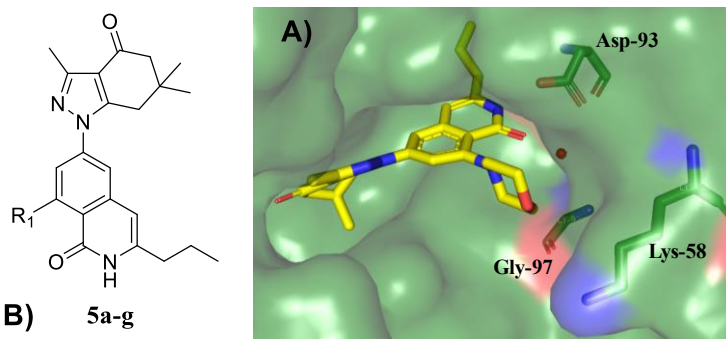
### Affinities for 5a-g.

Upon their preparation, compounds **5a-g** were evaluated for their binding affinity against the cytosolic Hsp90 isoforms (Figure 2.10). The binding profile of the morpholine-containing compound, **5a**, was consistent with the proposed hypothesis and exhibited excellent selectivity for Hsp90 $\beta$  with a  $K_d$  of ~121 nM.

The binding profile for **5a**

mirrored **4e**, which contains a *n*-butyl group at the 2'-position. This data informed us that with **5a**, the propyl chain aligns in Hsp90 $\beta$  in a manner similar to the butyl chain in **4e**, and thus affects selectivity. Compound **5b**, which contains a hydroxyl moiety, was hypothesized to interact with amino acids present at the gate of the binding pocket, such as Gly-97 and Lys-58 (Figure 2.10 A).

**Figure 2.10:** A) Modeled picture of **5a** in Hsp90 $\beta$  ATP binding site B) Apparent  $K_d$  values of compounds **5a-g** against Hsp90 $\alpha$  and Hsp90 $\beta$  determined using fluorescence polarization (FP) assay.



Compound	Hsp90 $\alpha$ $K_d$ ( $\mu$ M)	Hsp90 $\beta$ $K_d$ ( $\mu$ M)
<b>5a</b>	>50	0.121 $\pm$ 0.017
<b>5b</b>	38.00 $\pm$ 1.10	0.091 $\pm$ 0.010
<b>5c</b>	8.52 $\pm$ 0.24	0.426 $\pm$ 0.053
<b>5d</b>	>50	4.47 $\pm$ 0.278
<b>5e</b>	>50	0.463 $\pm$ 0.031
<b>5f</b>	17.083 $\pm$ 0.66	0.513 $\pm$ 0.067
<b>5g</b>	>50	4.46 $\pm$ 0.188

In fact, **5b** was found to exhibit ~91 nM  $K_d$  for Hsp90 $\beta$  with >400-fold selectivity over Hsp90 $\alpha$ , supporting our hypothetical model for binding.

Incorporation of N-methyl piperazine into compound **5c**, led to a decrease in affinity and selectivity when compared to **5a** and **5b**, which might result from unfavorable interactions of the tertiary amine with the Lys-58 that is present in both isoforms. A decrease in binding affinity for compound **5d**, could result from similar disfavored interactions. Furthermore, a *t*-butyloxycarbonyl (Boc) protected piperazine containing compound (**5e**) was also evaluated to determine whether incorporation of an acceptor group could be beneficial. Upon evaluation, it exhibited a binding affinity comparable to that of the N-methyl piperazine compound, **5c**, however, it manifested greater selectivity over Hsp90 $\alpha$ . 1-Methylpiperidin-4-amine was installed to produce **5f** and to investigate whether the tertiary amine could replace the *trans*-4-aminocyclohexanol, while increasing solubility. Unfortunately, a loss in affinity was observed with **5f**, while selectivity for Hsp90 $\beta$  was found to be similar to **4d**. An open chain amine was also installed as shown with **5g**, it too exhibited a loss in affinity. Both **5f** and **5g** were found to be more soluble than **4d**.

## II.5 Cellular Studies

### II.5.1 Determination of Growth-Inhibitory Effects on Cancer Cells.

Due to its high binding affinity, compound **4d** was evaluated for its growth inhibition activity against the NCI-60 cancer cell line panel with a single dose of 10  $\mu$ M, which resulted in potent

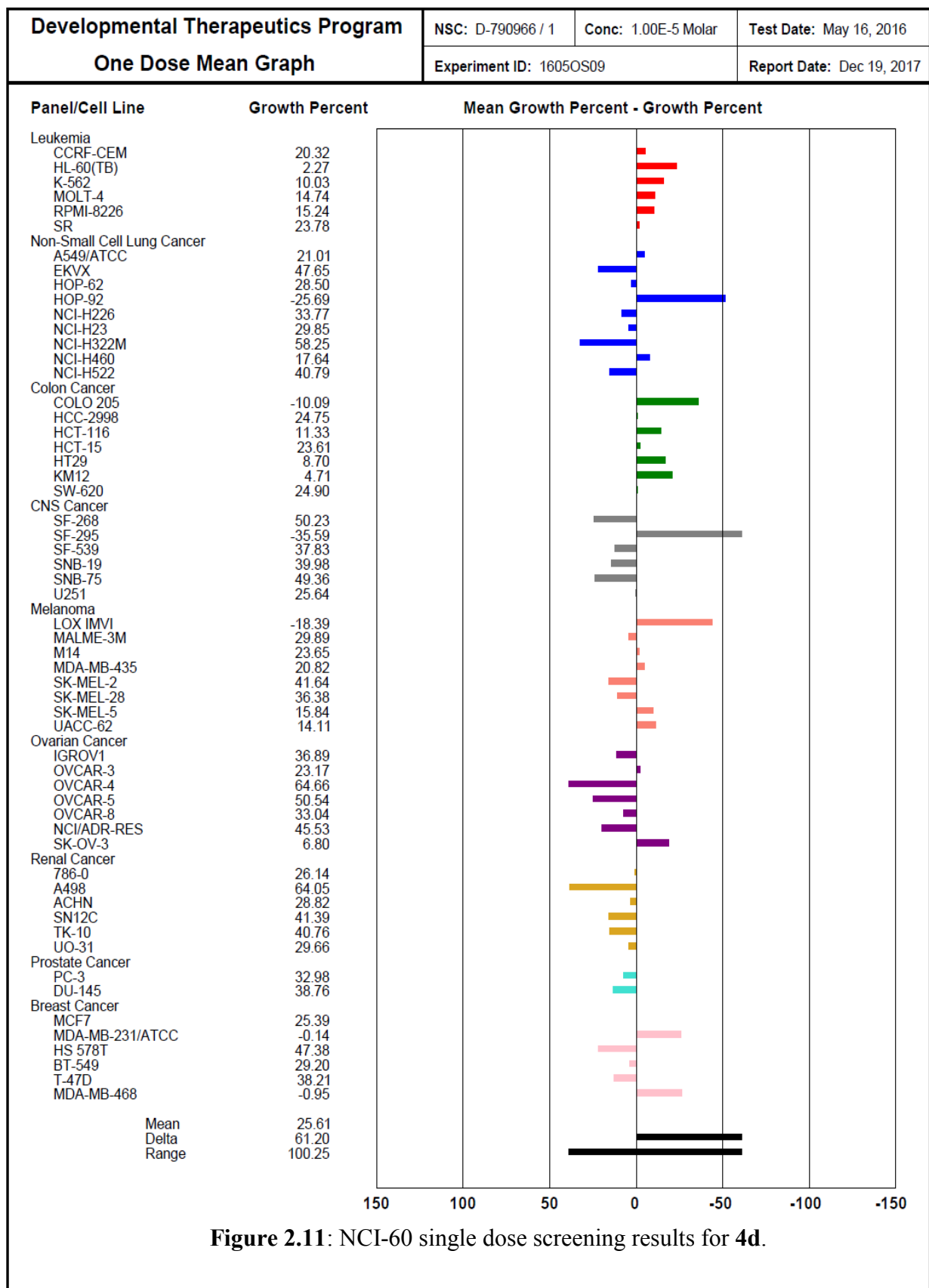


Figure 2.11: NCI-60 single dose screening results for 4d.



Panel/Cell Line	Log10 Concentration												GI50	
	Time Zero	Ctrl	Mean Optical Densities						Percent Growth					
			-8.0	-7.0	-6.0	-5.0	-4.0	-8.0	-7.0	-6.0	-5.0	-4.0		
<b>Leukemia</b>														
CCRF-CEM	0.461	2.251	2.212	1.517	0.775	0.609	0.658	98	59	18	8	11	1.65E-7	
HL-60(TB)	1.083	3.315	3.302	2.009	1.061	0.796	0.661	99	41	-2	-27	-39	7.13E-8	
K-562	0.291	2.175	2.085	0.669	0.549	0.429	0.446	95	20	14	7	8	4.00E-8	
MOLT-4	0.724	2.800	2.684	1.713	0.950	0.864	0.853	94	48	11	7	6	8.90E-8	
RPMI-8226	0.958	2.876	2.830	2.060	1.591	0.818	0.930	98	57	33	-15	-3	2.02E-7	
SR	0.525	1.864	1.754	0.966	0.758	0.606	0.610	92	33	17	6	6	5.12E-8	
<b>Non-Small Cell Lung Cancer</b>														
A549/ATCC	0.394	1.589	1.589	1.114	0.672	0.591	0.554	100	60	23	16	13	1.89E-7	
EKVX	0.601	1.832	1.804	1.393	1.217	1.094	1.048	98	64	50	40	36	1.01E-6	
HOP-62	0.716	1.553	1.534	1.089	1.003	0.895	0.780	98	45	34	21	8	7.89E-8	
HOP-92	1.270	1.828	1.841	1.635	1.163	0.947	0.989	102	65	-8	-25	-22	1.62E-7	
NCI-H226	1.017	1.836	1.773	1.596	1.462	1.271	1.268	92	71	54	31	31	1.52E-6	
NCI-H23	0.524	1.714	1.538	0.887	0.893	0.862	0.846	85	31	31	28	27	4.40E-8	
NCI-H322M	0.885	2.134	1.951	1.538	1.514	1.291	1.429	85	52	50	32	44	1.04E-6	
NCI-H460	0.306	2.723	2.794	1.337	0.688	0.643	0.569	103	43	16	14	11	7.55E-8	
NCI-H522	0.925	1.998	1.940	1.523	1.298	1.148	1.116	95	56	35	21	18	1.87E-7	
<b>Colon Cancer</b>														
COLO 205	0.469	1.611	1.624	0.811	0.457	0.375	0.405	101	30	-3	-20	-14	5.22E-8	
HCC-2998	0.837	2.902	2.629	1.785	1.144	0.997	1.141	87	46	15	8	15	7.94E-8	
HCT-116	0.561	3.003	2.854	1.426	1.009	0.708	0.958	94	35	18	6	16	5.63E-8	
HCT-15	0.384	2.295	2.185	1.396	0.803	0.674	0.655	94	53	22	15	14	1.24E-7	
HT29	0.313	1.678	1.388	0.441	0.372	0.356	0.329	79	9	4	3	1	2.60E-8	
KM12	0.500	2.756	2.584	1.354	0.640	0.616	0.594	92	38	6	5	4	5.99E-8	
SW-620	0.291	1.818	1.811	0.806	0.613	0.593	0.526	100	34	21	20	15	5.66E-8	
<b>CNS Cancer</b>														
SF-268	0.578	1.959	1.927	1.614	1.222	1.040	0.875	98	75	47	33	21	7.61E-7	
SF-295	0.996	2.748	2.682	2.485	1.317	0.600	0.738	96	85	18	-40	-26	3.35E-7	
SF-539	1.027	2.919	2.944	2.603	1.817	1.425	1.489	101	83	42	21	24	6.34E-7	
SNB-19	0.423	1.698	1.711	1.342	0.973	0.753	0.766	101	72	43	26	27	5.77E-7	
SNB-75	0.868	1.716	1.681	1.693	1.387	1.005	0.801	96	97	61	16	-8	1.77E-6	
U251	0.434	1.818	2.071	1.635	0.944	0.668	0.613	118	87	37	17	13	5.45E-7	
<b>Melanoma</b>														
LOX IMVI	0.380	2.440	2.343	1.359	0.397	0.299	0.330	95	48	1	-21	-13	8.88E-8	
MALME-3M	0.623	1.099	1.161	0.871	0.628	0.593	0.597	113	52	1	-5	-4	1.10E-7	
M14	0.574	2.167	2.084	1.111	0.993	0.554	0.763	95	34	26	-4	12	5.41E-8	
MDA-MB-435	0.465	2.334	2.355	1.232	0.910	0.678	0.674	101	41	24	11	11	7.09E-8	
SK-MEL-2	0.978	1.975	1.969	1.635	1.326	1.228	1.179	99	66	35	25	20	3.26E-7	
SK-MEL-28	0.742	2.170	2.138	1.577	1.158	0.963	1.083	98	58	29	15	24	1.95E-7	
SK-MEL-5	0.770	2.790	2.729	2.104	1.241	0.508	0.943	97	66	23	-34	9	2.37E-7	
UACC-257	1.062	2.047	2.080	1.886	1.274	1.289	1.298	103	84	22	23	24	3.48E-7	
UACC-62	0.761	2.872	2.726	1.822	1.006	0.726	0.881	93	50	12	-5	6	1.01E-7	
<b>Ovarian Cancer</b>														
IGROV1	0.585	1.949	1.940	1.247	0.845	0.854	0.785	99	49	19	20	15	9.35E-8	
OVCAR-3	0.533	1.878	1.915	1.647	0.908	0.675	0.675	103	83	28	11	11	3.96E-7	
OVCAR-4	0.776	1.596	1.617	1.535	1.345	1.246	1.202	103	93	69	57	52	> 1.00E-4	
OVCAR-5	0.742	1.941	1.808	1.688	1.276	1.129	1.104	89	79	44	32	30	6.91E-7	
OVCAR-8	0.509	2.011	2.081	1.862	1.029	0.866	0.825	105	90	35	24	21	5.27E-7	
NCI/ADR-RES	0.502	1.786	1.748	1.729	1.031	0.745	0.754	97	96	41	19	20	6.89E-7	
SK-OV-3	0.912	2.098	2.023	1.556	1.006	1.008	0.957	94	54	8	8	4	1.24E-7	
<b>Renal Cancer</b>														
786-0	0.656	2.224	2.151	1.716	1.338	0.772	0.876	95	68	44	7	14	5.38E-7	
A498	1.368	2.011	2.083	1.846	1.586	1.451	1.484	111	74	34	13	18	3.98E-7	
ACHN	0.446	2.030	2.005	1.105	0.848	0.702	0.750	98	42	25	16	19	7.12E-8	
RXF 393	0.773	1.581	1.571	1.157	1.027	0.466	0.556	99	47	31	-40	-28	8.92E-8	
SN12C	0.516	2.191	1.976	1.233	1.107	1.035	0.992	87	43	35	31	28	6.89E-8	
TK-10	1.079	2.167	2.126	1.617	1.376	1.384	1.309	96	49	27	28	21	9.71E-8	
UO-31	0.629	1.667	1.508	1.140	0.858	0.715	0.777	85	49	22	8	14	9.51E-8	
<b>Prostate Cancer</b>														
PC-3	0.617	1.674	1.545	1.217	1.116	0.931	0.884	88	57	47	30	25	5.09E-7	
DU-145	0.388	1.648	1.558	0.757	0.811	0.473	0.449	93	29	34	7	5	4.72E-8	
<b>Breast Cancer</b>														
MCF7	0.444	2.102	1.873	1.005	0.898	0.766	0.671	86	34	27	19	14	4.91E-8	
MDA-MB-231/ATCC	0.547	1.393	1.473	1.063	0.732	0.500	0.531	109	61	22	-9	-3	1.90E-7	
HS 578T	1.100	2.097	2.181	1.892	1.610	1.345	1.381	108	79	51	25	28	1.11E-6	
BT-549	1.182	2.414	2.399	1.746	1.775	0.999	1.399	99	46	48	-15	18	8.32E-8	
T-47D	0.873	1.590	1.514	1.190	1.023	1.005	1.024	89	44	21	18	21	7.45E-8	
MDA-MB-468	0.706	1.406	1.372	0.895	0.697	0.719	0.693	95	27	-1	2	-2	4.59E-8	

**Figure 2.12:** NCI-60 five dose GI<sub>50</sub> determination screening results for **4d**.

growth inhibition across various cancer types. Exciting and unusual results from the single dose screening of **4d** led to further investigations via the NCI to determine the GI<sub>50</sub> values against the cell lines represented in the NCI-60 cell panel (Figure 2.12 and 2.13).

Interestingly, **4d** exhibited GI<sub>50</sub>'s below 100 nM for many cancer types, including, leukemia, colon, breast and renal cancer cells. Amongst the colon cancer cell lines, HT29 cells were found to be most sensitive to **4d**, which manifested GI<sub>50</sub> of 26 nM, the other colon cancer cells also exhibited strong growth inhibition with GI<sub>50</sub>'s ranging 56-80 nM. Two prostate cancer cell lines were also found to be sensitive to **4d**, with a GI<sub>50</sub> value of ~0.5 μM for PC3 and ~47 nM for DU-145 cells. Among the breast cancer cell lines evaluated, MCF7, BT549, T-47D and MDA MB 468 exhibited the greatest growth inhibition. The K562 and SR cell lines were the most sensitive among leukemia cell lines. The NCI-60 cell panel assay established that **4d**, a 21-fold Hsp90β-selective inhibitor, exhibited GI<sub>50</sub> values comparable to clinically evaluated Hsp90 pan-inhibitors, validating Hsp90β-selective inhibition as a viable approach for the treatment of cancer.<sup>42-43</sup>

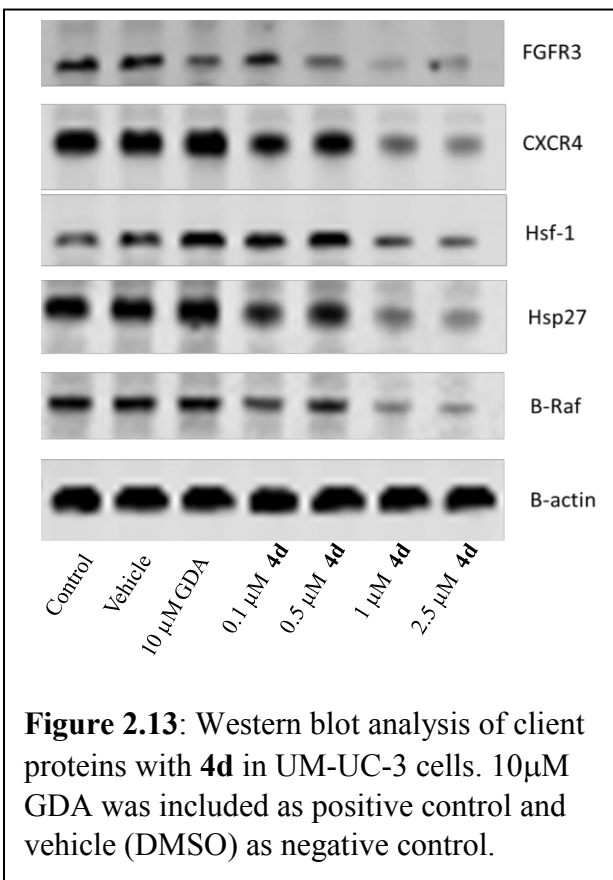
**II.5.2 Determination of the Growth-Inhibition and Client Protein Degradation in Urological Cancer Cells.** In collaboration with Dr. Jeffery Holzbeierlein at The University of Kansas Medical Center, compound **4d** was evaluated for

	Cell Line	GI50 (Moles)
Bladder Cancer	UM-UC3	5.084e-007
	T24	1.969e-007
Prostate Cancer	PC3MM2	1.240e-006
	LNcap-LN3	1.183e-006
	C4-2b	1.031e-006
	LAPC4	2.565e-006

**Table 2.2:** GI<sub>50</sub> values of **4d** against urological cancer cells.

growth inhibition against urological cancers, such as bladder and prostate cancer cells not represented in the NCI-60 cell panel. As noted in Table 2.2, **4d** exhibits GI<sub>50</sub> values of ~508 nM and ~196 nM against UM-UC-3 and T24 bladder cancer cells, respectively, whereas, the efficacy of **4d** against evaluated prostate cancer cells ranged between 1-2.5 μM (Table 2.2).

Since Hsp90 inhibition induces the degradation of Hsp90-dependent substrates via



the ubiquitin-proteasome pathway, the levels of both kinase and non-kinase Hsp90 clients were assessed via Western blot analysis. Known Hsp90 clients, fibroblast growth factor receptor 3 (FGFR3) (highly mutated and/or overexpressed in nonmuscle-invasive urothelial carcinomas),<sup>44-46</sup> CXCR4, and B-Raf, along with HSR elements Hsf-1 and Hsp27, were analyzed following the administration of **4d** to UM-UC-3 cells. After a 24-hour incubation with **4d**, Hsp90-dependent client proteins were reduced at concentrations that mirrored the cellular IC<sub>50</sub> value, clearly linking cell viability to Hsp90β inhibition (Figure 2.13). A marked dose-dependent reduction in FGFR3 level was observed along with Hsp90β-dependent clients, CXCR4 and B-Raf. Heat shock related

proteins Hsp27 and Hsf-1, were found to decline with increasing doses of **4d**, which mirrored the trend observed previously with the Hsp90 $\beta$ -selective compound, **KUNB31**.

**II.5.3 HER2 Dependency on Hsp90 Isoforms.** In collaboration with Dr. Len Neckers at the National Institute of Health, compound **5b**, being the most selective Hsp90 $\beta$  inhibitor, was evaluated in SkBr3 cells for its effect on the maturation of proteins known to drive oncogenesis. Hsp90 $\alpha$  knockdown via Hsp90 $\alpha$  siRNA was carried out to distinguish the roles of Hsp90 $\alpha$  and Hsp90 $\beta$  on the maturation of the known Hsp90 client, ErbB2 (HER2). HER2 belongs to the epidermal growth factor receptor family of proteins (EGFR), and exhibits intrinsic receptor tyrosine kinase activity that is overexpressed in ~30% of breast cancers and many other cancers.<sup>47-</sup>

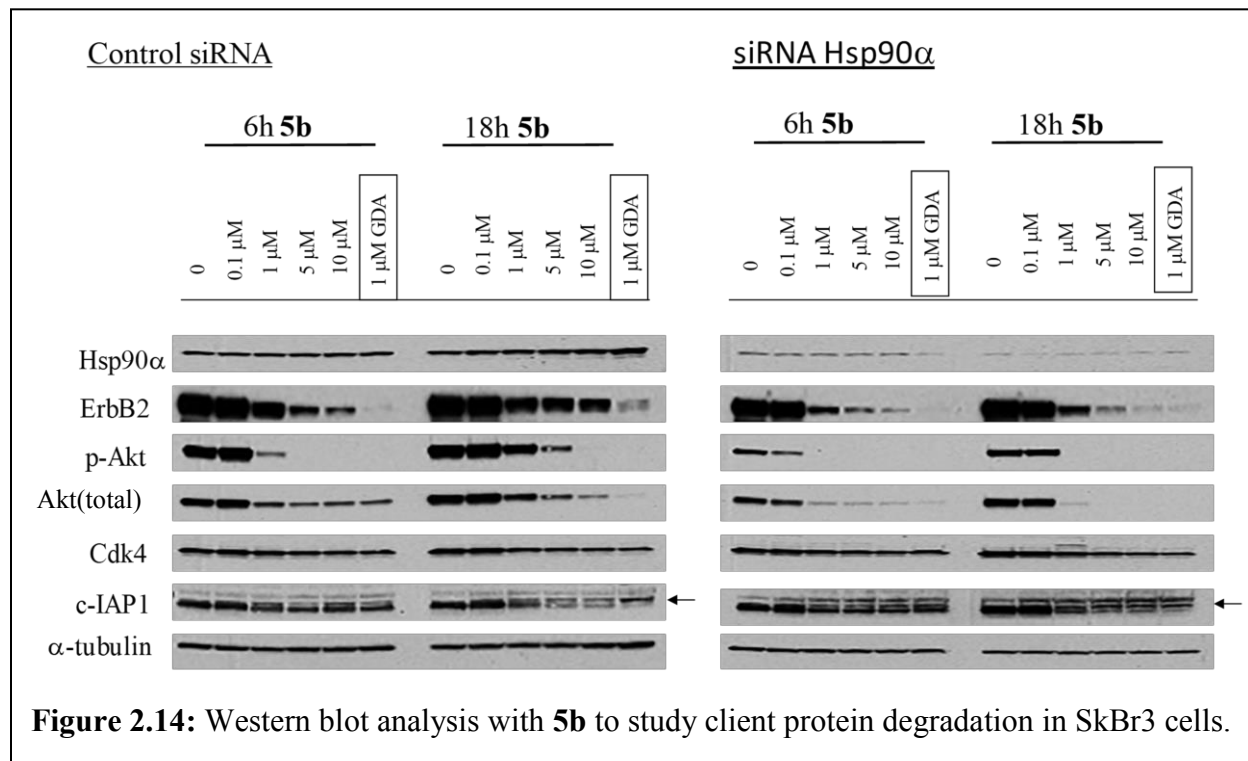


**Figure 2.14:** Western blot analysis with **5b** to study client protein degradation in SkBr3 cells.

<sup>49</sup> It is hypothesized in the literature that membrane bound HER2 in SkBr3 cells is dependent upon Grp94, however, the cytosolic HER2 population is maintained by Hsp90 $\alpha$  and Hsp90 $\beta$ .<sup>34</sup> Compound **5b** was utilized as a chemical tool to inhibit Hsp90 $\beta$ , which revealed HER2 to be dependent on both cytosolic isoforms, as

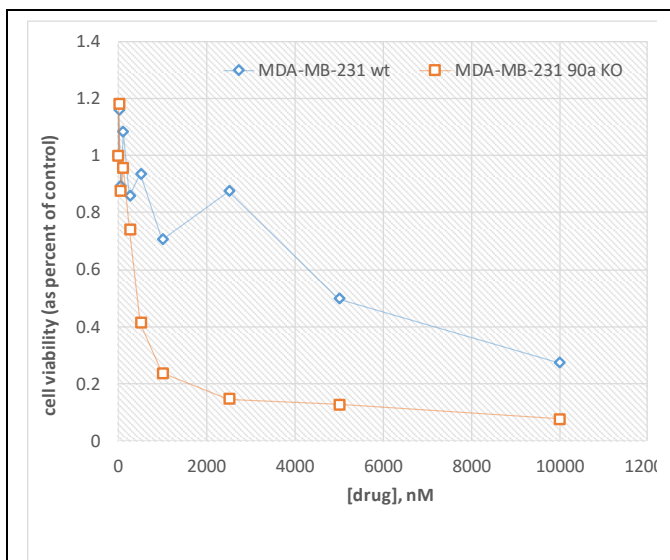


**Figure 2.15:** Effect of **5b** on viability of MDA-MB-231 wild type and MDA-MB-231 Hsp90 $\alpha$  knockout cells after 5-day of treatment

the inhibition of Hsp90 $\beta$  with **5b** was not effective at reducing HER2 maturation (control siRNA, 18h reading), however, upon knockdown of Hsp90 $\alpha$  with siRNA in the presence of **5b**, the levels of HER2 were significantly reduced. Therefore, maturation of HER2 exhibits redundant dependency upon both Hsp90 isoforms and therefore a functional loss of Hsp90 $\beta$  can be compensated by Hsp90 $\alpha$ . Unlike the pan-inhibitor, GDA, **5b** did not induce the heat shock response even at 10  $\mu$ M (control siRNA, 18h), which is an advantage manifested by Hsp90 $\beta$ -selective inhibitors. In addition, known Hsp90 $\beta$  dependent clients such as CDK4 and c-IAP1 were degraded in a dose-dependent manner upon increasing concentrations of **5b**, but were unaffected via Hsp90 $\alpha$  knockdown.

In a parallel study, triple negative breast cancer cells, MDA-MB-231 and a Hsp90 $\alpha$  knockout variant of MDA-MB-231 cells, were treated with increasing concentrations of **5b** (Figure 2.15). Interestingly, in MDA-MB-231 cells treated with control siRNA, **5b** exhibited growth inhibition that was significantly less (4.5  $\mu$ M- 5  $\mu$ M) than that in the Hsp90 $\alpha$  knockdown cells (~0.5  $\mu$ M). Again, this study highlighted that Hsp90 $\alpha$  and Hsp90 $\beta$  functions may overlap in certain cases, as cellular viability may be rescued by compensatory chaperones. The functional redundancy manifested by the Hsp90 cytosolic isoforms may not exist for all clients, and therefore, further investigation is needed to identify the oncogenic drivers that are specifically dependent upon each isoform.

## **II.6 Conclusions and Future Directions**

Using a structure-based approach, a new series of Hsp90 $\beta$ -selective inhibitors has been discovered. The developed series exhibits both high affinity and selectivity for the Hsp90 $\beta$  isoform versus other Hsp90 isoforms. Analogs based on the benzamide derived inhibitor, SNX2112 were developed, and exhibit Hsp90 $\beta$ -selectivity by differentiating between minor structural differences between the Hsp90 $\alpha$  and Hsp90 $\beta$  N-terminal binding site, which until recently, was considered indistinguishable by ligands. The reported isoquinolin-1(2H)-one series of compounds provides an improvement over the reported Hsp90 $\beta$ -selective compounds in terms of affinity (~40-90 nM), selectivity (20->400-fold) and cellular efficacy.

Compound **4d** was screened in the NCI-60 cancer cell panel which identified cancer types that may be sensitive to Hsp90 $\beta$  inhibition. Excitingly, a number of cancers showed growth inhibition at low nanomolar concentrations, which is comparable to the pan-inhibitors that have been evaluated clinically. Furthermore, Hsp90 $\beta$ -selective inhibition does not induce heat shock response, and consequently, may be a safer alternative to pan-Hsp90 inhibition.

Moving forward, the SAR trends observed with the current series will be utilized to develop more efficacious derivatives. As suggested by the modeling studies, the introduction of saturation into the **5b** may increase selectivity and affinity for Hsp90 $\beta$ . Co-crystallization studies with **4d** and **5b** are underway in collaboration with Dr. Robert Matts at Oklahoma State University to validate the proposed binding modes.

## II.7 Method and Experiments

All reactions were performed in oven-dried glassware under argon atmosphere unless otherwise stated. Dichloromethane (DCM), tetrahydrofuran (THF), and toluene were passed through a column of activated alumina prior to use. Anhydrous acetonitrile, methanol, *N,N*-dimethylformamide (DMF) were purchased and used without further purification. Flash column chromatography was performed using silica gel (40–63  $\mu\text{m}$  particle size). The  $^1\text{H}$  (500 and 400 MHz) and  $^{13}\text{C}$  NMR (125 and 100 MHz) spectra were recorded on 500 and 400 MHz spectrometer. Data are reported as p = pentet, q = quartet, t = triplet, d = doublet, s = singlet, bs =

broad singlet, m = multiplet; coupling constant(s) in Hz. High resolution mass spectral data were obtained on a time-of-flight mass spectrometer and analysis was performed using electrospray ionization.

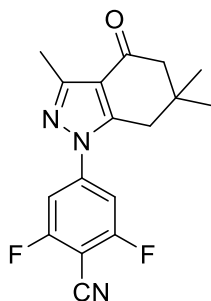
### **Fluorescence Polarization Assay**

Assay buffer (25  $\mu$ L, 20 mM HEPES pH 7.3, 50 mM KCl, 5 mM MgCl<sub>2</sub>, 1 mM DTT, 20 mM Na<sub>2</sub>MoO<sub>4</sub>, 0.01% NP-40, and 0.5 mg/mL BGG) was added to 96-well plate (black well, black bottom) followed by the desired compound at the indicated final concentrations in DMSO (1% DMSO final concentration). Subsequently, 10nM Recombinant Hsp90 $\alpha$  or Hsp90 $\beta$  or cGrp94 or Trap-1 and 6 nM FITC-GDA were added in 50  $\mu$ L and 25  $\mu$ L assay buffer respectively resulting in a 100  $\mu$ L final volume. Plates were incubated for 5 h at 4°C on a rocker. Fluorescence was determined using excitation and emission filters of 485 and 528 nm, respectively. Percent FITC-GDA bound was determined by assigning the DMSO millipolarization unit (mP) value as the 100% bound value and 0% for FITC-GDA in assay buffer without any protein. Plates were incubated at 4 °C with rocking for 2 hrs. Polarization values (in mP units) was measured at 37 °C with an excitation filter at 485 nm and an emission filter at 528 nm. Polarization values were correlated to % tracer bound and compound concentrations. The concentration of inhibitor at which the 50% displaced tracer was observed, represented apparent K<sub>d</sub>.

**Molecular Modeling.** Surflex-Docking module in SybylX was used for molecular modeling and docking studies. The co-crystal structures of SNX 2112 bound to Hsp90 (PDB code: 4NH7) , compound 31 bound to Hsp90a (PDB code:4O0B) and PU-3 bound to Hsp90b (PDB code:1UYM) were utilized for modeling experiments. Pymol was used for further visualization and figure preparation.



## Chemistry



### **2,6-difluoro-4-(3,6,6-trimethyl-4-oxo-4,5,6,7-tetrahydro-1H-indazol-1-yl)benzonitrile (2):**

**a)** To a solution of 2,4,6-trifluorobenzonitrile (**1**) (5g, 31.8 mmol, 1 eq.) in 50 mL of ethanol heated to 60°C, was added hydrazine hydrate (50-60% solution) (3.4g, 63.6 mmol, ~2 eq.). Upon consumption of **1** (monitored using TLC), the solvent was evaporated from the reaction mixture under vacuum. To the remaining white semisolid mass was added 50 mL water and the organic mass was extracted with ethyl acetate (3 X 50mL). The combined organic fractions were combined and washed with brine (100 mL). The organic fraction was separated and dried over sodium sulfate. Subsequently, evaporation of the organic layer provided ~6.5 g of white mixture that was utilized in the next reaction without further purification.

**b)** Above obtained crude product (6g, 35.5 mmol, 1 eq.) was suspended in 100mL ethanol in a 250mL capacity sealed reaction vessel. 2-acetyldimedone (16.1g, 88.75 mmol, 2.5 eq), an orange colored oil, was subsequently added to the reaction vessel which was sealed and heated to 100° C for 6 hr. The reaction vessel was allowed to cool to rt, ethanol was removed in vacuo, and the remaining mass was extracted with ethyl acetate (3X 100 mL) and water (200mL). Organic layers were combined and washed with 100 mL water. Separated organic layer was dried using sodium sulfate and adsorbed onto silica, and purified using column chromatography (SiO<sub>2</sub>, 3:2

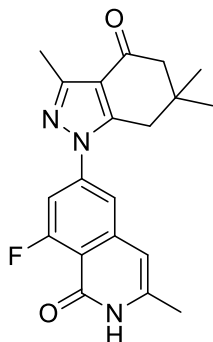
hexanes/ethyl acetate) to afford **2** (5.8 g, 52%) as light-yellow solid. <sup>1</sup>H NMR (500 MHz, Chloroform-d) δ 7.39 – 7.33 (m, 2H), 2.91 (s, 2H), 2.55 (s, 3H), 2.45 (s, 2H), 1.17 (s, 6H). <sup>13</sup>C NMR (126 MHz, Chloroform-d) δ 192.9, 164.5 (d, J = 6.5 Hz), 162.5 (d, J = 6.4 Hz), 151.8, 149.4, 144.5 – 144.1 (m), 118.8, 108.5, 106.2 (d, J = 4.1 Hz), 106.0 (d, J = 3.9 Hz), 99.9, 52.0, 38.0, 36.0, 28.4 (2), 13.3. HRMS (ESI) *m/z* [M+H] calculated for C<sub>17</sub>H<sub>16</sub>F<sub>2</sub>N<sub>3</sub>O, 316.1261, found 316.1237.

### **General Method for Preparation of 3a-i:**

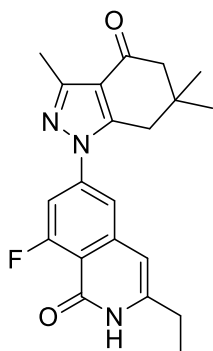
**a)** To a solution of Benzonitrile **2** (200 mg, 0.64 mmol, 1 eq) in 2 mL DMF in a 10 mL round bottom flask, desired β-ketoethyl ester (0.76 mmol, 1.2 eq), potassium carbonate (106 mg, 0.76 mmol, 1.2 eq) was added and stirred at 70° C until **2** was consumed, as determined by TLC. Upon completion, the reaction was acidified to pH 5 with 1N aq. HCl, subsequently, 10 mL NH<sub>4</sub>Cl saturated solution was added and extracted using ethyl acetate (3X 10 ml). The combined organic fractions were washed with brine and dried over sodium sulfate. The organic fraction was then adsorbed on silica and a quick flash column chromatography was performed using 3:7 ethyl acetate/hexane as solvent system. The product fractions were collected, dried and the resulting mass was utilized in the further reaction.

**b)** The crude mass obtained (~210 mg) was taken in a 15 ml sealed reaction vessel, to which 1mL sulfuric acid (36N), 8.5 mL acetic acid and 0.5 mL water were added. The vessel was sealed and heated to 140° C for 8h. The reaction was then quenched with addition of the reaction mixture to 100 mL water. Precipitated solid was filtered under vacuum to yield brown colored solid cake that was dried, dissolved in ethyl acetate and adsorbed onto silica for further purification. Upon column

chromatography with 5:5 Hexane/ethyl acetate, the desired product was isolated as white solid (30-40 % yield).

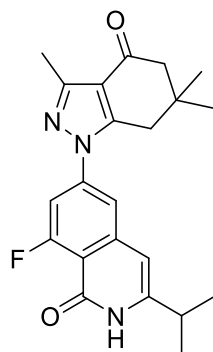


**8-fluoro-3-methyl-6-(3,6,6-trimethyl-4-oxo-4,5,6,7-tetrahydro-1H-indazol-1-yl)isoquinolin-1(2H)-one (3a):** 78 mg, Yield 35%;  $^1\text{H}$  NMR (500 MHz, Chloroform-*d*)  $\delta$  10.63 (s, 1H), 7.40 – 7.35 (m, 1H), 7.29 – 7.25 (m, 1H), 6.34 (s, 1H), 2.91 (s, 2H), 2.57 (s, 3H), 2.44 (s, 2H), 2.41 (d,  $J = 1.0$  Hz, 3H), 1.15 (s, 6H).  $^{13}\text{C}$  NMR (126 MHz, Chloroform-*d*)  $\delta$  193.3, 163.0 (d,  $J = 265.2$  Hz), 161.3 (d,  $J = 3.9$  Hz), 150.8, 149.2, 142.4 (d,  $J = 11.7$  Hz), 142.1 (d,  $J = 1.8$  Hz), 140.5, 117.8, 114.3 (d,  $J = 4.2$  Hz), 112.0 (d,  $J = 6.4$  Hz), 107.5 (d,  $J = 25.6$  Hz), 103.9 (d,  $J = 2.7$  Hz), 52.2, 37.7, 36.0, 28.4 (2), 19.3, 13.4. HRMS (ESI)  $m/z$  [M+H] calculated for  $\text{C}_{20}\text{H}_{20}\text{FN}_3\text{O}_2$ , 354.1617, found 354.1626.



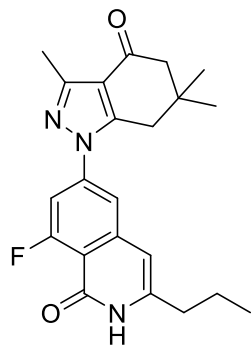
**3-ethyl-8-fluoro-6-(3,6,6-trimethyl-4-oxo-4,5,6,7-tetrahydro-1H-indazol-1-yl)isoquinolin-1(2H)-one (3b):** 77 mg, Yield: 36%;  $^1\text{H}$  NMR (600 MHz, Chloroform-*d*)  $\delta$  9.51 (s, 1H), 7.41 (d,

$J = 2.0$  Hz, 1H), 7.27 (d,  $J = 0.6$  Hz, 1H), 6.33 (s, 1H), 2.92 (s, 2H), 2.64 (q,  $J = 7.5$  Hz, 2H), 2.57 (s, 3H), 2.44 (s, 2H), 1.36 (t,  $J = 7.5$  Hz, 3H), 1.15 (s, 6H).  $^{13}\text{C}$  NMR (151 MHz, Chloroform-*d*)  $\delta$  193.3, 162.1, 160.8, 150.8, 149.2, 145.4, 142.5, 142.0, 117.9, 114.6 (d,  $J = 4.1$  Hz), 112.3, 107.6 (d,  $J = 25.5$  Hz), 102.8, 52.3, 37.7, 36.0, 28.4 (2), 26.4, 13.4, 12.0. HRMS (ESI)  $m/z$  [M+Na] calculated for  $\text{C}_{21}\text{H}_{22}\text{FN}_3\text{O}_2\text{Na}$ , 390.1594 found 390.1609.

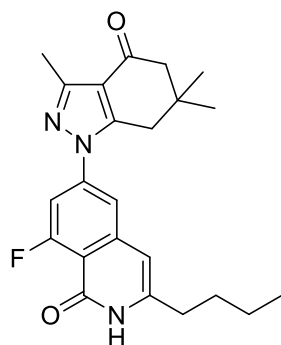


**8-fluoro-3-isopropyl-6-(3,6,6-trimethyl-4-oxo-4,5,6,7-tetrahydro-1H-indazol-1-**

**yl)isoquinolin-1(2H)-one (3c):** 96 mg, Yield: 40 %;  $^1\text{H}$  NMR (600 MHz, Chloroform-*d*)  $\delta$  9.31 (s, 1H), 7.41 (d,  $J = 2.0$  Hz, 1H), 7.27 (dd,  $J = 11.7, 2.0$  Hz, 1H), 6.32 (s, 1H), 2.91 (s, 2H), 2.86 – 2.79 (m, 1H), 2.57 (s, 3H), 2.44 (s, 2H), 1.36 (d,  $J = 6.9$  Hz, 6H), 1.15 (s, 6H).  $^{13}\text{C}$  NMR (151 MHz, Chloroform-*d*)  $\delta$  193.31, 162.99 (d,  $J = 265.3$  Hz), 160.6, 150.8, 149.4, 149.2, 142.4 (d,  $J = 11.7$  Hz), 142.0, 117.9, 114.8 (d,  $J = 4.3$  Hz), 112.4, 107.6 (d,  $J = 25.6$  Hz), 100.9 (d,  $J = 2.6$  Hz), 52.3, 37.7, 36.0, 32.2, 28.4 (2), 21.2 (2), 13.4. HRMS (ESI)  $m/z$  [M+Na] calculated for  $\text{C}_{22}\text{H}_{24}\text{FN}_3\text{O}_2\text{Na}$ , 404.1750, found 404.1743.

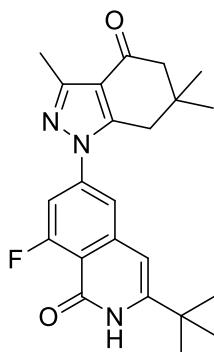


**8-fluoro-3-propyl-6-(3,6,6-trimethyl-4-oxo-4,5,6,7-tetrahydro-1H-indazol-1-yl)isoquinolin-1(2H)-one (3d)** : 113 mg, Yield 45 %;  $^1\text{H}$  NMR (500 MHz, Chloroform-*d*)  $\delta$  10.32 (s, 1H), 7.40 (d,  $J = 2.0$  Hz, 1H), 7.26 (d,  $J = 14.0$  Hz, 1H), 6.37 – 6.29 (s, 1H), 2.91 (s, 2H), 2.61 (t,  $J = 7.6$  Hz, 2H), 2.57 (s, 3H), 2.44 (s, 2H), 1.80 (h,  $J = 7.4$  Hz, 2H), 1.15 (s, 6H), 1.04 (t,  $J = 7.4$  Hz, 3H).  $^{13}\text{C}$  NMR (126 MHz, Chloroform-*d*)  $\delta$  193.3, 162.9 (d,  $J = 265.2$  Hz), 161.1 (d,  $J = 4.5$  Hz), 150.8, 149.3, 144.5, 142.8 (d,  $J = 11.9$  Hz), 142.0 (d,  $J = 2.4$  Hz), 117.8, 114.6 (d,  $J = 4.6$  Hz), 112.2 (d,  $J = 7.2$  Hz), 107.5 (d,  $J = 25.7$  Hz), 103.3 (d,  $J = 3.5$  Hz), 52.3, 37.8, 36.0, 35.2, 28.4 (2), 21.4, 13.5, 13.4. HRMS (ESI)  $m/z$   $[\text{M}+\text{Na}]$  calculated for  $\text{C}_{22}\text{H}_{24}\text{FN}_3\text{O}_2\text{Na}$ , 404.1750, found 404.1765.



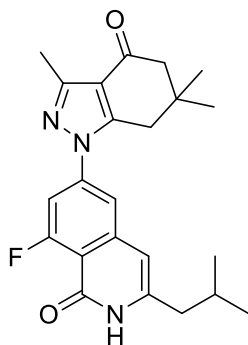
**3-butyl-8-fluoro-6-(3,6,6-trimethyl-4-oxo-4,5,6,7-tetrahydro-1H-indazol-1-yl)isoquinolin-1(2H)-one (3e)**: 100 mg, Yield 40%;  $^1\text{H}$  NMR (600 MHz, Chloroform-*d*)  $\delta$  9.99 (d,  $J = 20.1$  Hz, 1H), 7.40 (d,  $J = 1.9$  Hz, 1H), 7.25 (dd,  $J = 11.6, 2.0$  Hz, 1H), 6.32 (s, 1H), 2.91 (s, 2H), 2.61 (t,  $J = 7.7$  Hz, 2H), 2.58 – 2.55 (m, 3H), 2.44 (s, 2H), 1.73 (p,  $J = 7.7$  Hz, 2H), 1.45 (h,  $J = 7.4$  Hz, 2H),

1.15 (s, 6H), 1.01 – 0.95 (m, 3H). <sup>13</sup>C NMR (151 MHz, Chloroform-*d*) δ 193.3, 163.0 (d, *J* = 265.5 Hz), 161.1 (d, *J* = 3.6 Hz), 150.8, 149.2, 144.6, 142.4 (d, *J* = 11.5 Hz), 142.1, 117.9, 114.6 (d, *J* = 4.1 Hz), 112.3 (d, *J* = 6.3 Hz), 107.5 (d, *J* = 25.5 Hz), 103.2 (d, *J* = 2.6 Hz), 52.3, 37.8, 36.0, 33.1, 30.1, 28.4 (2), 22.1, 13.7, 13.4. HRMS (ESI) *m/z* [M+Na] calculated for C<sub>23</sub>H<sub>26</sub>FN<sub>3</sub>O<sub>2</sub>Na, 418.1907, found 418.1902.

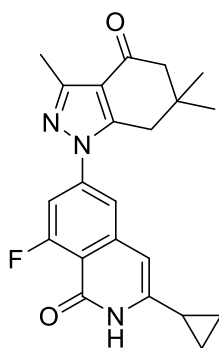


**3-(tert-butyl)-8-fluoro-6-(3,6,6-trimethyl-4-oxo-4,5,6,7-tetrahydro-1H-indazol-1-**

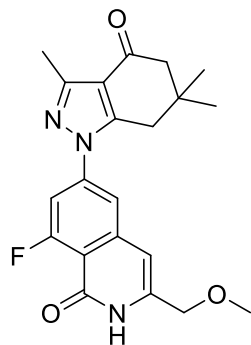
**yl)isoquinolin-1(2H)-one (3f)** : 95 mg, Yield 38%; <sup>1</sup>H NMR (600 MHz, Chloroform-*d*) δ 8.78 (s, 1H), 7.44 (d, *J* = 1.9 Hz, 1H), 7.27 (d, *J* = 0.7 Hz, 1H), 6.37 (s, 1H), 2.91 (s, 2H), 2.56 (s, 3H), 2.44 (s, 2H), 1.38 (s, 9H), 1.15 (s, 6H). <sup>13</sup>C NMR (151 MHz, Chloroform-*d*) δ 193.3, 161.2 (d, *J* = 254.3 Hz), 155.6, 151.3, 150.8, 149.2, 142.4 (d, *J* = 11.5 Hz) 141.9, 140.8, 117.9, 115.1, 107.7 (d, *J* = 25.8 Hz), 100.3, 52.3, 37.8, 36.0, 34.5, 28.8 (3), 28.4 (2), 13.4. HRMS (ESI) *m/z* [M+Na] calculated for C<sub>23</sub>H<sub>26</sub>FN<sub>3</sub>O<sub>2</sub>Na, 418.1907, found 418.1897.



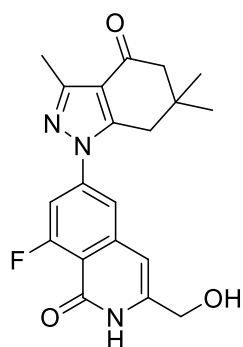
**8-fluoro-3-isobutyl-6-(3,6,6-trimethyl-4-oxo-4,5,6,7-tetrahydro-1H-indazol-1-yl)isoquinolin-1(2H)-one (3g):** 88 mg, Yield 35 % ;  $^1\text{H}$  NMR (600 MHz, Chloroform-*d*)  $\delta$  8.74 (s, 1H), 7.43 (d,  $J = 2.0$  Hz, 1H), 7.24 (dd,  $J = 11.7, 2.0$  Hz, 1H), 6.28 (s, 1H), 2.91 (s, 2H), 2.56 (s, 3H), 2.44 (s, 2H), 2.41 (d,  $J = 7.4$  Hz, 2H), 1.15 (s, 6H), 1.02 (d,  $J = 6.6$  Hz, 6H).  $^{13}\text{C}$  NMR (151 MHz, Chloroform-*d*)  $\delta$  197.0, 171.0, 161.3 (d,  $J = 3.9$  Hz), 150.8, 149.2, 148.7, 142.5 (d,  $J = 11.7$  Hz), 142.1 (d,  $J = 1.8$  Hz), 139.2, 122.4, 114.3 (d,  $J = 4.2$  Hz), 112.0 (d,  $J = 6.4$  Hz), 107.5 (d,  $J = 25.6$  Hz), 103.9 (d,  $J = 2.7$  Hz), 53.4, 42.8, 37.7, 36.0, 28.4, 22.2 (2), 14.2 (2). HRMS (ESI)  $m/z$  [M+Na] calculated for  $\text{C}_{23}\text{H}_{26}\text{FN}_3\text{O}_2\text{Na}$ , 418.1907, found 418.1913.



**3-cyclopropyl-8-fluoro-6-(3,6,6-trimethyl-4-oxo-4,5,6,7-tetrahydro-1H-indazol-1-yl)isoquinolin-1(2H)-one (3h):** 80 mg, Yield 33%;  $^1\text{H}$  NMR (600 MHz, Chloroform-*d*)  $\delta$  9.43 (s, 1H), 7.38 – 7.35 (m, 1H), 7.23 (dd,  $J = 11.8, 2.0$  Hz, 1H), 6.24 – 6.20 (m, 1H), 2.90 (s, 2H), 2.56 (s, 3H), 2.43 (s, 2H), 1.90 – 1.83 (m, 1H), 1.14 (s, 6H), 1.10 – 1.08 (m, 2H), 0.93 – 0.90 (m, 2H).  $^{13}\text{C}$  NMR (151 MHz, Chloroform-*d*)  $\delta$  193.3, 163.0 (d,  $J = 265.1$  Hz), 160.6, 150.8, 149.2, 145.7, 142.5, 142.0, 117.9, 114.4 (d,  $J = 4.2$  Hz), 112.2 (d,  $J = 6.3$  Hz), 107.4 (d,  $J = 25.5$  Hz), 101.1 (d,  $J = 2.7$  Hz), 52.3, 37.8, 35.9, 28.4 (2), 13.5, 13.4, 7.4 (2). HRMS (ESI)  $m/z$  [M+Na] calculated for  $\text{C}_{22}\text{H}_{22}\text{FN}_3\text{O}_2\text{Na}$ , 402.1594, found 402.1603.



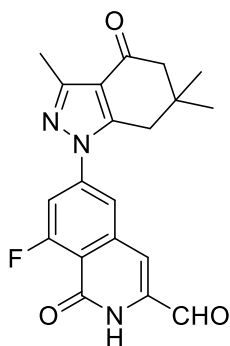
**8-fluoro-3-(methoxymethyl)-6-(3,6,6-trimethyl-4-oxo-4,5,6,7-tetrahydro-1H-indazol-1-yl)isoquinolin-1(2H)-one (3i):** 80 mg, Yield 33%;  $^1\text{H}$  NMR (600 MHz, Chloroform-*d*)  $\delta$  8.74 (s, 1H), 7.38 (d,  $J = 2.0$  Hz, 1H), 7.22 (dd,  $J = 11.7, 2.0$  Hz, 1H), 6.30 (s, 1H), 4.30 (s, 2H), 3.39 (s, 3H), 2.83 (s, 2H), 2.49 (s, 3H), 2.36 (s, 2H), 1.07 (s, 6H).  $^{13}\text{C}$  NMR (126 MHz, Chloroform-*d*)  $\delta$  193.2, 162.9 (d,  $J = 265.1$  Hz), 159.7, 150.9, 149.2, 142.6, 141.2 (d,  $J = 2.2$  Hz), 139.5, 117.9, 114.9 (d,  $J = 4.6$  Hz), 113.3 (d,  $J = 6.2$  Hz), 108.2 (d,  $J = 25.7$  Hz), 102.6 (d,  $J = 3.3$  Hz), 70.0, 58.7, 52.2, 37.8, 35.9, 28.4 (2), 13.4. HRMS (ESI)  $m/z$  [M+H] calculated for  $\text{C}_{21}\text{H}_{23}\text{FN}_3\text{O}_3$ , 384.1723, found 384.1716.



**8-fluoro-3-(hydroxymethyl)-6-(3,6,6-trimethyl-4-oxo-4,5,6,7-tetrahydro-1H-indazol-1-yl)isoquinolin-1(2H)-one (3j):** To a solution of 3i (100 mg, 0.26 mmol, 1eq) in 3 mL DCM cooled to 0°C was added 0.8 mL of 1M BBr<sub>3</sub> solution in DCM (0.78 mmol, 3 eq) dropwise, the reaction completion was monitored using TLC. After 2h, the reaction was quenched dropwise using 2mL



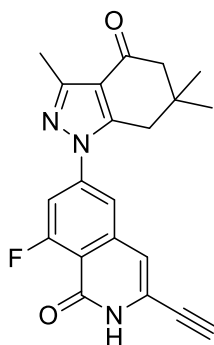
saturated sodium bicarbonate solution, resulting biphasic mixture was extracted using ethyl acetate (10mL X 2). The organic fractions were collected, washed with water and dried over sodium sulfate. Organic fraction was adsorbed onto silica for column chromatography purification using (4:6 ethyl acetate/hexanes) to furnish 55 mg (0.155 mmol, Yield 60%) as white solid. <sup>1</sup>H NMR (600 MHz, Chloroform-*d*) δ 10.28 (s, 1H), 7.35 (d, *J* = 1.9 Hz, 1H), 7.24 (dd, *J* = 11.8, 2.0 Hz, 1H), 6.36 (s, 1H), 4.59 (s, 2H), 2.83 (s, 2H), 2.49 (s, 3H), 2.36 (s, 2H), 1.07 (s, 6H). <sup>13</sup>C NMR (126 MHz, Chloroform-*d*) δ 193.25, 166.29(d, *J* = 265.1 Hz) 151.0, 149.3, 142.3, 141.4, 118.0, 114.9 (d, *J* = 4.6 Hz), 112.7, 108.2 (d, *J* = 25.4 Hz), 102.7 (d, *J* = 2.9 Hz), 100.8, 99.9, 61.1, 52.2, 37.7, 35.9, 28.4(2), 13.4. HRMS (ESI) *m/z* [M+H] calculated for C<sub>20</sub>H<sub>21</sub>FN<sub>3</sub>O<sub>3</sub>, 370.1567, found 370.1581.



**8-fluoro-1-oxo-6-(3,6,6-trimethyl-4-oxo-4,5,6,7-tetrahydro-1H-indazol-1-yl)-1,2-**

**dihydroisoquinoline-3-carbaldehyde (3k):** To a solution of **3j** (30 mg, 0.081 mmol, 1 eq) in 3 mL DCM in a 15 mL sealed reaction vessel, was added activated MnO<sub>2</sub> (70 mg, 0.81 mmol, 10 eq). The reaction vessel was sealed and heated to 45°C for 6 h. Upon completion, the reaction mixture was cooled, filtered through a plug of celite, and a quick flash column chromatography (5:5 ethyl acetate/hexanes) afforded **3k** (28 mg, 0.076 mmol, 94%) as white solid. <sup>1</sup>H NMR (500 MHz, Chloroform-*d*) δ 9.63 (s, 1H), 8.91 (s, 1H), 7.77 (s, 1H), 7.53 (dd, *J* = 11.6, 2.0 Hz, 1H), 7.14 (d, *J* = 1.7 Hz, 1H), 2.96 (s, 2H), 2.58 (s, 3H), 2.46 (s, 2H), 1.17 (s, 6H). <sup>13</sup>C NMR (126 MHz,

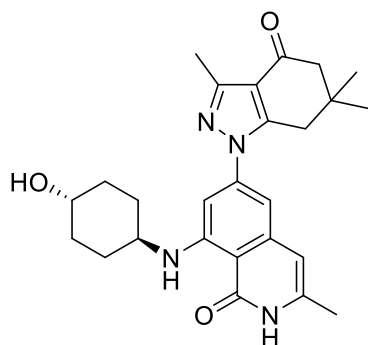
Chloroform-*d*)  $\delta$  193.1, 183.6, 161.3 (d,  $J = 265.2$  Hz), 151.4, 143.1, 149.3, 139.1, 136.3, 124.1, 118.4, 117.2 (d,  $J = 4.8$  Hz), 116.2 (d,  $J = 6.2$  Hz), 116.0 (d,  $J = 3.7$  Hz), 111.5 (d,  $J = 26.0$  Hz), 52.2, 37.9, 36.0, 28.5 (2), 13.4. HRMS (ESI)  $m/z$  [M+H] calculated for C<sub>20</sub>H<sub>24</sub>NO<sub>3</sub>, 326.1756, found 326.1781.



**3-ethynyl-8-fluoro-6-(3,6,6-trimethyl-4-oxo-4,5,6,7-tetrahydro-1H-indazol-1-yl)isoquinolin-1(2H)-one (31):** Dimethyl-1-diazo-2-oxopropylphosphonate (60  $\mu$ L, 0.40 mmol, 1.2 eq.) was added to a stirred solution of aldehyde **3k** (50 mg, 0.13 mmol, 1.0 eq.) and potassium carbonate (36 mg, 0.26 mmol, 2.0 eq) in 3 mL methanol. The resulting mixture was stirred for 24 h at rt. Subsequently, methanol was evaporated in vacuo and remaining mass was diluted with water and ethyl acetate 10 mL each. The organic layer was washed with saturated sodium bicarbonate solution (10 mL), dried over anhydrous sodium sulfate, filtered and concentrated. The residue was purified by flash chromatography (SiO<sub>2</sub>, 1:3 ethyl acetate/hexanes) to afford **31** (40 mg, 0.11 mmol, 85%). <sup>1</sup>H NMR (400 MHz, Chloroform-*d*)  $\delta$  8.97 (s, 1H), 7.48 (s, 1H), 7.38 (dd,  $J = 11.7$ , 1.7 Hz, 1H), 6.78 (d,  $J = 1.8$  Hz, 1H), 3.41 (s, 1H), 2.92 (s, 2H), 2.57 (s, 3H), 2.45 (s, 2H), 1.15 (s, 6H). <sup>13</sup>C NMR (101 MHz, Chloroform-*d*)  $\delta$  193.2, 159.1, 151.1, 149.2, 142.9, 140.4, 135.9, 135.1, 123.5, 118.1, 115.2, 111.3, 109.4 (d,  $J = 25.9$  Hz), 82.7, 52.2, 37.8, 36.0, 29.7, 28.5 (2), 13.4. HRMS (ESI)  $m/z$  [M+H] calculated for C<sub>21</sub>H<sub>26</sub>NO<sub>3</sub>, 340.1912, found 340.1916.

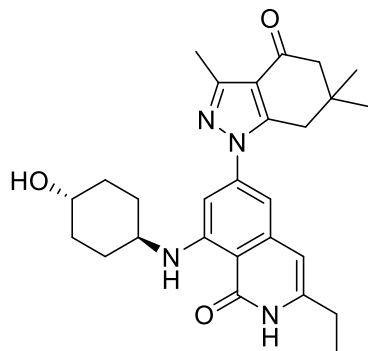
**General procedure for preparation of 4a-k and 5a-g:**

A solution of the desired intermediate **3a-l** (0.07 mmol, 1 eq) in 1 mL DMSO was taken in a 5mL sealed reaction vessel, the corresponding amine (trans-4-aminocyclohexanol for **4a-k**) (0.212 mmol, 3 eq) then diisopropyl ethyl amine (DIPEA)(0.212 mmol, 3eq) was introduced. The reaction vessel was then sealed and heated to 140° C for 12 h, cooled and water (25 mL) was added. The aqueous layer was extracted with ethyl acetate (25 mL X 3), the organic fractions were combined and washed with brine (25mL) and dried over sodium sulfate. Purification with column chromatography (SiO<sub>2</sub>, 4:96 methanol:DCM for **4a-k**, **5a,5b,5e** and 5:1:94 methanol:7M NH<sub>3</sub> in methanol:DCM for **5c,5d,5f,5g**) resulted in the desired products which were further purified by preparative TLC to give the desired compounds **4a-k**, **5a-g** as light yellow solids.

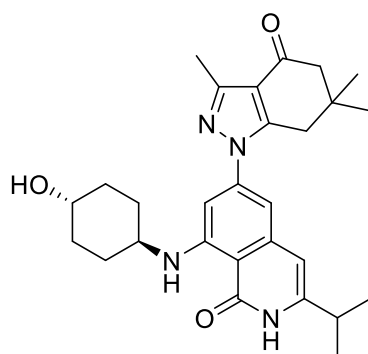


**8-(((1r,4r)-4-hydroxycyclohexyl)amino)-3-methyl-6-(3,6,6-trimethyl-4-oxo-4,5,6,7-**

**tetrahydro-1H-indazol-1-yl)isoquinolin-1(2H)-one (4a):** 22 mg, Yield 70%; <sup>1</sup>H NMR (400 MHz, Chloroform-*d*) δ 9.16 (d, *J* = 7.5 Hz, 1H), 9.05 (s, 1H), 6.51 – 6.40 (m, 2H), 6.09 (s, 1H), 3.74 – 3.59 (m, 2H), 3.31 (d, *J* = 24.2 Hz, 1H), 2.78 (s, 2H), 2.49 (s, 3H), 2.34 (s, 2H), 2.19 (s, 3H), 2.17 – 2.08 (m, 2H), 2.04 – 1.95 (m, 2H), 1.38 (q, *J* = 11.1, 9.9 Hz, 4H), 1.04 (s, 6H). <sup>13</sup>C NMR (101 MHz, CDCl<sub>3</sub>) δ 193.4, 185.3, 169.7, 165.5, 151.4, 150.0, 149.1, 143.5, 143.2, 142.1, 137.4, 107.3, 105.7, 104.8, 100.3, 69.7, 52.4, 50.2, 37.8, 35.8, 33.5, 29.9, 28.4 (2), 19.0, 13.4. HRMS (ESI) *m/z* [M+H] calculated for C<sub>26</sub>H<sub>33</sub>N<sub>4</sub>O<sub>3</sub>, 449.2553, found 449.2566.

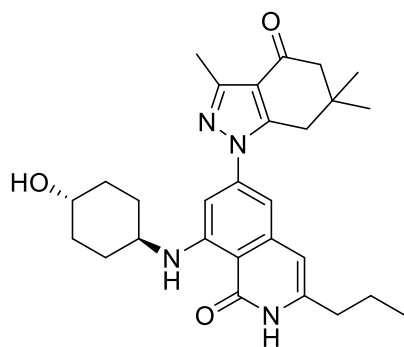


**3-ethyl-8-(((1r,4r)-4-hydroxycyclohexyl)amino)-6-(3,6,6-trimethyl-4-oxo-4,5,6,7-tetrahydro-1H-indazol-1-yl)isoquinolin-1(2H)-one (4b):** 19 mg, Yield 58 %;  $^1\text{H}$  NMR (500 MHz, Chloroform-*d*)  $\delta$  9.77 (s, 1H), 9.45 (s, 1H), 6.67 (d,  $J = 28.0$  Hz, 2H), 6.26 – 6.16 (m, 1H), 3.77 (dd,  $J = 8.7, 4.4$  Hz, 1H), 3.44 (s, 1H), 2.89 (s, 2H), 2.62 – 2.55 (m, 5H), 2.43 (s, 2H), 2.30 – 2.17 (m, 2H), 2.10 (d,  $J = 10.4$  Hz, 3H), 1.54 – 1.42 (m, 4H), 1.32 (q,  $J = 7.6$  Hz, 3H), 1.14 (s, 6H).  $^{13}\text{C}$  NMR (126 MHz,  $\text{CDCl}_3$ )  $\delta$  193.4, 165.6, 150.9, 150.1, 149.5, 149.1, 143.4, 143.1, 142.1, 119.4, 117.3, 104.3, 99.9, 88.4, 69.6, 52.4, 37.8, 35.8 (2), 33.5 (2), 29.7, 29.7, 28.4 (2), 26.1, 13.5, 12.4. HRMS (ESI)  $m/z$   $[M+H]$  calculated for  $\text{C}_{28}\text{H}_{38}\text{N}_5\text{O}_2$ , 476.3026, found 476.3049.



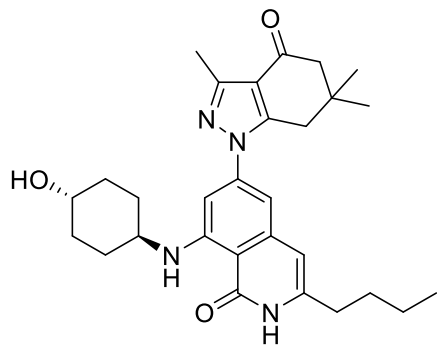
**8-(((1r,4r)-4-hydroxycyclohexyl)amino)-3-isopropyl-6-(3,6,6-trimethyl-4-oxo-4,5,6,7-tetrahydro-1H-indazol-1-yl)isoquinolin-1(2H)-one (4c):** 21 mg, Yield 65 %;  $^1\text{H}$  NMR (500 MHz, Chloroform-*d*)  $\delta$  11.01 – 10.60 (m, 1H), 9.29 (d,  $J = 7.4$  Hz, 1H), 6.59 (d,  $J = 2.0$  Hz, 1H),

6.52 (d,  $J = 1.9$  Hz, 1H), 6.21 (d,  $J = 1.8$  Hz, 1H), 3.79-3.70 (m, 1H), 3.47-3.38 (m, 1H), 2.88 – 2.77 (m, 3H), 2.56 (s, 3H), 2.41 (s, 2H), 2.25 – 2.18 (m, 2H), 2.10 – 2.04 (m, 2H), 1.52 – 1.38 (m, 4H), 1.34 (d,  $J = 6.9$  Hz, 6H), 1.11 (s, 6H).  $^{13}\text{C}$  NMR (126 MHz, Chloroform- $d$ )  $\delta$  193.6, 166.8 – 165.9 (m), 151.3 (d,  $J = 15.4$  Hz), 149.9, 149.2, 147.6 (d,  $J = 17.2$  Hz), 143.1, 142.2, 117.1, 107.6 (d,  $J = 2.7$  Hz), 105.1 (d,  $J = 2.7$  Hz), 102.9 (t,  $J = 2.6$  Hz), 100.1, 69.7, 52.4, 50.1 (d,  $J = 11.0$  Hz), 37.7, 35.9, 33.6 (2), 31.9 (d,  $J = 6.7$  Hz), 30.2 (2), 28.4 (2), 21.4 (2), 13.48. HRMS (ESI)  $m/z$  [M+Na] calculated for  $\text{C}_{28}\text{H}_{37}\text{N}_4\text{O}_3\text{Na}$ , 499.2685, found 499.2672.

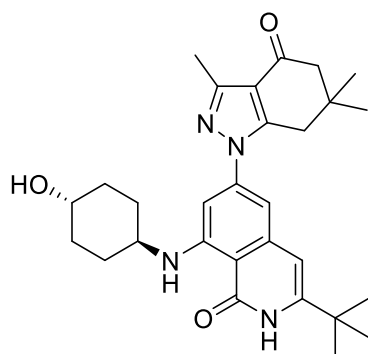


**8-(((1r,4r)-4-hydroxycyclohexyl)amino)-3-propyl-6-(3,6,6-trimethyl-4-oxo-4,5,6,7-**

**tetrahydro-1H-indazol-1-yl)isoquinolin-1(2H)-one (4d):** 22 mg, Yield 65%;  $^1\text{H}$  NMR (500 MHz, Chloroform- $d$ )  $\delta$  10.44 (s, 1H), 9.29 (d,  $J = 7.4$  Hz, 1H), 6.56 (dd,  $J = 41.9, 1.9$  Hz, 2H), 6.21 (d,  $J = 1.9$  Hz, 1H), 3.80-3.73 (m, 1H), 3.47-3.38 (m, 1H), 2.87 (s, 2H), 2.58 (s, 3H), 2.54 (t,  $J = 7.5$  Hz, 2H), 2.43 (s, 2H), 2.28 – 2.20 (m, 2H), 2.12 – 2.03 (m, 2H), 1.76 (h,  $J = 7.4$  Hz, 2H), 1.55-1.36 (m, 4H), 1.13 (s, 6H), 1.01 (t,  $J = 7.3$  Hz, 3H).  $^{13}\text{C}$  NMR (126 MHz, Chloroform- $d$ )  $\delta$  193.5, 166.3, 151.4, 149.9, 149.1, 143.1, 142.2, 141.9, 117.2, 107.5, 105.4, 104.9, 100.0, 69.8, 52.4, 50.2, 37.7, 35.9, 34.8, 33.6 (2), 30.1 (2), 28.4 (2), 21.3, 13.5, 13.5. HRMS (ESI)  $m/z$  [M+Na] calculated for  $\text{C}_{28}\text{H}_{36}\text{N}_4\text{O}_3\text{Na}$ , 499.2685, found 499.2688.

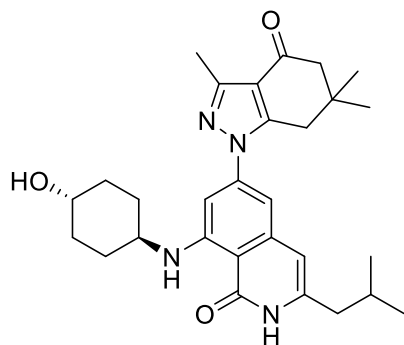


**3-butyl-8-(((1r,4r)-4-hydroxycyclohexyl)amino)-6-(3,6,6-trimethyl-4-oxo-4,5,6,7-tetrahydro-1H-indazol-1-yl)isoquinolin-1(2H)-one (4e):** 20 mg, Yield 58%;  $^1\text{H}$  NMR (500 MHz, Chloroform-*d*)  $\delta$  10.21 (s, 1H), 9.27 (d,  $J = 7.5$  Hz, 1H), 6.55 (dd,  $J = 39.0, 1.9$  Hz, 2H), 6.20 (d,  $J = 2.0$  Hz, 1H), 3.79-3.72 (m, , 1H), 3.47-3.37 (m, 1H), 2.87 (s, 2H), 2.60-2.52 (m, 5H), 2.42 (s, 2H), 2.26 – 2.19 (m, 2H), 2.11 – 2.05 (m, 2H), 1.74 – 1.64 (m, 2H), 1.54 – 1.32 (m, 6H), 1.12 (s, 6H), 0.96 (t,  $J = 7.3$  Hz, 3H).  $^{13}\text{C}$  NMR (126 MHz, Chloroform-*d*)  $\delta$  193.5, 166.1, 151.4, 149.9, 149.1, 143.1, 142.2, 142.1, 117.2, 107.5, 105.2, 104.9, 100.1, 69.8, 52.4, 50.2, 37.7, 35.8, 33.7 (2), 32.6, 30.1 (2), 30.0, 28.4 (2), 22.1, 13.9, 13.5. HRMS (ESI)  $m/z$   $[\text{M}+\text{H}]$  calculated for  $\text{C}_{29}\text{H}_{39}\text{N}_4\text{O}_3$ , 491.3022, found 491.3011.

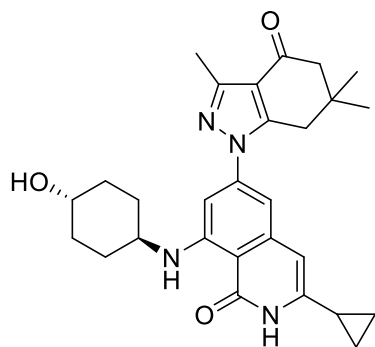


**3-(tert-butyl)-8-(((1r,4r)-4-hydroxycyclohexyl)amino)-6-(3,6,6-trimethyl-4-oxo-4,5,6,7-tetrahydro-1H-indazol-1-yl)isoquinolin-1(2H)-one (4f):** 22 mg, Yield 65%;  $^1\text{H}$  NMR (500 MHz, Chloroform-*d*)  $\delta$  9.53 (s, 1H), 9.28 (d,  $J = 6.9$  Hz, 1H), 6.68 – 6.51 (m, 2H), 6.27 (d,  $J = 2.1$

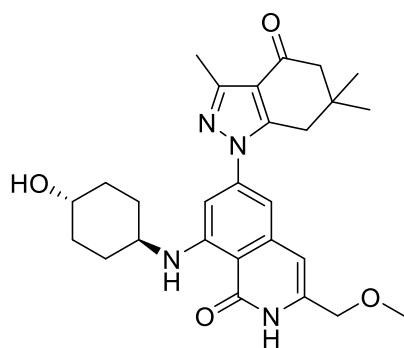
Hz, 1H), 3.80-3.73 (m, 1H), 3.47-3.43 (m, 1H), 2.88 (s, 2H), 2.58 (s, 3H), 2.43 (s, 2H), 2.25 – 2.18 (m, 2H), 2.13 – 2.06 (m, 2H), 1.53 – 1.40 (m, 4H), 1.38 (s, 9H), 1.13 (s, 6H). <sup>13</sup>C NMR (126 MHz, Chloroform-*d*) δ 193.5, 165.7, 150.9, 150.0, 149.3, 149.1, 143.2, 141.9, 117.2, 107.6, 105.8, 102.3, 100.7, 69.8, 52.4, 50.6, 37.8, 35.9, 34.3, 33.7 (2), 30.1 (2), 28.9 (3), 28.4 (2), 13.5. HRMS (ESI) *m/z* [M+Na] calculated for C<sub>29</sub>H<sub>38</sub>N<sub>4</sub>O<sub>3</sub>Na, 513.2842, found 513.2821.



**8-(((1*r*,4*r*)-4-hydroxycyclohexyl)amino)-3-isobutyl-6-(3,6,6-trimethyl-4-oxo-4,5,6,7-tetrahydro-1H-indazol-1-yl)isoquinolin-1(2H)-one (4g):** 19 mg, Yield 55%; <sup>1</sup>H NMR (500 MHz, Chloroform-*d*) δ 9.57 (s, 1H), 9.24 (d, *J* = 7.5 Hz, 1H), 6.60 (d, *J* = 1.9 Hz, 1H), 6.50 (d, *J* = 1.9 Hz, 1H), 6.17 (d, *J* = 2.0 Hz, 1H), 3.80-3.72 (m, 1H), 3.46-3.37 (m, 1H), 2.87 (s, 2H), 2.63 (s, 4H), 2.42 (s, 2H), 2.39 (d, *J* = 7.4 Hz, 2H), 2.23 (dd, *J* = 9.4, 5.0 Hz, 2H), 2.11 – 1.97 (m, 3H), 1.53 – 1.39 (m, 4H), 1.12 (s, 6H), 0.99 (d, *J* = 6.6 Hz, 6H). <sup>13</sup>C NMR (126 MHz, Chloroform-*d*) δ 193.5, 165.9, 151.4, 150.0, 149.1, 143.1, 142.0, 141.0, 117.2, 107.5, 106.1, 105.0, 100.1, 69.8, 52.4, 50.3, 42.4, 37.7, 35.8, 33.7 (2), 30.1 (2), 28.4, 27.9 (2), 22.3 (2), 13.5. HRMS (ESI) *m/z* [M+H] calculated for C<sub>29</sub>H<sub>39</sub>N<sub>4</sub>O<sub>3</sub>, 491.3022, found 491.3019.



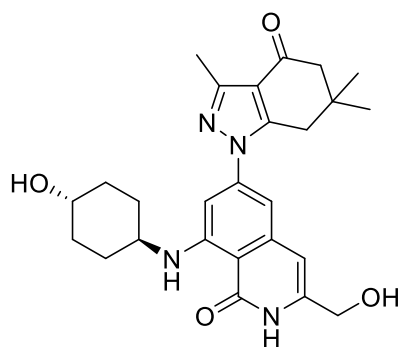
**3-cyclopropyl-8-(((1r,4r)-4-hydroxycyclohexyl)amino)-6-(3,6,6-trimethyl-4-oxo-4,5,6,7-tetrahydro-1H-indazol-1-yl)isoquinolin-1(2H)-one (4h):** 22 mg, Yield 66%;  $^1\text{H}$  NMR (500 MHz, Chloroform-*d*)  $\delta$  9.67 (s, 1H), 9.26 (d,  $J = 7.2$  Hz, 1H), 6.58 (d,  $J = 1.9$  Hz, 1H), 6.53 (d,  $J = 2.0$  Hz, 1H), 6.15 (d,  $J = 1.9$  Hz, 1H), 3.80-3.73 (m, 1H), 3.48 – 3.39 (m, 1H), 2.88 (s, 2H), 2.59 (s, 3H), 2.44 (s, 2H), 2.26 – 2.18 (m, 2H), 2.12 – 2.04 (m, 2H), 1.87 – 1.78 (m, 1H), 1.55 – 1.38 (m, 4H), 1.14 (s, 6H), 1.04 – 0.99 (m, 2H), 0.95 – 0.90 (m, 2H).  $^{13}\text{C}$  NMR (126 MHz, Chloroform-*d*)  $\delta$  193.5, 165.7, 150.0, 149.1, 143.2, 143.2, 142.0, 117.2, 107.5, 105.0, 103.4, 100.2, 69.8, 52.4, 50.3, 37.7, 35.8, 33.7 (2), 30.0 (2), 28.4 (2), 13.5, 13.4, 7.1 (2). HRMS (ESI)  $m/z$  [M+H] calculated for  $\text{C}_{28}\text{H}_{35}\text{N}_4\text{O}_3$ , 475.2709, found 475.2698.



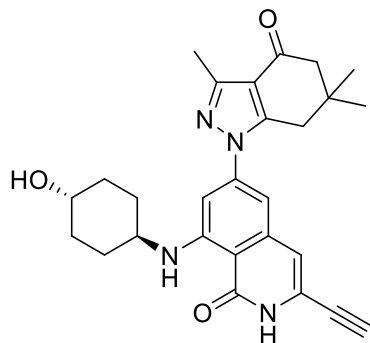
**8-(((1r,4r)-4-hydroxycyclohexyl)amino)-3-(methoxymethyl)-6-(3,6,6-trimethyl-4-oxo-4,5,6,7-tetrahydro-1H-indazol-1-yl)isoquinolin-1(2H)-one (4i):** 20 mg, Yield 60%;  $^1\text{H}$  NMR (400 MHz, Chloroform-*d*)  $\delta$  9.27 (d,  $J = 7.5$  Hz, 1H), 8.63 (s, 1H), 6.62 (d,  $J = 1.8$  Hz, 1H), 6.56



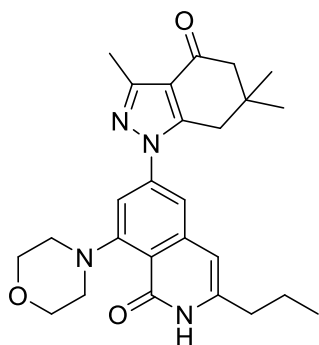
(s, 1H), 6.25 (s, 1H), 4.32 (s, 2H), 3.42 (s, 3H), 2.86 (s, 2H), 2.57 (s, 3H), 2.42 (s, 2H), 2.21 (s, 2H), 2.07 (s, 2H), 1.49 (q,  $J = 11.9, 10.3$  Hz, 4H), 1.12 (s, 6H).  $^{13}\text{C}$  NMR (101 MHz,  $\text{CDCl}_3$ )  $\delta$  193.3, 164.9, 151.5, 150.0, 149.0, 143.2, 141.2, 137.1, 117.3, 108.4, 105.3, 105.1, 101.0, 70.2, 69.7, 58.4, 52.4, 50.3, 37.8, 35.8, 33.5 (2), 29.9 (2), 28.4 (2), 13.4. HRMS (ESI)  $m/z$   $[\text{M}+\text{H}]$  calculated for  $\text{C}_{27}\text{H}_{35}\text{N}_4\text{O}_4$ , 479.2658, found 479.2665.



**8-(((1r,4r)-4-hydroxycyclohexyl)amino)-3-(hydroxymethyl)-6-(3,6,6-trimethyl-4-oxo-4,5,6,7-tetrahydro-1H-indazol-1-yl)isoquinolin-1(2H)-one (4j):** 20 mg, Yield 63 %;  $^1\text{H}$  NMR (400 MHz, Chloroform-*d*)  $\delta$  9.31 (s, 1H), 9.19 (d,  $J = 7.4$  Hz, 1H), 6.53 (dd,  $J = 16.9, 1.8$  Hz, 2H), 6.22 (s, 1H), 4.49 (s, 2H), 3.79 – 3.64 (m, 1H), 3.40 (d,  $J = 16.0$  Hz, 1H), 2.83 (s, 2H), 2.55 (s, 3H), 2.40 (s, 2H), 2.19 (d,  $J = 11.2$  Hz, 2H), 2.09 – 2.00 (m, 2H), 1.44 (dd,  $J = 18.9, 9.5$  Hz, 4H), 1.10 (s, 6H).  $^{13}\text{C}$  NMR (101 MHz,  $\text{CDCl}_3$ )  $\delta$  193.6, 172.2, 151.4, 150.1, 149.3, 143.1, 141.5, 139.9, 117.2, 108.2, 105.4, 103.9, 100.8, 69.5, 60.7, 52.3, 50.2, 37.7, 35.8, 33.4 (2), 29.9 (2), 28.3 (2), 13.3. HRMS (ESI)  $m/z$   $[\text{M}+\text{H}]$  calculated for  $\text{C}_{26}\text{H}_{33}\text{N}_4\text{O}_4$ , 465.2502, found 465.2501.

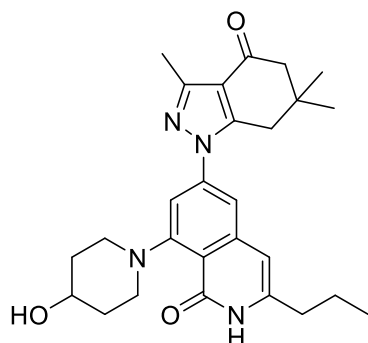


**3-ethynyl-8-(((1r,4r)-4-hydroxycyclohexyl)amino)-6-(3,6,6-trimethyl-4-oxo-4,5,6,7-tetrahydro-1H-indazol-1-yl)isoquinolin-1(2H)-one (4k):** 11 mg, Yield 35%;  $^1\text{H}$  NMR (400 MHz, Chloroform-*d*)  $\delta$  9.09 (d,  $J = 7.2$  Hz, 1H), 8.06 (s, 1H), 6.57-6.52 (m, 3H), 3.69 (s, 2H), 3.31 (d,  $J = 22.1$  Hz, 2H), 3.23 (s, 1H), 2.78 (s, 2H), 2.49 (s, 3H), 2.35 (s, 2H), 2.13 (s, 2H), 1.98 (s, 2H), 1.39 (d,  $J = 4.7$  Hz, 4H), 1.05 (s, 6H).  $^{13}\text{C}$  NMR (101 MHz,  $\text{CDCl}_3$ )  $\delta$  199.1, 167.6, 167.3, 157.5, 153.7, 152.0, 148.1, 132.0, 131.3, 126.4, 121.3, 107.4, 97.5, 77.2, 76.8, 72.7, 52.5, 48.7, 42.8, 36.5, 36.2, 34.3 (2), 31.2 (2), 23.5 (2). HRMS (ESI)  $m/z$  [M+H] calculated for  $\text{C}_{27}\text{H}_{31}\text{N}_4\text{O}_3$ , 459.2396, found 459.2375.

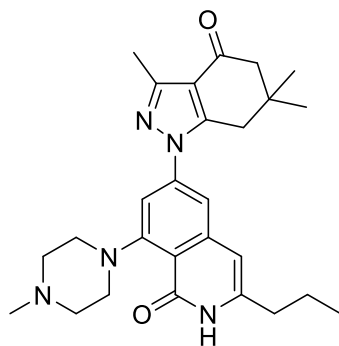


**8-morpholino-3-propyl-6-(3,6,6-trimethyl-4-oxo-4,5,6,7-tetrahydro-1H-indazol-1-yl)isoquinolin-1(2H)-one (5a):** 20 mg, Yield 65%;  $^1\text{H}$  NMR (400 MHz, Chloroform-*d*)  $\delta$  9.53 (s, 1H), 7.07 (dd,  $J = 18.7, 1.9$  Hz, 2H), 6.25 (s, 1H), 4.00 (t,  $J = 4.5$  Hz, 4H), 3.22 (s, 4H), 2.86 (s, 2H), 2.57 (s, 5H), 2.43 (s, 2H), 1.76 (h,  $J = 7.4$  Hz, 2H), 1.12 (s, 6H), 1.03 (t,  $J = 7.3$  Hz, 3H).  $^{13}\text{C}$

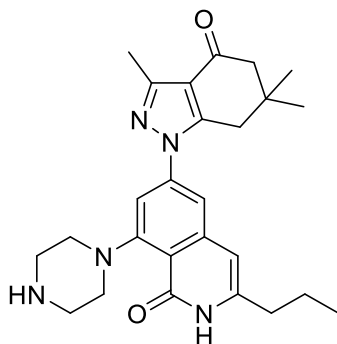
NMR (126 MHz, CDCl<sub>3</sub>)  $\delta$  193.4, 162.1, 155.4, 150.4, 149.1, 143.1, 142.8, 141.9, 117.5, 115.4, 112.9, 109.7, 104.3, 67.2 (2), 53.4 (2), 52.4, 37.6, 35.9, 34.8, 28.4 (2), 21.2, 13.5, 13.5. HRMS (ESI)  $m/z$  [M+H] calculated for C<sub>26</sub>H<sub>33</sub>N<sub>4</sub>O<sub>3</sub>, 449.2553, found 449.2557.



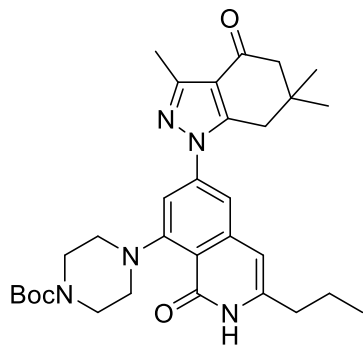
**8-(4-hydroxypiperidin-1-yl)-3-propyl-6-(3,6,6-trimethyl-4-oxo-4,5,6,7-tetrahydro-1H-indazol-1-yl)isoquinolin-1(2H)-one (5b):** 18 mg, Yield 55%; <sup>1</sup>H NMR (500 MHz, Chloroform-*d*)  $\delta$  9.03 (s, 1H), 6.98 (d, *J* = 3.3 Hz, 2H), 6.15 (s, 1H), 3.86 (s, 1H), 3.41 (s, 2H), 2.87 (s, 2H), 2.78 (s, 2H), 2.52-2.44 (m, 5H), 2.35 (s, 2H), 2.12-2.03 (m, 2H), 1.92-1.81 (m, 2H), 1.67 (h, *J* = 7.4 Hz, 2H), 1.05 (s, 6H), 0.95 (t, *J* = 7.4 Hz, 3H). <sup>13</sup>C NMR (126 MHz, CDCl<sub>3</sub>)  $\delta$  193.5, 162.0, 155.8, 150.3, 149.1, 142.9, 142.4, 141.8, 117.4, 115.5, 112.4, 110.1, 104.2, 53.4, 52.4 (2), 37.6, 35.9, 34.9 (2), 30.9, 29.7, 28.4 (2), 21.1, 13.5, 13.5. HRMS (ESI)  $m/z$  [M+H] calculated for C<sub>27</sub>H<sub>35</sub>N<sub>4</sub>O<sub>3</sub>, 463.2709, found 463.2710.



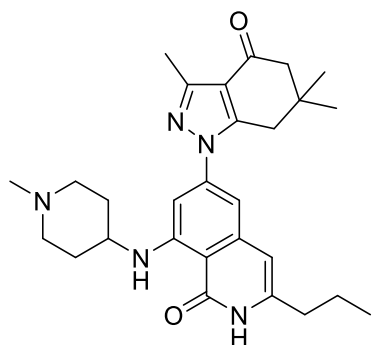
**8-(4-methylpiperazin-1-yl)-3-propyl-6-(3,6,6-trimethyl-4-oxo-4,5,6,7-tetrahydro-1H-indazol-1-yl)isoquinolin-1(2H)-one (5c):** 18 mg, Yield 55%; <sup>1</sup>H NMR (400 MHz, Chloroform-*d*) δ 9.56 (s, 1H), 9.35 (d, *J* = 7.3 Hz, 1H), 6.55 (dd, *J* = 26.8, 2.0 Hz, 2H), 6.19 (d, *J* = 1.9 Hz, 1H), 2.87 (s, 2H), 2.80 (s, 1H), 2.57 (s, 3H), 2.52 (t, *J* = 7.4 Hz, 2H), 2.43 (s, 2H), 2.33 (s, 3H), 2.26 (t, *J* = 10.5 Hz, 2H), 2.16 – 2.08 (m, 2H), 1.79 – 1.58 (m, 7H), 1.13 (s, 6H), 1.01 (t, *J* = 7.4 Hz, 3H). <sup>13</sup>C NMR (101 MHz, CDCl<sub>3</sub>) δ 193.5, 165.8, 151.2, 149.9, 149.0, 143.1, 142.1, 141.6, 140.8, 107.7, 105.3, 105.0, 100.2, 52.4, 46.3, 37.7, 35.8, 34.9 (2), 32.1, 31.6, 31.4, 28.4 (2), 21.2 (2), 13.5, 13.4. HRMS (ESI) *m/z* [M+Na] calculated for C<sub>28</sub>H<sub>37</sub>N<sub>5</sub>O<sub>2</sub>Na, 498.2845, found 498.2823.



**8-(piperazin-1-yl)-3-propyl-6-(3,6,6-trimethyl-4-oxo-4,5,6,7-tetrahydro-1H-indazol-1-yl)isoquinolin-1(2H)-one (5d):** 14 mg, Yield 45%; <sup>1</sup>H NMR (400 MHz, Chloroform-*d*) δ 9.59 (s, 1H), 6.99 (dd, *J* = 26.4, 2.1 Hz, 2H), 6.17 (s, 1H), 3.13 (s, 6H), 2.79 (s, 2H), 2.50 (s, 5H), 2.35 (s, 2H), 2.27 – 2.01 (m, 2H), 1.68 (h, *J* = 7.4 Hz, 2H), 1.05 (s, 6H), 0.95 (t, *J* = 7.3 Hz, 3H). <sup>13</sup>C NMR (126 MHz, CDCl<sub>3</sub>) δ 193.4, 161.7, 155.8, 150.3, 149.1, 143.0, 142.2, 141.9, 117.4, 115.5, 112.7, 109.8, 104.3, 54.3, 52.4 (2), 46.1 (2), 37.6, 35.9, 34.9, 28.5 (2), 21.2, 13.5, 13.5. HRMS (ESI) *m/z* [M+H] calculated for C<sub>26</sub>H<sub>34</sub>N<sub>5</sub>O<sub>2</sub>, 448.2713, found 448.2706.

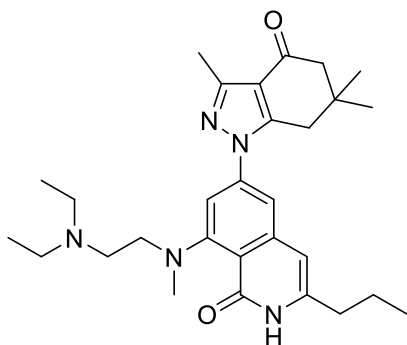


**tert-butyl 4-(1-oxo-3-propyl-6-(3,6,6-trimethyl-4-oxo-4,5,6,7-tetrahydro-1H-indazol-1-yl)-1,2-dihydroisoquinolin-8-yl)piperazine-1-carboxylate (5e):** 20 mg, Yield 53%;  $^1\text{H}$  NMR (500 MHz, Chloroform-*d*)  $\delta$  8.93 (s, 1H), 7.01 (d,  $J = 2.0$  Hz, 1H), 6.96 (d,  $J = 2.1$  Hz, 1H), 6.16 (d,  $J = 2.0$  Hz, 1H), 3.75 (s, 4H), 3.08 (s, 4H), 2.79 (s, 2H), 2.51 – 2.43 (m, 5H), 2.35 (s, 2H), 1.66 (h,  $J = 7.4$  Hz, 2H), 1.42 (s, 9H), 1.05 (s, 6H), 0.94 (t,  $J = 7.3$  Hz, 3H).  $^{13}\text{C}$  NMR (126 MHz,  $\text{CDCl}_3$ )  $\delta$  193.4, 161.8, 155.4, 154.9, 150.4, 149.1, 143.0, 142.5, 141.9, 117.5, 115.6, 112.9, 110.0, 104.2, 79.8, 53.0 (2), 52.4 (2), 37.6, 35.9, 34.9, 31.6, 28.5 (4), 21.1, 13.5, 13.5. HRMS (ESI)  $m/z$  [M+H] calculated for  $\text{C}_{31}\text{H}_{42}\text{N}_5\text{O}_4$ , 548.3237, found 548.3226.



**8-((1-methylpiperidin-4-yl)amino)-3-propyl-6-(3,6,6-trimethyl-4-oxo-4,5,6,7-tetrahydro-1H-indazol-1-yl)isoquinolin-1(2H)-one (5f):** 13 mg, Yield 40 %;  $^1\text{H}$  NMR (400 MHz, Chloroform-*d*)  $\delta$  9.56 (s, 1H), 9.35 (d,  $J = 7.3$  Hz, 1H), 6.55 (dd,  $J = 26.8, 2.0$  Hz, 2H), 6.19 (d,  $J = 1.9$  Hz, 1H), 2.87 (s, 2H), 2.80 (s, 1H), 2.57 (s, 3H), 2.52 (t,  $J = 7.4$  Hz, 2H), 2.43 (s, 2H), 2.33 (s, 3H),

2.26 (t,  $J = 10.5$  Hz, 2H), 2.16 – 2.08 (m, 2H), 1.79 – 1.58 (m, 7H), 1.13 (s, 6H), 1.01 (t,  $J = 7.4$  Hz, 3H).  $^{13}\text{C}$  NMR (101 MHz,  $\text{CDCl}_3$ )  $\delta$  193.5, 165.8, 151.3, 149.9, 149.1, 143.1, 142.1, 141.6, 140.8, 107.6, 105.3, 105.0, 100.2, 52.4, 46.3, 37.7, 35.8, 34.9 (2), 32.1, 31.6, 31.4, 28.4 (2), 21.2 (2), 13.5, 13.4. HRMS (ESI)  $m/z$   $[\text{M}+\text{Na}]$  calculated for  $\text{C}_{28}\text{H}_{37}\text{N}_5\text{O}_2\text{Na}$ , 498.2845, found 498.2823.



**8-((2-(diethylamino)ethyl)(methyl)amino)-3-propyl-6-(3,6,6-trimethyl-4-oxo-4,5,6,7-**

**tetrahydro-1H-indazol-1-yl)isoquinolin-1(2H)-one (5g):** 14 mg, Yield 45%;  $^1\text{H}$  NMR (500 MHz, Chloroform-*d*)  $\delta$  9.22 (s, 1H), 7.02 (dd,  $J = 16.0, 2.0$  Hz, 2H), 6.21 (s, 1H), 3.44 – 3.37 (m, 2H), 3.02 (s, 3H), 2.86 (s, 2H), 2.77 (t,  $J = 7.4$  Hz, 2H), 2.57 (s, 3H), 2.56-2.48 (m, 6H), 2.42 (s, 2H), 1.81 – 1.71 (m, 2H), 1.12 (s, 6H), 1.03 (t,  $J = 7.3$  Hz, 3H), 0.97 (t,  $J = 7.1$  Hz, 6H).  $^{13}\text{C}$  NMR (126 MHz,  $\text{CDCl}_3$ )  $\delta$  193.5, 162.0, 155.2, 150.1, 149.1, 142.9, 141.5, 117.3, 114.5, 111.4, 110.0, 104.3, 55.5, 52.4, 50.4, 47.3 (2), 41.7, 37.5, 35.9, 35.0, 29.9, 28.4 (2), 21.2, 13.6, 13.5 (2), 11.7. HRMS (ESI)  $m/z$   $[\text{M}+\text{H}]$  calculated for  $\text{C}_{29}\text{H}_{42}\text{N}_5\text{O}_2$ , 492.3338, found 492.3352.

## II.8 References

1. Chen, B.; Piel, W. H.; Gui, L.; Bruford, E.; Monteiro, A. The HSP90 family of genes in the human genome: insights into their divergence and evolution. *Genomics* **2005**, *86*, 627-37.
2. Subbarao Sreedhar, A.; Kalmár, É.; Csermely, P.; Shen, Y.-F. Hsp90 isoforms: functions, expression and clinical importance. *FEBS Lett.* **2004**, *562*, 11-15.

3. Milicevic, Z.; Bogojevic, D.; Mihailovic, M.; Petrovic, M.; Krivokapic, Z. Molecular characterization of hsp90 isoforms in colorectal cancer cells and its association with tumour progression. *Int. J. Oncol.* **2008**, *32*, 1169-78.
4. Liu, W.; Vielhauer, G. A.; Holzbeierlein, J. M.; Zhao, H.; Ghosh, S.; Brown, D.; Lee, E.; Blagg, B. S. KU675, a Concomitant Heat-Shock Protein Inhibitor of Hsp90 and Hsc70 that Manifests Isoform Selectivity for Hsp90alpha in Prostate Cancer Cells. *Mol. Pharmacol.* **2015**, *88*, 121-30.
5. Wang, Q.; He, Z.; Zhang, J.; Wang, Y.; Wang, T.; Tong, S.; Wang, L.; Wang, S.; Chen, Y. Overexpression of endoplasmic reticulum molecular chaperone GRP94 and GRP78 in human lung cancer tissues and its significance. *Cancer Detect. Prev.* **2005**, *29*, 544-51.
6. Li, C. F.; Huang, W. W.; Wu, J. M.; Yu, S. C.; Hu, T. H.; Uen, Y. H.; Tian, Y. F.; Lin, C. N.; Lu, D.; Fang, F. M.; Huang, H. Y. Heat shock protein 90 overexpression independently predicts inferior disease-free survival with differential expression of the alpha and beta isoforms in gastrointestinal stromal tumors. *Clin. Cancer. Res.* **2008**, *14*, 7822-31.
7. Gao, Y.; Yechikov, S.; Vazquez, A. E.; Chen, D.; Nie, L. Distinct roles of molecular chaperones HSP90alpha and HSP90beta in the biogenesis of KCNQ4 channels. *PLoS One* **2013**, *8*, e57282.
8. Karagoz, G. E.; Rudiger, S. G. Hsp90 interaction with clients. *Trends Biochem. Sci* **2015**, *40*, 117-25.
9. Prince, T. L.; Kijima, T.; Tatokoro, M.; Lee, S.; Tsutsumi, S.; Yim, K.; Rivas, C.; Alarcon, S.; Schwartz, H.; Khamit-Kush, K.; Scroggins, B. T.; Beebe, K.; Trepel, J. B.; Neckers, L. Client Proteins and Small Molecule Inhibitors Display Distinct Binding Preferences for Constitutive and Stress-Induced HSP90 Isoforms and Their Conformationally Restricted Mutants. *PLoS One* **2015**, *10*, e0141786.
10. Peterson, L. B.; Eskew, J. D.; Vielhauer, G. A.; Blagg, B. S. The hERG channel is dependent upon the Hsp90alpha isoform for maturation and trafficking. *Mol. Pharm.* **2012**, *9*, 1841-6.
11. Ernst, J. T.; Liu, M.; Zuccola, H.; Neubert, T.; Beaumont, K.; Turnbull, A.; Kallel, A.; Vought, B.; Stamos, D. Correlation between chemotype-dependent binding conformations of HSP90alpha/beta and isoform selectivity-Implications for the structure-based design of HSP90alpha/beta selective inhibitors for treating neurodegenerative diseases. *Bioorg. Med. Chem. Lett.* **2014**, *24*, 204-8.
12. Khandelwal, A. Unfolding the Hsp90 Foldasome: Structure-Activity Relationship Studies on EGCG and Development of Isoform-Selective Inhibitors, Ph.D Dissertation, The University of Kansas. **2016**.
13. Didelot, C.; Lanneau, D.; Brunet, M.; Bouchot, A.; Cartier, J.; Jacquelin, A.; Ducoroy, P.; Cathelin, S.; Decolonne, N.; Chiosis, G.; Dubrez-Daloz, L.; Solary, E.; Garrido, C. Interaction of heat-shock protein 90 beta isoform (HSP90 beta) with cellular inhibitor of apoptosis 1 (c-IAP1) is required for cell differentiation. *Cell Death Differ.* **2008**, *15*, 859-66.
14. Shinozaki, F.; Minami, M.; Chiba, T.; Suzuki, M.; Yoshimatsu, K.; Ichikawa, Y.; Terasawa, K.; Emori, Y.; Matsumoto, K.; Kurosaki, T.; Nakai, A.; Tanaka, K.; Minami, Y. Depletion of hsp90beta induces multiple defects in B cell receptor signaling. *J. Biol. Chem.* **2006**, *281*, 16361-9.

15. Liu, X.; Ye, L.; Wang, J.; Fan, D. Expression of heat shock protein 90 beta in human gastric cancer tissue and SGC7901/VCR of MDR-type gastric cancer cell line. *Chin. Med. J. (Engl.)* **1999**, *112*, 1133-7.
16. Sreedhar, A. S.; Csermely, P. Heat shock proteins in the regulation of apoptosis: new strategies in tumor therapy: a comprehensive review. *Pharmacol. Ther.* **2004**, *101*, 227-57.
17. Gruppi, C. M.; Zakeri, Z. F.; Wolgemuth, D. J. Stage and lineage-regulated expression of two hsp90 transcripts during mouse germ cell differentiation and embryogenesis. *Mol. Reprod. Dev* **1991**, *28*, 209-17.
18. Dugyala, R. R.; Claggett, T. W.; Kimmel, G. L.; Kimmel, C. A. HSP90alpha, HSP90beta, and p53 expression following in vitro hyperthermia exposure in gestation day 10 rat embryos. *Toxicol. Sci.* **2002**, *69*, 183-90.
19. Cambiazo, V.; Gonzalez, M.; Isamit, C.; Maccioni, R. B. The beta-isoform of heat shock protein hsp-90 is structurally related with human microtubule-interacting protein Mip-90. *FEBS Lett.* **1999**, *457*, 343-7.
20. Zuehlke, A. D.; Beebe, K.; Neckers, L.; Prince, T. Regulation and function of the human HSP90AA1 gene. *Gene* **2015**, *570*, 8-16.
21. Yufu, Y.; Nishimura, J.; Nawata, H. High constitutive expression of heat shock protein 90 alpha in human acute leukemia cells. *Leuk. Res.* **1992**, *16*, 597-605.
22. Taipale, M.; Tucker, G.; Peng, J.; Krykbaeva, I.; Lin, Z. Y.; Larsen, B.; Choi, H.; Berger, B.; Gingras, A. C.; Lindquist, S. A quantitative chaperone interaction network reveals the architecture of cellular protein homeostasis pathways. *Cell* **2014**, *158*, 434-448.
23. Chadli, A.; Felts, S. J.; Toft, D. O. GCUNC45 Is the First Hsp90 Co-chaperone to Show  $\alpha/\beta$  Isoform Specificity. *J. Biol. Chem.* **2008**, *283*, 9509-9512.
24. Bertram, J.; Palfner, K.; Hiddemann, W.; Kneba, M. Increase of P-glycoprotein-mediated drug resistance by hsp 90b. *Anti-Cancer Drugs* **1996**, *7*, 838-845.
25. Nguyen, M. T. N.; Knieß, R. A.; Daturpalli, S.; Le Breton, L.; Ke, X.; Chen, X.; Mayer, M. P. Isoform-Specific Phosphorylation in Human Hsp90 $\beta$  Affects Interaction with Clients and the Cochaperone Cdc37. *J. Mol. Biol.* **2017**, *429*, 732-752.
26. Xiong, X.; Wang, Y.; Liu, C.; Lu, Q.; Liu, T.; Chen, G.; Rao, H.; Luo, S. Heat shock protein 90 $\beta$  stabilizes focal adhesion kinase and enhances cell migration and invasion in breast cancer cells. *Exp. Cell Res.* **2014**, *326*, 78-89.
27. Li, S.; Li, J.; Hu, T.; Zhang, C.; Lv, X.; He, S.; Yan, H.; Tan, Y.; Wen, M.; Lei, M.; Zuo, J. Bcl-2 overexpression contributes to laryngeal carcinoma cell survival by forming a complex with Hsp90beta. *Oncol. Rep.* **2017**, *37*, 849-856.
28. Meng, J.; Liu, Y.; Han, J.; Tan, Q.; Chen, S.; Qiao, K.; Zhou, H.; Sun, T.; Yang, C. Hsp90beta promoted endothelial cell-dependent tumor angiogenesis in hepatocellular carcinoma. *Mol. Cancer* **2017**, *16*, 72.
29. de la Mare, J.-A.; Jurgens, T.; Edkins, A. L. Extracellular Hsp90 and TGF $\beta$  regulate adhesion, migration and anchorage independent growth in a paired colon cancer cell line model. *BMC cancer* **2017**, *17*, 202.
30. Correia, A. L.; Mori, H.; Chen, E. I.; Schmitt, F. C.; Bissell, M. J. The hemopexin domain of MMP3 is responsible for mammary epithelial invasion and morphogenesis through extracellular interaction with HSP90beta. *Genes Dev* **2013**, *27*, 805-17.



31. Rong, B.; Zhao, C.; Liu, H.; Ming, Z.; Cai, X.; Gao, W.; Yang, S. Identification and verification of Hsp90-beta as a potential serum biomarker for lung cancer. *Am. J. Cancer Res.* **2014**, *4*, 874-885.
32. Rong, B.; Cai, X.; Liu, H.; Fu, T.; Gao, W.; Zhao, C.; Lin, Y. Increased level of Hsp90-beta in bronchoalveolar lavage fluid correlates with lymphatic invasion and advanced stage of lung cancer patients. *Am. J. Transl. Res* **2016**, *8*, 4147-4159.
33. Duerfeldt, A. S.; Peterson, L. B.; Maynard, J. C.; Ng, C. L.; Eletto, D.; Ostrovsky, O.; Shinogle, H. E.; Moore, D. S.; Argon, Y.; Nicchitta, C. V.; Blagg, B. S. J. Development of a Grp94 inhibitor. *J. Am. Chem. Soc.* **2012**, *134*, 9796-9804.
34. Patel, P. D.; Yan, P.; Seidler, P. M.; Patel, H. J.; Sun, W.; Yang, C.; Que, N. S.; Taldone, T.; Finotti, P.; Stephani, R. A.; Gewirth, D. T.; Chiosis, G. Paralog-selective Hsp90 inhibitors define tumor-specific regulation of HER2. *Nat. Chem. Biol.* **2013**, *9*, 677-84.
35. Mishra, S. J.; Ghosh, S.; Stothert, A. R.; Dickey, C. A.; Blagg, B. S. Transformation of the Non-Selective Aminocyclohexanol-Based Hsp90 Inhibitor into a Grp94-Selective Scaffold. *ACS Chem. Biol.* **2017**, *12*, 244-253.
36. Lavery, L. A.; Partridge, J. R.; Ramelot, T. A.; Elnatan, D.; Kennedy, M. A.; Agard, D. A. Structural asymmetry in the closed state of mitochondrial Hsp90 (TRAP1) supports a two-step ATP hydrolysis mechanism. *Mol. Cell* **2014**, *53*, 330-43.
37. Davies, N. G.; Browne, H.; Davis, B.; Drysdale, M. J.; Foloppe, N.; Geoffrey, S.; Gibbons, B.; Hart, T.; Hubbard, R.; Jensen, M. R.; Mansell, H.; Massey, A.; Matassova, N.; Moore, J. D.; Murray, J.; Pratt, R.; Ray, S.; Robertson, A.; Roughley, S. D.; Schoepfer, J.; Scriven, K.; Simmonite, H.; Stokes, S.; Surgenor, A.; Webb, P.; Wood, M.; Wright, L.; Brough, P. Targeting conserved water molecules: design of 4-aryl-5-cyanopyrrolo[2,3-d]pyrimidine Hsp90 inhibitors using fragment-based screening and structure-based optimization. *Bioorg. Med. Chem.* **2012**, *20*, 6770-89.
38. Patel, H. J.; Modi, S.; Chiosis, G.; Taldone, T. Advances in the discovery and development of heat-shock protein 90 inhibitors for cancer treatment. *Expert Opin. Drug Discov* **2011**, *6*, 559-587.
39. Haystead, T.; Hughes, P. F. Compounds and methods for targeting hsp90. WO/2014/025395, Feb 13: **2014**.
40. Ernst, J. T.; Neubert, T.; Liu, M.; Sperry, S.; Zuccola, H.; Turnbull, A.; Fleck, B.; Kargo, W.; Woody, L.; Chiang, P.; Tran, D.; Chen, W.; Snyder, P.; Alcacio, T.; Nezami, A.; Reynolds, J.; Alvi, K.; Goulet, L.; Stamos, D. Identification of novel HSP90alpha/beta isoform selective inhibitors using structure-based drug design. demonstration of potential utility in treating CNS disorders such as Huntington's disease. *J. Med. Chem.* **2014**, *57*, 3382-400.
41. Xia, M.; Zhang, T.; Wang, Y.; Xing, G. Tetrahydroindole derivatives and tetrahydroindazole derivatives, and use thereof. WO2006133634: **2006**.
42. Jensen, M. R.; Schoepfer, J.; Radimerski, T.; Massey, A.; Guy, C. T.; Brueggen, J.; Quadt, C.; Buckler, A.; Cozens, R.; Drysdale, M. J.; Garcia-Echeverria, C.; Chène, P. NVP-AUY922: a small molecule HSP90 inhibitor with potent antitumor activity in preclinical breast cancer models. *Breast Cancer Res.* **2008**, *10*, R33.
43. Graham, B.; Curry, J.; Smyth, T.; Fazal, L.; Feltell, R.; Harada, I.; Coyle, J.; Williams, B.; Reule, M.; Angove, H.; Cross, D. M.; Lyons, J.; Wallis, N. G.; Thompson, N. T. The heat shock protein 90 inhibitor, AT13387, displays a long duration of action in vitro and in vivo in non-small cell lung cancer. *Cancer Sci.* **2012**, *103*, 522-7.

44. Guancial, E. A.; Werner, L.; Bellmunt, J.; Bamias, A.; Choueiri, T. K.; Ross, R.; Schutz, F. A.; Park, R. S.; O'Brien, R. J.; Hirsch, M. S.; Barletta, J. A.; Berman, D. M.; Lis, R.; Loda, M.; Stack, E. C.; Garraway, L. A.; Riester, M.; Michor, F.; Kantoff, P. W.; Rosenberg, J. E. FGFR3 expression in primary and metastatic urothelial carcinoma of the bladder. *Cancer Medicine* **2014**, *3*, 835-844.
45. Pouessel, D.; Neuzillet, Y.; Mertens, L. S.; van der Heijden, M. S.; de Jong, J.; Sanders, J.; Peters, D.; Leroy, K.; Manceau, A.; Maille, P.; Soyeux, P.; Moktefi, A.; Semprez, F.; Vordos, D.; de la Taille, A.; Hurst, C. D.; Tomlinson, D. C.; Harnden, P.; Bostrom, P. J.; Mirtti, T.; Horenblas, S.; Llorca, Y.; Houédé, N.; Chevreau, C.; Beuzeboc, P.; Shariat, S. F.; Sagalowsky, A. I.; Ashfaq, R.; Burger, M.; Jewett, M. A. S.; Zlotta, A. R.; Broeks, A.; Bapat, B.; Knowles, M. A.; Lotan, Y.; van der Kwast, T. H.; Culine, S.; Allory, Y.; van Rhijn, B. W. G. Tumor heterogeneity of fibroblast growth factor receptor 3 (FGFR3) mutations in invasive bladder cancer: implications for perioperative anti-FGFR3 treatment. *Ann. Oncol.* **2016**, *27*, 1311-1316.
46. Laederich, M. B.; Degnin, C. R.; Lunstrum, G. P.; Holden, P.; Horton, W. A. Fibroblast growth factor receptor 3 (FGFR3) is a strong heat shock protein 90 (Hsp90) client: implications for therapeutic manipulation. *J. Biol. Chem.* **2011**, *286*, 19597-604.
47. Slamon, D. J.; Clark, G. M.; Wong, S. G.; Levin, W. J.; Ullrich, A.; McGuire, W. L. Human breast cancer: correlation of relapse and survival with amplification of the HER-2/neu oncogene. *Science* **1987**, *235*, 177-82.
48. Stern, D. F.; Heffernan, P. A.; Weinberg, R. A. p185, a product of the neu proto-oncogene, is a receptorlike protein associated with tyrosine kinase activity. *Mol. Cell. Biol.* **1986**, *6*, 1729-40.
49. Moasser, M. M. The oncogene HER2; Its signaling and transforming functions and its role in human cancer pathogenesis. *Oncogene* **2007**, *26*, 6469-6487.

## Chapter III

### Development of Hsp90 $\alpha$ -Selective Inhibitors

#### III.1 Hsp90 $\alpha$ and its Significance in Cancer

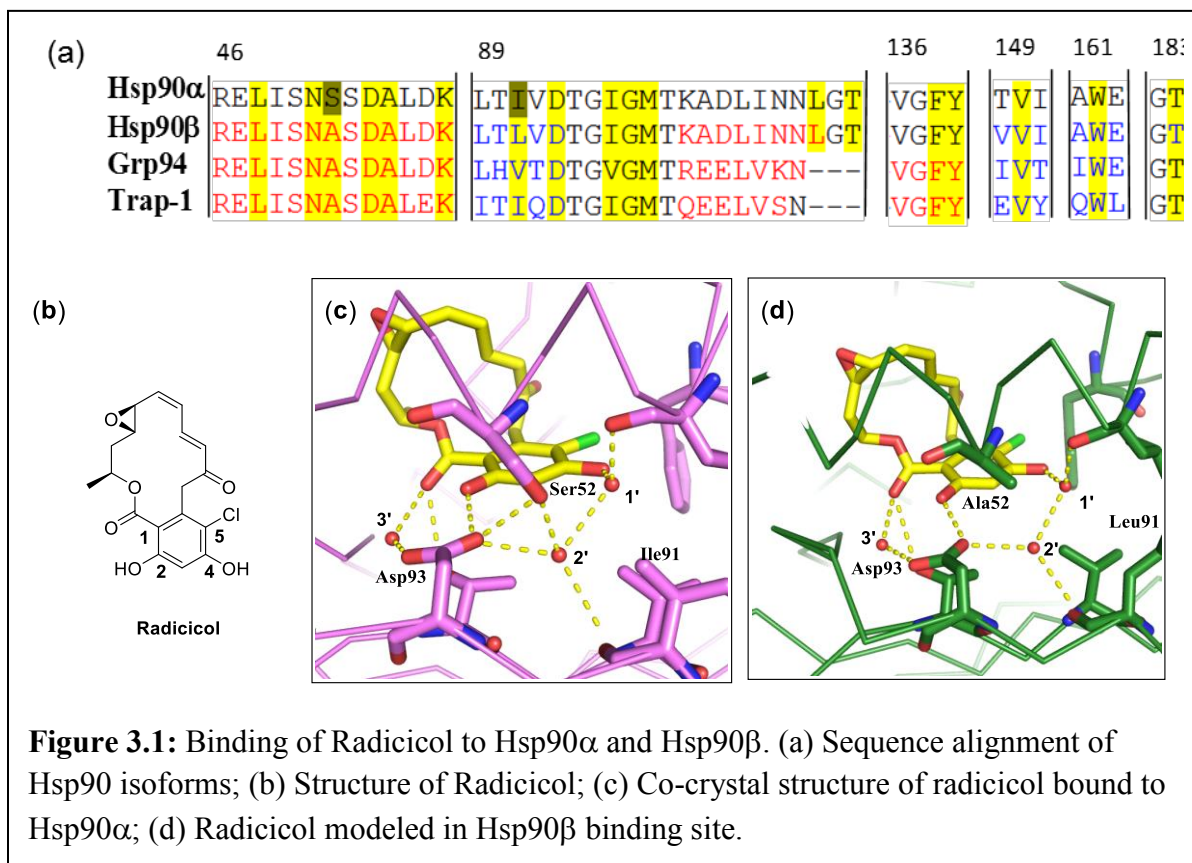
Hsp90 $\alpha$  represents the inducible cytosolic isoform of Hsp90. Despite high structural similarity with the constitutively expressed isoform, Hsp90 $\beta$ , Hsp90 $\alpha$  exhibits differential expression, function and regulation.<sup>1</sup> Genetic knockdown of Hsp90 $\alpha$  results in the desirable degradation of oncogenic client proteins, suggesting that the administration of Hsp90 $\alpha$ -selective inhibitors could disrupt the progression of cancers that are driven by Hsp90 $\alpha$ -dependent client proteins.<sup>2</sup> In addition to its cytosolic presence, Hsp90 $\alpha$  is secreted extracellularly to promote wound healing and inflammation.<sup>3</sup> In highly invasive cancers, significant levels of Hsp90 $\alpha$  are secreted from the cell to activate matrix metalloprotease 2 (MMP-2) and induce expression of MMP-3, which in turn promotes tumor invasion.<sup>4-5</sup> Exposure of prostate stromal fibroblasts to extracellular Hsp90 $\alpha$  (eHsp90 $\alpha$ ) via a MEK/ERK and NF- $\kappa$ B dependent pathway, increases the production and secretion of IL-6 and IL-8, which contribute to an inflammatory microenvironment that supports prostate cancer progression.<sup>5</sup> The same study also concluded that eHsp90 $\alpha$  acts upon activation of oncogenic inflammatory mediator, signal transducer and activator of transcription (STAT3).

Extracellular Hsp90 $\alpha$  (eHsp90 $\alpha$ ) induces inflammation through activation of NF- $\kappa$ B. Interestingly, NF- $\kappa$ B induces the expression Hsp90 $\alpha$  via positive feedback resulting in a surge of inflammation that promotes cancer progression. Additionally, eHsp90 $\alpha$  induces expression of Transcription Factor 12 (TCF 12) in colorectal cancer cells, improving their ability to migrate and invade.<sup>6</sup> Hsp90 $\alpha$  also effectively contributes to the DNA damage repair response, wherein, it stabilizes and repairs DNA following exposure to ionizing or infrared radiation. During this

process, Hsp90 $\alpha$  gets activated via phosphorylation by the ataxia-telangiectasia-mutated kinase (ATM).<sup>7-8</sup> Therefore, Hsp90 $\alpha$ -selective inhibitors could serve as radiosensitizing agents. Furthermore, Hsp90 $\alpha$  plays a key role in the self-renewal of breast cancer stem cells (BCSCs) by facilitating the nuclear translocation of c-Myc and EZH2 to regulate levels of B lymphoma Mo-MLV insertion region 1 homolog (BMI1), a polycomb family member with oncogenic activity in breast cancer.<sup>9</sup> Moreover, high levels of plasma Hsp90 $\alpha$  is recognized as a biomarker for liver cancer.<sup>10-11</sup> Increased levels of cytoplasmic Hsp90 $\alpha$  represents a poor prognosis of esophageal squamous cell carcinoma and acute leukemia.<sup>12-13</sup> In pancreatic cancers, Hsp90 $\alpha$  regulates cell invasion capacity via a pathway that involves MMP-2.<sup>14-15</sup>

In an analysis of the Hsp90 interactome, it was observed that Hsp90 $\alpha$  and Hsp90 $\beta$  collectively interact with 725 proteins, of which Hsp90 $\alpha$  interacts exclusively with 135 proteins, while Hsp90 $\beta$  interacts exclusively with 410 proteins, and both isoforms share 183 substrates.<sup>16</sup> In addition, analysis of gene ontology terms revealed that although Hsp90 $\beta$  interacts with a larger number of proteins, Hsp90 $\alpha$  is involved in added biological processes. Functionally, Hsp90 $\beta$  is more relevant to maintaining viability, while the processes dependent on Hsp90 $\alpha$  contribute to adaptation during stress or specialized functions.<sup>17-19</sup> Therefore, intra- and extracellular Hsp90 $\alpha$  represent excellent targets for the generation of new anti-cancer agents.

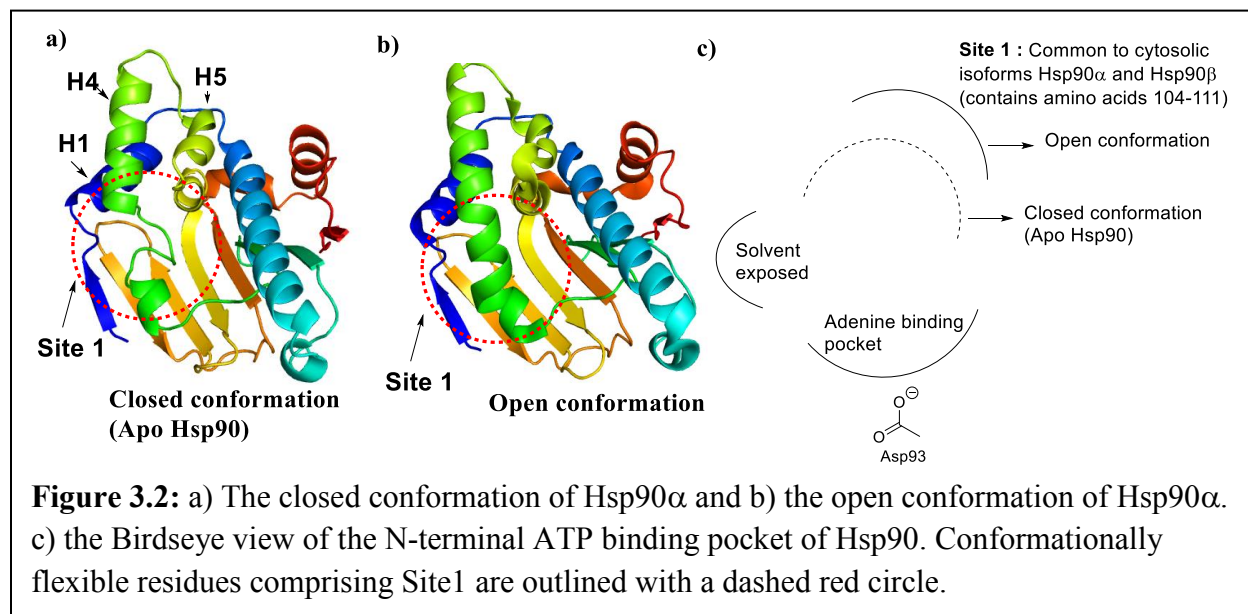
### III.2 Variations in the N-terminal ATP-Binding Site in the Hsp90 Isoforms.



As discussed in the previous chapter, the Hsp90 N-terminal ATP-binding site is highly conserved amongst the four Hsp90 isoforms. The primary amino acid sequence of Hsp90 $\alpha$  is ~86% identical to Hsp90 $\beta$ , however, the N-terminal ATP binding site is > 95% identical between the two cytosolic isoforms.<sup>20</sup> In fact, only two residues differ between the ATP-binding sites of Hsp90 $\alpha$  (Ser52, Ile91) and Hsp90 $\beta$  (Ala52, Leu91). The high conservation that is shared between the Hsp90 $\alpha$  and Hsp90 $\beta$  binding sites has prevented the development of Hsp90 $\alpha$ - or Hsp90 $\beta$ -selective inhibitors (Figure 3.1a). Radicicol (RDC) was selected as a reference ligand to study the Hsp90-ligand interactions (Figure 3.1b). The crystal structure of RDC bound to Hsp90 $\alpha$  and RDC modeled into Hsp90 $\beta$  were carefully analyzed to study the binding interactions that may differ between these two isoforms. As depicted in Figure 3.1, two conserved water molecules exist in

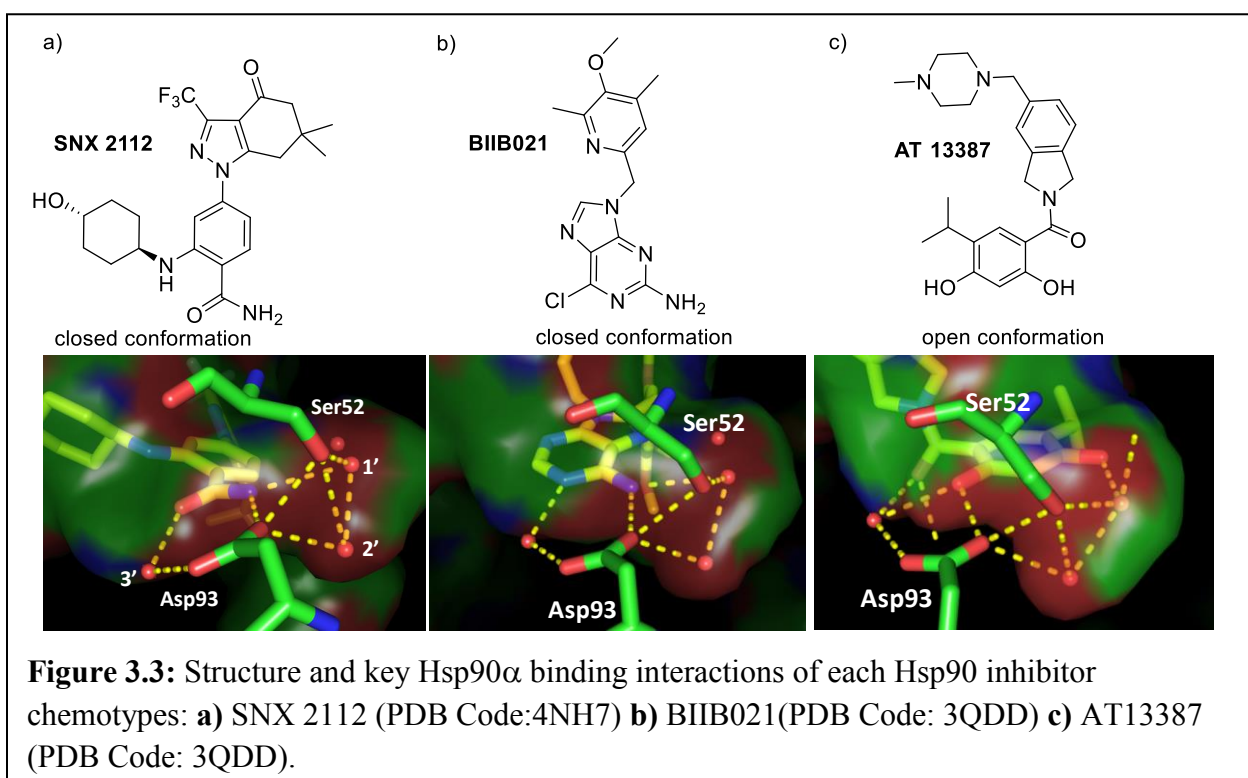
both Hsp90 $\alpha$  and Hsp90 $\beta$  (labeled as 1' and 2' in Figure 3.1c and d) and are responsible for mediating a hydrogen-bonding network involving Asp93, Ser52, and the phenols of RDC in Hsp90 $\alpha$ , whereas in Hsp90 $\beta$ , Ala52 alters this spatial arrangement and limits the hydrogen-bond network. The resorcinol moiety interacts with Asp93 in both isoforms and is a key interaction that drives potency.<sup>21</sup>

**III.3 Binding of the Small Molecule Inhibitors to the N-terminal ATP-Binding Site of Hsp90 $\alpha$ .** The cytosolic isoforms, Hsp90 $\alpha$  and Hsp90 $\beta$ , appear to be superimposable upon overlay of the N-terminal ATP-binding site amino acid sequences. In contrast, Grp94 and Trap1 exhibit



structural features that differ between Hsp90 $\alpha$  and Hsp90 $\beta$ . Figure 3.2a depicts the closed conformation (apo conformation) of Hsp90 $\alpha$ , which is the minimum energy conformation of the protein and is formed when Helix 4 (H4) exists as a disordered and closed loop, which leads to a smaller hydrophobic Site 1 (illustrated with a dashed curve in Figure 3.2c).<sup>22</sup> Expansion of Site 1 (open conformation) occurs when Helix 4 undergoes a conformational change that results in an ordered  $\alpha$ -helical structure of amino acids 104-111, as illustrated in Figure 3.2b and c. There are

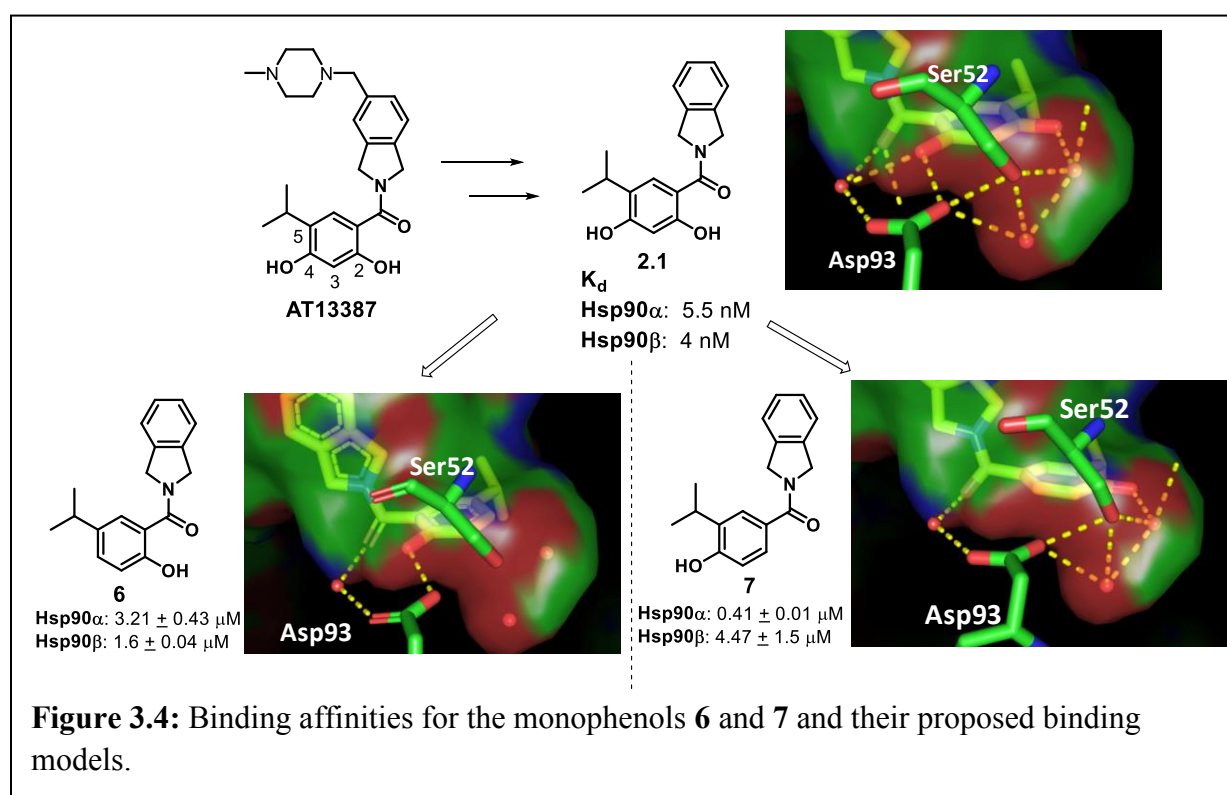
three chemotypes that summarize the Hsp90 small molecule inhibitors being evaluated in clinic; 1) benzamides, 2) purines, and 3) resorcinols. The crystal structure of compounds representing each Hsp90 inhibitor chemotype revealed that some chemotypes bind the open conformation of the Hsp90, whereas others can be accommodated in the resting state, i.e. the closed form.<sup>22</sup> The benzamide containing molecule, SNX 2112, binds and induces a conformational change to the open conformation, wherein, the tetrahydroindazolone fragment is accommodated into Site 1.



Similarly, the purine containing compound, BIIB021 also binds the open conformation of the protein. However, the resorcinol containing compounds, such as AT13387 (Onalespib), can only access and bind to closed conformation, which results in a reduced entropic penalty that translates into increased affinity. Each chemotype contains a pharmacophore that provides key interactions with the adenine binding region within the ATP-binding pocket (Figure 3.2). These pharmacophores represent a hydrogen bond donor-acceptor motif, such as the amide,

aminopyridine, or the resorcinol, which serve to anchor the ligand via a hydrogen-bond network that are coordinated via three conserved water molecules (labelled as 1'-3' in Figure 3.1 a).

Analysis of the co-crystal structures containing the three chemotypes that bind Hsp90 $\alpha$  and Hsp90 $\beta$  equipotently, reveals that the key binding interaction occurs between Asp93 and the H-bond donor from the ligand.<sup>23</sup> The carbonyl oxygen from the benzamide, the heterocyclic nitrogen from purine, and the 2-position phenol of the resorcinol act as a hydrogen-bond acceptors that interact via the 3' conserved water molecule. It is worth noting that the amide NH<sub>2</sub> and the aminopurine NH<sub>2</sub> interact simultaneously with Asp93 and Ser52 via conserved water molecules 1' and 2', however, in the resorcinol case, the 2-phenol directly interacts with Asp93, and the 4-phenol interacts with both Asp93 and Ser52 indirectly via water molecules 1' and 2'. Interestingly,

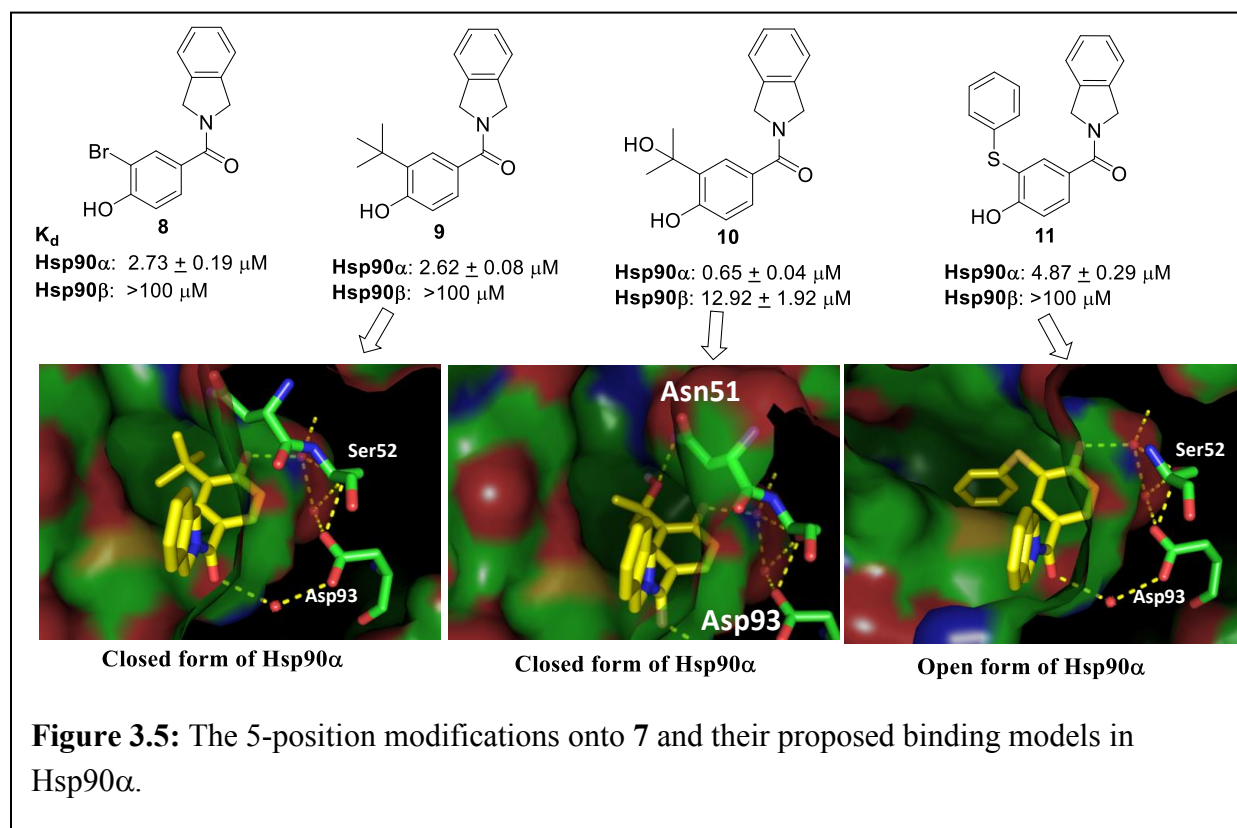


none of the examined scaffolds interact directly with Ser52, which is the only amino acid that varies between Hsp90 $\alpha$  and  $\beta$  that could be exploited to discriminate ligand binding. The other



residues, (Ile91( $\alpha$ )/Leu91( $\beta$ )) lead to a smaller pocket in Hsp90 $\alpha$  in comparison to Hsp90 $\beta$ , and cannot be probed for Hsp90 $\alpha$  binding (Figure 3.1c and d)

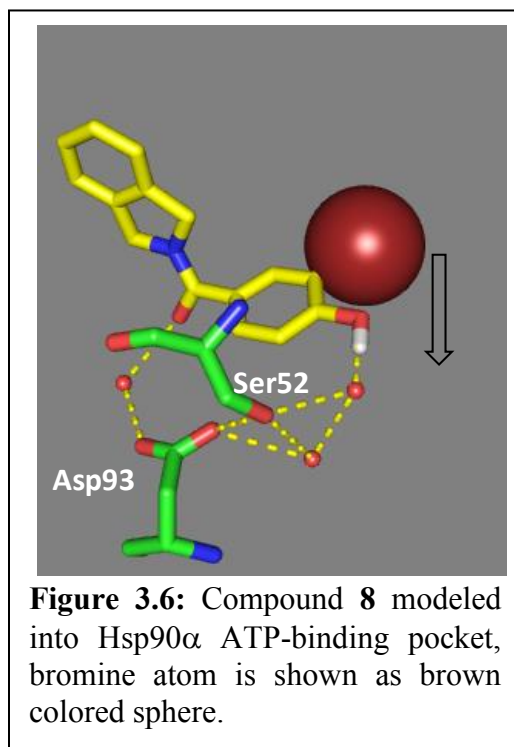
**III.4 The Discovery of the Monophenol-Based Hsp90 $\alpha$ -selective Inhibitor** As noted in the overlay studies, modifications to the benzamide and purine scaffolds were hypothesized to interrupt the planarity of the pharmacophores, which are essential for establishing contacts with protein via interactions with Asp93 (Figure 3.3). However, the resorcinol pharmacophore allowed



an opportunity to evaluate the polar binding requirements of the Hsp90 $\alpha$  surface via systematic removal of each phenol. For this purpose, the simplified resorcinolic compound, 2.1, a non-selective compound ( $\alpha/\beta$   $K_d=5.5/4$  nM), was chosen for investigation. Removal of the phenols resulted in the 2-phenol, 6, and the 4-phenol, 7.<sup>24</sup> In line with the hypothesis, compound 7, which

interacts with Ser52 via two conserved water molecules, manifested ~10-fold selectivity for Hsp90 $\alpha$  versus Hsp90 $\beta$  ( $\alpha/\beta$   $K_d=0.41/4.47$   $\mu\text{M}$ ). In contrast, **6** manifested moderate binding affinity with ~2-fold selectivity for Hsp90 $\beta$ , as the 2-phenol interacts with conserved water molecule 3' and Asp93. Collectively, polar interactions between Hsp90 $\alpha$  and **6** appear weaker as compared to the interactions manifested by **7**.<sup>24</sup> Encouraged by the binding profile of **7**, modifications to the 4-monophenol to improve affinity and selectivity were pursued. Figure 3.5 depicts the proposed binding mode of the compounds **8-11** that result from modifications at the 5-position of **7**. Notably, introduction of bulk at the 5-position improves selectivity, however, a loss of affinity (~5-fold) was also observed as compared to **7**. Figure 3.6 shows the 5-bromo containing compound (**8**) modeled into the Hsp90 $\alpha$  ATP-binding pocket (Figure 3.5). The bromine atom in Figure 3.6 is depicted as a brown sphere to aid in visualization that the bulk of bromine and other groups at the 5-position (**9-11**) restrict rotation of the 4-phenol and force it toward conserved water molecules and Ser52, and thereby, impart selectivity.

The presence of Asn51 in close proximity to the 5-position (Figure 3.5) allowed the installation of a hydroxyl onto **7** to yield the tertiary alcohol compound, **10**, which exhibits improved Hsp90 $\alpha$  binding affinity over **9** with ~20-fold selectivity against Hsp90 $\beta$ . 5-substitutions that may induce the open conformation of Hsp90 were also investigated. These efforts resulted in **11**, a compound that contains a phenyl thioether substitution that manifests selectivity similar to **8**, however, it also exhibits decreased affinity (Figure



3.5).<sup>24</sup> As hypothesized, **11**, may enlist an entropic penalty during the opening of Site 1, which may also reduce binding affinity. In the following sections, strategies that were employed to optimize the binding affinity and selectivity of the monophenol will be discussed.

### III.5 Optimization Studies of **7** and its 5-position Substituents.

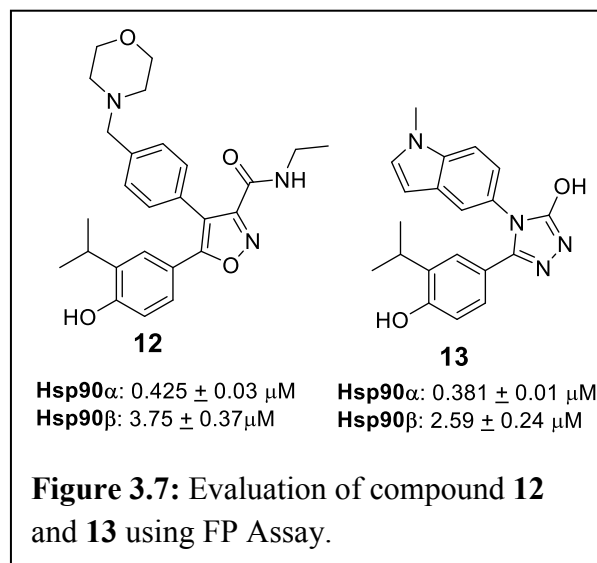
#### III.5.1 Exploration of Alternative 4-Phenol Scaffolds.

Apart from AT13887, there exist two other small molecule Hsp90 inhibitor scaffolds that are based on the resorcinol pharmacophore, the isoxazole containing NVPAUY922, and the triazolone-based, STA9090 (Figure 3.7).

Collectively, these three scaffolds represent the second generation of *pan*-Hsp90 inhibitors that have undergone clinical examination.

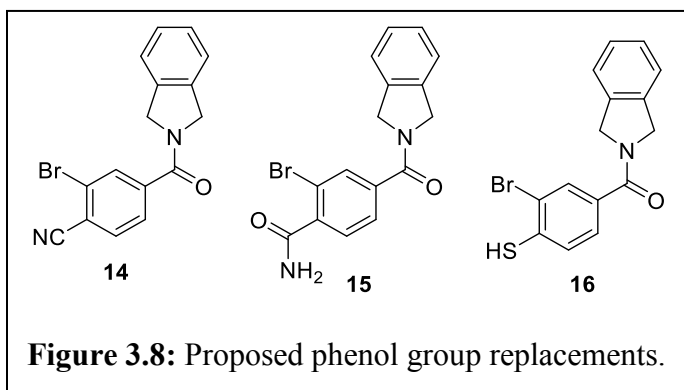
Derivatives **12** and **13** were prepared according

to the methods reported in literature to investigate the consequences of removing the 2-phenol in NVPAUY922 and STA9090 (Figure 3.7).<sup>25-26</sup> Upon evaluation of **12** and **13** in a fluorescence polarization (FP) assay, both compounds were shown to bind Hsp90 $\alpha$ / $\beta$  with affinities similar to **7**, however, a decrease in selectivity was observed (~8-fold for **12** and ~5-fold for **13**). These data support the isoxazole/triazolone containing scaffolds to bind Hsp90 $\alpha$  in similar orientation as the isoindoline scaffold, **7**.



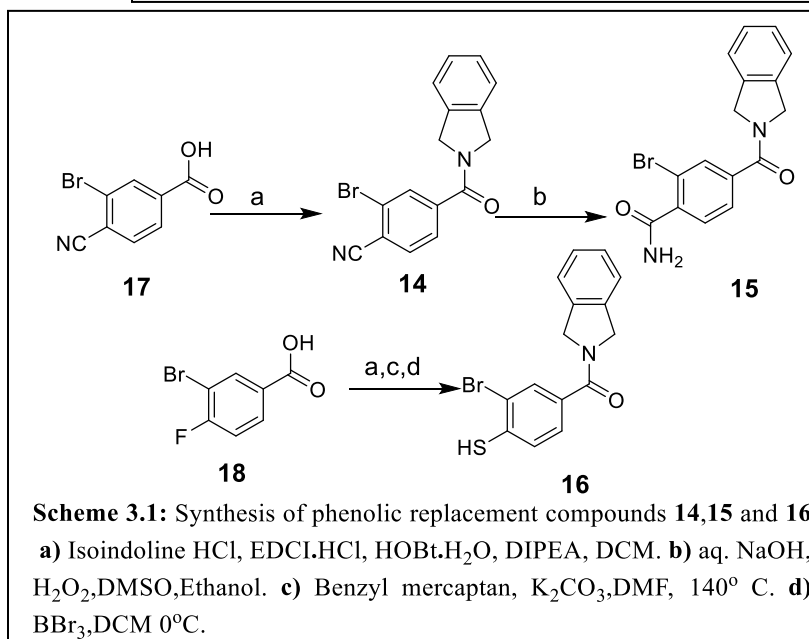
### III.5.2 Investigation of 4-Phenol Replacements. Compound **8** was chosen as a reference scaffold

for the construction of the proposed molecules to investigate phenol replacements. For this purpose, the phenol was replaced with a nitrile in **14** (Figure 3.8), whereas, **15** contained an amide group, both of which were



hypothesized to extend into the hydrogen bonding network and replace water molecules 1' and 2'. A thiol was incorporated into **16** in lieu of the phenol, which may define the spatial requirements of the pocket. An aniline was also investigated as a surrogate, but this substitution resulted in a complete loss of affinity.<sup>24</sup>

Synthesis of **14** commenced with acid **17**, which was coupled with isindoline in the presence of 1-ethyl-3-(3-dimethylaminopropyl) carbodiimide (EDCI) and hydroxybenzotriazole hydrate (HOBt·H<sub>2</sub>O). The nitrile in **14** was then hydrated in the presence of sodium hydroxide (NaOH) and



Compounds	Hsp90α	Hsp90β
	K <sub>d</sub> (μM)	K <sub>d</sub> (μM)
<b>14</b>	>50	>50
<b>15</b>	>50	>50
<b>16</b>	>50	>50

**Table 3.1:** K<sub>d</sub> values of phenolic replacement compound obtained from FP assay.

hydrogen peroxide to produce **15**. Synthesis of thiol **16**, began with an amide coupling reaction utilizing acid **18**, followed by aromatic nucleophilic substitution and debenzylation in the presence of boron tribromide (BBr<sub>3</sub>) to produce **16**.

Unfortunately, evaluation of these compounds in the fluorescence polarization (FP) assay revealed that neither the nitrile, the amide, nor the thiol group can mimic the phenol, as the K<sub>d</sub>'s were >50 μM for all three compounds.

### III.5.3 Modifications to the Tertiary Alcohol

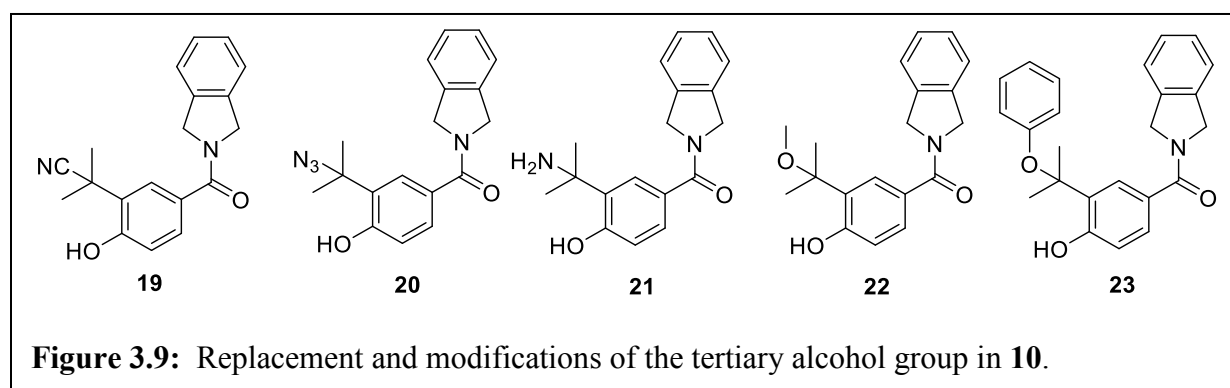


**Figure 3.9:** Replacement and modifications of the tertiary alcohol group in **10**.

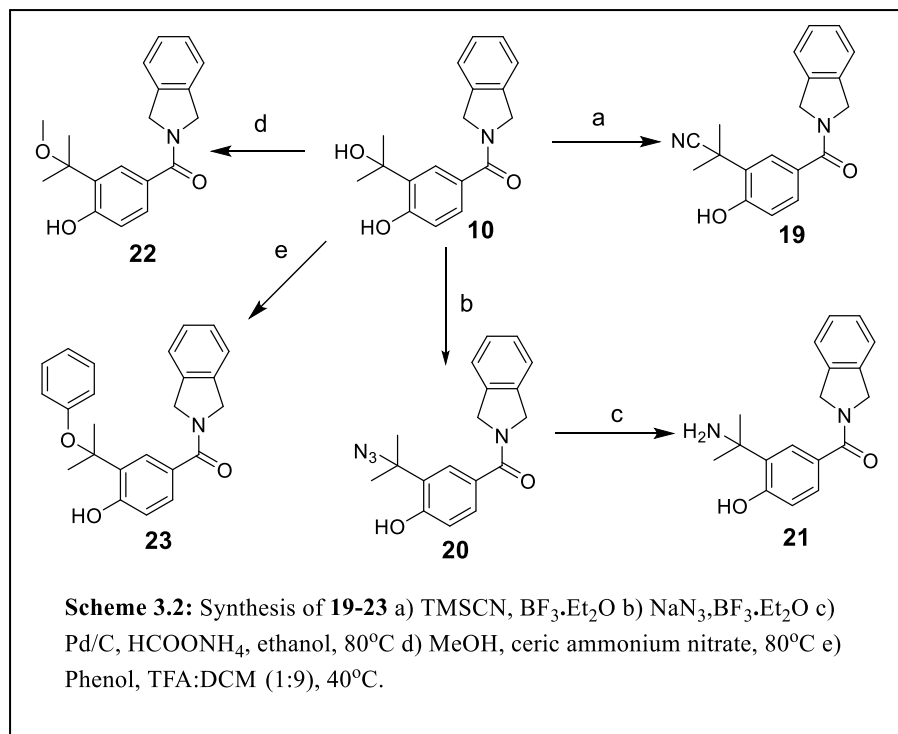
The tertiary alcohol containing, **10** (Figure 3.5) manifested higher affinity for Hsp90α versus Hsp90β when compared to the *t*-butyl containing compound, **9**. The alcohol may also act as a hydrogen bond acceptor and/or a donor, and therefore, functionalities were investigated to determine the role of the alcohol by calculating the binding affinity and selectivity. One of the proposed modifications included the introduction of a nitrile group onto **19**, which was hypothesized to interact with Asn51, as a hydrogen-bond acceptor. The azide containing compound, **20**, represented another derivative that could replace the alcohol with a hydrogen-bond acceptor in the binding pocket. In addition, an amine was installed to give **21** for investigation of charged interactions with the protein surface. Modeling of the alcohol into the binding site (Figure 3.5) suggested that a methoxy group could also be accommodated *in lieu* of the alcohol, which would allow for the differentiation of the hydrogen-bond acceptor/donor nature. Finally, the

phenolic ether was proposed in compound **23** to induce a conformational change in Hsp90 $\alpha$ , resulting in an open form, and subsequently allow occupation of the larger Site 1, that could resemble compound **11** (Figure 3.5).

Synthesis of compound **19**, was performed by treating previously developed **10** with trimethylsilyl cyanide (TMSCN) in the presence of boron trifluoride diethyl etherate (BF<sub>3</sub>.etherate).

Similarly, **20** was produced using sodium azide (NaN<sub>3</sub>). Upon hydrogenation via ammonium formate and palladium, **20** yielded the corresponding amine, **21**.

Preparation of the methoxy containing analog, **22**, required



treatment of **10** with ceric ammonium nitrate in methanol. Additionally, the phenol was reacted with **10** in the presence of trifluoroacetic acid to produce the phenoxy containing compound, **23**.

Interestingly, evaluation of **19** in the FP assay revealed that a nitrile could effectively replace the alcohol in **10**, as the binding affinity of **19** was shown to resemble **10**. This data implied that alcohol in **10** interacts with Asn51 as a hydrogen-bond acceptor. In line with the proposed hypothesis, the azide containing compound, **20**, exhibited ~2.74  $\mu$ M K<sub>d</sub>, which indicated

azide may also interact with Asn51, however, the size and linearity of the azido group may result in steric clash. The amine containing compound, **21**, exhibited a complete loss of affinity, suggesting that a charged moiety is undesired. Surprisingly, the methoxy containing analog, **22**, did not bind well. The loss in the affinity of **22** could result from steric interactions between the binding site and methoxy group. Similarly, the phenoxy containing compound, **23**, manifested a loss in binding affinity and did not interact with Hsp90 $\alpha$  as anticipated.

Compounds	Hsp90 $\alpha$ K <sub>d</sub> ( $\mu$ M)	Hsp90 $\beta$ K <sub>d</sub> ( $\mu$ M)
<b>19</b>	0.51 $\pm$ 0.008	5.1 $\pm$ 0.11
<b>20</b>	2.74 $\pm$ 0.20	14.91 $\pm$ 0.11
<b>21</b>	>50	>50
<b>22</b>	36 $\pm$ 1.56	>50
<b>23</b>	>50	>50

**Table 3.2:** K<sub>d</sub> values for **19-23** obtained from FP assay.

### III.5.4 Modifications to the gem-Dimethyl

Since the evaluated functionalities (Figure 3.9) did not produce an improvement in affinity and selectivity as was observed with **10**, the alcohol was established as the optimal group for Hsp90 $\alpha$  binding. In the following studies, a gem-dimethyl group was investigated. As shown in Figure 3.8, the dimethyl moiety could be modified to access the open form (Figure 3.2, 3.5 and 3.8) as well as the solvent channel (marked with red arrow in Figure

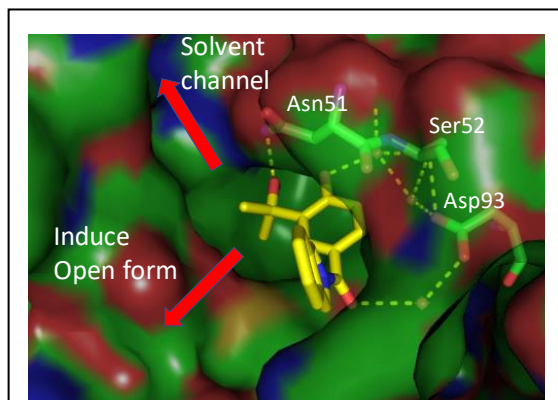
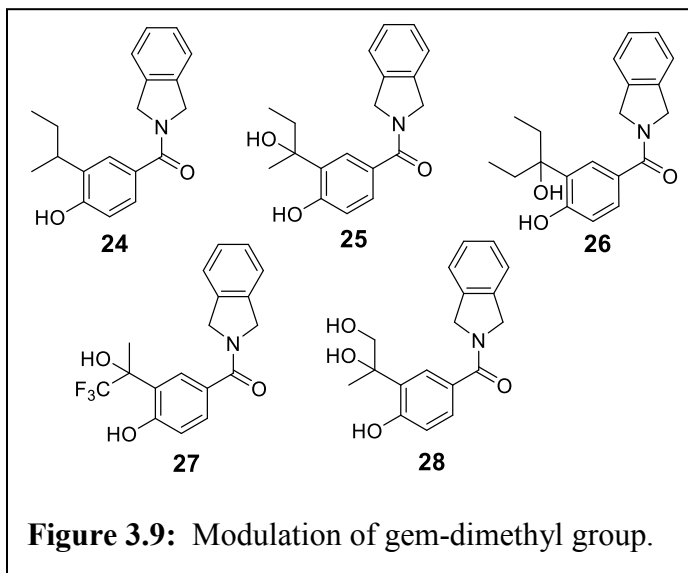


**Figure 3.10:** Proposed model of **10** binding to closed form of Hsp90 $\alpha$ . Arrows indicate the projection of the dimethyl replacements potentially into different pockets.

3.8), and lead to entropic stabilization via displacement of water. However, proposed

modifications introduced a chiral center, and therefore the evaluation of binding may be more complicated.

A *sec*-butyl was introduced onto **24**, to replace the isopropyl group present in **7**, for investigation of chain elongation. A similar modification was also introduced onto **8** to produce compound **25**. The extension of both methyl groups to form diethyl, **26**, was pursued to explore the mutual exclusivity of the methyl substituents. In addition, installation of a trifluoromethyl onto **27** was hypothesized to explore the steric bulk about the alcohol. A vicinal diol was incorporated into **26** to investigate additional hydrogen bonding interactions within the binding site.



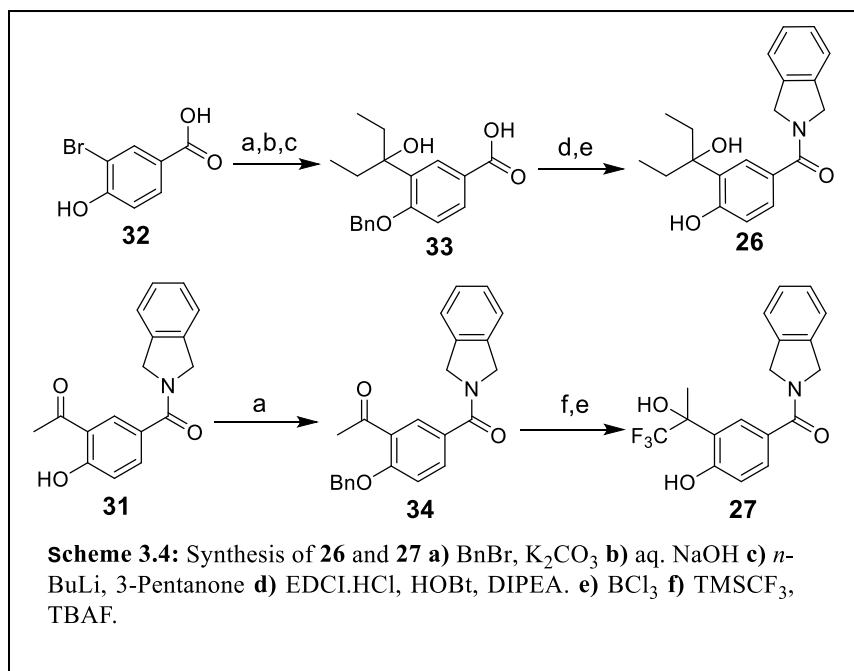
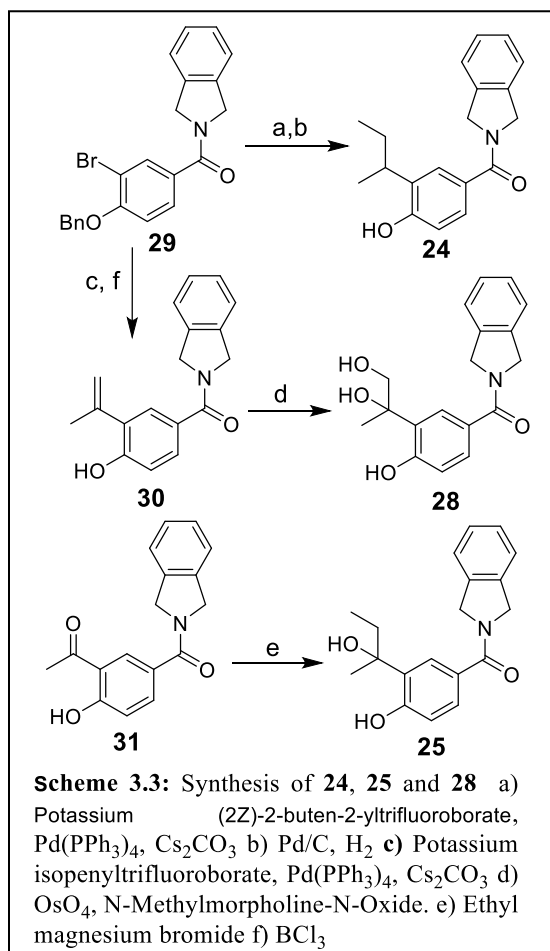
Preparation of **24** required a tetrakis(triphenylphosphine)palladium(0) ( $\text{Pd}(\text{PPh}_3)_4$ )-catalyzed coupling of benzyl protected bromophenol **29** with potassium (*E,Z*)-2-butenyltrifluoroborate (Scheme 3.3),<sup>24</sup> which underwent subsequent hydrogenation to produce **24**. The isopropenyl containing intermediate **30**, was produced using conditions similar to those used to



construct **24**. Dihydroxylation of intermediate **30** was performed with osmium tetroxide and resulted in **28**. The 5-acetylated monophenol **31**,<sup>24</sup> was treated with ethyl magnesium bromide to produce the tertiary alcohol, **25**.

Commercially available acid **32**, was protected with a benzyl moiety and then hydrolyzed with sodium hydroxide to yield the benzyloxy protected acid. A subsequent a lithium halogen exchange was then utilized and then quenched with 3-pentanone to give **33**. Coupling of **33** with isoindoline followed by removal of the protecting group led to the desired product, **26**. Installation of the trifluoromethyl group required

benzyl protection of **31**, to yield **34**, which upon treatment with



Compounds	Hsp90 $\alpha$ K <sub>d</sub> ( $\mu$ M)	Hsp90 $\beta$ K <sub>d</sub> ( $\mu$ M)
<b>24</b>	1.5 $\pm$ 0.357	30.29 $\pm$ 2.64
<b>25</b>	0.478 $\pm$ 0.01	5.23 $\pm$ 0.018
<b>26</b>	37.87 $\pm$ 1.24	>50
<b>27</b>	36 $\pm$ 1.56	>50
<b>28</b>	6.15 $\pm$ 0.76	>50

**Table 3.3:** K<sub>d</sub> values for **24-28** obtained from FP assay.

trifluoromethyltrimethylsilane (TMSCF<sub>3</sub>) and tetrabutyl ammonium fluoride (TBAF) resulted in **27**.

Upon evaluation in the FP assay, *sec*-butyl **24**, exhibited reduced affinity (~3-fold) as compared to the isopropyl containing compound, **7**. In contrast, introduction of an ethyl group (**25**)

resulted in an increase in binding affinity. These results suggest that **7** and **10** bind to different conformations of the protein and affects the orientation of ethyl chain. The binding affinity of **10** also indicates that the ethyl group may project toward the solvent channel (Figure 3.8), and displace water to reduce the dielectric constant within the binding site. Unfortunately, replacement of the dimethyl group in **26** with diethyl decreased binding affinity, indicating that substitutions can only be tolerated at one location. The trifluoromethyl group (**27**) also proved to be an ineffective binder. Finally, the vicinal diol (**28**) did not produce an increase in binding affinity, in contrast, a 10-fold decrease was observed.

**III.5.5 Installation of Appendages onto the Tertiary Alcohol.** The gain in binding affinity observed for **25** led to the hypothesis that further elongation of the chain may increase ligand binding. Therefore, both linear and branched aliphatic appendages were installed to distinguish the conformational changes that exist among the Hsp90 isoforms. Construction of analogs **35a-h** was

achieved via Grignard reagents prepared by reported methods.<sup>27</sup> The *n*-propyl containing compound, **35a**, maintained affinity similar to **25**, which led

<p><b>Scheme 3.5:</b> Synthesis of <b>35a-k</b> a) RMgBr, THF, 80°C b) AllylMgBr, -20°C c) EthylMgBr, methyl propargyl ether d) OsO<sub>4</sub>, NMO e) NaBH<sub>3</sub>CN.</p>	<b>Compound</b>	<b>Hsp90α K<sub>d</sub> (μM)</b>	<b>Hsp90β K<sub>d</sub> (μM)</b>	<b>Fold selectivity</b>
	<b>35a</b>	0.480±0.05	4.57±0.07	~10
	<b>35b</b>	0.184±0.02	2.4±0.39	~13
	<b>35c</b>	0.229±0.01	2.07±0.08	~8
	<b>35d</b>	11.81±0.87	>50	>5
	<b>35e</b>	4.60±0.87	>50±0.02	~10
	<b>35f</b>	0.596±0.03	5.16	~10
	<b>35g</b>	0.447±0.02	4.98±0.285	~10
	<b>35h</b>	2.49±0.25	30.5±2.29	~12
	<b>35i</b>	2.22±0.21	>50	~21
	<b>35j</b>	0.045±0.02	0.426±0.07	~10
	<b>35k</b>	3.71±0.25	17.94±2.80	~5

**Table 3.4:** K<sub>d</sub> values for **35a-k** obtained from FP assay.

to evaluation of the *n*-butyl appendage, **35b**. Surprisingly, **35b** manifested a ~3-fold increase in binding affinity, but selectivity against Hsp90β remained unchanged (~13-fold). Extension of the chain to a *n*-pentyl (**35c**) led to a minor loss in affinity. Collectively, the binding data obtained with compounds **35d-f** suggested that branching in close proximity to the tertiary alcohol is not tolerable. The hypothesis that alkyl side chains project into the solvent channel (Figure 3.8) was further explored via the methoxy (**35g**) and terminal alcohol (**35k**) that could mimic water molecules present in the channel. Interestingly, the methoxy-group containing compound **35g**,

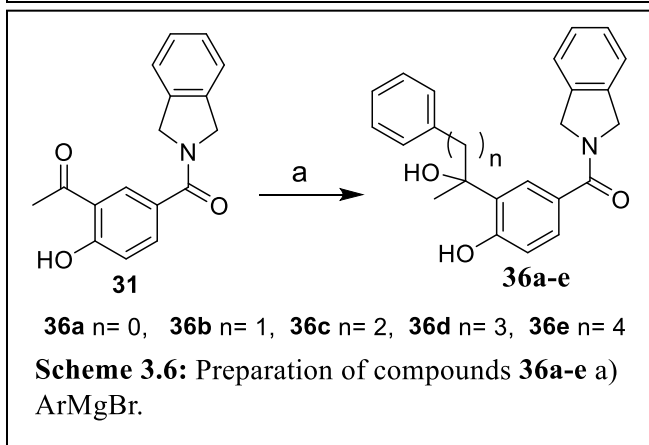
manifested a ~3-fold loss in affinity (compared to **35b**), whereas the alcohol containing compound **35k**, manifested ~24-fold loss in affinity. These data suggested that the unprotected alcohol (**35k**) may interact with solvent molecules and dilute enthalpic interactions. However, the methoxy (**35k**) appears to prevent solvent access to the binding site. Unfortunately, the introduction of a terminal alkene as in **35h** and **35i** led to compounds that manifested a loss in affinity, suggesting that the alkene exhibits disfavored interactions by imparting rigidity. Subsequently, **35g** was constrained via a propargyl ether to produce **35j**, which could orient the ether toward the solvent channel (Figure 3.10) and make contact with Asn51 and Phe138, and thereby reduce the entropic penalty. In agreement with this hypothesis, compound **35j** exhibited a  $K_d$  of ~45nM, however, selectivity versus Hsp90 $\beta$  remained unaffected (~10-fold).

Evaluation of compounds **35a-k** implied that the solvent channel could be probed via substitutions on the tertiary alcohol, and ultimately produced compound that improved affinity. However, except for allyl (**35i**), selectivity versus Hsp90 $\beta$  ranged between 5-10-fold, suggesting that modification to this region drive affinity, but have no effect on selectivity.

### III.5.6 Substitutions to Probe the Hsp90 $\alpha$ Open Conformation. As discussed in the earlier

Compound	Hsp90 $\alpha$ K <sub>d</sub> ( $\mu$ M)	Hsp90 $\beta$ K <sub>d</sub> ( $\mu$ M)	Fold selectivity
<b>36a</b>	3.87 $\pm$ 0.32	39.32 $\pm$ 2.64	~10
<b>36b</b>	3.84 $\pm$ 0.31	>50	>13
<b>36c</b>	3.03 $\pm$ 0.19	>50	>13
<b>36d</b>	0.25 $\pm$ 0.01	3.67 $\pm$ 0.14	~15
<b>36e</b>	0.33 $\pm$ 0.87	4.28 $\pm$ 0.07	~13

**Table 3.5:** K<sub>d</sub> values for **36a-e** obtained from FP assay.



binding may arise from differences in the transition state energies for the ligand-Hsp90 $\alpha/\beta$  complex. Compounds **36a-e** were prepared to probe and potentially bind Site 1 in Hsp90 $\alpha$ , by treating **31** with the appropriate Grignard reagent.

Following their preparation, **36a-e** were evaluated for binding affinities toward Hsp90 $\alpha$  and  $\beta$ . In comparison to **10**, **36a-c** exhibited a loss of binding

sections, Hsp90 undergoes a conformational change upon ligand binding to result in a larger Site 1 (Figure 3.2 and 3.8). Although Site 1 is conserved among the cytosolic isoforms, quaternary changes in the Hsp90 structure have been observed as

a consequence of ligand binding.<sup>28</sup> Compounds have been reported to exhibit moderate preference for binding to Hsp90 $\alpha$  over Hsp90 $\beta$ , but the rationale for their binding preference is lacking.<sup>29-30</sup> The observed Hsp90 $\alpha$ -selectivity for ligand

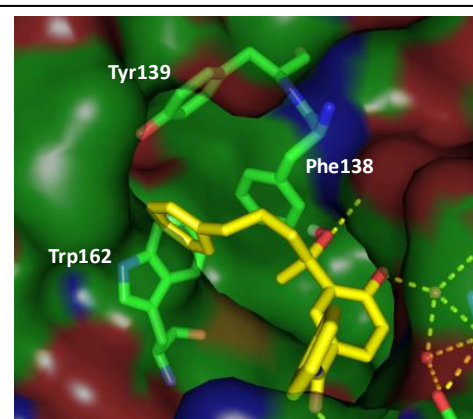
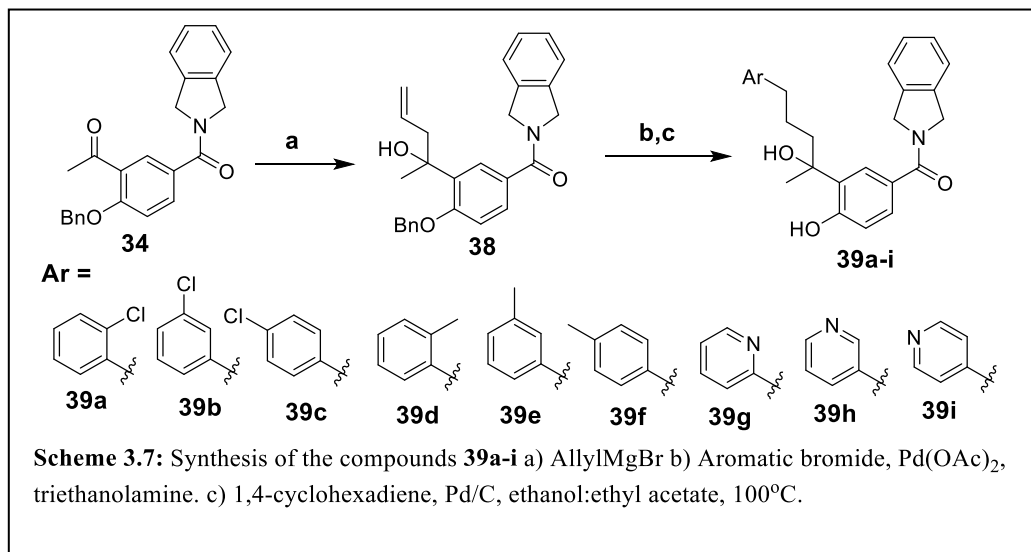


**Figure 3.11:** Proposed binding mode of **36d** in the open conformation of the Hsp90 $\alpha$  ATP-binding site.

affinity and selectivity (~10-13-folds vs ~20-folds for **10**). This observation led to the hypothesis



that compounds with linker ranging from 0 to 2 carbons were unfit for binding and/or inducing the open conformation. However, the 3-carbon linker as in compound **36d**, exhibited improved affinity ( $K_d \sim 0.25 \mu\text{M}$ ) and ~15-fold selectivity. Surprisingly, **36d** overcame the combined entropic penalty by rotation of the propylene linker to induce a conformational change

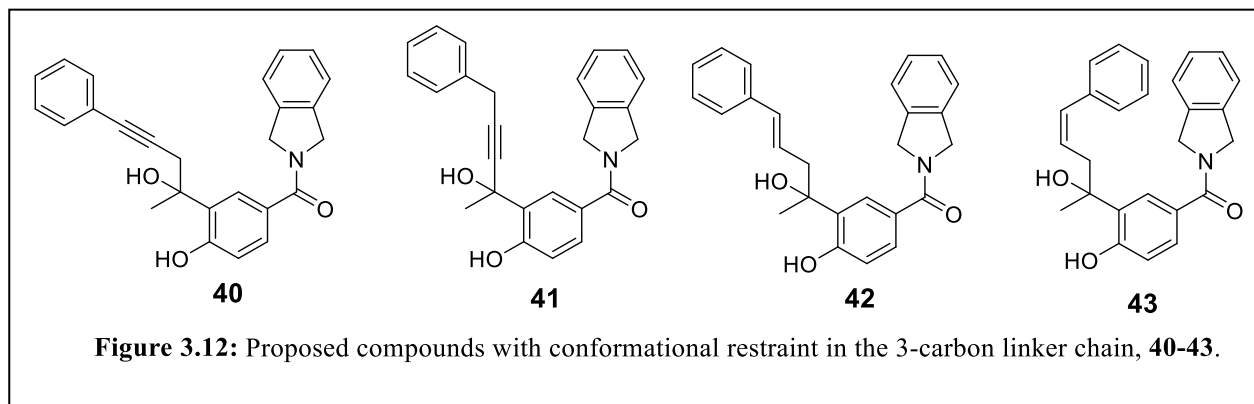
Compound	Hsp90 $\alpha$ $K_d$ ( $\mu\text{M}$ )	Hsp90 $\beta$ $K_d$ ( $\mu\text{M}$ )	Fold selectivity
<b>39a</b>	0.279 $\pm$ 0.048	2.74 $\pm$ 0.34	~10
<b>39b</b>	0.256 $\pm$ 0.31	2.55 $\pm$ 0.19	~10
<b>39c</b>	0.381 $\pm$ 0.001	4.84 $\pm$ 0.19	~12
<b>39d</b>	0.726 $\pm$ 0.03	3.98 $\pm$ 0.04	~6
<b>39e</b>	0.243 $\pm$ 0.006	4.15 $\pm$ 0.65	~17
<b>39f</b>	0.278 $\pm$ 0.064	2.12 $\pm$ 0.08	~8
<b>39g</b>	0.056 $\pm$ 0.004	0.328 $\pm$ 0.059	~6
<b>39h</b>	0.086 $\pm$ 0.009	0.563 $\pm$ 0.026	~7
<b>39i</b>	0.057 $\pm$ 0.004	0.639 $\pm$ 0.119	~11

**Table 3.6:**  $K_d$  values for **39a-i** obtained from FP assay.

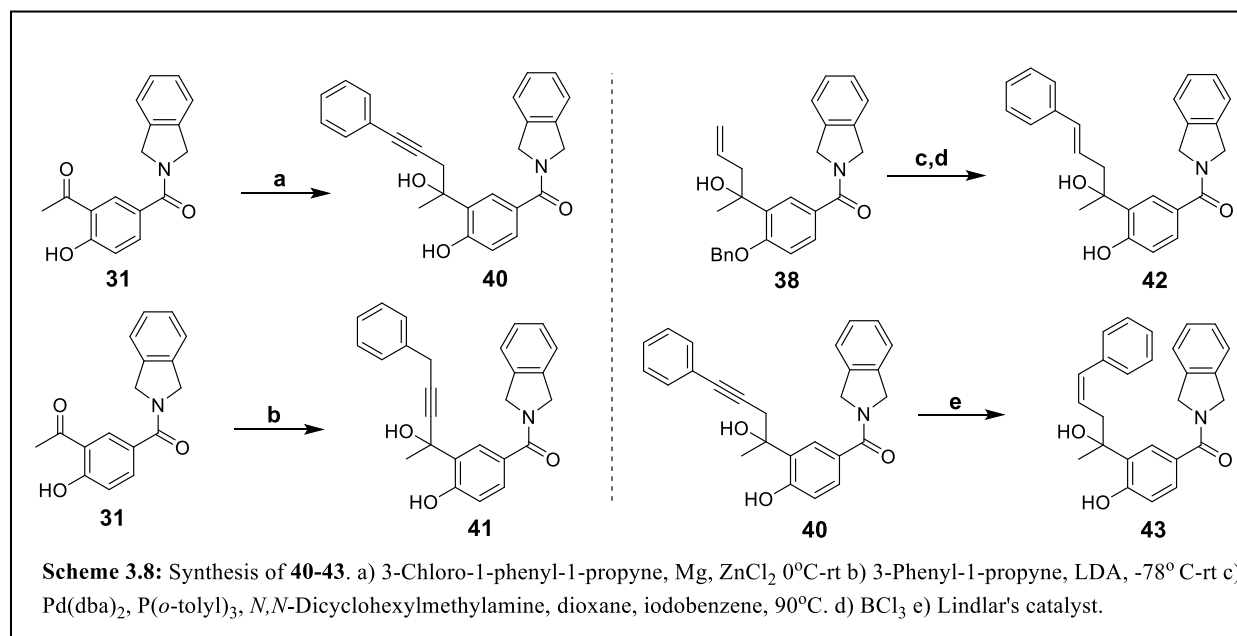
in the protein. The four-carbon linker as in compound **36e**, also exhibited a similar binding profile, albeit with a minor loss in affinity.

The binding profile of **36d** led us to speculate that further modification to the phenyl ring may provide compounds with improved affinity and selectivity through binding to probing Site 1. Therefore, substituted phenyl derivatives, **39a-i**, were produced using the benzyl protected intermediate **34**, which upon treatment with allyl magnesium bromide yielded the chiral alcohol, **37**. Intermediate **37**, was then coupled with the desired aromatic bromides via Heck coupling conditions, followed by simultaneous removal of the benzyl group and reduction of the alkene to afford the desired products, **39a-i**.

Evaluation of the chlorine substituted compounds **39a-c**, determined that binding affinity and selectivity largely remained unaffected. In fact, a slight loss of affinity was observed with the 4-chlorine substituted compound, **39i**. This implied that the chlorine atom could be accommodated on the ring without a significant loss of affinity. Methyl groups were also installed on the phenyl ring, which determined that the 2-methyl substituted compound, **39d**, lost affinity as well as selectivity. In contrast, the 3-methyl containing compound, **39e**, improved selectivity (~17-fold) while maintaining affinity, whereas, the 4-methyl containing compound **39f**, retained affinity but lost selectivity. Finally, a nitrogen-scan was performed to probe potential hydrogen-bonds with Tyr139, and/or improved *pi-pi* stacking with Phe138 and Trp162 (Figure 3.10). Expectedly, binding improved for all pyridyl analogs (**39g-i**), but a gain in selectivity was not observed. Instead, the 2- and 4-pyridyl analogs, **39g** and **39i**, lost selectivity (~6-fold) respectively.



Flexibility of the 3-carbon linker chain was investigated by introduction of an alkyne or an alkene. It was hypothesized that restricting rotation with an alkene or an alkyne would project the phenyl ring directly into Site 1 while reducing entropy. Therefore, the alkyne group was introduced



within the linker chain at various positions (**40** and **41**). Additionally, *trans* (**42**) and *cis* (**43**) variants of compound **36d** were

also investigated (Figure 3.12).

Synthesis of **40** commenced upon the treatment of **31** with a Grignard reagent containing the desired alkyne (Scheme 3.8). Construction of **41** required generation of the alkynyl

anion via lithium diisopropylamide (LDA), which then reacted with **31** to yield **41**. The synthesis of *trans*-alkene **42** was achieved utilizing Heck coupling conditions, enlisting palladium(0) bis(dibenzylideneacetone) (Pd(dba)<sub>2</sub>) and tri-*o*-tolylphosphine (P(*o*-tolyl)<sub>3</sub>) before deprotection to

Compound	Hsp90α K <sub>d</sub> (μM)	Hsp90β K <sub>d</sub> (μM)	Fold selectivity
<b>40</b>	0.861±0.011	22.35±0.64	~26
<b>41</b>	0.034±0.001	0.048±0.011	~1
<b>42</b>	0.260±0.09	3.97±0.15	~15
<b>43</b>	0.343±0.004	4.55±0.08	~13

**Table 3.7:** K<sub>d</sub> values of **40-43** obtained from FP assay.



give **42**. However, the *cis* variant was accessed via reduction of alkyne **40** in the presence of Lindlar's catalyst.

Evaluation of these compounds using an FP assay was performed and revealed interesting binding profiles. For example, compound **40** exhibited a loss of affinity (~3-fold), however, selectivity was found to be improved by ~26-fold, which represents an improvement over the parent compound, **36d**. Compound **41** manifested improved binding affinity ( $K_d \sim 35\text{nM}$ ), but also a similar affinity for Hsp90 $\beta$ , resulting in lack of selectivity. The *trans* analog, **42**, exhibited affinity and selectivity comparable to the parent compound, **36d**, whereas, the *cis* analog (**43**) was ineffective.

### III.6 Cellular Studies

Biological evaluation of the prepared compounds will be discussed in the next chapter.

### III.7 Conclusions

Monophenol, **7**, represents the first rationally designed Hsp90 $\alpha$ -selective inhibitor. The 4-monophenol analogs of the resorcinol chemotypes, NVPAUY922 and STA9090, were prepared (**12** and **13**) and evaluated. Studies determined **7** was best suited for subsequent optimization. Substitutions at the 5-position in **7** led to the compounds **8-11**, which established the presence of a bulky group regulates Hsp90 $\alpha$  binding affinity, and gave ~30-fold selectivity over Hsp90 $\beta$ . These compounds served as hits for further development. In particular, **10** was selected for its superior binding affinity toward Hsp90 $\alpha$  and ~20-fold selectivity versus Hsp90 $\beta$ .

Initial derivatives of **10** were sought to replace the alcohol with various functional groups, which uncovered the nitrile to mimic the binding affinity of **10**. The introduction of appendages onto the tertiary alcohol was pursued and both elongated and branched chain compounds, **25** and **35a-k** were prepared, the *n*-butyl analog provided optimal binding affinity, whereas, branching of

the chain was found unfavorable. Of note, introduction of propargyl ether into **35j** led to an enhancement in affinity, without any improvement of selectivity.

While the alkyl chain was explored to investigate the closed conformation of Hsp90, the introduction of a phenyl ring was pursued to investigate the open conformation of Hsp90 $\alpha$ . It was determined that the 3-carbon linker found in **36d** is optimal and manifested ~250nM  $K_d$  for Hsp90 $\alpha$  and ~15-fold selectivity over Hsp90 $\beta$ . Furthermore, structure-activity relationship studies on the phenyl ring determined that a 3-methyl substitution (**39e**) maintained affinity and selectivity, and warrants further investigation. Finally, flexibility of the linker chain in **36d** was pursued via **40-43**. It was discovered that placement of the alkyne is critical for regulating selectivity and potency, as **40** lost affinity but gained selectivity, whereas, **41**, lost selectivity but was equipotent against Hsp90 $\alpha$  and Hsp90 $\beta$ .

In order to understand the mechanisms of binding of the compounds **35b** and **36d**, co-crystallization studies are underway in collaboration with Dr. Robert Matts at Oklahoma State University.

### **III.8 Methods and Experiments**

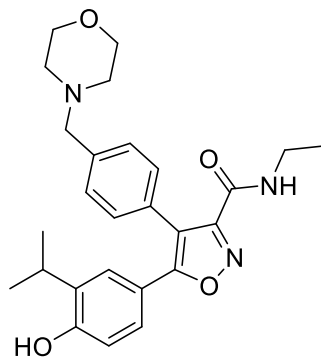
#### **Chemistry**

All reactions were performed in oven-dried glassware under argon atmosphere unless otherwise stated. Dichloromethane (DCM), tetrahydrofuran (THF), and toluene were passed through a column of activated alumina prior to use. Anhydrous dimethyl sulfoxide (DMSO), methanol, and *N,N*-dimethylformamide (DMF) were purchased and used without further purification. Flash column chromatography was performed using silica gel (40–63  $\mu$ m particle size). The  $^1\text{H}$  (500 and 400 MHz) and  $^{13}\text{C}$  NMR (125 and 100 MHz) spectra were recorded on 500 and 400 MHz

spectrometer. Data are reported as p = pentet, q = quartet, t = triplet, d = doublet, s = singlet, bs = broad singlet, m = multiplet; coupling constant(s) in Hz. High resolution mass spectral data were obtained on a time-of-flight mass spectrometer and analysis was performed using electrospray

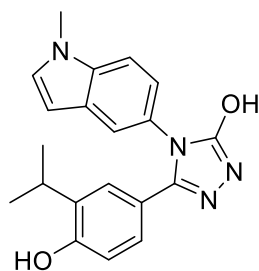
### **Fluorescence Polarization Assay**

Assay buffer (25  $\mu$ L, 20 mM HEPES pH 7.3, 50 mM KCl, 5 mM MgCl<sub>2</sub>, 1 mM DTT, 20 mM Na<sub>2</sub>MoO<sub>4</sub>, 0.01% NP-40, and 0.5 mg/mL BGG) was added to 96-well plate (black well, black bottom) followed by the desired compound at the indicated final concentrations in DMSO (1% DMSO final concentration). Subsequently, 10nM Recombinant Hsp90 $\alpha$  or Hsp90 $\beta$  or cGrp94 or Trap-1 and 6 nM FITC-GDA were added in 50  $\mu$ L and 25  $\mu$ L assay buffer respectively resulting in a 100  $\mu$ L final volume. Plates were incubated for 24 h at 4°C on a rocker. Fluorescence was determined using excitation and emission filters of 485 and 528 nm, respectively. Percent FITC-GDA bound was determined by assigning the DMSO millipolarization unit (mP) value as the 100% bound value and 0% for FITC-GDA in assay buffer without any protein. Polarization values (in mP units) was measured at 37 °C with an excitation filter at 485 nm and an emission filter at 528 nm. Polarization values were correlated to % tracer bound and compound concentrations. The concentration of inhibitor at which the 50% displaced tracer was observed, represented apparent  $K_d$ .



**N-ethyl-5-(4-hydroxy-3-isopropylphenyl)-4-(4-(morpholinomethyl)phenyl)isoxazole-3-**

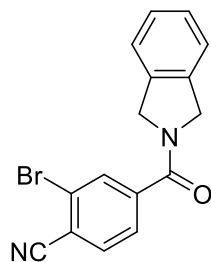
**carboxamide (12)<sup>25</sup>:** Yield 70%; <sup>1</sup>H NMR (500 MHz, Chloroform-*d*) δ 7.41 – 7.32 (m, 4H), 7.29 (dd, *J* = 8.4, 2.2 Hz, 1H), 7.24 (d, *J* = 2.1 Hz, 1H), 6.74 (t, *J* = 5.8 Hz, 1H), 6.66 (d, *J* = 8.4 Hz, 1H), 3.73 (t, *J* = 4.7 Hz, 4H), 3.55 (s, 2H), 3.42 (qd, *J* = 7.3, 5.8 Hz, 2H), 3.11 (hept, *J* = 6.9 Hz, 1H), 2.51 (s, 4H), 1.21 (t, *J* = 7.3 Hz, 3H), 1.02 (d, *J* = 6.9 Hz, 6H). <sup>13</sup>C NMR (126 MHz, CDCl<sub>3</sub>) δ 167.6, 159.2, 156.5, 154.7, 134.8, 130.5 (2), 129.5, 128.7, 125.7 (2), 119.7, 115.5, 114.5, 66.9 (2), 63.2 (2), 53.6, 34.3, 26.5, 22.2 (2), 14.6. HRMS (ESI) *m/z* [M+H] calculated for C<sub>26</sub>H<sub>32</sub>N<sub>3</sub>O<sub>4</sub>, 450.2387, found 450.2400.



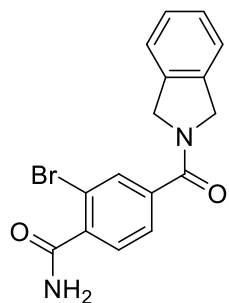
**5-(4-hydroxy-3-isopropylphenyl)-4-(1-methyl-1H-indol-5-yl)-4H-1,2,4-triazol-3-ol (13)<sup>26</sup>:**

Yield 35%; <sup>1</sup>H NMR (500 MHz, Chloroform-*d*) δ 7.43 (d, *J* = 2.0 Hz, 1H), 7.28 (d, *J* = 8.6 Hz, 1H), 7.03 (dd, *J* = 10.5, 2.7 Hz, 2H), 7.00- 6.93 (m, 2H), 6.50 (d, *J* = 8.4 Hz, 1H), 6.40 (dd, *J* = 3.2, 0.8 Hz, 1H), 3.74 (s, 3H), 3.01 (hept, *J* = 6.9 Hz, 1H), 0.84 (d, *J* = 6.9 Hz, 6H). <sup>13</sup>C NMR (126 MHz, CDCl<sub>3</sub>) δ 156.0, 155.3, 147.6, 136.4, 134.8, 130.4, 128.8, 126.3, 126.2, 125.3, 120.9, 120.3,

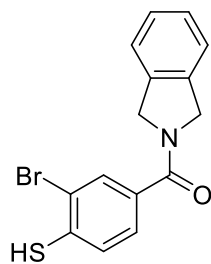
118.2, 114.8, 110.0, 101.6, 33.0, 26.4, 22.0 (2). HRMS (ESI)  $m/z$  [M+H] for C<sub>20</sub>H<sub>21</sub>N<sub>4</sub>O<sub>2</sub>, 349.1659, found 349.1699.



**2-bromo-4-(isoindoline-2-carbonyl)benzonitrile (14):** To a solution of **17** (200 mg, 0.88 mmol, 1 eq. ) in DCM (5 mL) were added *N*-(3-Dimethylaminopropyl)-*N'*-ethylcarbodiimide hydrochloride (338 mg, 1.76 mmol, 2.0 eq.), hydroxybenzotriazole hydrate (238mg, 1.76 mmol, 2 eq.) , *N,N*-Diisopropylethylamine (567 mg, 4.4 mmol, 5 eq.) and isoindoline hydrochloride (155 mg, 1 mmol, 1.1 eq.). Reaction was stirred overnight at rt, before solvent was removed in vacuo, then water (10 mL) was added to the remaining crude mass, acidified with 1N HCl and extracted with ethyl acetate (10 mL x2). The organic layer was dried over sodium sulfate, filtered and concentrated. The residue was purified by flash chromatography (SiO<sub>2</sub>, 1:3 hexanes/ethyl acetate) to afford **14** (240 mg, 85%) as a white solid. <sup>1</sup>H NMR (500 MHz, Chloroform-*d*) δ 7.91 (d, *J* = 1.4 Hz, 1H), 7.78 (d, *J* = 7.9 Hz, 1H), 7.62 (dd, *J* = 7.9, 1.5 Hz, 1H), 7.39 – 7.29 (m, 3H), 7.20 (dt, *J* = 7.4, 1.1 Hz, 1H), 5.02 (t, *J* = 1.2 Hz, 2H), 4.75 (q, *J* = 1.3 Hz, 2H). <sup>13</sup>C NMR (126 MHz, CDCl<sub>3</sub>) δ 166.7, 141.9, 135.6, 135.5, 134.5, 131.6, 128.2, 127.8, 125.9, 125.8, 123.0, 122.5, 117.1, 116.5, 54.8, 52.7. HRMS (ESI)  $m/z$  [M+H] calculated for C<sub>16</sub>H<sub>12</sub>BrN<sub>2</sub>O, 327.0133, found 327.0076.

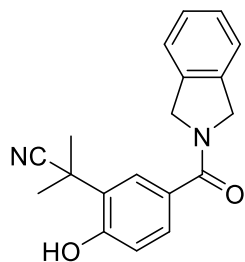


**2-bromo-4-(isoindoline-2-carbonyl)benzamide (15):** To a solution of 14 (50 mg, 0.15 mmol, 1 eq.) in DMSO:ethanol (1:3) (3 mL) were added 2N sodium hydroxide solution (0.15 mL, 0.3 mmol, 2 eq.) and 30 % hydrogen peroxide solution (0.034 mL, 0.3 mmol). The resulting mixture was extracted with ethyl acetate (3 × 5 mL). The resulting mixture was stirred for 2 h before the addition of water (5 mL). The organic layers were combined, washed with saturated sodium chloride solution (10 mL), dried over anhydrous sodium sulfate, filtered, and concentrated. The residue was purified by flash chromatography (SiO<sub>2</sub>, 1:3 hexane/ ethyl acetate) to give **15** as a white amorphous solid (35 mg, 71 %). <sup>1</sup>H NMR (500 MHz, Chloroform-*d*) δ 7.83 (d, *J* = 1.5 Hz, 1H), 7.74 (d, *J* = 7.8 Hz, 1H), 7.58 (dd, *J* = 7.8, 1.6 Hz, 1H), 7.38 – 7.28 (m, 3H), 7.19 (d, *J* = 7.6 Hz, 1H), 6.15 (s, 1H), 5.88 (s, 1H), 5.02 (s, 2H), 4.75 (d, *J* = 1.5 Hz, 2H). <sup>13</sup>C NMR (126 MHz, CDCl<sub>3</sub>) δ 168.3, 167.6, 139.9, 137.9, 135.9, 135.8, 131.9, 130.1, 128.0, 127.7, 125.9, 123.0, 122.5, 119.5, 54.9, 52.6. HRMS (ESI) *m/z* [M+H] calculated for C<sub>16</sub>H<sub>14</sub>BrN<sub>2</sub>O<sub>2</sub>, 345.0239, found 345.0243.

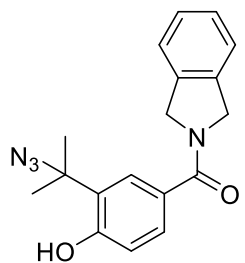


**(3-bromo-4-mercaptophenyl) (isoindolin-2-yl)methanone (16):** The intermediate **18** (100mg, 0.46 mmol, 1 eq.) was dissolved in DCM (3 mL), to this solution were introduced, N-(3-Dimethylaminopropyl)-N'-ethylcarbodiimide hydrochloride (175 mg, 0.92 mmol, 2.0 eq.), hydroxybenzotriazole hydrate (124.2 mg, 0.92 mmol, 2 eq.), N,N-Diisopropylethylamine (296 mg, 2.3 mmol, 5 eq.) and isoindoline hydrochloride (80 mg, 0.5 mmol, 1.1 eq.) Reaction was stirred overnight at rt, before solvent was removed in vacuo, subsequently, water (10 mL) was added to the remaining crude mass, acidified with 1N HCl and extracted with ethyl acetate (10 mL x2). The organic fractions were combined, dried over sodium sulfate, filtered and concentrated. The resulting residue was purified by flash chromatography (SiO<sub>2</sub>, 1:3 hexanes/ethyl acetate) to obtain (3-bromo-4-fluorophenyl)(isoindolin-2-yl)methanone, which was dissolved in DMF (3 mL). To this solution, benzyl mercaptan (171 mg, 1.38 mmol, 3 eq.) and potassium carbonate (190 mg, 1.38 mmol, 3 eq.) were added and heated to 140° C for 3h. The reaction was quenched with water (10 mL) and extracted with ethyl acetate (10 mL X 3). The organic fractions were combined, washed with brine (10 mL X 2), dried over sodium sulfate and subsequently, evaporated to result in a residue, which was passed through a pad of silica to yield (elution with 1:1 ethyl acetate:hexanes) to yield a crude mass. DCM (3 mL) was added to this mass, cooled to 0°C and 1M boron tribromide solution in DCM (1.38 mL, 1.38 mmol, 3 eq.) was added slowly. Reaction was quenched with a brine (10 mL), extracted with ethyl acetate (10 X 3), dried over sodium sulfate and purified using column chromatography (SiO<sub>2</sub>, 1:3 ethyl acetate/hexanes) to produce **16** (44 mg, 26% overall) as a white solid. <sup>1</sup>H NMR (500 MHz, Chloroform-*d*) δ 7.84 (dd, *J* = 6.5, 2.1 Hz, 1H), 7.55 (ddd, *J* = 8.4, 4.6, 2.1 Hz, 1H), 7.38 – 7.34 (m, 2H), 7.33 – 7.28 (m, 1H), 7.22 (q, *J* = 8.2 Hz, 2H), 7.15 – 7.14 (m, 1H), 5.02 (s, 2H), 4.80 (d, *J* = 1.4 Hz, 2H). <sup>13</sup>C NMR (126 MHz, CDCl<sub>3</sub>) δ 167.8, 136.0, 132.6, 130.1, 128.0, 128.0, 127.9, 127.7, 125.9, 123.0, 122.5, 116.7,

116.6, 55.0, 52.6. HRMS (ESI)  $m/z$  [M+H] calculated for  $C_{15}H_{13}BrNOS$ , 335.9875, found 335.9849.

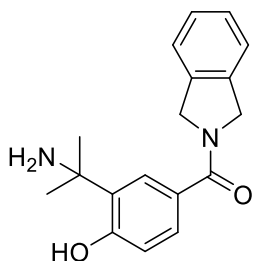


**2-(2-hydroxy-5-(isoindoline-2-carbonyl)phenyl)-2-methylpropanenitrile (19):** A solution of **10** (25 mg, 0.084 mmol, 1 eq.) in DCM (3 mL) under argon, was treated with trimethylsilyl cyanide (10 mg, 0.1 mmol, 1.2 eq.), cooled to 0°C, treated with  $BF_3$  etherate (15 mg, 0.1 mmol, 1.2 eq.), allowed to warm to room temperature and stirred for 2 h. The mixture was treated with sodium bicarbonate solution (5 mL), extracted with DCM ( $2 \times 5$  mL), the combined extracts washed with water (10 mL), dried over sodium sulfate, concentrated in vacuo and purified by chromatography [ $SiO_2$ ; heptane-EtOAc (6:4)] to furnish **19** (13 mg, 55 %) isolated as a white solid.  $^1H$  NMR (500 MHz, Chloroform-*d*)  $\delta$  7.42 (m, 1H), 7.37 (d,  $J = 2.1$  Hz, 1H), 7.35 – 7.29 (m, 3H), 7.18 (d,  $J = 7.5$  Hz, 1H), 6.90 (d,  $J = 8.2$  Hz, 1H), 5.02 (s, 2H), 4.83 (s, 2H), 1.70 (s, 6H).  $^{13}C$  NMR (126 MHz,  $CDCl_3$ )  $\delta$  170.5, 157.6, 136.5, 131.2, 127.8 (2), 127.5, 127.4, 125.3 (2), 122.9, 122.4, 117.2 (2), 76.0, 55.2, 52.6, 30.3 (2). HRMS (ESI)  $m/z$  [M+H] calculated for  $C_{19}H_{19}N_2O_2$ , 307.1447, found 307.0349.



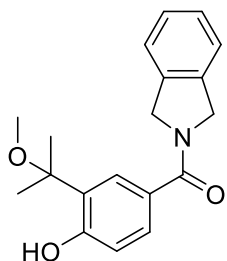


**(3-(2-azidopropan-2-yl)-4-hydroxyphenyl)(isoindolin-2-yl)methanone (20):** A solution of **10** (25 mg, 0.084 mmol, 1 eq.) in DCM (3 mL) under argon, was treated with sodium azide (17 mg, 0.25 mmol, 3 eq.), cooled to 0°C, treated with BF<sub>3</sub> etherate (15 mg, 0.1 mmol, 1.2 eq.), allowed to warm to room temperature and stirred for 4 h. The mixture was treated with 1N sodium bicarbonate solution (5 mL), extracted with DCM (2 × 5 mL), the combined extracts washed with water (10 mL), dried over sodium sulfate, concentrated in vacuo and purified by chromatography [SiO<sub>2</sub>; heptane-EtOAc (6:4)] to furnish **20** (15 mg, 65 %) isolated as a white solid. <sup>1</sup>H NMR (500 MHz, Chloroform-*d*) δ 7.82 (s, 1H), 7.51 – 7.49 (m, 2H), 7.39 – 7.29 (m, 3H), 7.21 (d, *J* = 7.4 Hz, 1H), 6.99 (d, *J* = 8.8 Hz, 1H), 5.05 (s, 2H), 4.86 (s, 2H), 1.77 (s, 6H). <sup>13</sup>C NMR (126 MHz, CDCl<sub>3</sub>) δ 170.0, 156.5, 136.5, 136.3, 128.8, 128.3 (2), 127.8, 127.5, 125.7, 122.9, 122.4, 117.7, 64.4, 55.2, 52.7, 26.7 (2). HRMS (ESI) *m/z* [M+Na] calculated for C<sub>18</sub>H<sub>18</sub>N<sub>4</sub>O<sub>2</sub>Na, 345.1327, found 345.1348.

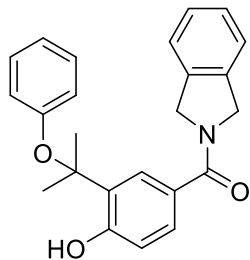


**(3-(2-aminopropan-2-yl)-4-hydroxyphenyl) (isoindolin-2-yl)methanone (21):** Intermediate **20** (10 mg, 0.031 mmol, 1 eq.) was dissolved in ethanol (3 mL) contained in a 15 mL sealed vessel. Subsequently, ammonium formate (20 mg, 0.3 mmol, 10 eq.) and Palladium on carbon (10%) were introduced in the reaction vessel, which was sealed, and heated to 80° C for 10 h. Solvent was removed in vacuo, and water (5 mL) was then added to the remaining mass and extracted with ethyl acetate (10 mL X 3), dried, evaporated to result in a mass that was purified using preparative thin layer chromatography. (SiO<sub>2</sub>, 1:9 methanol:DCM) to yield **21** (7 mg, 68%) as a white solid. <sup>1</sup>H NMR (500 MHz, Chloroform-*d*) δ 7.45 (d, *J* = 2.1 Hz, 1H), 7.41 (dd, *J* = 8.3, 2.1 Hz, 1H), 7.31

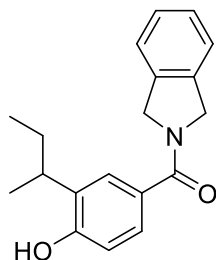
(m, 3H), 7.17 (d,  $J = 7.4$  Hz, 1H), 6.86 (d,  $J = 8.3$  Hz, 1H), 5.01 (s, 2H), 4.85 (s, 2H), 1.60 (s, 6H).  $^{13}\text{C}$  NMR (126 MHz,  $\text{CDCl}_3$ )  $\delta$  170.6, 159.7, 136.7, 136.5, 130.8, 127.8, 127.7, 127.4, 126.8, 125.8, 122.9, 122.4, 116.9, 55.2, 54.4, 52.6, 31.4 (2). HRMS (ESI)  $m/z$  [M+H] calculated for  $\text{C}_{18}\text{H}_{21}\text{N}_2\text{O}_2$ , 297.1603, found 297.1619.



**(4-hydroxy-3-(2-methoxypropan-2-yl)phenyl)(isoindolin-2-yl)methanone (22):** Ceric ammonium nitrate (15 mg, 0.027 mmol, 0.3 eq.) was added to a solution of **10** (25 mg, 0.084 mmol, 1 eq.) in methanol (5 mL), contained in a sealed reaction vessel, which was heated to 80°C for 12 h, cooled, solvent evaporated under vacuum, and extracted with water (10 mL) and ethyl acetate (20 mL X 2). The organic fractions were collected, dried using sodium sulfate, concentrated to yield a residue that was purified using column chromatography ( $\text{SiO}_2$ , 4:6 ethyl acetate:hexanes) to produce **22** (13 mg, 50%) as white solid.  $^1\text{H}$  NMR (500 MHz, Chloroform- $d$ )  $\delta$  9.04 (s, 1H), 7.46 (dd,  $J = 8.3, 2.1$  Hz, 1H), 7.39 (d,  $J = 2.1$  Hz, 1H), 7.37 – 7.23 (m, 3H), 7.18 (d,  $J = 7.2$  Hz, 1H), 6.91 (d,  $J = 8.4$  Hz, 1H), 5.02 (s, 2H), 4.85 (d,  $J = 6.6$  Hz, 2H), 3.25 (s, 3H), 1.63 (s, 6H).  $^{13}\text{C}$  NMR (126 MHz,  $\text{CDCl}_3$ )  $\delta$  170.3, 157.6, 136.6, 136.4, 128.8, 128.2, 127.8, 127.8, 127.5, 126.8, 122.9, 122.4, 116.5, 80.2, 55.1, 52.6, 50.9, 26.4 (2). HRMS (ESI)  $m/z$  [M+H] calculated for  $\text{C}_{19}\text{H}_{21}\text{NO}_3\text{Na}$ , 334.1419, found 334.1412.



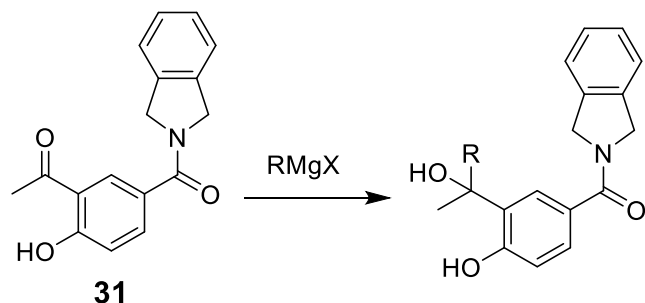
**(4-hydroxy-3-(2-phenoxypropan-2-yl)phenyl)(isoindolin-2-yl)methanone (23):** Phenol (60 mg, 0.67 mmol, 8 eq.) was introduced to a solution of **10** (25 mg, 0.084 mmol, 1 eq.) in trifluoroacetic acid :DCM (1:9, 5 mL) contained in a sealed vessel. The reaction was heated to 45°C for 24 h, cooled, and the solvent removed under vacuum. Water (10 mL) and Ethyl acetate (20 mL X 2) was used for extraction. Organic layers were combined, dried over sodium sulfate and concentrated to result in a residue mass that was purified using preparative thin layer chromatography. (SiO<sub>2</sub>, 3:7 ethyl acetate:hexanes) to yield **23** (8 mg, 25%) as a white solid. <sup>1</sup>H NMR (400 MHz, Chloroform-*d*) δ 7.72 (d, *J* = 2.0 Hz, 1H), 7.40 (m, 1H), 7.31 (d, *J* = 28.4 Hz, 4H), 7.20 (d, *J* = 7.3 Hz, 1H), 7.18 – 7.10 (m, 2H), 6.77 (m, 3H), 5.05 (s, 2H), 4.88 (s, 2H), 1.64 (s, 6H). <sup>13</sup>C NMR (101 MHz, CDCl<sub>3</sub>) δ 171.0, 155.9, 155.5, 138.4, 136.5, 136.3, 135.7, 128.0, 127.8, 127.5, 127.2 (2), 127.0, 126.2 (2), 122.9, 122.4, 117.2, 116.1, 55.2, 53.4, 52.7, 29.6 (2). HRMS (ESI) *m/z* [M+H] calculated for C<sub>24</sub>H<sub>24</sub>NO<sub>3</sub>, 374.1756, found 374.1773.



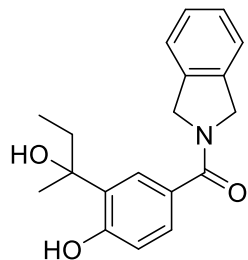
**(3-(sec-butyl)-4-hydroxyphenyl)(isoindolin-2-yl)methanone (24):** (4-(benzyloxy)-3-bromophenyl)(isoindolin-2-yl)methanone (**29**) (100 mg, 0.24 mmol, 1 eq.) was dissolved in

THF:water (8:2) (10 mL). Subsequently, Potassium (2Z)-2-buten-2-yltrifluoroborate (60 mg, 0.36 mmol, 1.5 eq.), cesium carbonate (156 mg, 0.48 mmol, 2 eq.) and tetrakis(triphenylphosphine)palladium (0) (27 mg, 0.024 mmol, 0.1 eq) were introduced to this solution in a 15 mL sealed reaction vessel, purged with argon before closing the cap and heating to 100°C for 10 h. The reaction mass was transferred to a round bottom flask and solvent was removed under vacuum. Water (10 mL) was added to the crude and ethyl acetate (20 mL X 2) was used for extraction. Organic layers were combined, dried over sodium sulfate and concentrated to result in a residue that was passed through a small pad of silica (eluted with 4:6 ethyl acetate:hexanes), concentrated, to give a brown residue. Obtained residue was dissolved in ethyl acetate (10 mL), and hydrogenation was performed using palladium on carbon (10%). Upon completion of reaction as indicated by TLC, the reaction mixture was filtered through a pad of Celite and column chromatography (SiO<sub>2</sub>, 3:7 ethyl acetate:hexanes) then furnished 24 (28 mg, 40%) as a white solid. <sup>1</sup>H NMR (500 MHz, Chloroform-*d*) δ 7.35 (d, *J* = 2.2 Hz, 1H), 7.29 – 7.16 (m, 4H), 7.10 (d, *J* = 7.4 Hz, 1H), 6.72 (d, *J* = 8.2 Hz, 1H), 5.20 (s, 1H), 4.95 (s, 2H), 4.74 (s, 2H), 2.94 (q, *J* = 7.0 Hz, 1H), 1.66 – 1.52 (m, 2H), 1.20 – 1.17 (d, 3H), 0.82 (t, *J* = 7.4 Hz, 3H). <sup>13</sup>C NMR (126 MHz, CDCl<sub>3</sub>) δ 170.7, 154.7, 133.3, 128.9, 127.7, 127.4, 126.7, 125.9, 122.9, 122.4, 115.0, 55.2, 52.6, 33.9, 29.7, 20.3, 12.1. HRMS (ESI) *m/z* [M+H] calculated for C<sub>19</sub>H<sub>22</sub>NO<sub>2</sub>, 296.1651, found 296.1668.

### General procedure A:

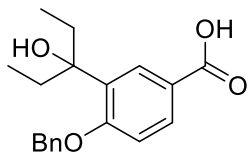


A solution of the desired Grignard's reagent (0.85 mmol, 5 eq.) in THF was added to a solution of **31** (50 mg, 0.17 mmol, 1 eq.) in THF (5 mL) at 0°C. The reaction mixture was stirred at 0°C for 15 min, allowed to warm to rt. Upon completion of the reaction, as indicated by TLC, reaction was quenched with 1N HCl (2 mL) and then extraction was performed using ethyl acetate (10 mL X 3). Organic layers were combined, washed with water (10 mL), dried over sodium sulfate and concentrated. The resulting residue was purified using flash chromatography (SiO<sub>2</sub>, 4:6 ethyl acetate:hexanes) to result in the desired final products, which purified again using a preparative TLC (SiO<sub>2</sub>, 2:98 methanol:DCM).



**(4-hydroxy-3-(2-hydroxybutan-2-yl)phenyl)(isoindolin-2-yl)methanone (25):** Prepared using general procedure A, yield 74 %, off white solid. <sup>1</sup>H NMR (400 MHz, Chloroform-*d*) δ 9.59 (s, 1H), 7.31 (dd, *J* = 8.3, 2.1 Hz, 1H), 7.19 (s, 3H), 7.17 (d, *J* = 2.1 Hz, 1H), 7.09 (d, *J* = 7.3 Hz, 1H), 6.79 (d, *J* = 8.3 Hz, 1H), 4.93 (s, 2H), 4.80 – 4.66 (m, 2H), 1.85 (m, 2H), 1.57 (s, 3H), 0.83 (t, *J* = 7.5 Hz, 3H). <sup>13</sup>C NMR (101 MHz, CDCl<sub>3</sub>) δ 170.6, 158.1, 136.5, 136.4, 129.6, 127.8, 127.6, 127.5,

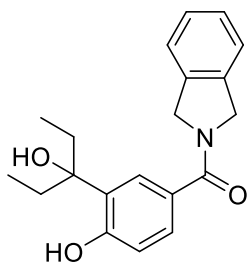
127.1, 126.1, 122.9, 122.4, 117.2, 78.9, 55.2, 52.6, 35.3, 28.1, 8.4. HRMS (ESI)  $m/z$  [M+H] calculated for C<sub>19</sub>H<sub>22</sub>NO<sub>3</sub>, 312.1600, 312.1624.



**4-(benzyloxy)-3-(3-hydroxypentan-3-yl)benzoic acid (33):** A solution of **32** (1 g, 4.6 mmol, 1 eq.) in acetone (20 mL) was treated with benzyl bromide (2g, 11.5 mmol, 2.5 eq.) and potassium carbonate (1.9 g, 13.8 mmol, 3 eq.). The resulting mixture was stirred, heated at 50° C for 10 h. Solvent was removed under vacuum, then, water (50 mL) and ethyl acetate (50 mL X 3) were used for extraction. Organic fractions were combined, dried over sodium sulfate, and concentrated under vacuum to result in a white solid mass. This residue was dissolved in Ethanol (30 mL), 2N aq. Sodium hydroxide solution was then added, and the reaction was heated to 60°C till completion of the reaction, which was monitored using TLC. Ethanol was then removed from the reaction mixture and the water (50 mL) was added to the concentrated reaction mass. Subsequently, 1N HCl was added to adjust the pH ~3. Extraction was then performed using ethyl acetate (50 mL X 2). Organic layers were then combined, washed with water, dried over sodium sulfate and concentrated to produce a white mass. A quick chromatography (SiO<sub>2</sub>, 3:7 ethyl acetate:hexane) was performed to obtain 4-(benzyloxy)-3-bromobenzoic acid as white solid.

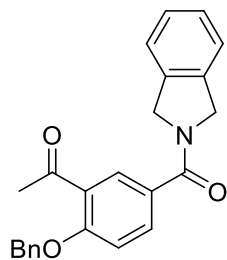
In the following step, 4-(benzyloxy)-3-bromobenzoic acid (200 mg, 0.65 mmol, 1 eq.) was dissolved in THF (10 mL), cooled to -78°C, and a 2.5 M solution of *n*-BuLi (0.8 mL, 2 mmol, 3 eq.) in hexanes was added slowly. The reaction was stirred at -78°C for 30 mins, before 3-Pentanone (0.35 mL, 3.25 mmol, 5 eq.) was introduced. Reaction was allowed to warm to 0° C, and stirred for additional 1 h before it was quenched with saturated ammonium chloride solution

(10 mL). Extraction was then performed using ethyl acetate (30 mL X 2). The resulting organic fractions were combined, dried, evaporated to result in a residue, which was purified using column chromatography (SiO<sub>2</sub>, 4:6 ethyl acetate:hexanes) to yield **33** (30 mg, 15 %) as a white solid. <sup>1</sup>H NMR (400 MHz, Chloroform-*d*) δ 8.17 (d, *J* = 2.2 Hz, 1H), 8.02 (dd, *J* = 8.6, 2.2 Hz, 1H), 7.46 – 7.35 (m, 5H), 7.04 (d, *J* = 8.6 Hz, 1H), 5.20 (s, 2H), 2.13 (m, 2H), 1.90 – 1.78 (m, 2H), 0.78 (t, *J* = 7.4 Hz, 6H). <sup>13</sup>C NMR (101 MHz, CDCl<sub>3</sub>) δ 170.9, 160.3, 133.3, 130.9, 130.7, 128.9 (2), 128.5, 127.6 (2), 121.5, 111.9, 99.9, 77.9, 70.9, 32.4 (2), 8.3 (2). HRMS (ESI) *m/z* [M+H] calculated for C<sub>19</sub>H<sub>23</sub>O<sub>4</sub>, 315.1596, found 315.1615.



**(4-hydroxy-3-(3-hydroxypentan-3-yl)phenyl)(isoindolin-2-yl)methanone (26):** **33** (25 mg, 0.08 mmol, 1 eq.) was dissolved in DCM (3 mL) together with *N*-(3-Dimethylaminopropyl)-*N'*-ethylcarbodiimide hydrochloride (30 mg, 0.16 mmol, 2.0 eq.), hydroxybenzotriazole hydrate (22 mg, 0.16 mmol, 2 eq.), *N,N*-Diisopropylethylamine (51 mg, 0.4 mmol, 5 eq.) and isoindoline hydrochloride (14 mg, 0.09 mmol, 1.1 eq.). The resulting mixture was stirred at rt for 12 h, before solvent was removed in vacuo, subsequently, water (10 mL) was added to the remaining crude mass, acidified with 1N HCl and extracted with ethyl acetate (10 mL x2). The organic fractions were combined, dried over sodium sulfate, filtered and concentrated. The resulting residue was purified by a quick flash chromatography (SiO<sub>2</sub>, 1:3 hexanes/ethyl acetate) to obtain a white crude mass. In the subsequent reaction, the obtained solid mass (~20 mg) was dissolved in DCM (5mL), cooled to 0°C, subsequently, 1M DCM solution of boron tribromide (0.144 mL, 0.144 mmol, 3

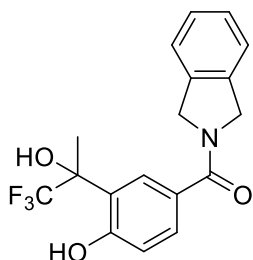
eq.) was added. The reaction was stirred and allowed to gradually warm to rt over 1 h, before the reaction was quenched with water (10 mL). DCM fraction was separated, and aqueous layer was washed with DCM (10 mL X2). Organic fractions were combined, dried over sodium sulfate, and concentrated to yield a residue that was purified using preparative TLC (SiO<sub>2</sub>, 3:7 ethyl acetate:hexanes) to result in **26** (9 mg, 34 %) as white solid. <sup>1</sup>H NMR (500 MHz, Chloroform-*d*) δ 9.67 (s, 1H), 7.34 (dd, *J* = 8.4, 2.1 Hz, 1H), 7.29 – 7.16 (m, 3H), 7.14 (d, *J* = 2.1 Hz, 1H), 7.10 (d, *J* = 7.2 Hz, 1H), 6.82 (d, *J* = 8.4 Hz, 1H), 4.94 (s, 2H), 4.75 (s, 2H), 1.94 (m, 2H), 1.80 (m, 2H), 0.84 (t, *J* = 7.4 Hz, 6H). <sup>13</sup>C NMR (126 MHz, CDCl<sub>3</sub>) δ 170.4, 159.1, 136.5, 136.5, 127.8, 127.7, 127.5, 127.2, 126.8, 126.5, 122.9, 122.4, 117.4, 82.7, 55.2, 52.7, 34.3 (2), 7.88 (2). HRMS (ESI) *m/z* [M+H] calculated for C<sub>20</sub>H<sub>24</sub>NO<sub>3</sub>, 326.1756, found 326.1779.



**1-(2-(benzyloxy)-5-(isoindoline-2-carbonyl)phenyl)ethan-1-one (34):** To a round bottom flask containing **31** (1 g, 3.5 mmol, 1 eq.) dissolved in acetone (30 mL) were added potassium carbonate (580 mg, 4.2 mmol, 1.2 eq) and benzyl bromide (0.53 mL, 4.2 mmol, 1.2 eq.). Reaction was then refluxed for 12 h, cooled, solvent removed under vacuum, and remaining mass was extracted using water (50 mL) and ethyl acetate (50 X 2). Organic fractions were collected, washed with water (50 mL), dried over sodium sulfate, concentrated and purified using column chromatography (SiO<sub>2</sub>, 3:7 ethyl acetate:hexanes) to afford **34** (1.1 g, 84%) as white solid. <sup>1</sup>H NMR (500 MHz, Chloroform-*d*) δ 8.05 (d, *J* = 2.3 Hz, 1H), 7.77 (dd, *J* = 8.6, 2.3 Hz, 1H), 7.50 – 7.27 (m, 8H), 7.15 (dd, *J* = 27.6, 8.0 Hz, 2H), 5.25 (s, 2H), 5.03 (s, 2H), 4.86 (s, 2H), 2.64 (s, 3H). <sup>13</sup>C NMR (126



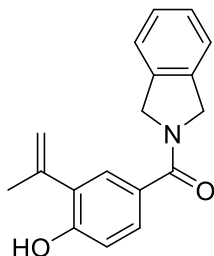
MHz, CDCl<sub>3</sub>)  $\delta$  198.9, 169.0, 159.2, 136.4, 136.2, 135.6, 133.2, 129.5, 129.1, 128.8 (2), 128.5, 128.0, 127.8, 127.6 (2), 127.5, 122.9, 122.4, 113.0, 70.9, 55.0, 52.7, 32.1. HRMS (ESI)  $m/z$  [M+Na] calculated for C<sub>24</sub>H<sub>21</sub>NO<sub>3</sub>Na, 394.1419, found 394.1435.



**(4-hydroxy-3-(1,1,1-trifluoro-2-hydroxypropan-2-yl)phenyl)(isoindolin-2-yl)methanone**

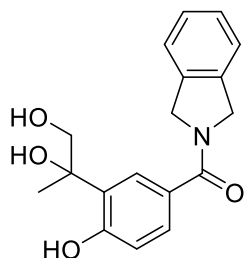
**(27):** A solution of **34** (25 mg, 0.07 mmol, 1 eq.) in THF (5 mL) was cooled to 0°C, trifluoromethyltrimethylsilane (35  $\mu$ L, 0.21 mmol, 3 eq.) and 1M THF solution of tetra-*n*-butylammonium fluoride (TBAF) (0.21 mL, 0.21 mmol, 3 eq.) were then introduced. The reaction was then allowed to warm to rt and reaction was monitored for consumption of starting material using TLC. Upon completion, reaction was quenched with sat. ammonium chloride solution, extracted with ethyl acetate (10 mL X 3). Organic fractions were combined, dried over sodium sulfate and evaporated to produce a residue that was subjected to subsequent reaction without purification. In the following step, the obtained residue was dissolved in DCM (5 mL), cooled to 0°C, and 1M DCM solution of BCl<sub>3</sub> (0.21 mL, 0.21 mmol, 3 eq.) was then added slowly. Reaction was stirred at 0°C till completion, as monitored via TLC. Water (5mL) was then added to the reaction mixture, and extraction was performed using ethyl acetate (10 mL X 3). Organic fractions were combined washed with water (20 mL), dried (Na<sub>2</sub>SO<sub>4</sub>), and evaporated under vacuum to result in a mass that was purified using column chromatography (SiO<sub>2</sub>, 3:7 ethyl acetate:hexanes) to afford **27** (11 mg, 45%) as white solid. <sup>1</sup>H NMR (500 MHz, Chloroform-*d*)  $\delta$  9.41 (s, 1H), 7.31 – 7.20 (m, 4H), 7.10 (q,  $J$  = 3.0 Hz, 2H), 6.71 (d,  $J$  = 8.4 Hz, 1H), 6.22 (s, 1H), 4.92 (s, 2H), 4.65

(q,  $J = 14.4$  Hz, 2H), 1.69 (s, 3H).  $^{13}\text{C}$  NMR (126 MHz,  $\text{CDCl}_3$ )  $\delta$  170.9, 158.9, 136.0, 135.8, 128.8 (2), 127.9, 127.7, 127.0, 126.6, 122.9, 122.5, 121.6, 118.6, 77.2, 55.1, 52.7, 22.6. HRMS (ESI)  $m/z$  [M+H] calculated for  $\text{C}_{18}\text{H}_{17}\text{F}_3\text{NO}_3$ , 352.1161, found 352.1176.



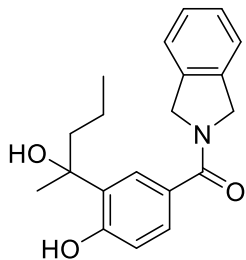
**(4-hydroxy-3-(prop-1-en-2-yl)phenyl)(isoindolin-2-yl)methanone (30):** A reaction vessel was charged with **29** (100 mg, 0.24 mmol, 1 eq.), potassium isopropenyltrifluoroborate (53 mg, 0.36 mmol, 1.5 eq.), cesium carbonate (156 mg, 0.48 mmol, 2 eq.), tetrakis(triphenylphosphine)palladium (0) (27 mg, 0.024 mmol, 0.1 eq.). Into this vessel, solvent (10 mL, 1:9, water: THF) was added, purged with argon, sealed with Teflon lined cap and heated to 100°C for 10 h. Reaction was cooled, solvent removed under pressure, and the remaining mass extracted using water (30 mL) and ethyl acetate (30 mL X 2). Organic fractions were combined, dried, and evaporated to a white mass. Boron trichloride solution (0.72 mL of 1M DCM solution, 0.72 mmol, 3 eq.) was then added to a 0°C cooled solution of the obtained mass in DCM (5 mL). Upon completion as monitored by TLC, the reaction was quenched with sat. ammonium chloride solution (10 mL). Extraction was performed using water (20 mL) and DCM (20 mL X 2), subsequently, DCM fractions were combined, dried over sodium sulfate and adsorbed on silica for purification using flash chromatography ( $\text{SiO}_2$ , 3:7 ethyl acetate:hexanes) to afford **30** (46 mg, 70%) as off white solid.  $^1\text{H}$  NMR (500 MHz, Chloroform- $d$ )  $\delta$  7.37 – 7.32 (m, 2H), 7.29 – 7.17 (m, 4H), 7.10 (d,  $J = 7.5$  Hz, 1H), 6.90 (d,  $J = 8.3$  Hz, 1H), 6.07 (s, 1H), 5.37 (p,  $J = 1.6$  Hz, 1H), 5.12 (dd,  $J = 1.8, 0.9$  Hz, 1H), 4.95 (s, 2H), 4.77 (s, 2H), 2.07 (t,  $J = 1.2$  Hz, 3H).  $^{13}\text{C}$  NMR (126

MHz, CDCl<sub>3</sub>)  $\delta$  170.1, 153.7, 141.5, 136.5, 136.4, 128.9, 128.4, 127.8, 127.7, 127.5, 127.4, 122.9, 122.4, 116.5, 115.4, 55.2, 52.6, 24.1. HRMS (ESI)  $m/z$  [M+H] calculated for C<sub>18</sub>H<sub>18</sub>NO<sub>2</sub>, 280.1338, found 280.1335.

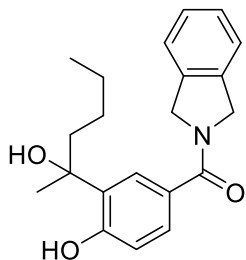


**(3-(1,2-dihydroxypropan-2-yl)-4-hydroxyphenyl)(isoindolin-2-yl)methanone (28):**

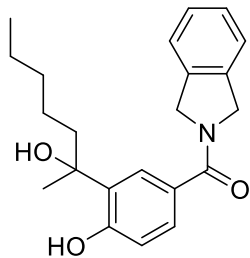
Compound **30** (25 mg, 0.09 mmol, 1 eq.) was dissolved in 2mL of acetone: *t*-butanol: water solvent mixture. Osmium tetroxide (0.1 mL of 4% aq. solution) and N-methylmorpholine-N-Oxide (40 mg, 0.34 mmol, 3.8 eq.) were then added and the reaction was stirred for 1 h at rt, quenched with water and extracted with ethyl acetate (20 mLX 2). Organic layers were combined washed with water and adsorbed on silica for purification (SiO<sub>2</sub>, 4:6 ethyl acetate:hexanes) which afforded **28** (19 mg, 67%) as white solid. <sup>1</sup>H NMR (500 MHz, Chloroform-*d*)  $\delta$  9.76 (s, 1H), 7.39 (dd,  $J$  = 8.4, 2.0 Hz, 1H), 7.35 – 7.27 (m, 4H), 7.17 (d,  $J$  = 7.3 Hz, 1H), 6.88 (d,  $J$  = 8.3 Hz, 1H), 5.07 – 4.92 (m, 2H), 4.90 – 4.76 (m, 2H), 4.54 (s, 1H), 3.95 (d,  $J$  = 11.2 Hz, 1H), 3.60 – 3.43 (m, 2H), 1.55 (s, 3H). <sup>13</sup>C NMR (126 MHz, CDCl<sub>3</sub>)  $\delta$  170.7, 158.8, 136.3, 136.0, 127.9, 127.8, 127.7, 127.6, 126.8, 126.1, 122.9, 122.4, 117.4, 78.0, 68.6, 55.2, 52.7, 24.9. HRMS (ESI)  $m/z$  [M+H] calculated for C<sub>18</sub>H<sub>20</sub>NO<sub>4</sub>, 314.1392, found 314.1401.



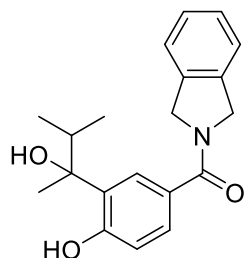
**(4-hydroxy-3-(2-hydroxypentan-2-yl)phenyl)(isoindolin-2-yl)methanone (35a):** Prepared using general procedure A, 40 mg, Yield 72%, white solid:  $^1\text{H}$  NMR (500 MHz, Chloroform-*d*)  $\delta$  9.90 (s, 1H), 7.38 – 7.25 (m, 4H), 7.21 (q,  $J = 3.0$  Hz, 1H), 7.17 (d,  $J = 7.0$  Hz, 1H), 6.82 (dd,  $J = 8.3, 3.8$  Hz, 1H), 5.11 – 4.93 (m, 2H), 4.81 (m, 3.8 Hz, 2H), 4.18 – 3.87 (m, 1H), 1.82 (m, 2H), 1.62 (s, 3H), 1.40 – 1.19 (m, 2H), 0.89 (m, 3H).  $^{13}\text{C}$  NMR (126 MHz,  $\text{CDCl}_3$ )  $\delta$  170.8, 158.1, 136.4, 136.3, 130.4, 127.8, 127.5, 127.4, 126.7, 125.9, 122.9, 122.4, 117.2, 78.2, 55.2, 52.7, 45.0, 28.3, 17.3, 14.3. HRMS (ESI)  $m/z$   $[\text{M}+\text{H}]$  calculated for  $\text{C}_{20}\text{H}_{24}\text{NO}_3$ , 326.1756, found 326.1768.



**(4-hydroxy-3-(2-hydroxyhexan-2-yl)phenyl)(isoindolin-2-yl)methanone (35b):** Prepared using general procedure A, 44 mg, Yield 77%, white solid:  $^1\text{H}$  NMR (500 MHz, Chloroform-*d*)  $\delta$  9.95 (s, 1H), 7.37 – 7.23 (m, 4H), 7.19 (d,  $J = 2.1$  Hz, 1H), 7.16 (d,  $J = 7.4$  Hz, 1H), 6.81 (d,  $J = 8.3$  Hz, 1H), 5.05 – 4.93 (m, 2H), 4.86 – 4.73 (m, 2H), 1.93 – 1.74 (m, 2H), 1.61 (s, 3H), 1.27 (tdd,  $J = 14.3, 9.0, 5.0$  Hz, 4H), 0.87 (t,  $J = 7.0$  Hz, 3H).  $^{13}\text{C}$  NMR (126 MHz,  $\text{CDCl}_3$ )  $\delta$  170.9, 158.1, 136.4, 136.2, 130.4, 127.8, 127.5, 127.4, 126.6, 125.8, 122.9, 122.4, 117.2, 78.1, 55.2, 52.7, 42.5, 28.2, 26.3, 22.9, 14.1. HRMS (ESI)  $m/z$   $[\text{M}+\text{H}]$  calculated for  $\text{C}_{21}\text{H}_{26}\text{NO}_3$ , 340.1913, found 340.1920.

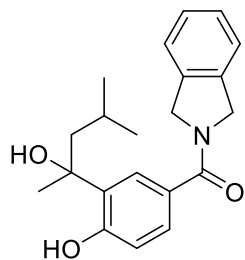


**(4-hydroxy-3-(2-hydroxyheptan-2-yl)phenyl)(isoindolin-2-yl)methanone (35c):** Prepared using general procedure A, 39 mg, Yield 65%, white solid:  $^1\text{H}$  NMR (500 MHz, Chloroform-*d*)  $\delta$  7.37 (dd,  $J = 8.3, 2.1$  Hz, 1H), 7.35 – 7.27 (m, 3H), 7.24 (d,  $J = 2.1$  Hz, 1H), 7.16 (d,  $J = 7.5$  Hz, 1H), 6.85 (d,  $J = 8.3$  Hz, 1H), 5.00 (s, 2H), 4.82 (d,  $J = 16.1$  Hz, 2H), 1.94 – 1.76 (m, 2H), 1.64 (s, 3H), 1.36 – 1.19 (m, 6H), 0.88 – 0.82 (m, 3H).  $^{13}\text{C}$  NMR (126 MHz,  $\text{CDCl}_3$ )  $\delta$  170.7, 158.0, 136.3, 130.0, 127.8, 127.6, 127.5, 126.9, 125.9, 122.9, 122.4, 117.3, 78.6, 55.2, 52.7, 42.7, 31.9, 28.5, 23.7, 22.6, 14., 14.0. HRMS (ESI)  $m/z$   $[\text{M}+\text{H}]$  calculated for  $\text{C}_{22}\text{H}_{28}\text{NO}_3$ , 354.2069, found 354.2076.



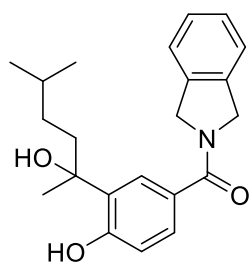
**(4-hydroxy-3-(2-hydroxy-3-methylbutan-2-yl)phenyl)(isoindolin-2-yl)methanone (35d):** Prepared using general procedure A, 38 mg, Yield 70%, white solid:  $^1\text{H}$  NMR (500 MHz, Chloroform-*d*)  $\delta$  9.80 (s, 1H), 7.40 – 7.25 (m, 4H), 7.21 (d,  $J = 2.1$  Hz, 1H), 7.18 (d,  $J = 7.4$  Hz, 1H), 6.84 (d,  $J = 8.3$  Hz, 1H), 5.08 – 4.94 (m, 2H), 4.80 (q,  $J = 14.3$  Hz, 2H), 3.36 (s, 1H), 2.17 (p,  $J = 6.8$  Hz, 1H), 1.60 (s, 3H), 0.99 (d,  $J = 6.8$  Hz, 3H), 0.86 (d,  $J = 6.8$  Hz, 3H).  $^{13}\text{C}$  NMR (126 MHz,  $\text{CDCl}_3$ )  $\delta$  170.7, 158.1, 136.5, 136.3, 129.6, 127.8, 127.6, 127.5, 126.7, 126.7, 122.9, 122.4,

117.3, 81.2, 55.2, 52.7, 37.5, 24.8, 17.5, 17.1. HRMS (ESI)  $m/z$  [M+H] calculated for C<sub>20</sub>H<sub>24</sub>NO<sub>3</sub>, 326.1756, found 326.1763.



**(4-hydroxy-3-(2-hydroxy-4-methylpentan-2-yl)phenyl)(isoindolin-2-yl)methanone (35e):**

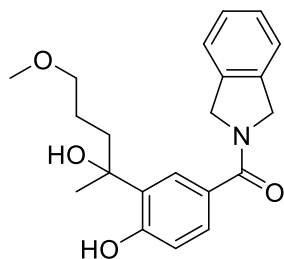
Prepared using general procedure A, 35 mg, Yield 61%, white solid: <sup>1</sup>H NMR (500 MHz, Chloroform-*d*)  $\delta$  9.79 (s, 1H), 7.38 (dd,  $J$  = 8.3, 2.1 Hz, 1H), 7.36 – 7.28 (m, 3H), 7.26 (d,  $J$  = 2.1 Hz, 1H), 7.18 (d,  $J$  = 7.4 Hz, 1H), 6.86 (d,  $J$  = 8.3 Hz, 1H), 5.00 (t,  $J$  = 11.1 Hz, 2H), 4.81 (q,  $J$  = 14.3 Hz, 2H), 1.92 – 1.84 (m, 1H), 1.79 – 1.71 (m, 2H), 1.68 (s, 3H), 0.92 (d,  $J$  = 6.4 Hz, 3H), 0.85 (d,  $J$  = 6.3 Hz, 3H). <sup>13</sup>C NMR (126 MHz, CDCl<sub>3</sub>)  $\delta$  170.6, 158.0, 136.5, 136.3, 130.3, 127.8, 127.5, 127.5, 127.0, 126.0, 122.9, 122.4, 117.2, 79.1, 55.2, 52.7, 51.3, 29.4, 24.6, 24.5, 24.5. HRMS (ESI)  $m/z$  [M+H] calculated for C<sub>21</sub>H<sub>26</sub>NO<sub>3</sub>, 340.1913, found 340.1926.



**(4-hydroxy-3-(2-hydroxy-5-methylhexan-2-yl)phenyl)(isoindolin-2-yl)methanone (35f):**

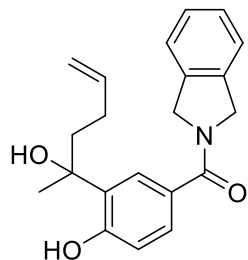
Prepared using general procedure A, 40 mg, Yield 65%, white solid: <sup>1</sup>H NMR (500 MHz, Chloroform-*d*)  $\delta$  9.81 (s, 1H), 7.39 – 7.24 (m, 4H), 7.21 (d,  $J$  = 2.1 Hz, 1H), 7.16 (d,  $J$  = 7.4 Hz, 1H), 6.83 (d,  $J$  = 8.3 Hz, 1H), 5.00 (s, 2H), 4.80 (s, 2H), 3.80 (s, 1H), 1.77-1.93 (m, 2H), 1.63 (s,

3H), 1.49 (dp,  $J = 13.3, 6.6$  Hz, 1H), 1.29 – 1.11 (m, 2H), 0.86 (dd,  $J = 8.9, 6.6$  Hz, 6H).  $^{13}\text{C}$  NMR (126 MHz,  $\text{CDCl}_3$ )  $\delta$  170.8, 158.1, 136.5, 136.3, 130.2, 127.8, 127.5, 127.5, 126.8, 125.8, 122.9, 122.3, 117.3, 78.4, 55.2, 52.6, 40.5, 32.9, 28.3, 28.2, 22.6, 22.6. HRMS (ESI)  $m/z$  [M+H] calculated for  $\text{C}_{22}\text{H}_{28}\text{NO}_3$ , 354.2069, found 354.2065.



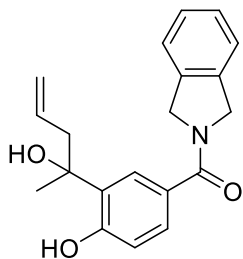
**(4-hydroxy-3-(2-hydroxy-5-methoxypentan-2-yl)phenyl)(isoindolin-2-yl)methanone (35g):**

Prepared using general procedure A, 33 mg, Yield 55%, white solid:  $^1\text{H}$  NMR (500 MHz, Chloroform- $d$ )  $\delta$  10.44 (s, 1H), 7.40 (dd,  $J = 8.3, 2.1$  Hz, 1H), 7.36 – 7.28 (m, 3H), 7.18 (d,  $J = 7.4$  Hz, 1H), 6.88 (d,  $J = 8.3$  Hz, 1H), 5.85 (s, 1H), 5.01 (s, 2H), 4.84 (s, 2H), 3.50 – 3.42 (m, 2H), 3.39 (s, 3H), 2.34 (m, 1H), 1.93 (m, 1H), 1.87 – 1.72 (m, 2H), 1.60 (s, 3H).  $^{13}\text{C}$  NMR (126 MHz,  $\text{CDCl}_3$ )  $\delta$  170.5, 158.7, 136.6, 136.5, 130.1, 127.7, 127.4, 127.1, 126.2, 122.9, 122.4, 117.2, 77.6, 77.2, 73.3, 58.7, 55.2, 52.6, 40.6, 30.0, 24.5. HRMS (ESI)  $m/z$  [M+H] calculated for  $\text{C}_{21}\text{H}_{26}\text{NO}_4$ , 356.1862, found 356.1878.



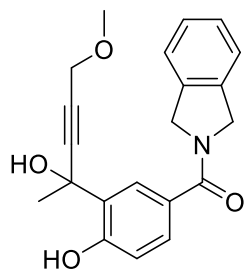
**(4-hydroxy-3-(2-hydroxyhex-5-en-2-yl)phenyl)(isoindolin-2-yl)methanone (35h):** Prepared using general procedure A, 31 mg, Yield 55%, white solid:  $^1\text{H}$  NMR (500 MHz, Chloroform- $d$ )  $\delta$

9.65 (s, 1H), 7.40 (dd,  $J = 8.3, 2.1$  Hz, 1H), 7.36 – 7.27 (m, 3H), 7.17 (d,  $J = 7.5$  Hz, 1H), 6.87 (d,  $J = 8.3$  Hz, 1H), 5.87 – 5.75 (m, 1H), 5.07 – 4.94 (m, 4H), 4.88 – 4.75 (m, 2H), 3.23 (t,  $J = 1.5$  Hz, 1H), 2.17 – 2.02 (m, 3H), 1.93 (m, 1H), 1.68 (s, 3H).  $^{13}\text{C}$  NMR (126 MHz,  $\text{CDCl}_3$ )  $\delta$  170.5, 158.0, 138.0, 136.5, 136.3, 129.6, 127.8, 127.7, 127.5, 127.2, 126.0, 122.9, 122.4, 117.4, 115.2, 78.8, 55.2, 52.7, 41.6, 28.9, 28.4. HRMS (ESI)  $m/z$   $[\text{M}+\text{H}]$  calculated for  $\text{C}_{21}\text{H}_{24}\text{NO}_3$ , 338.1756, found 338.1769.



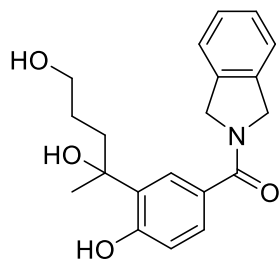
**(4-hydroxy-3-(2-hydroxypent-4-en-2-yl)phenyl)(isoindolin-2-yl)methanone (35h):** A solution of the allyl magnesium bromide (0.85 mmol, 5 eq.) in THF was added to a solution of **31** (50 mg, 0.17 mmol, 1 eq.) in THF (5 mL) at  $-20^\circ\text{C}$ . The reaction mixture was stirred at  $-20^\circ\text{C}$  for 15 min, allowed to warm to rt. Upon completion of the reaction, as indicated by TLC, reaction was quenched with 1N HCl (2 mL) and then extraction was performed using ethyl acetate (10 mL X 3). Organic layers were combined, washed with water (10 mL), dried over sodium sulfate and concentrated. The resulting residue was purified using flash chromatography ( $\text{SiO}_2$ , 4:6 ethyl acetate:hexanes) to produce **35h** (27mg, 50%) as white solid.  $^1\text{H}$  NMR (500 MHz, Chloroform- $d$ )  $\delta$  9.55 (s, 1H), 7.43 (dd,  $J = 8.3, 2.1$  Hz, 1H), 7.39 – 7.29 (m, 4H), 7.20 (d,  $J = 7.5$  Hz, 1H), 6.91 (d,  $J = 8.3$  Hz, 1H), 5.82 (m, 1H), 5.28 – 5.19 (m, 2H), 5.03 (s, 2H), 4.84 (s, 2H), 2.84 (m, 1H), 2.59 (m, 1H), 1.66 (s, 3H).  $^{13}\text{C}$  NMR (126 MHz,  $\text{CDCl}_3$ )  $\delta$  170.4, 157.9, 136.5, 136.4, 132.6, 129.5, 127.8, 127.8, 127.5, 127.4, 125.9, 122.9, 122.4, 120.8, 117.4, 77.2, 55.2, 52.6, 46.5, 28.5. HRMS (ESI)  $m/z$   $[\text{M}+\text{H}]$  calculated for  $\text{C}_{20}\text{H}_{22}\text{NO}_3$ , 324.1600, found 324.1616.





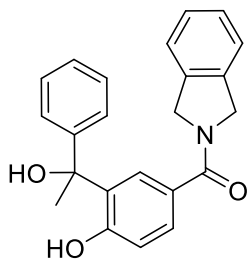
**(4-hydroxy-3-(2-hydroxy-5-methoxypent-3-yn-2-yl)phenyl)(isoindolin-2-yl)methanone**

**(35j):** Methyl propargyl ether (0.06 mL, 0.7 mmol) was added to benzene (2 mL) in a round bottom flask. Ethyl magnesium bromide (0.3 mL 3M solution in THF, 1 mmol) was then introduced dropwise at rt. Reaction was stirred for 30 mins, **31** (25 mg, 0.09 mmol, 1 eq.) was quickly added to this solution and heated to 80° C. Reaction was monitored via TLC for completion, subsequently, sat ammonium chloride solution was added to the reaction, acidified with 1N HCl and extracted with ethyl acetate (10 mL X 2). Purification with column chromatography (SiO<sub>2</sub>, 3:7 ethyl acetate:hexanes) afforded **35j** (18 mg, 58%) as white solid. <sup>1</sup>H NMR (600 MHz, Chloroform-*d*) δ 8.97 (s, 1H), 7.59 (d, *J* = 2.1 Hz, 1H), 7.34 (dd, *J* = 8.3, 2.2 Hz, 1H), 7.28 – 7.17 (m, 3H), 7.09 (d, *J* = 7.6 Hz, 1H), 6.80 (d, *J* = 8.3 Hz, 1H), 4.93 (s, 2H), 4.76 (t, *J* = 11.3 Hz, 3H), 4.09 (s, 2H), 3.28 (s, 3H), 1.79 (s, 3H). <sup>13</sup>C NMR (151 MHz, CDCl<sub>3</sub>) δ 170.4, 156.9, 136.5, 136.2, 128.6, 128.1, 127.8, 127.5, 127.2, 126.4, 122.9, 122.4, 117.6, 87.9, 82.2, 71.9, 59.8, 57.8, 55.2, 52.7, 31.2. HRMS (ESI) *m/z* [M+H] calculated for C<sub>21</sub>H<sub>22</sub>NO<sub>4</sub>, 352.1549, found 352.1561.

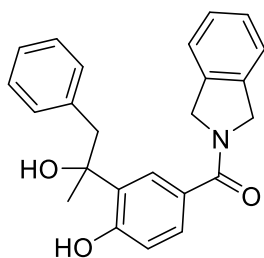


**(3-(2,5-dihydroxypentan-2-yl)-4-hydroxyphenyl)(isoindolin-2-yl)methanone (35k):** In a vial containing solution of **35h** (20 mg, 0.06 mmol, 1 eq.) in dioxane:water (2 mL, 8:2) was added

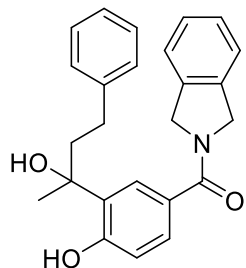
osmium tetroxide (0.1 mL of 4% aq. solution), 2,6-Lutidine (0.05 mL, 0.45 mmol, 8 eq.), and sodium metaperiodate (26 mg, 0.12 mmol, 2 eq.). Reaction was stirred for 12 h at rt, before quenching the reaction with 10 mL water and extraction with ethyl acetate (10 mL X 3). Organic layers were combined, washed with brine, dried with sodium sulfate, concentrated and purified using a quick flash chromatography (5:5 ethyl acetate:hexane) to result in a mass containing the desired aldehyde. The resulting mass was dissolved in THF (5 mL), cooled to 0° C and sodium cyanoborohydride (18 mg, 0.3 mmol, 5 eq.) was introduced. Reaction was warmed to rt and the progress was monitored using TLC for consumption of the aldehyde via 2,4-Dinitrophenylhydrazine stain. Upon completion, reaction was concentrated extracted with water (5 ml) and ethyl acetate (10 mL). organic layer was dried over sodium sulfate, concentrated and purified using column chromatography (SiO<sub>2</sub>, 3:7 ethyl acetate:hexane) to afford 35k (12 mg, 62%) as white solid. <sup>1</sup>H NMR (500 MHz, Chloroform-*d*) δ 10.22 (s, 1H), 7.31 (dd, *J* = 8.3, 2.1 Hz, 1H), 7.29 – 7.20 (m, 4H), 7.14 – 7.08 (m, 1H), 6.81 (d, *J* = 8.3 Hz, 1H), 4.93 (s, 2H), 4.76 (s, 2H), 3.70 – 3.55 (m, 2H), 2.23 (m, 1H), 1.88 (m, 1H), 1.75 – 1.59 (m, 2H), 1.56 (s, 3H). <sup>13</sup>C NMR (126 MHz, CDCl<sub>3</sub>) δ 170.56, 158.60, 136.58, 136.38, 130.12, 127.79, 127.48, 127.11, 126.22, 122.93, 122.42, 117.26, 99.99, 77.74, 77.23, 55.23, 52.67, 40.24, 29.96, 26.76. <sup>13</sup>C NMR (126 MHz, CDCl<sub>3</sub>) δ 170.6, 158.6, 136.6, 136.4, 130.1, 127.8, 127.5, 127.1, 126.2, 122.9, 122.4, 117.2, 99.9, 77.7, 77.2, 55.2, 52.7, 40.2, 29.9, 26.7. HRMS (ESI) *m/z* [M+H] calculated for C<sub>20</sub>H<sub>24</sub>NO<sub>4</sub>, 342.1705, found 342.1712.



**(4-hydroxy-3-(1-hydroxy-1-phenylethyl)phenyl)(isoindolin-2-yl)methanone (36a):** Prepared using general procedure A, 41 mg, Yield 68%, white solid:  $^1\text{H}$  NMR (500 MHz, Chloroform-*d*)  $\delta$  9.08 (s, 1H), 7.46 – 7.41 (m, 3H), 7.38 – 7.28 (m, 6H), 7.25 (d,  $J = 2.1$  Hz, 1H), 7.16 (d,  $J = 7.3$  Hz, 1H), 6.89 (d,  $J = 8.3$  Hz, 1H), 4.98 (s, 2H), 4.82 – 4.61 (m, 2H), 2.00 (s, 2H).  $^{13}\text{C}$  NMR (126 MHz,  $\text{CDCl}_3$ )  $\delta$  170.3, 157.6, 145.7, 136.5, 136.3, 130.8, 128.4, 128.3, 127.8, 127.7, 127.5, 127.0, 126.9, 125.6, 122.9, 122.3, 117.5, 78.9, 55.1, 52.7, 30.6. HRMS (ESI)  $m/z$  [M+H] calculated for  $\text{C}_{23}\text{H}_{22}\text{NO}_3$ , 360.1600, found 360.1599.

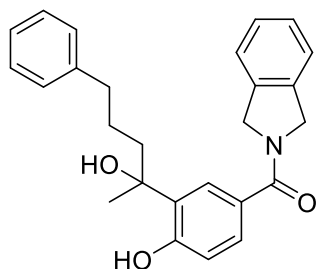


**(4-hydroxy-3-(2-hydroxy-1-phenylpropan-2-yl)phenyl)(isoindolin-2-yl)methanone (36b):** Prepared using general procedure A, 45 mg, Yield 72%, white solid:  $^1\text{H}$  NMR (500 MHz, Chloroform-*d*)  $\delta$  9.62 (s, 1H), 7.38 (dd,  $J = 8.4, 2.0$  Hz, 1H), 7.31 (m, 3H), 7.25 (m, 3H), 7.18 (d,  $J = 7.1$  Hz, 1H), 7.05 – 6.98 (m, 3H), 6.89 (d,  $J = 8.3$  Hz, 1H), 5.06 – 4.82 (m, 2H), 4.62 – 4.42 (m, 2H), 3.83 (s, 1H), 3.25 – 3.05 (m, 2H), 1.59 (s, 3H).  $^{13}\text{C}$  NMR (126 MHz,  $\text{CDCl}_3$ )  $\delta$  170.7, 157.9, 136.5, 136.3, 130.8 (2), 129.4, 128.2 (2), 128.0, 127.8, 127.5, 126.8, 126.8, 125.7, 122.9, 122.4, 117.5, 77.8, 77.3, 54.9, 52.6, 48.1, 27.2. HRMS (ESI)  $m/z$  [M+H] calculated for  $\text{C}_{24}\text{H}_{24}\text{NO}_3$ , 374.1756, found 374.1751.



**(4-hydroxy-3-(2-hydroxy-4-phenylbutan-2-yl)phenyl)(isoindolin-2-yl)methanone (36c):**

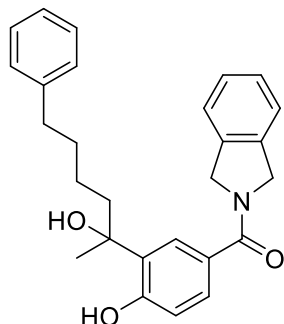
Prepared using general procedure A, 46 mg, Yield 70%, white solid:  $^1\text{H}$  NMR (500 MHz, Chloroform-*d*)  $\delta$  9.70 (s, 1H), 7.30 (dd,  $J = 8.3, 2.1$  Hz, 1H), 7.28 – 7.14 (m, 6H), 7.11 – 7.03 (m, 4H), 6.78 (d,  $J = 8.3$  Hz, 1H), 5.02 – 4.86 (m, 2H), 4.80 – 4.64 (m, 2H), 3.65 – 3.55 (s, 1H) 2.61 (m, 2H), 2.22 – 1.97 (m, 2H), 1.63 (s, 3H).  $^{13}\text{C}$  NMR (126 MHz,  $\text{CDCl}_3$ )  $\delta$  170.6, 158.1, 141.6, 136.4, 136.3, 129.8, 128.5, 128.3, 127.8, 127.6, 127.5, 127.1, 125.9, 125.8, 122.9, 122.4, 117.4, 78.4, 55.2, 52.7, 44.6, 30.4, 28.6. HRMS (ESI)  $m/z$  [M+H] calculated for  $\text{C}_{25}\text{H}_{26}\text{NO}_3$ , 388.1913, found 388.1891.



**(4-hydroxy-3-(2-hydroxy-5-phenylpentan-2-yl)phenyl)(isoindolin-2-yl)methanone (36d):**

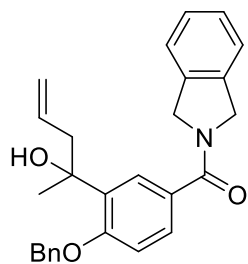
Prepared using general procedure A, 48 mg, Yield 70%, white solid:  $^1\text{H}$  NMR (500 MHz, Chloroform-*d*)  $\delta$  10.08 (s, 1H), 7.52 – 7.45 (m, 3H), 7.45 – 7.36 (m, 3H), 7.32 – 7.20 (m, 5H), 6.96 (d,  $J = 8.3$  Hz, 1H), 5.14 (d,  $J = 4.1$  Hz, 2H), 4.95 – 4.81 (m, 2H), 4.51 – 4.43 (m, 1H), 2.73 (t,  $J = 7.7$  Hz, 2H), 2.04 (m, 2H), 1.89 – 1.69 (m, 5H).  $^{13}\text{C}$  NMR (126 MHz,  $\text{CDCl}_3$ )  $\delta$  170.9, 158.1, 142.0, 136.3, 136.2, 130.2, 128.3 (2), 128.3 (2), 127.8, 127.5, 127.5, 126.6, 125.8, 125.6, 122.9,

122.4, 117.3, 77.9, 55.2, 52.7, 42.2, 35.9, 28.2, 25.9. HRMS (ESI)  $m/z$  [M+H] calculated for  $C_{26}H_{28}NO_3$ , 402.2069, found 402.2071.



**(4-hydroxy-3-(2-hydroxy-6-phenylhexan-2-yl)phenyl)(isoindolin-2-yl)methanone (36e):**

Prepared using general procedure A, 46 mg, Yield 65%, white solid:  $^1H$  NMR (500 MHz, Chloroform- $d$ )  $\delta$  9.84 (s, 1H), 7.37 – 7.27 (m, 3H), 7.27 – 7.18 (m, 3H), 7.17 – 7.09 (m, 5H), 6.83 (d,  $J = 8.3$  Hz, 1H), 5.06 – 4.91 (m, 2H), 4.88 – 4.69 (m, 2H), 3.95 (s, 1H), 2.57 (t,  $J = 7.8$  Hz, 2H), 1.88 (m, 2H), 1.62 (s, 5H), 1.46 – 1.27 (m, 2H).  $^{13}C$  NMR (126 MHz,  $CDCl_3$ )  $\delta$  170.8, 158.1, 142.3, 136.4, 136.2, 130.3, 128.3 (2), 128.2 (2), 127.8, 127.5, 127.5, 126.8, 125.8, 125.6, 122.9, 122.4, 117.3, 78.2, 55.2, 52.7, 42.4, 35.7, 31.6, 28.2, 23.7. HRMS (ESI)  $m/z$  [M+H] calculated for  $C_{27}H_{30}NO_3$ , 416.2226, found 416.2230.

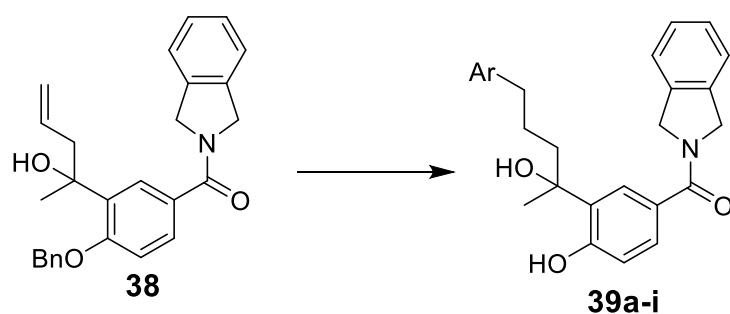


**(4-(benzyloxy)-3-(2-hydroxypent-4-en-2-yl)phenyl)(isoindolin-2-yl)methanone (38):**

A solution of the allyl magnesium bromide (7.8 mmol, 3 eq.) in THF was added to a solution of **34** (1 g mg, 2.6 mmol, 1 eq.) in THF (5 mL) at  $-20^\circ C$ . The reaction mixture was stirred at  $-20^\circ C$  for

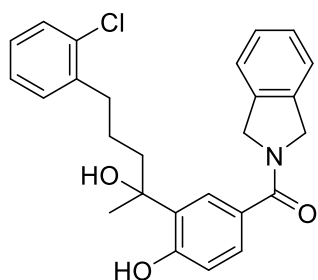
15 min, allowed to warm to rt. Upon completion of the reaction, as indicated by TLC, reaction was quenched with 1N HCl (20 mL) and then extraction was performed using ethyl acetate (20 mL X 3). Organic layers were combined, washed with water (10 mL), dried over sodium sulfate and concentrated. The resulting residue was purified using flash chromatography (SiO<sub>2</sub>, 4:6 ethyl acetate:hexanes) to produce **38** (0.72 g, 73%) as white solid. <sup>1</sup>H NMR (500 MHz, Chloroform-*d*) δ 7.68 (d, *J* = 2.1 Hz, 1H), 7.52 (dd, *J* = 8.4, 2.2 Hz, 1H), 7.48 – 7.38 (m, 5H), 7.38 – 7.26 (m, 3H), 7.18 (d, *J* = 7.4 Hz, 1H), 7.06 (d, *J* = 8.4 Hz, 1H), 5.65 (dddd, *J* = 15.7, 11.5, 7.9, 6.8 Hz, 1H), 5.21 (s, 2H), 5.10 – 5.00 (m, 4H), 4.87 – 4.74 (m, 2H), 3.57 (s, 1H), 2.92 (ddt, *J* = 13.8, 6.7, 1.3 Hz, 1H), 2.63 (ddt, *J* = 13.6, 7.8, 1.2 Hz, 1H), 1.64 (s, 3H). <sup>13</sup>C NMR (126 MHz, CDCl<sub>3</sub>) δ 170.2, 157.0, 136.5, 136.4, 135.9, 134.9, 134.3, 129.1, 128.9, 128.5, 127.8, 127.6, 127.5, 127.4, 126.3, 122.9, 122.4, 118.4, 118.4, 112.1, 112.0, 74.1, 70.7, 55.1, 52.6, 46.1, 27.1. HRMS (ESI) *m/z* [M+H] calculated for C<sub>27</sub>H<sub>28</sub>NO<sub>3</sub>, 414.2069, found 414.2050.

### General procedure B:



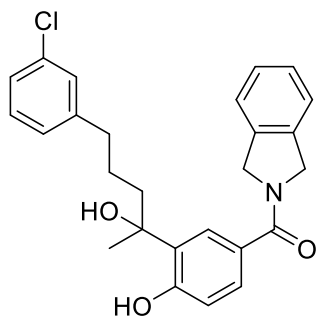
Intermediate **38** (50 mg, 0.12 mmol, 1 eq.) and the desired aromatic bromide (0.144 mmol, 1.2 eq.) were suspended in triethanolamine (0.5 mL) contained in a 5mL reaction vessel. Palladium acetate (Pd(OAc)<sub>2</sub>) (2.5 mg, 0.012 mmol) was added to this reaction mixture, vessel was sealed with

Teflon lined cap and heated to 110°C for 10 h. The reaction was cooled, Water (20 mL) was added to dilute the reaction and extracted with ethyl acetate (20 mL X 2). Organic fractions were combined, washed with brine, dried over sodium sulfate, and passed through a short column (SiO<sub>2</sub>, 5:5 ethyl acetate:hexanes) to result in the residue containing the desired coupled product which was dissolved in ethyl acetate:ethanol (5 mL, 4:1) in a sealed reaction vessel. Palladium on carbon (10%) and cyclohexene (0.12 mL, 1.2 mmol, 10 eq.) were added then and the sealed vessel was then heated to 100° C for 12 h. Subsequently, reaction mixture was passed through a pad of celite, solvent was removed under vacuum and the remaining mass was purified using preparative TLC (SiO<sub>2</sub>, 3:7 ethyl acetate:hexanes) to afford products **39a-i** as white solid.



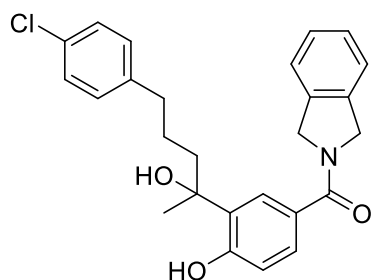
**(3-(5-(2-chlorophenyl)-2-hydroxypentan-2-yl)-4-hydroxyphenyl)(isoindolin-2-yl)methanone**

**(39a):** Prepared using general procedure B, 16 mg, Yield 32%, white solid: <sup>1</sup>H NMR (500 MHz, Chloroform-*d*) δ 9.68 (s, 1H), 7.40 – 7.29 (m, 3H), 7.28 – 7.23 (m, 2H), 7.20 (t, *J* = 2.7 Hz, 1H), 7.18 – 7.09 (m, 4H), 6.86 (d, *J* = 8.3 Hz, 1H), 5.01 (s, 2H), 4.81 – 4.73 (m, 2H), 3.36 (s, 1H), 2.61 (t, *J* = 7.6 Hz, 2H), 2.01 – 1.84 (m, 2H), 1.74-1.63 (m, 5H). <sup>13</sup>C NMR (126 MHz, CDCl<sub>3</sub>) δ 170.4, 158.0, 155.2, 141.8, 136.5, 136.3, 129.5, 128.3 (2), 128.3 (2), 127.8, 127.4, 127.2, 125.9, 125.8, 122.9, 122.4, 117.4, 78.7, 55.2, 52.6, 42.2, 35.8, 28.9, 25.7. HRMS (ESI) *m/z* [M+Na] calculated for C<sub>26</sub>H<sub>26</sub>ClNO<sub>3</sub>Na, 458.1499, found 458.1488.



**(3-(5-(3-chlorophenyl)-2-hydroxypentan-2-yl)-4-hydroxyphenyl)(isoindolin-2-yl)methanone**

**(39b):** Prepared using general procedure B, 13 mg, Yield 25%, white solid:  $^1\text{H}$  NMR (500 MHz, Chloroform-*d*)  $\delta$  9.49 (s, 1H), 7.31 (dd,  $J = 8.4, 2.1$  Hz, 1H), 7.28 – 7.12 (m, 5H), 7.10 – 6.99 (m, 4H), 6.79 (d,  $J = 8.3$  Hz, 1H), 4.93 (s, 2H), 4.69 (s, 2H), 2.86 (s, 1H), 2.52 (t,  $J = 7.6$  Hz, 2H), 1.94-1.74 (m, 2H), 1.65 – 1.54 (m, 5H).  $^{13}\text{C}$  NMR (126 MHz,  $\text{CDCl}_3$ )  $\delta$  170.4, 158.0, 141.8, 136.5, 136.3, 129.5, 128.4, 128.3, 128.3, 128.2, 127.8, 127.5, 127.2, 125.9, 125.8, 122.9, 122.4, 117.4, 78.7, 55.2, 55.2, 52.6, 42.2, 35.8, 28.9, 25.8. HRMS (ESI)  $m/z$   $[\text{M}+\text{Na}]$  calculated for  $\text{C}_{26}\text{H}_{26}\text{ClNO}_3\text{Na}$ , 458.1499, found 458.1480.

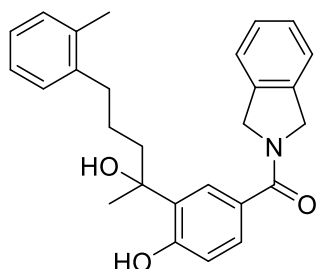


**(3-(5-(4-chlorophenyl)-2-hydroxypentan-2-yl)-4-hydroxyphenyl)(isoindolin-2-yl)methanone**

**(39c):** Prepared using general procedure B, 17 mg, Yield 35%, white solid:  $^1\text{H}$  NMR (500 MHz, Chloroform-*d*)  $\delta$  9.69 (s, 1H), 7.39 – 7.28 (m, 4H), 7.23 – 7.16 (m, 3H), 7.13 – 7.02 (m, 3H), 6.84 (d,  $J = 8.3$  Hz, 1H), 5.00 (s, 2H), 4.82 – 4.66 (m, 2H), 3.56 – 3.48 (m, 1H), 2.64 – 2.47 (m, 2H), 1.88 (m, 2H), 1.70 – 1.54 (m, 5H).  $^{13}\text{C}$  NMR (126 MHz,  $\text{CDCl}_3$ )  $\delta$  170.6, 158.0, 140.3, 136.3,

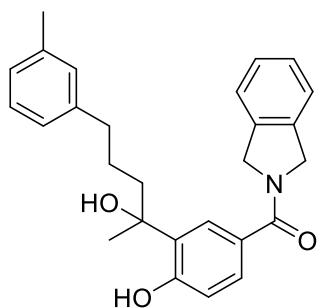


136.2, 131.5, 129.8, 129.7 (2), 128.4 (2), 127.8, 127.6, 127.5, 127.0, 125.8, 122.9, 122.4, 117.4, 78.3, 55.2, 52.7, 42.1, 35.1, 28.5, 25.7. HRMS (ESI)  $m/z$  [M+H] calculated for  $C_{26}H_{27}ClNO_3$ , 436.1679, found 436.1709.



**(4-hydroxy-3-(2-hydroxy-5-(o-tolyl)pentan-2-yl)phenyl)(isoindolin-2-yl)methanone (39d):**

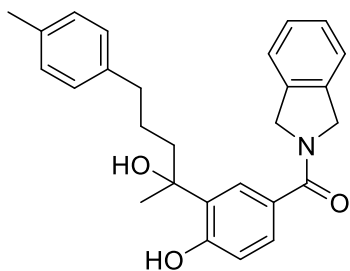
Prepared using general procedure B, 15 mg, Yield 30%, white solid:  $^1H$  NMR (500 MHz, Chloroform-*d*)  $\delta$  9.51 (s, 1H), 7.31 (dd,  $J = 8.3, 2.1$  Hz, 1H), 7.19 (s, 3H), 7.15 (d,  $J = 2.1$  Hz, 1H), 7.01 (m, 5H), 6.79 (d,  $J = 8.3$  Hz, 1H), 4.97 – 4.85 (m, 2H), 4.74 – 4.59 (m, 2H), 2.88 (s, 1H), 2.50 (m, 2H), 2.16 (s, 3H), 1.89 (m, 2H), 1.54 (m, 5H).  $^{13}C$  NMR (126 MHz,  $CDCl_3$ )  $\delta$  170.4, 157.9, 140.0, 136.5, 136.3, 135.8, 130.2, 129.6, 128.6, 127.8, 127.8, 127.5, 127.2, 126.0, 125.9, 125.9, 122.9, 122.4, 117.4, 78.7, 55.2, 52.6, 42.5, 33.1, 28.8, 24.5, 19.3. HRMS (ESI)  $m/z$  [M+H] calculated for  $C_{27}H_{30}NO_3$ , 416.2226, found 416.2240.



**(4-hydroxy-3-(2-hydroxy-5-(m-tolyl)pentan-2-yl)phenyl)(isoindolin-2-yl)methanone (39e):**

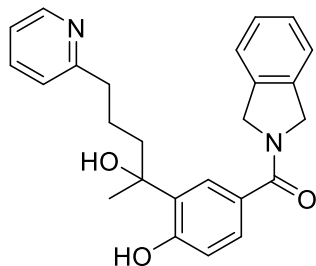
Prepared using general procedure B, 16 mg, Yield 33%, white solid:  $^1H$  NMR (500 MHz,

Chloroform-*d*)  $\delta$  9.74 (s, 1H), 7.38 – 7.29 (m, 3H), 7.27 (s, 1H), 7.17 (d,  $J = 2.1$  Hz, 1H), 7.15 – 7.07 (m, 2H), 6.99 – 6.90 (m, 3H), 6.84 (d,  $J = 8.3$  Hz, 1H), 5.00 (d,  $J = 3.9$  Hz, 2H), 4.81 – 4.69 (m, 2H), 3.62 (d,  $J = 2.8$  Hz, 1H), 2.61 – 2.48 (m, 2H), 1.91 (dddd,  $J = 45.2, 13.8, 11.6, 4.9$  Hz, 2H), 2.29 (s, 3H), 1.75 – 1.54 (m, 5H).  $^{13}\text{C}$  NMR (126 MHz,  $\text{CDCl}_3$ )  $\delta$  170.6, 158.0, 141.9, 137.9, 136.4, 136.2, 129.9, 129.2, 128.2, 127.8, 127.6, 127.5, 126.9, 126.6, 125.8, 125.3, 122.9, 122.4, 117.4, 78.3, 55.2, 52.7, 42.3, 35.8, 28.5, 25.9, 21.4. HRMS (ESI)  $m/z$  [M+H] calculated for  $\text{C}_{27}\text{H}_{30}\text{NO}_3$ , 416.2226, found 416.2232.



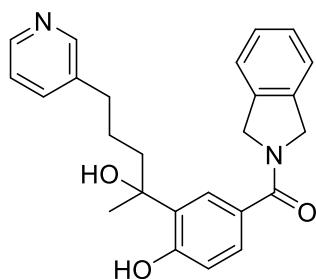
**(4-hydroxy-3-(2-hydroxy-5-(p-tolyl)pentan-2-yl)phenyl)(isoindolin-2-yl)methanone (39f):**

Prepared using general procedure B, 14 mg, Yield 28%, white solid:  $^1\text{H}$  NMR (500 MHz, Chloroform-*d*)  $\delta$  9.64 (s, 1H), 7.37 (dd,  $J = 8.3, 2.1$  Hz, 1H), 7.36 – 7.27 (m, 3H), 7.19 (d,  $J = 2.1$  Hz, 1H), 7.09 (d,  $J = 7.4$  Hz, 1H), 7.07 – 7.00 (m, 4H), 6.85 (d,  $J = 8.3$  Hz, 1H), 5.00 (s, 2H), 4.82 – 4.66 (m, 2H), 3.19 (d,  $J = 2.7$  Hz, 1H), 2.58 – 2.51 (m, 2H), 2.28 (s, 3H), 1.91 (m, 2H), 1.63 (s, 5H).  $^{13}\text{C}$  NMR (126 MHz,  $\text{CDCl}_3$ )  $\delta$  170.5, 158.0, 138.8, 136.5, 136.3, 135.3, 129.6, 129.0 (2), 128.2 (2), 127.8, 127.7, 127.4, 127.1, 125.8, 122.9, 122.4, 117.4, 78.5, 55.2, 52.6, 42.2, 35.4, 28.7, 25.9, 20.9. HRMS (ESI)  $m/z$  [M+H] calculated for  $\text{C}_{27}\text{H}_{30}\text{NO}_3$ , 416.2226, found 416.2227.



**(4-hydroxy-3-(2-hydroxy-5-(pyridin-2-yl)pentan-2-yl)phenyl)(isoindolin-2-yl)methanone**

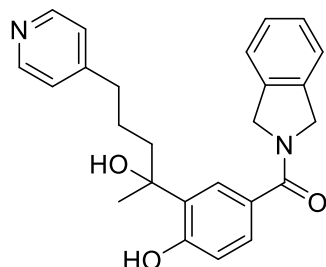
**(39g):** Prepared using general procedure B, 12 mg, yield 26%, white solid:  $^1\text{H}$  NMR (500 MHz, Chloroform-*d*)  $\delta$  11.15 (s, 1H), 8.50 – 8.45 (m, 1H), 7.66-7.63 (m, 1H), 7.39 (dd,  $J = 8.3, 2.1$  Hz, 1H), 7.36-7.27 (m, 3H), 7.20 – 7.14 (m, 3H), 6.88 (d,  $J = 8.4$  Hz, 1H), 5.02 (s, 2H), 4.85 (s, 2H), 3.01-2.96 (m, 1H), 2.86-2.81 (m, 1H), 2.20 – 2.10 (m, 1H), 1.99 – 1.88 (m, 2H), 1.87-1.75 (s, 1H), 1.63 (s, 3H).  $^{13}\text{C}$  NMR (126 MHz,  $\text{CDCl}_3$ )  $\delta$  170.5, 160.8, 159.0, 147.6, 137.4, 136.7, 136.5, 129.8, 127.7, 127.4, 127.3, 126.9, 126.5, 124.1, 122.9, 122.4, 121.4, 117.2, 79.2, 55.2, 52.6, 39.7, 35.2, 32.0, 22.7. HRMS (ESI)  $m/z$   $[\text{M}+\text{H}]$  calculated for  $\text{C}_{25}\text{H}_{27}\text{N}_2\text{O}_3$ , 403.2022, found 403.2007.



**(4-hydroxy-3-(2-hydroxy-5-(pyridin-3-yl)pentan-2-yl)phenyl)(isoindolin-2-yl)methanone**

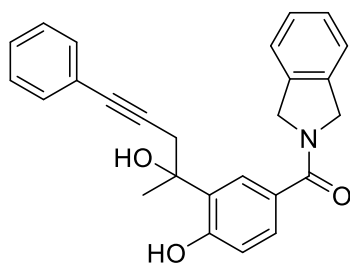
**(39h):** Prepared using general procedure B, 12mg, Yield 25%, white solid:  $^1\text{H}$  NMR (500 MHz, Cfhloroform-*d*)  $\delta$  9.98 (s, 1H), 8.26 (d,  $J = 39.4$  Hz, 2H), 7.42 – 7.36 (m, 1H), 7.32 (dd,  $J = 8.3, 2.1$  Hz, 1H), 7.29 – 7.20 (m, 3H), 7.16 – 7.04 (m, 2H), 6.80 (d,  $J = 8.3$  Hz, 1H), 4.93 (s, 2H), 4.82 – 4.65 (m, 2H), 2.50 (hept,  $J = 7.0$  Hz, 2H), 1.84-1.73 (m, 2H), 1.59-1.52 (m, 5H).  $^{13}\text{C}$  NMR (126 MHz,  $\text{CDCl}_3$ )  $\delta$  170.5, 158.2, 149.3, 149.3, 146.9, 146.9, 136.5, 136.3, 130.0, 127.8, 127.7, 127.5,

127.1, 126.0, 122.9, 122.4, 117.2, 117.2, 78.1, 77.3, 55.2, 52.7, 42.3, 28.9, 25.5. HRMS (ESI)  $m/z$  [M+H] calculated for  $C_{25}H_{26}N_2O_3Na$ , 425.1841, found 425.1843.



**(4-hydroxy-3-(2-hydroxy-5-(pyridin-4-yl)pentan-2-yl)phenyl)(isoindolin-2-yl)methanone**

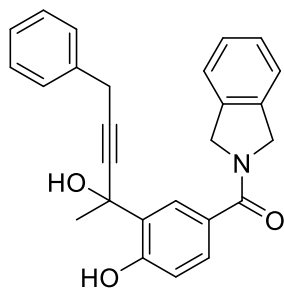
**(39i):** Prepared using general procedure B, 15 mg, Yield 32%, white solid:  $^1H$  NMR (500 MHz, Chloroform-*d*)  $\delta$  8.23 – 8.18 (m, 2H), 7.30 (dd,  $J = 8.4, 2.1$  Hz, 1H), 7.28 – 7.17 (m, 4H), 7.06 (d,  $J = 7.5$  Hz, 1H), 7.00 – 6.95 (m, 2H), 6.78 (d,  $J = 8.3$  Hz, 1H), 4.91 (d,  $J = 13.6$  Hz, 2H), 4.79 – 4.65 (m, 2H), 3.41 (s, 1H), 2.57-2.44 (m, 2H), 1.89 – 1.70 (m, 2H), 1.69-1.60 (m, 2H), 1.57 (s, 3H).  $^{13}C$  NMR (126 MHz,  $CDCl_3$ )  $\delta$  170.46, 158.3, 151.7, 148.7 (2), 136.4, 136.3, 130.1, 127.8, 127.5, 126.9, 126.0, 124.2 (2), 122.9, 122.4, 122.3, 117.1, 77.6, 55.2, 52.7, 42.1, 34.9, 29.0, 24.4. HRMS (ESI)  $m/z$  [M+H] calculated for  $C_{25}H_{27}N_2O_3$ , 403.2022, found 403.2049.



**(4-hydroxy-3-(2-hydroxy-5-phenylpent-4-yn-2-yl)phenyl)(isoindolin-2-yl)methanone (40):** 3-Chloro-1-phenyl-1-propyne (0.15 mL, 1 mmol, 3 eq.) was added to a round bottom flask containing THF (5 mL) under argon. Subsequently, the reaction mixture was cooled to 0°C, zinc

chloride (13.6 mg, 0.1 mmol, 0.3 eq.) and magnesium turnings (50 mg, 2 mmol, 6 eq) were added and stirred and allowed to warm to rt for 30 mins. In this duration, reaction turned into a red colored solution. This solution was transferred quickly to a reaction vessel containing **31** (100 mg, 0.3 mmol, 1 eq) dissolved in THF (5 mL), at 0°C via glass syringe. The resulting reaction mixture was stirred, warmed to rt and monitored via TLC for the consumption of **31**. Upon completion the reaction was quenched with 1N HCl (3 mL) and extracted with ethyl acetate (20 mL X 2). Organic layers were combined, dried over sodium sulfate, evaporated to yield a residue that was purified using flash chromatography (SiO<sub>2</sub>, 3:7 ethyl acetate:hexanes) to afford **40** (45 mg, 31%) as beige solid. <sup>1</sup>H NMR (500 MHz, Chloroform-*d*) δ 9.40 (s, 1H), 7.42 (dd, *J* = 8.3, 2.1 Hz, 1H), 7.39 – 7.34 (m, 3H), 7.34 – 7.16 (m, 7H), 6.92 (d, *J* = 8.3 Hz, 1H), 6.84 (d, *J* = 7.6 Hz, 1H), 5.05 – 4.93 (m, 2H), 4.75 (s, 2H), 3.15 (d, *J* = 16.9 Hz, 1H), 2.98 (d, *J* = 16.9 Hz, 1H), 1.80 (s, 3H). <sup>13</sup>C NMR (126 MHz, CDCl<sub>3</sub>) δ 170.6, 157.8, 136.4, 136.2, 131.6 (2), 128.6, 128.4 (2), 128.3, 128.2, 127.7, 127.4, 127.3, 125.7, 122.8, 122.7, 122.4, 117.7, 84.8, 84.5, 77.2, 55.1, 52.6, 33.9, 27.6. HRMS (ESI) *m/z* [M+H] calculated for C<sub>26</sub>H<sub>24</sub>NO<sub>3</sub>, 398.1756, found

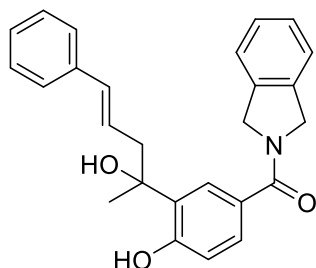
398.1772.



**(4-hydroxy-3-(2-hydroxy-5-phenylpent-3-yn-2-yl)phenyl)(isoindolin-2-yl)methanone (41):** 3-Phenyl-1-propyne (41 mg, 0.35 mmol, 2 eq.) dissolved in THF (3 mL) was cooled to -78°C, subsequently, lithium diisopropylamide (LDA) (0.38 mL 1M solution in THF, 0.38 mmol, 2.2 eq.) was introduced and the reaction was stirred at -78°C for 15 min, and at 0°C for 30 min. This

solution was transferred, via a syringe into a round bottom flask containing **31** (50 mg, 0.177 mmol, 1 eq) in THF (3 mL) at 0°C. Upon addition, the reaction was warmed to 40° C and stirred for 1 h, before quenching with ammonium chloride solution and extraction with ethyl acetate (20 mL X 2). Organic layers were combined, dried over sodium sulfate, and evaporated to yield a residue that was purified using flash chromatography to produce **41** (36 mg, 51%) as white solid. <sup>1</sup>H NMR (500 MHz, Chloroform-*d*) δ 9.40 (s, 1H), 7.42 (dd, *J* = 8.3, 2.1 Hz, 1H), 7.39 – 7.34 (m, 3H), 7.34 – 7.16 (m, 7H), 6.92 (d, *J* = 8.3 Hz, 1H), 6.84 (d, *J* = 7.6 Hz, 1H), 5.05 – 4.93 (m, 2H), 4.75 (s, 2H), 3.15 (d, *J* = 16.9 Hz, 1H), 2.98 (d, *J* = 16.9 Hz, 1H), 1.80 (s, 3H). <sup>13</sup>C NMR (126 MHz, CDCl<sub>3</sub>) δ 170.6, 157.8, 136.4, 136.2, 131.6 (2), 128.6, 128.4 (2), 128.3, 128.2, 127.7, 127.4, 127.3, 125.7, 122.8, 122.7, 122.4, 117.7, 84.8, 84.5, 77.2, 55.2, 52.6, 33.9, 27.6. HRMS (ESI) *m/z* [M+H] calculated for C<sub>26</sub>H<sub>24</sub>NO<sub>3</sub>, 398.1756, found

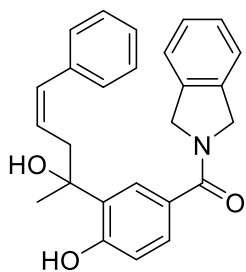
398.1772.



**(E)-(4-hydroxy-3-(2-hydroxy-5-phenylpent-4-en-2-yl)phenyl)(isoindolin-2-yl)methanone**

**(42):** 38 (50 mg, 0.12 mmol, 1 eq.) was dissolved in dioxane (2 mL) contained in a reaction vessel. Subsequently, palladium(0) bis(dibenzylideneacetone) (Pd(dba)<sub>2</sub>) (4 mg, 5 mol %) and tri-*o*-tolylphosphine (P(*o*-tolyl)<sub>3</sub>) (3.6 mg, 10 mol %) and N,N-Dicyclohexylmethylamine (47mg, 0.24 mmol, 2 eq.), iodobenzene (27 mg, 0.13 mmol, 1.1 eq.) were added to the reaction vessel, the solution was purged with argon, sealed with a teflon cap, and heated to 90° C for 6 h. Water (5 mL) was added to the reaction mixture and extracted with ethyl acetate (10 mL X 2). Organic

layers were washed with brine, dried over sodium sulfate and evaporated to result in a residue that was passed through a short column (SiO<sub>2</sub>, 3:7 ethyl acetate:hexanes) to obtain fractions containing the desired product. The combined fractions were evaporated to yield a residue that was dissolved in DCM (3 mL), cooled to 0° C and treated with boron trichloride solution (0.36 mL 1M solution in DCM, 0.36 mmol, 3 eq.). Reaction was stirred at 0°C for 30 mins, quenched with water (10 mL), DCM removed under vacuum and extracted with ethyl acetate (10 mL X 2). Organic layers were combined, washed with brine, dried over sodium sulfate and evaporated to yield a crude mass, which upon purification (SiO<sub>2</sub>, 3:7 ethyl acetate:hexanes) produced **42** (18 mg, 38%) as a beige solid. <sup>1</sup>H NMR (500 MHz, Chloroform-*d*) δ 9.55 (s, 1H), 7.32 (dd, *J* = 8.3, 2.1 Hz, 1H), 7.27 – 7.10 (m, 7H), 6.92 (d, *J* = 7.5 Hz, 1H), 6.81 (d, *J* = 8.3 Hz, 1H), 6.40 (d, *J* = 15.8 Hz, 1H), 6.09 (dt, *J* = 15.5, 7.5 Hz, 1H), 4.92 (s, 2H), 4.67 (s, 2H), 3.64 (s, 1H), 2.84 (ddd, *J* = 13.9, 7.2, 1.4 Hz, 1H), 2.64 (ddd, *J* = 13.9, 7.8, 1.2 Hz, 1H), 1.59 (s, 3H). <sup>13</sup>C NMR (126 MHz, CDCl<sub>3</sub>) δ 170.6, 158.0, 136.8, 136.4, 136.2, 135.1, 129.7, 128.6 (2), 127.9, 127.8, 127.6, 127.4, 127.2, 126.2 (2), 125.7, 123.9, 122.9, 122.4, 117.5, 77.6, 55.2, 52.6, 45.8, 28.2. HRMS (ESI) *m/z* [M+H] calculated for C<sub>26</sub>H<sub>25</sub>NO<sub>3</sub>Na, 422.1732, found 422.1729.



**(Z)-(4-hydroxy-3-(2-hydroxy-5-phenylpent-4-en-2-yl)phenyl)(isoindolin-2-yl)methanone**

**(43):** Intermediate **40** (25 mg, 0.06 mmol) was dissolved in ethyl acetate (3 mL). Lindlar's catalyst (3 mg) was then added and reaction mixture was hydrogenated at rt for 2 h. The reaction mixture was filtered through a pad of Celite and obtained filtrate was evaporated to give a crude mass that

was purified using preparative TLC (SiO<sub>2</sub>, 3:7 ethyl acetate:hexanes) to furnish **43** (11mg, 46 %) as a beige solid. <sup>1</sup>H NMR (400 MHz, Chloroform-*d*) δ 9.58 (s, 1H), 7.39 (dd, *J* = 8.3, 2.1 Hz, 1H), 7.35 – 7.28 (m, 3H), 7.27 – 7.10 (m, 5H), 6.95 – 6.81 (m, 1H), 6.64 (d, *J* = 11.8 Hz, 1H), 5.80-5.65 (m, 1H), 5.00 (s, 2H), 4.76 (s, 2H), 3.58 (s, 1H), 3.10-2.855 (m, 2H), 1.64 (s, 3H). <sup>13</sup>C NMR (101 MHz, CDCl<sub>3</sub>) δ 170.5, 158.1, 136.8, 136.3, 133.0, 129.5, 128.6 (2), 128.3, 128.3 (2), 127.9, 127.8, 127.5, 127.1, 127.0, 126.0, 125.8, 122.9, 122.4, 117.5, 78.0, 55.1, 52.6, 40.7, 28.5. HRMS (ESI) *m/z* [M+H] calculated for C<sub>26</sub>H<sub>25</sub>NO<sub>3</sub>, 400.1907, found 400.1907.

### III.9 References

1. Zuehlke, A. D.; Beebe, K.; Neckers, L.; Prince, T. Regulation and function of the human HSP90AA1 gene. *Gene* **2015**, *570*, 8-16.
2. Wang, X.; Song, X.; Zhuo, W.; Fu, Y.; Shi, H.; Liang, Y.; Tong, M.; Chang, G.; Luo, Y. The regulatory mechanism of Hsp90α secretion and its function in tumor malignancy. *Proceedings of the National Academy of Sciences* **2009**, *106*, 21288-21293.
3. Li, W.; Sahu, D.; Tsen, F. Secreted Heat Shock Protein-90 (Hsp90) in Wound Healing and Cancer. *Biochim. Biophys. Acta* **2012**, *1823*, 730-741.
4. Eustace, B. K.; Sakurai, T.; Stewart, J. K.; Yimlamai, D.; Unger, C.; Zehetmeier, C.; Lain, B.; Torella, C.; Henning, S. W.; Beste, G.; Scroggins, B. T.; Neckers, L.; Ilag, L. L.; Jay, D. G. Functional proteomic screens reveal an essential extracellular role for hsp90 alpha in cancer cell invasiveness. *Nature cell biology* **2004**, *6*, 507-14.
5. Bohonowych, J. E.; Hance, M. W.; Nolan, K. D.; Defee, M.; Parsons, C. H.; Isaacs, J. S. Extracellular Hsp90 mediates an NF-kappaB dependent inflammatory stromal program: implications for the prostate tumor microenvironment. *Prostate* **2014**, *74*, 395-407.
6. Chen, W. S.; Chen, C. C.; Chen, L. L.; Lee, C. C.; Huang, T. S. Secreted heat shock protein 90alpha (HSP90alpha) induces nuclear factor-kappaB-mediated TCF12 protein expression to down-regulate E-cadherin and to enhance colorectal cancer cell migration and invasion. *The Journal of biological chemistry* **2013**, *288*, 9001-10.
7. Elaimy, A. L.; Ahsan, A.; Marsh, K.; Pratt, W. B.; Ray, D.; Lawrence, T. S.; Nyati, M. K. ATM is the primary kinase responsible for phosphorylation of Hsp90α after ionizing radiation. *Oncotarget* **2016**, *7*, 82450-82457.
8. Pennisi, R.; Antocchia, A.; Leone, S.; Ascenzi, P.; di Masi, A. Hsp90alpha regulates ATM and NBN functions in sensing and repair of DNA double-strand breaks. *The FEBS journal* **2017**, *284*, 2378-2395.
9. Lee, Y. C.; Chang, W. W.; Chen, Y. Y.; Tsai, Y. H.; Chou, Y. H.; Tseng, H. C.; Chen, H. L.; Wu, C. C.; Chang-Chien, J.; Lee, H. T.; Yang, H. F.; Wang, B. Y. Hsp90alpha Mediates BMI1 Expression in Breast Cancer Stem/Progenitor Cells through Facilitating Nuclear Translocation of c-Myc and EZH2. *International journal of molecular sciences* **2017**, *18*.



10. Fu, Y.; Xu, X.; Huang, D.; Cui, D.; Liu, L.; Liu, J.; He, Z.; Liu, J.; Zheng, S.; Luo, Y. Plasma Heat Shock Protein 90alpha as a Biomarker for the Diagnosis of Liver Cancer: An Official, Large-scale, and Multicenter Clinical Trial. *EBioMedicine* **2017**, *24*, 56-63.
11. Sourbier, C. Plasma HSP90 $\alpha$  and liver cancer: a potential biomarker? *EBioMedicine* *25*, 7-8.
12. Huang, T.; Chen, S.; Han, H.; Li, H.; Huang, Z.; Zhang, J.; Yin, Q.; Wang, X.; Ma, X.; Dai, P.; Duan, D.; Zou, F.; Chen, X. Expression of Hsp90alpha and cyclin B1 were related to prognosis of esophageal squamous cell carcinoma and keratin pearl formation. *International journal of clinical and experimental pathology* **2014**, *7*, 1544-52.
13. Tian, W. L.; He, F.; Fu, X.; Lin, J. T.; Tang, P.; Huang, Y. M.; Guo, R.; Sun, L. High expression of heat shock protein 90 alpha and its significance in human acute leukemia cells. *Gene* **2014**, *542*, 122-8.
14. Rybarczyk, P.; Vanlaeys, A.; Brassart, B.; Dhennin-Duthille, I.; Chatelain, D.; Sevestre, H.; Ouadid-Ahidouch, H.; Gautier, M. The Transient Receptor Potential Melastatin 7 Channel Regulates Pancreatic Cancer Cell Invasion through the Hsp90alpha/uPA/MMP2 pathway. *Neoplasia (New York, N.Y.)* **2017**, *19*, 288-300.
15. Jiang, H.; Duan, B.; He, C.; Geng, S.; Shen, X.; Zhu, H.; Sheng, H.; Yang, C.; Gao, H. Cytoplasmic HSP90alpha expression is associated with perineural invasion in pancreatic cancer. *International journal of clinical and experimental pathology* **2014**, *7*, 3305-11.
16. Taipale, M.; Tucker, G.; Peng, J.; Krykbaeva, I.; Lin, Z.-Y.; Larsen, B.; Choi, H.; Berger, B.; Gingras, A.-C.; Lindquist, S. A quantitative chaperone interaction network reveals the architecture of cellular protein homeostasis pathways. *Cell* **2014**, *158*, 434-448.
17. Voss, A. K.; Thomas, T.; Gruss, P. Mice lacking HSP90beta fail to develop a placental labyrinth. *Development (Cambridge, England)* **2000**, *127*, 1-11.
18. Grad, I.; Cederroth, C. R.; Walicki, J.; Grey, C.; Barluenga, S.; Winssinger, N.; De Massy, B.; Nef, S.; Picard, D. The molecular chaperone Hsp90alpha is required for meiotic progression of spermatocytes beyond pachytene in the mouse. *PloS one* **2010**, *5*, e15770.
19. Kajiwara, C.; Kondo, S.; Uda, S.; Dai, L.; Ichianagi, T.; Chiba, T.; Ishido, S.; Koji, T.; Udono, H. Spermatogenesis arrest caused by conditional deletion of Hsp90alpha in adult mice. *Biology open* **2012**, *1*, 977-82.
20. Chen, B.; Piel, W. H.; Gui, L.; Bruford, E.; Monteiro, A. The HSP90 family of genes in the human genome: insights into their divergence and evolution. *Genomics* **2005**, *86*, 627-37.
21. Patel, H. J.; Modi, S.; Chiosis, G.; Taldone, T. Advances in the discovery and development of heat-shock protein 90 inhibitors for cancer treatment. *Expert opinion on drug discovery* **2011**, *6*, 559-587.
22. Ernst, J. T.; Liu, M.; Zuccola, H.; Neubert, T.; Beaumont, K.; Turnbull, A.; Kallel, A.; Vought, B.; Stamos, D. Correlation between chemotype-dependent binding conformations of HSP90alpha/beta and isoform selectivity-Implications for the structure-based design of HSP90alpha/beta selective inhibitors for treating neurodegenerative diseases. *Bioorg. Med. Chem. Lett.* **2014**, *24*, 204-8.
23. Obermann, W. M.; Sondermann, H.; Russo, A. A.; Pavletich, N. P.; Hartl, F. U. In vivo function of Hsp90 is dependent on ATP binding and ATP hydrolysis. *The Journal of cell biology* **1998**, *143*, 901-10.

24. Khandelwal, A. Unfolding the Hsp90 Foldasome: Structure-Activity Relationship Studies on EGCG and Development of Isoform-Selective Inhibitors, Ph.D Dissertation, The University of Kansas. **2016**.
25. Brough, P. A.; Aherne, W.; Barril, X.; Borgognoni, J.; Boxall, K.; Cansfield, J. E.; Cheung, K. M.; Collins, I.; Davies, N. G.; Drysdale, M. J.; Dymock, B.; Eccles, S. A.; Finch, H.; Fink, A.; Hayes, A.; Howes, R.; Hubbard, R. E.; James, K.; Jordan, A. M.; Lockie, A.; Martins, V.; Massey, A.; Matthews, T. P.; McDonald, E.; Northfield, C. J.; Pearl, L. H.; Prodromou, C.; Ray, S.; Raynaud, F. I.; Roughley, S. D.; Sharp, S. Y.; Surgenor, A.; Walmsley, D. L.; Webb, P.; Wood, M.; Workman, P.; Wright, L. 4,5-diarylisoxazole Hsp90 chaperone inhibitors: potential therapeutic agents for the treatment of cancer. *J. Med. Chem.* **2008**, *51*, 196-218.
26. Lee, C. W.; James, D.; Zhang, S.; Ying, W.; Chimmanamada, D. U.; Chae, J.; Przewloka, T. Method for the preparation of triazole compounds with hsp90 modulating activity. WO2007139952 A2: **6th Dec 2007**.
27. Tatarinov, D. A.; Kuznetsov, D. M.; Voloshina, A. D.; Lyubina, A. P.; Strobykina, A. S.; Mukhitova, F. K.; Polyancev, F. M.; Mironov, V. F. Synthesis of 2-(2-hydroxyaryl)alkenylphosphonium salts from phosphine oxides via ring-closing ring-opening approach and their antimicrobial evaluation. *Tetrahedron* **2016**, *72*, 8493-8501.
28. Li, J.; Soroka, J.; Buchner, J. The Hsp90 chaperone machinery: Conformational dynamics and regulation by co-chaperones. *Biochimica et Biophysica Acta (BBA) - Molecular Cell Research* **2012**, *1823*, 624-635.
29. Patel, P. D.; Yan, P.; Seidler, P. M.; Patel, H. J.; Sun, W.; Yang, C.; Que, N. S.; Taldone, T.; Finotti, P.; Stephani, R. A.; Gewirth, D. T.; Chiosis, G. Paralog-selective Hsp90 inhibitors define tumor-specific regulation of HER2. *Nat. Chem. Biol.* **2013**, *9*, 677-84.
30. Sun, J.; Lin, C.; Qin, X.; Dong, X.; Tu, Z.; Tang, F.; Chen, C.; Zhang, J. Synthesis and biological evaluation of 3,5-disubstituted-4-alkynylisoxozales as a novel class of HSP90 inhibitors. *Bioorganic & medicinal chemistry letters* **2015**, *25*, 3129-3134.

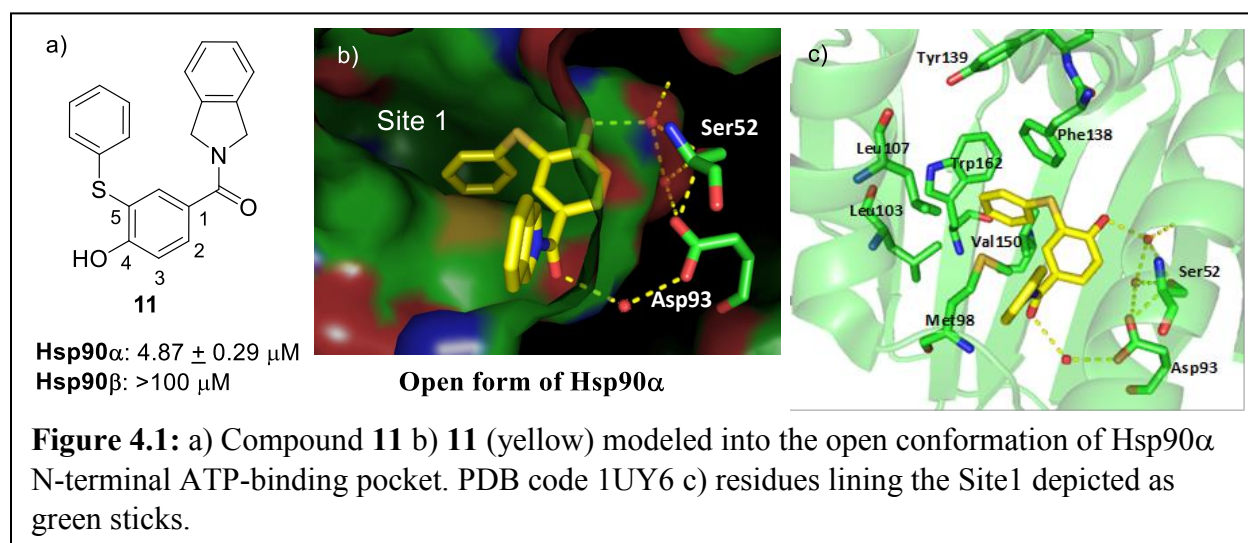
## Chapter IV

### Optimization of the Hsp90 $\alpha$ -selective Compounds

#### IV.1 Benzenethiols Containing Hsp90 $\alpha$ -selective Inhibitors

As discussed in the previous chapter, benzenethiol containing hit **11**, was hypothesized to preferentially bind Hsp90 $\alpha$  and induce a conformational change by projecting the benzenethiol moiety into Site 1 (Figure 4.1b). The Hsp90 tertiary structure resulting from ligand binding is regulated by transition states of Hsp90-ligand complexes that differ energetically between Hsp90 isoforms  $\alpha$  and  $\beta$ , which are cytosolic isoforms that exhibit >95% identity in their N-terminal ATP-binding site.<sup>1-4</sup>

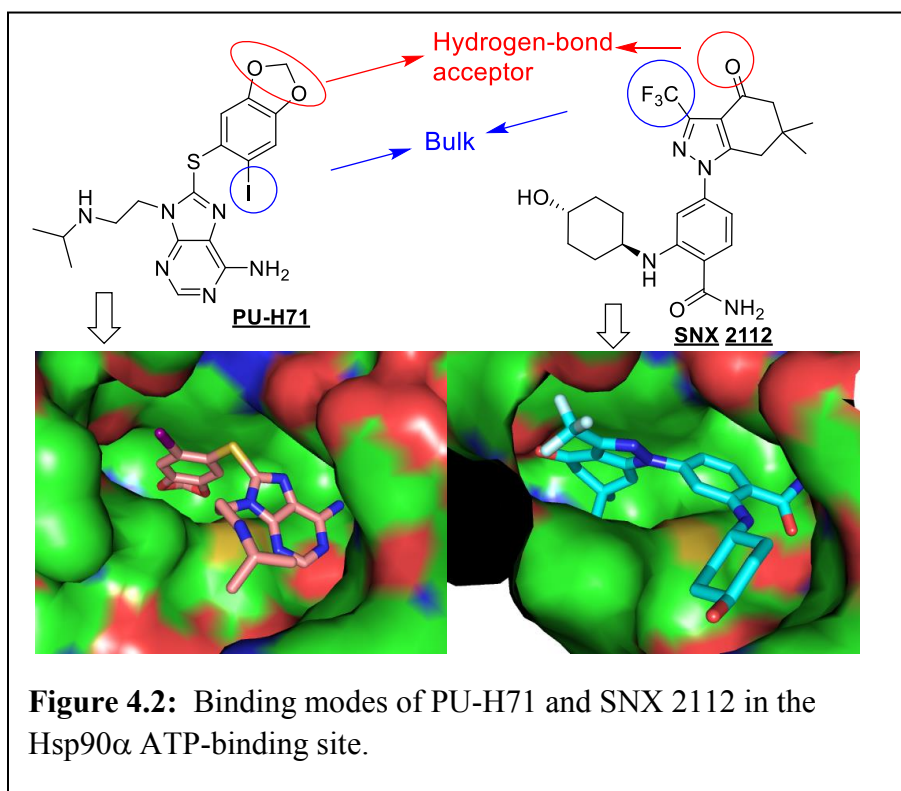
The benzenethiol provides steric bulk at the 5-position that orients the 4-phenol into a conformation that is favored for interaction with Ser52 (Ala52 in Hsp90 $\beta$ ), imparting the observed selectivity versus Hsp90 $\beta$ . In the open conformation of Hsp90 $\alpha$ , Site 1 is outlined with residues



that contain aromatic and non-polar side chains, as illustrated in Figure 4.1c, which together create a hydrophobic environment in the binding pocket. Analysis of the co-crystal structures of purine-

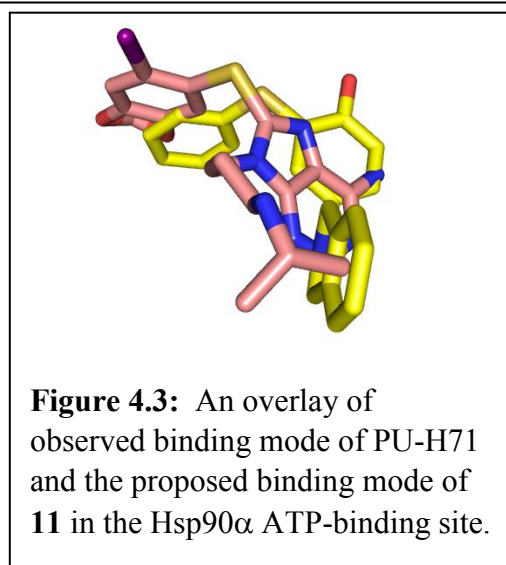
and benzamide-based Hsp90 inhibitors revealed that both scaffolds open Site 1.<sup>5-6</sup> The methylenedioxyphenyl ring in the purine-based compounds and the tetrahydroindazolone fragment of SNX 2112, induce opening by occupying the extended Site1. An overlay of these

scaffolds also uncovered that Site 1 occupying fragments share two pharmacophores; 1) a steric bulk (iodine atom, and CF<sub>3</sub> group, Figure 4.2), which displace water molecules present near the binding pocket, resulting in an entropically stable



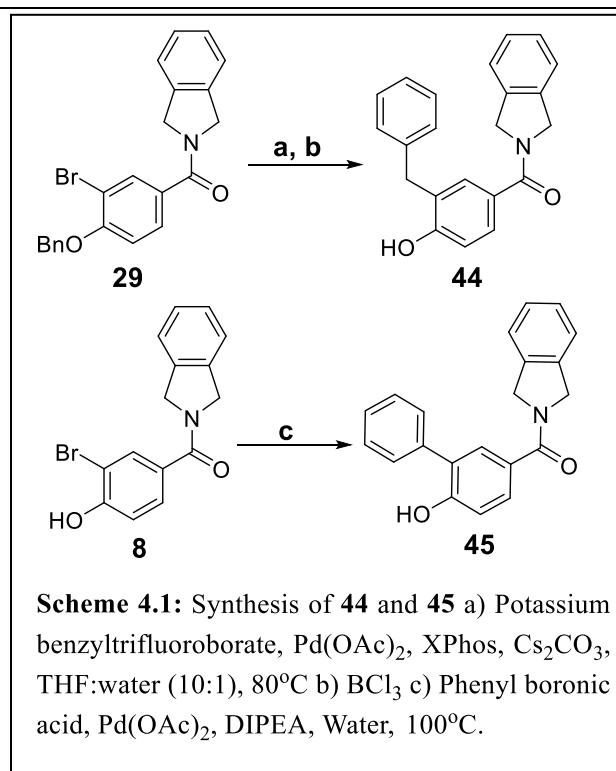
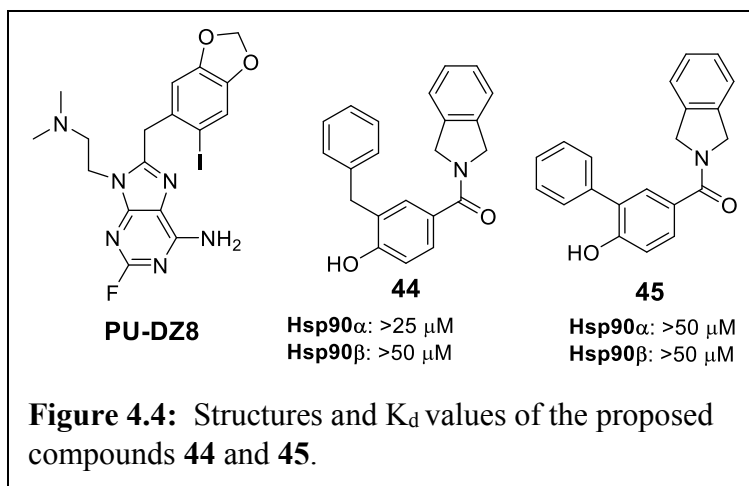
ligand-Hsp90 complex; 2) a hydrogen-bond acceptor (methylenedioxy and ketone) that interacts with Tyr139 (Figure 4.2).

Since PU-H71 and **11** share a thioether linkage, an overlay was performed with the proposed binding mode of **11** and the observed binding pose of PU-H71 in the Hsp90 $\alpha$  co-crystal structure. Interestingly, this study revealed that the benzenethiol in **11** does not align with



the methylenedioxyphenyl ring (Figure 4.3), and implies that **11** exhibits a binding pose that differs from PU-H71. PU-DZ8, another purine containing compound, which contains a methylene *in lieu* of the thioether linker (Figure 4.4),<sup>7</sup>

maintains cellular efficacy and client degradation as observed for PU-H71.<sup>7</sup> In addition, the methylene linker projects the methylenedioxyphenyl ring into Site 1 at an angle that is minimally different than the thioether linkage.<sup>5</sup> As such, the thioether linkage contained in **11** was replaced with a methylene to produce **44**. In addition, a compound lacking the linker was also sought (**45**).



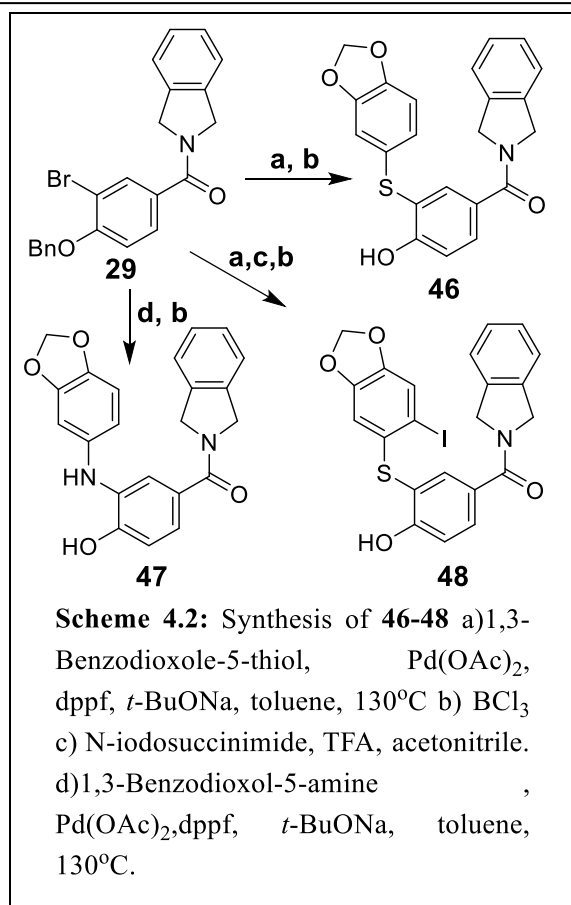
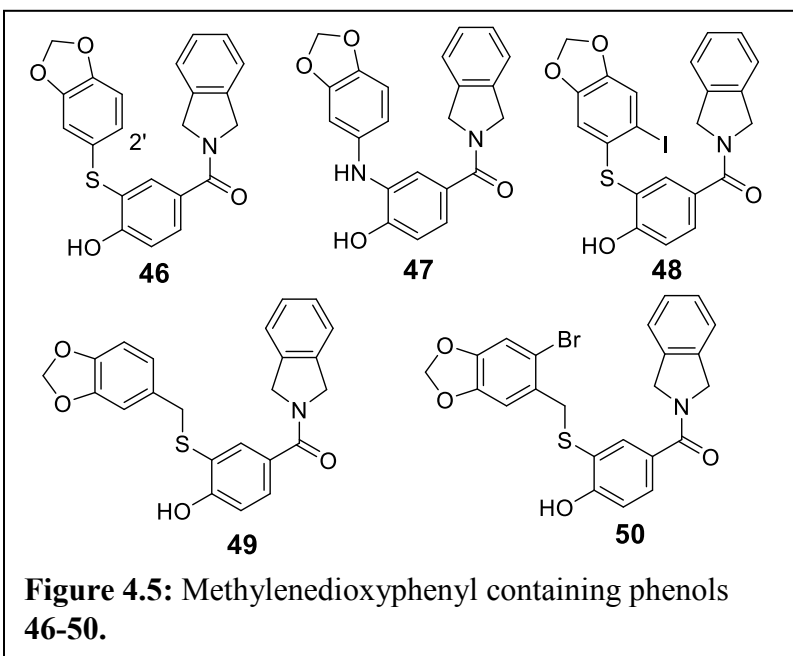
Synthesis of the proposed compounds is outlined in Scheme 4.1, wherein, benzyl protected monophenol **29**,<sup>3</sup> was coupled with benzyltrifluoroborate via palladium acetate (Pd(OAc)<sub>2</sub>). The desired product, **44**, was obtained upon unmasking the phenol using a solution of boron trichloride (BCl<sub>3</sub>). Compound **45** was prepared via a Pd(OAc)<sub>2</sub> catalyzed reaction between **8** and phenyl boronic acid in the presence of diisopropylethylamine (DIPEA). Upon their preparation, **44** and

**45** were evaluated in an FP assay to determine their apparent  $K_{dS}$ . Unlike **11**, compound **44** and **45** bound poorly to Hsp90 $\alpha$ , while **45** manifested no affinity.

#### IV.2 Chimeric Hsp90 $\alpha$ -selective Compounds.

In an attempt to hybridize the purine and monophenol scaffolds, a methylenedioxyphenyl ring was proposed to replace the thiophenol moiety in **11**.

Although overlay studies indicated that the methylenedioxy may not orient in a manner similar to purine compounds, the potential for hydrogen bonding interactions with Tyr139 (Figure 4.1c) warranted the evaluation of **46** (Figure 4.5). Construction of **46** was achieved via a Buchwald-Hartwig coupling reaction between protected phenol **29** and 1,3-Benzodioxole-5-thiol, which was prepared following a reported method.<sup>8</sup> **46** was found to exhibit ~5-folds improvement in affinity ( $K_d \sim 0.71 \mu\text{M}$ , Table 4.1) in an FP assay, which aligned with the original hypothesis. Furthermore, as the presence of a bulky

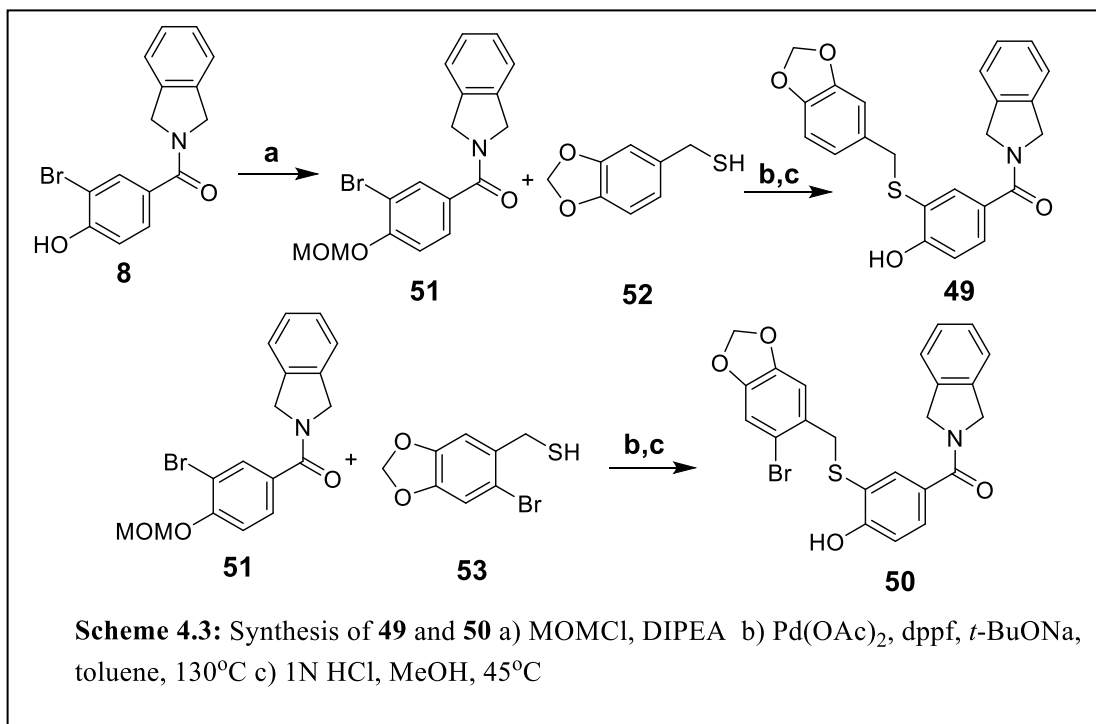


atom or group was proven to be beneficial for increased affinity with the purine (at 2'-position of methylenedioxyphenyl ring) and benzamide scaffold (CF<sub>3</sub> group),<sup>9-10</sup> an iodine atom was installed onto the 2'-position of **46** to mimic this bulk (**48**). Upon its preparation, **48** was evaluated for binding affinity to reveal that **48** exhibits a minimal loss in affinity (K<sub>d</sub> ~0.91 μM) as compared to the unsubstituted compound, **46** (Table 4.1). An aniline was also incorporated *in lieu* of the thioether to produce **47**, which lacked

Compounds	Hsp90α K <sub>d</sub> (μM)	Hsp90β K <sub>d</sub> (μM)	Fold selectivity
<b>46</b>	0.715± 0.03	>50	>70
<b>47</b>	>25	>50	>2
<b>48</b>	0.91± 0.05	>50	>55
<b>49</b>	0.92± 0.03	>50	>55
<b>50</b>	>50	>50	-

**Table 4.1:** K<sub>d</sub> determination of **46-50**, using the FP assay.

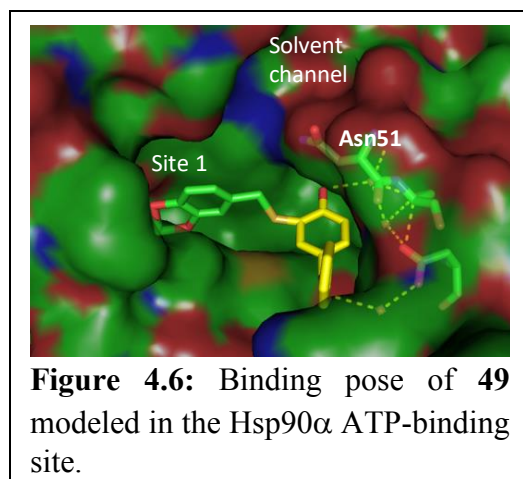
binding to both isoforms, suggesting that the rotational freedom afforded by thioether is beneficial



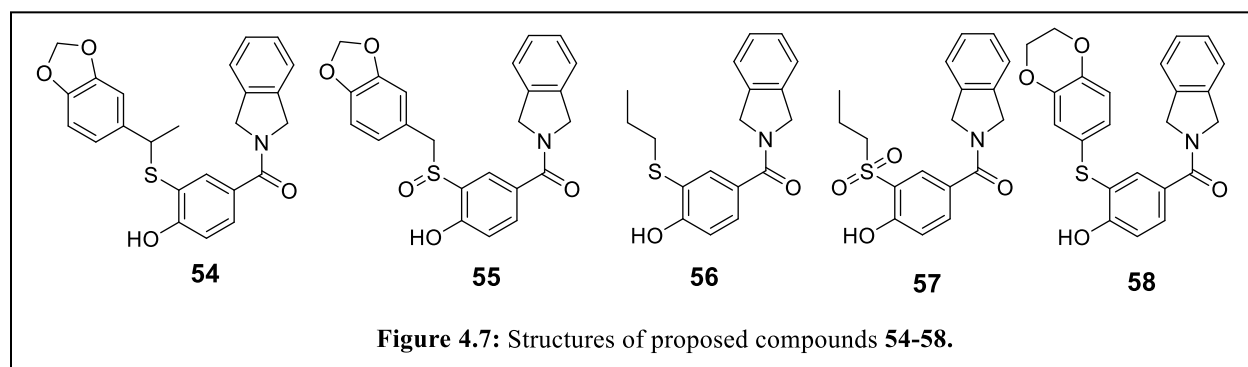
for orientation of the methylenedioxyphenyl ring. Upon reviewing the overlays of PU-H71 and **11**,

it became apparent that a methylene linker could be accommodated between the thiol and methylenedioxyphenyl ring, and was therefore incorporated into **49**. Compound **49** was constructed similar to the route used for the preparation of **46**, wherein **51** was treated with the requisite thiol, **52**.<sup>11</sup> Upon evaluation, **49** was shown to exhibit a loss of affinity as compared to **46**. A bulky group was then pursued to investigate the binding orientation of **49**, by coupling **53** with **51** to produce the bromine containing compound, **50**.<sup>9, 12</sup> Unfortunately, **50**, did not bind either Hsp90 $\alpha$  or Hsp90 $\beta$ , suggesting that the bulky bromide is a poor fit and exhibits a steric clash with the protein surface.

Modeling of **49** into the binding site suggested that a methylene linker, may provide access to the solvent as noted in Figure 4.6. Occupation of the solvent channel has resulted in an enhancement in



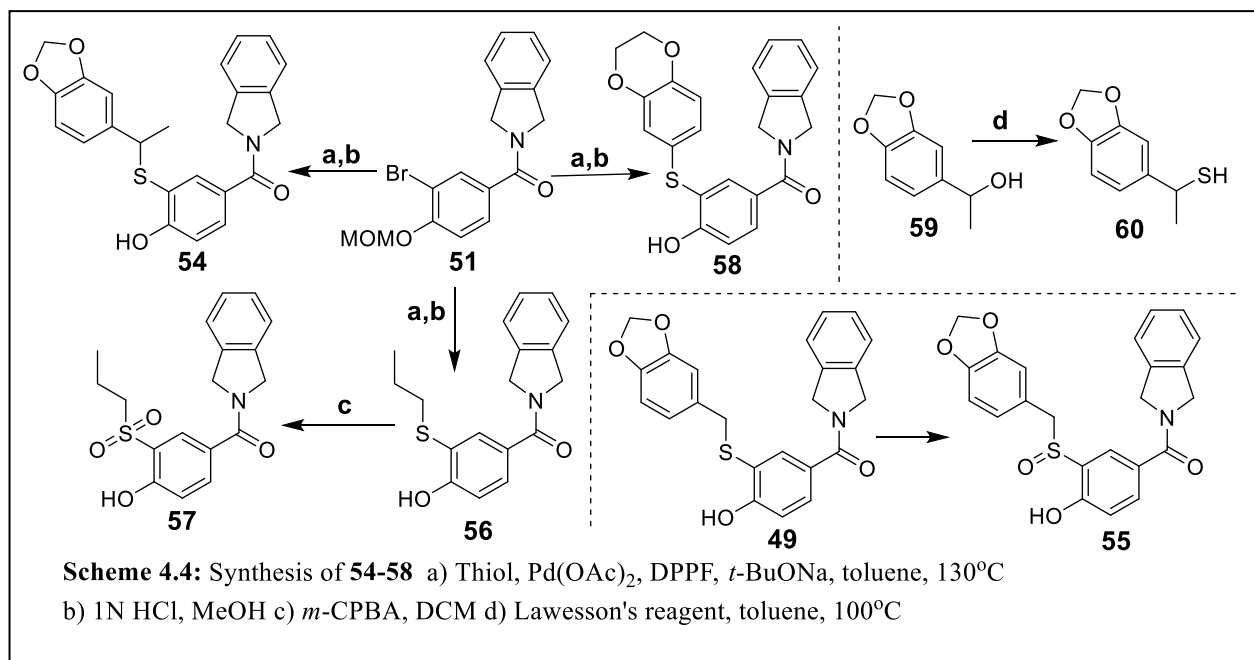
affinity as noted in prior chapters, therefore, a methyl was introduced onto the linker as shown with **54**. Treatment of the required alcohol **59** with Lawesson's reagent resulted in thiol **60**,<sup>13</sup> which was subsequently coupled with **51** to furnish the desired product, **54**. Unfortunately, upon the



evaluation of **54**, it was determined that the additional methyl group was detrimental to affinity (Table 4.2). Compound **55** was prepared by oxidation of **49** with *m*-chloroperbenzoic acid (*m*-



CPBA), which contained a sulfoxide to potentially interact with Asn51. But it too manifested little



affinity toward both isoforms. Compound **56**, which was also hypothesized to project into the solvent channel, contained a *n*-propyl chain as a mimic of the *n*-butyl observed in compound **35b** as discussed in the prior chapter. Interestingly, **56** exhibited moderate affinity ( $K_d \sim 2.28 \mu\text{M}$ ) and

$\sim 20$ -fold selectivity for Hsp90 $\beta$ .

Therefore, **56** presented a scaffold akin to the *t*-butyl containing compound, **9** (Chapter 3), used for the development of Hsp90 $\alpha$ -selective inhibitors. A sulfonyl group was also installed into **57** to investigate potential binding interactions with

Compound	Hsp90 $\alpha$ $K_d$ ( $\mu\text{M}$ )	Hsp90 $\beta$ $K_d$ ( $\mu\text{M}$ )	Fold selectivity
<b>54</b>	$3.476 \pm 0.40$	>50	>15
<b>55</b>	>50	>50	-
<b>56</b>	$2.28 \pm 0.14$	$44.25 \pm 0.14$	$\sim 20$
<b>57</b>	>50	>50	-
<b>58</b>	$0.521 \pm 0.018$	$27.74 \pm 3.07$	$\sim 53$

**Table 4.2:**  $K_d$  determination of **54-58**, using the FP assay.

Asn51. However, the sulfonyl containing compound manifested a complete loss in affinity.

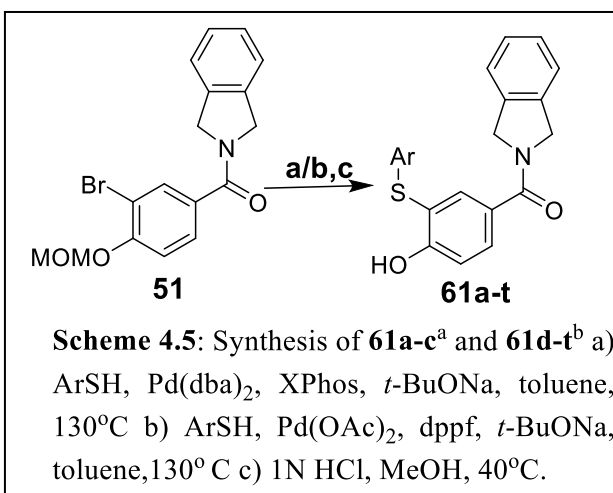
Finally, an ethylenedioxyphenyl ring was introduced into compound **58**, which led to the

improvement in affinity ( $K_d \sim 0.521 \mu\text{M}$ ) over the methylenedioxy (**46**), with  $\sim 53$ -fold selectivity versus Hsp90 $\beta$ .

Collectively, the binding data from the hybridized 4-phenol series of compounds (Figure 4.2 and 4.5) suggested that binding affinity improved with the introduction of hydrogen-bond acceptor groups through interactions with Tyr139, but 2'-substituted derivatives produced decreased affinity, which is unlike the trend observed for purine-based compounds. Therefore, structure-activity relationship studies were proposed on compound **11** and about the benzenethiol ring to investigate Site 1.

### IV.3 Structure-Activity Relationship Studies on the Benzenethiol Ring.

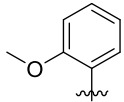
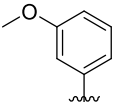
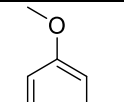
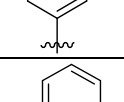
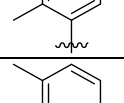
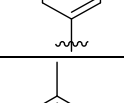
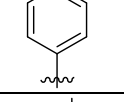
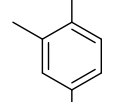
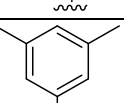
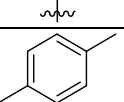
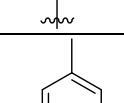
As outlined in Figure 4.1c, residues that comprise Site 1 exhibit primarily hydrophobic side chains. Therefore, a methyl scan was initiated in addition to the proposed methoxy substitutions, which could mimic the methylenedioxy interactions with Tyr139. The unsubstituted compound, **11**, binds



Hsp90 $\alpha$  with  $K_d \sim 4.87 \mu\text{M}$  and is  $>20$ -fold selective versus Hsp90 $\beta$ .

The preparation of compounds **61a-t** was achieved by coupling the methoxymethyl acetal (MOM) intermediate **51**, with the corresponding thiols via a Buchwald-Hartwig conditions. While palladium acetate (Pd(OAc)<sub>2</sub>) and 1,1'-Ferrocenediyl-bis(diphenylphosphine) (dppf) worked

efficiently for the synthesis of **61d-t**, coupling of the methyl ether-containing compounds **61a-c**, required the (dibenzylideneacetone)palladium(0) ( $\text{Pd}(\text{dba})_2$ ) and 2-dicyclohexylphosphino-2',4',6'-

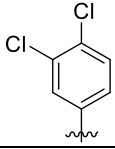
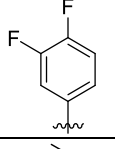
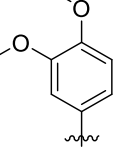
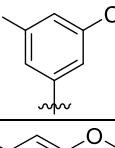
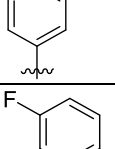
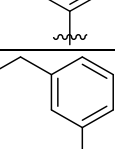
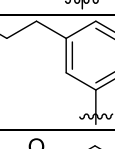
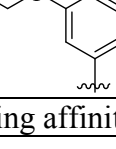
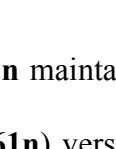
Compounds	Ar group	Hsp90 $\alpha$ $K_d$ ( $\mu\text{M}$ )	Hsp90 $\beta$ $K_d$ ( $\mu\text{M}$ )	Fold selectivity
<b>61a</b>		4.34 $\pm$ 0.58	>50	>12
<b>61b</b>		1.44 $\pm$ 0.12	>50	>35
<b>61c</b>		2.57 $\pm$ 0.15	>50	>20
<b>61d</b>		2.94 $\pm$ 0.24	>50	>17
<b>61e</b>		1.74 $\pm$ 0.44	>50	>28
<b>61f</b>		2.70 $\pm$ 0.40	44.25 $\pm$ 0.14	~16
<b>61g</b>		0.845 $\pm$ 0.13	>50	>63
<b>61h</b>		0.724 $\pm$ 0.08	37.51 $\pm$ 3.8 7	~51
<b>61i</b>		7.736 $\pm$ 0.93	>50	>7
<b>61j</b>		>50	>50	-
<b>61k</b>		3.029 $\pm$ 0.26	>50	>16

**Table 4.3:** Binding affinities of **61a-k** as determined with FP assay

triisopropylbiphenyl (XPhos) catalytic system (Scheme 4.4). Upon evaluation of the methoxy containing compounds, **61a-c** in an FP assay, the 3-methoxy (**61b**) derivative was found to exhibit improved affinity as compared to **61c**, while the 2-methoxy (**61a**) also increased affinity. A subsequent methyl scan with compounds **61d-f**, revealed the 3-methyl compound (**61e**) to exhibit improved affinity ( $K_d \sim 1.74 \mu\text{M}$ ), whereas the 2-methyl (**61d**) ( $K_d \sim 2.94 \mu\text{M}$ ) and 4-methyl derivatives (**61f**) ( $K_d \sim 2.74 \mu\text{M}$ ) provided moderate improvement in affinity. Furthermore, substitutions were installed onto the phenyl ring to determine mutual exclusivity for occupation of Site1. Since **58** manifested high affinity ( $K_d \sim 0.521 \mu\text{M}$ ), other di-substituted products were pursued. The 3,4-dimethyl substituted compound, **61g**, was prepared and found to manifest  $\sim 0.845 \mu\text{M}$  binding affinity with  $>60$ -fold selectivity, whereas the 3,5-dimethyl derivative (**61h**) bound Hsp90 $\alpha$  with a  $K_d \sim 0.724 \mu\text{M}$ . Unfortunately, selectivity was limited when compared to **61g**. When compounds containing, 2,5- and 2,4-dimethyl substituents were investigated a loss of affinity was observed (**61i**  $K_d \sim 7.73 \mu\text{M}$ ).

Preparation of the 3,4,5-trimethyl substituted compound, **61k**, was sought to explore the potential for occupation of Site 1 in an orientation that resembled the binding pose of compounds **61g** and **61h**. 3,4,5-Trimethylbenzenethiol was prepared using an approach previously reported and was used to construct **61k**.<sup>14</sup> Unfortunately, **61k** did not bind Hsp90 $\alpha$  as effectively as **61g** or **61h**, suggesting that the conformation of **61k** is different than **61g** and **61h**.

Incorporation of a 3,4-dichlorophenyl ring led to **61l** (Table 4.4), however, it did not manifest similar affinity as **58**. Similarly, the 3,4-difluorophenyl analog (**61m**) exhibited decreased affinity (~4.77 $\mu$ M), suggesting the presence of the difluoro substitution is not beneficial for Site 1. The 3,4-dimethoxy containing compound, **61n**, resembles **58**, but contains the open form

Compounds	Ar group	Hsp90 $\alpha$ K <sub>d</sub> ( $\mu$ M)	Hsp90 $\beta$ K <sub>d</sub> ( $\mu$ M)	Fold selectivity
<b>61l</b>		4.34 $\pm$ 0.58	>50	>12
<b>61m</b>		4.77 $\pm$ 0.21	>50	>11
<b>61n</b>		0.529 $\pm$ 0.07	11.66 $\pm$ 1.07	~22
<b>61o</b>		4.45 $\pm$ 0.58	>50	>12
<b>61p</b>		0.899 $\pm$ 0.02	>50	>56
<b>61q</b>		7.04 $\pm$ 0.15	>50	>7
<b>61r</b>		0.463 $\pm$ 0.06	22.28 $\pm$ 2.79	~48
<b>61s</b>		0.565 $\pm$ 0.06	>50	>88
<b>61t</b>		4.38 $\pm$ 0.24	>50	>12

**Table 4.4:** Binding affinities of **61l-t** as determined with FP assay

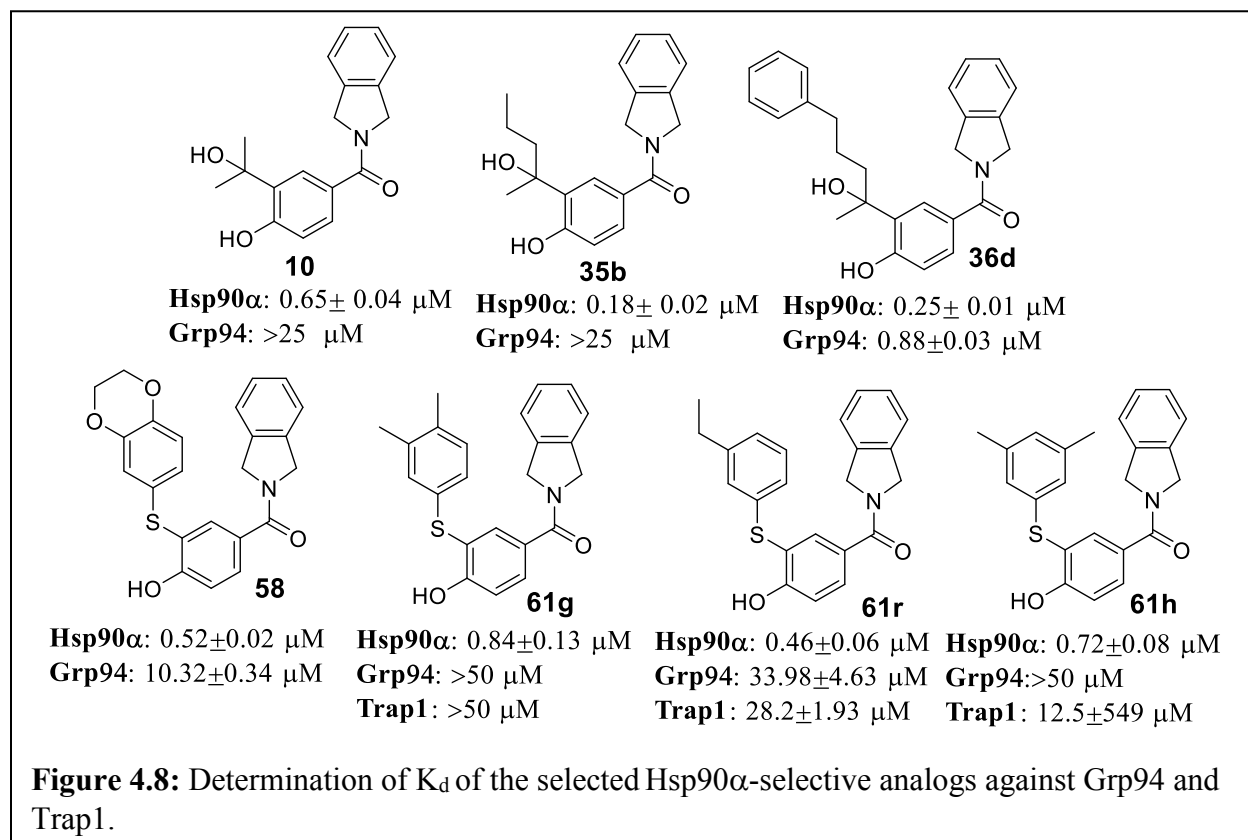
of the ethylenedioxy ring. Surprisingly, **61n** maintained binding affinity as compared to **58**, but resulted in a loss of selectivity (22-fold (**61n**) versus 53-fold (**58**)), implying ring constraint is accommodated by Hsp90 $\beta$  more effectively. Improvement in binding affinity afforded by the 3,5-dimethyl compound, **61h**, warranted investigation of the 3,5-dichloro compound, **61o**.

Disappointingly, **61o** did not increase affinity, reinforcing the notion that the chlorine atom is not beneficial. Noting the 3-methyl and 3-methoxy substitutions manifest improved affinities, a 3-methoxy-5-methyl substituted derivative, **61p**, was synthesized via the 3-methoxy-5-methyl benzenethiol,<sup>15</sup> and was found exhibit similar affinity as 3,5-dimethyl (**61h**). A fluorine atom at the 3-position was also introduced into **61q**, to investigate the role of the fluorine atom as a hydrogen-bond acceptor and for interactions with Tyr139. However, FP assay results determined **61q** to manifest decreased binding affinity. Evaluation of the 3-ethyl derivative, **61r**, resulted in ~4-fold improvement ( $K_d \sim 463$  nM, ~48-fold selective) in binding affinity compared to the 3-methyl analog, **61e**. Consequently, the 3-position was homologated to the corresponding *n*-propyl analog (**61s**), that resulted in slight loss of affinity ( $K_d \sim 565$  nM) relative to **61r**, however, selectivity against Hsp90 $\beta$  improved (>88-fold). Similarly, the 3-ethoxy derivative (**61t**) was proposed (**61r**), but unfortunately, a loss of ~3-fold affinity was observed.

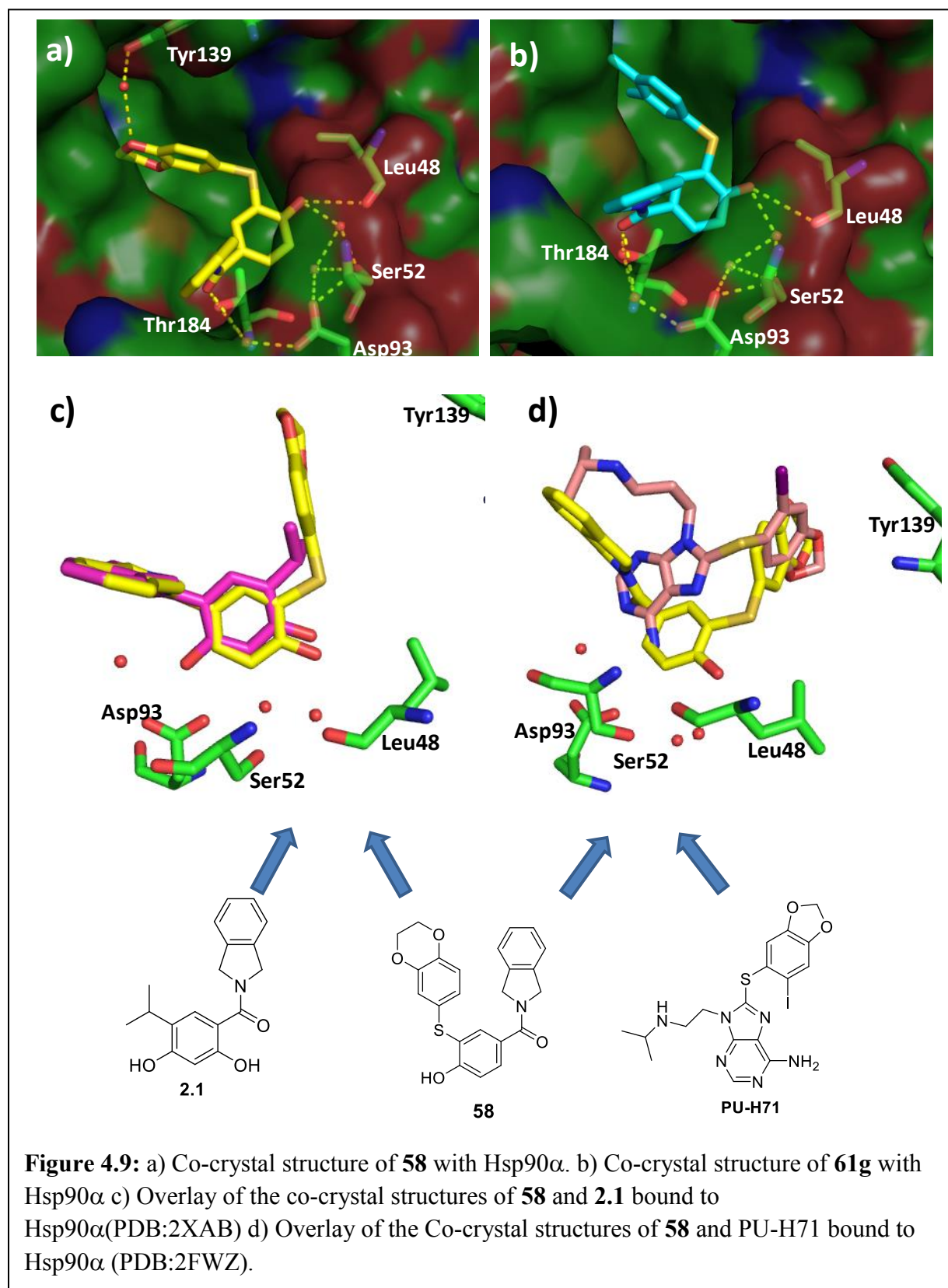
#### **IV.4 Selectivity of the Hsp90 $\alpha$ -selective Compounds Against Grp94 and Trap1**

The developed Hsp90 $\alpha$ -selective scaffolds were screened for their affinity towards the endoplasmic reticulum residing isoform, Grp94 and then select compounds were also screened against the mitochondrial isoform, Trap1.

Upon evaluation in the FP assay, the tertiary alcohol, **10**, showed reduced binding toward Grp94. Similarly, the alcohol derivative containing a *n*-butyl chain (**35b**) exhibited binding affinity



$>25\mu\text{M}$  against Grp94. However, the phenpropyl containing compound (**36d**) bound Grp94 with only ~4-fold selectivity, implying that occupation of Site1 with a flexible propylene linker increases affinity for Grp94 as well. The benzenethiol compound, **58**, exhibited ~20-fold selectivity versus Grp94, whereas, the 3,4-dimethyl (**61g**) showed  $>50$ -fold selectivity against both Grp94 and Trap1. Furthermore, the 3-ethyl derivative (**61r**) bound Grp94 with ~74-fold selectivity and Trap1 with ~60-fold selectivity. Finally, the 3,5-dimethyl analog (**61h**) exhibited ~70-fold selectivity versus Grp94, while it bound Trap1 with only ~17-fold selectivity. These binding preferences suggest that the substitution pattern on the benzenethiol ring plays a critical role for selectivity against the organelle residing Hsp90 isoforms. The future design of Hsp90α-selective



compounds may avoid binding to Grp94 or Trap1 by incorporating these substituents as optimized

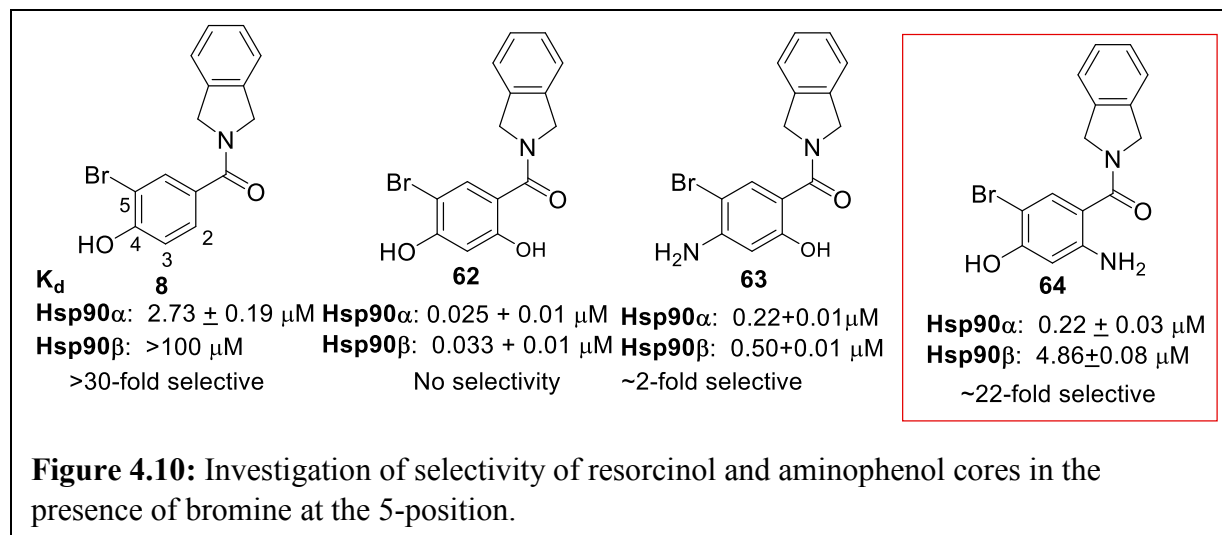


in this SAR study.

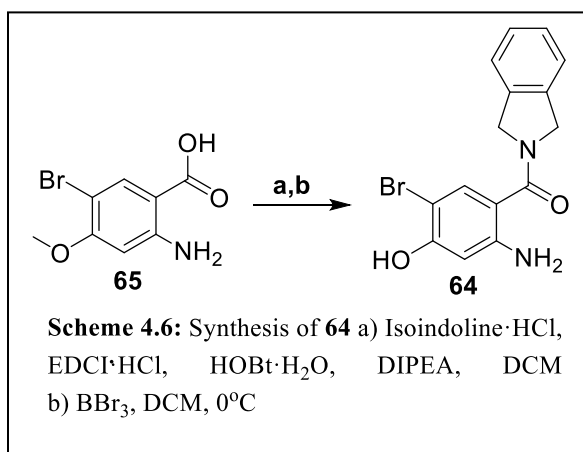
#### IV.5 Analysis of the Co-Crystal Structures of **58** and **61g** with Hsp90 $\alpha$

In collaboration with Dr. Robert Matts at Oklahoma State University, Hsp90 $\alpha$ -selective compounds, **58** and **61g**, were successfully co-crystallized with the Hsp90 $\alpha$  N-terminal domain. Not surprisingly, binding poses of the analyzed compounds, **58** and **61g**, were identical to the binding pose identified during modeling studies (Figure 4.9 a and b). Participation of the 4-phenol in the hydrogen bonding network resembles the proposed model. In fact, compounds **58** and **61g** induce the opening of Site 1 and interact with residues Leu48, Ser52, Asp93 and Thr184 through conserved water molecules. In addition, the ethylenedioxyphenyl ring present in **58**, was found to interact with Tyr139 via a non-conserved water molecule (Figure 4.9a), whereas, **61h** lacked such interactions. The selectivity of benzenethiol series of compounds for Hsp90 $\alpha$  is rationalized by using the overlay of the binding poses for the non-selective compound, **2.1** and **58** bound to Hsp90 $\alpha$  (Figure 4.9c). As can be observed, inclusion of the benzenethiol at the 5-position in the 4-monophenol induced a conformational change that resulted in the opening of Site 1, unlike **2.1**, which binds to the closed form (resting state) of Hsp90 $\alpha$ . Orientation of the benzenethiol fragment in Site 1 is dissimilar to the thioether that is projected with PU-H71 (Figure 4.9d). Accommodation of the thioether in the 4-phenol series requires a shift in the binding plane toward the adenine binding pocket (Figure 4.9c), which brings the 4-phenol closer to Ser52, a residue that differentiates the Hsp90 $\alpha$ -subpocket from Hsp90 $\beta$ , and Asp93, which exhibits critical interactions with ligands in the Hsp90 N-terminal ATP-binding site.<sup>16-17</sup> Consequently, Hsp90 $\alpha$  preferentially accommodates the benzenethiol containing 4-monophenols better than Hsp90 $\beta$ .

#### IV.6 Discovery of the Aminophenol-containing Hsp90 $\alpha$ -selective Scaffold



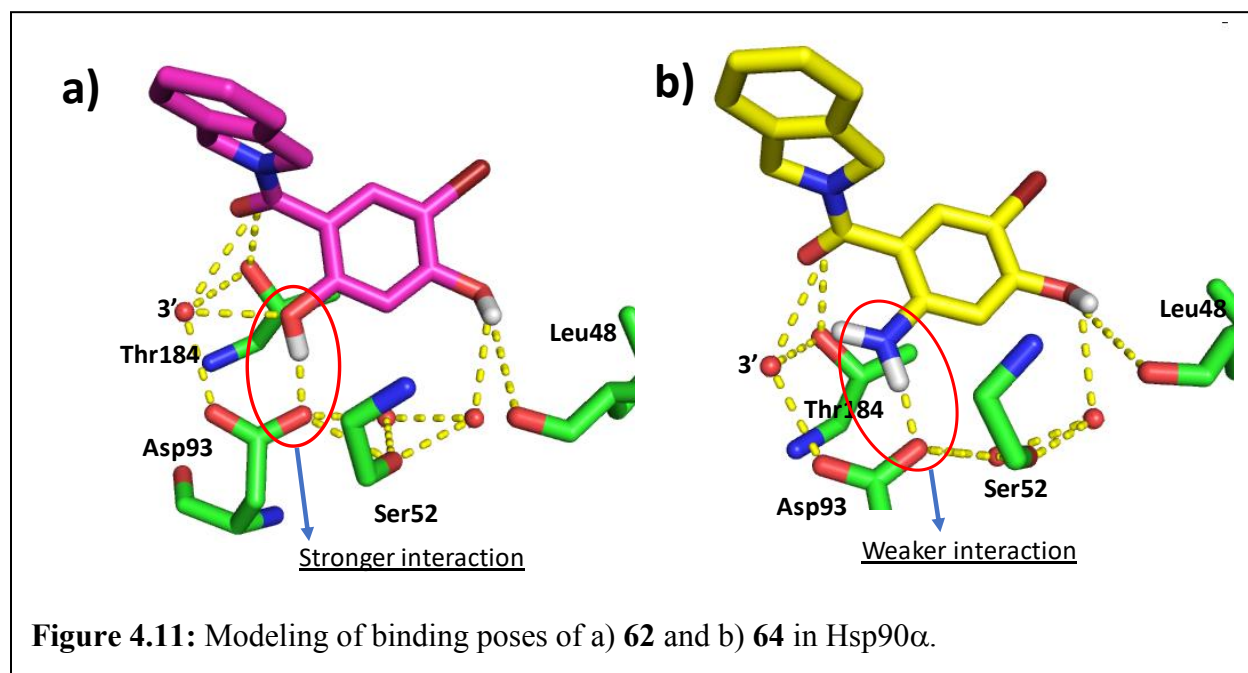
The presence of a bromine atom at the 5-position appeared to enhance Hsp90 $\alpha$ -selectivity for the monophenol **8**, as previously explained (Figure 4.10). Therefore, the impact of a bromine atom at the 5-position in resorcinol compound **62** was hypothesized to increase selectivity while maintaining affinity. However, upon evaluation in an FP assay, **62** lost complete selectivity. The lack of selectivity can be explained by the contact that the 2-phenol makes with Asp93, as well as interactions with Thr184 via water molecule 3', which negates any preferential interaction between the 4-phenol and Ser52. However, the incorporation of an aniline group into the 4-position (**63**) led to ~2-fold selectivity for



Hsp90 $\alpha$ , but >10-fold reduction in affinity was also observed.<sup>3</sup> Consequently, it was concluded that the phenol at the 2-position is detrimental to selectivity. Therefore, replacements of the 2-phenol were sought. Computational studies established that the binding energy between an unsubstituted phenol and an acetate ion could be ~25.4 kcal/mol, whereas an unsubstituted aniline

may only manifest a binding energy of  $\sim 18$  kcal/mol.<sup>18-19</sup> Therefore, aniline in **64** was theorized to interact with Asp93 poorly in comparison to the 2-phenol of **62**, and thus, provide a non-specific gain in binding affinity toward both isoforms without a loss in selectivity. It was reasoned that interaction of the aniline with Asp93 could be compensated via the 4-phenol in **64**.

**65** was prepared using a previously reported procedure,<sup>20</sup> and was then coupled with isoindoline by enlisting 1-ethyl-3-(3-dimethylaminopropyl) carbodiimide (EDCI) and hydroxybenzotriazole (HOBt), and subsequently treating with boron tribromide (BBR<sub>3</sub>) to produce **64** (Scheme 4.6).



Upon evaluation in an FP assay, **64** was found to bind Hsp90 $\alpha$  and Hsp90 $\beta$  with a  $K_d$  of  $\sim 0.22$   $\mu$ M and  $\sim 4.86$   $\mu$ M respectively, exhibited  $\sim 22$ -fold selectivity.

## IV.7 Biological Studies

### IV.7.1 Antiproliferative Effect on Cancer Cells

Hsp90 $\alpha$ -selective compounds, **35b** and **36d** which belong to the tertiary-alcohol series, and **61g**, a compound belonging to the benzenethiol series, were evaluated against the NCI-60 cancer cell panel at a single dose of 10 $\mu$ M. Results obtained are shown in Figure 4.12 (**35b**), 4.13 (**36d**) and 4.14 (**61g**). These inhibitors exhibited moderate antiproliferative activity in the NCI-60 cell panel, however, particular cell lines were consistently affected upon treatment with these Hsp90 $\alpha$ -selective inhibitors. The leukemia cell line, K562, NSCLC cells, NCI-H522, colon cancer cell line, KM12, melanoma cell lines, UACC-62, ovarian cancer cell line, SK-OV-3 and more specifically, the renal cancer cell line, UO-31 resulted in decreased proliferation when Hsp90 $\alpha$ -selective inhibitors. Further studies are underway to identify the dependency of these cancer cell lines upon Hsp90 $\alpha$  and to elucidate Hsp90 $\alpha$ -dependent clients that drive proliferation and metastasis of these cancers.

P.T.O.

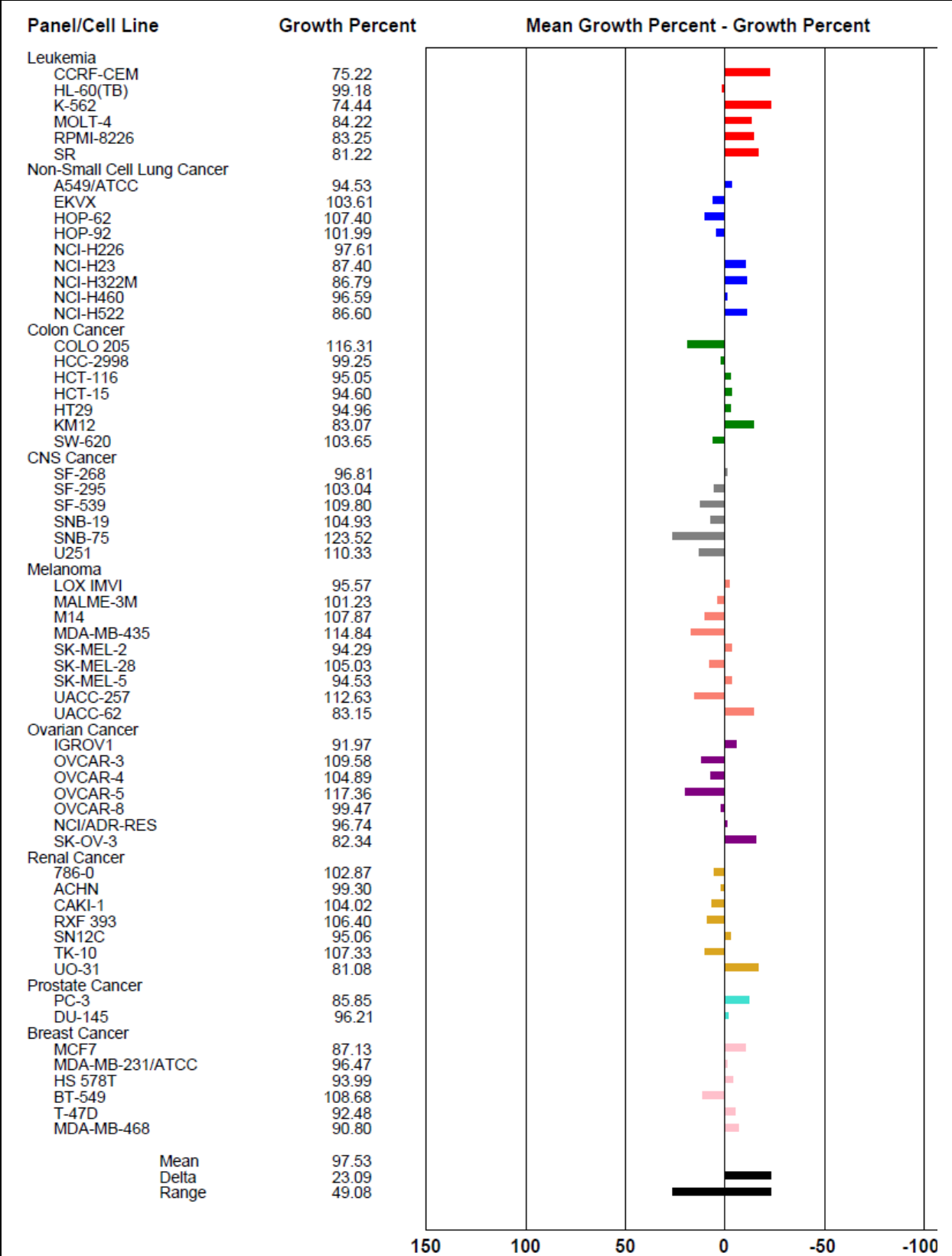


**Figure 4.12:** NCI-60 cancer cell screening results from the single dose experiment of **35b**.

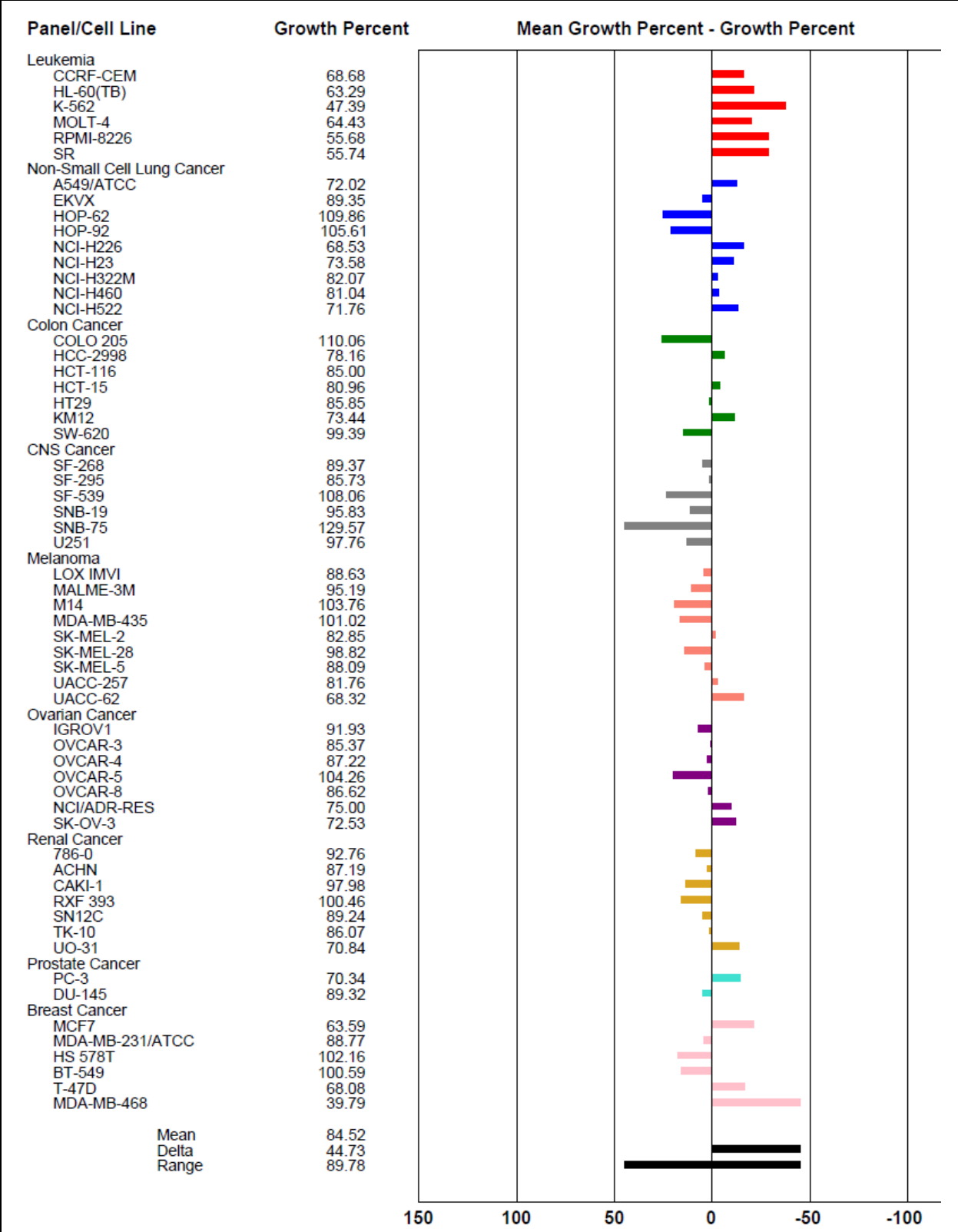


**Figure 4.13:** NCI-60 cancer cell screening results from the single dose experiment of 36d.

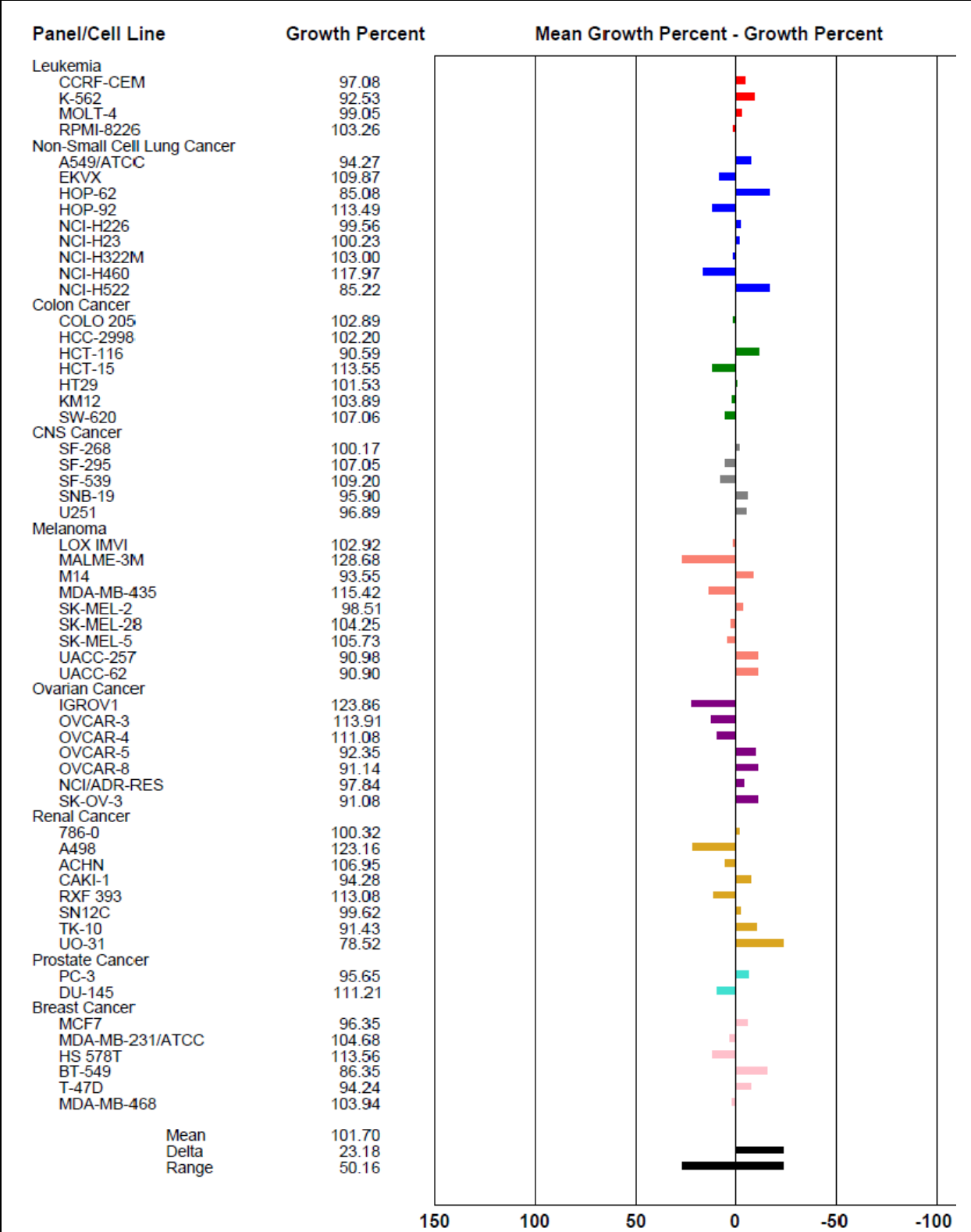


**Figure 4.14:** NCI-60 cancer cell screening results from the single dose experiment of 61g.

## IV.8 Conclusions and Future Directions

The benzenethiol containing Hsp90 $\alpha$ -selective compounds have been optimized for the occupation of Site 1, which ultimately led to compounds **58**, **61g**, **61r** and **61h**. These inhibitors exhibited superior affinity and selectivity over the parent compound, **11**. The binding modes of **58** and **61g** were confirmed to align well with the modelling studies and uncovered the plane of monophenol to shift closer to residues Ser52 and Asp93, which allows for the selective binding of Hsp90 $\alpha$ . In addition, it was also discovered that aminophenol, **64**, could rescue the affinity loss by the resorcinol, while maintaining ~22-fold selectivity versus Hsp90 $\beta$ . In the future, the aminophenol and the optimized thioether fragment will be combined to guide the development of Hsp90 $\alpha$ -selective inhibitors that should exhibit affinities <50 nM and selectivities >50-fold versus Hsp90 $\beta$ .

The NCI-60 screening of compounds representing various Hsp90 $\alpha$ -selective scaffolds has allowed the identification of cell lines that appear to be depend upon Hsp90 $\alpha$  for their growth. Critical evaluation of the upregulated biological pathways and clients driving the growth of these cancer cell lines may highlight the therapeutic relevance on Hsp90 $\alpha$ -selective inhibition. Ultimately, these findings will aid in the rationalization and development of Hsp90 $\alpha$ -selective compounds as an alternative chemotherapeutic approach to treat cancers.

## IV.9 Methods and Experiments

### Chemistry

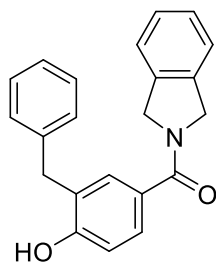
All reactions were performed in oven-dried glassware under argon atmosphere unless otherwise stated. Dichloromethane (DCM), tetrahydrofuran (THF), and toluene were passed through a column of



activated alumina prior to use. Anhydrous methanol, dimethyl sulfoxide (DMSO), and *N,N*-dimethylformamide (DMF) were purchased and used without further purification. Flash column chromatography was performed using silica gel (40-63  $\mu\text{m}$  particle size). The  $^1\text{H}$  (500 and 400 MHz) and  $^{13}\text{C}$  NMR (125 and 100 MHz) spectra were recorded on 500 and 400 MHz spectrometer. Data are reported as p = pentet, q = quartet, t = triplet, d = doublet, s = singlet, br s = broad singlet, m = multiplet; coupling constant(s) in Hz. High resolution mass spectral data were obtained on a time-of-flight (TOF) mass spectrometer and analysis was performed using electrospray ionization (ESI).

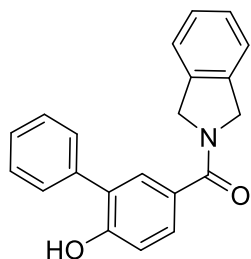
### **Fluorescence Polarization Assay**

Assay buffer (25  $\mu\text{L}$ , 20 mM HEPES pH 7.3, 50 mM KCl, 5 mM  $\text{MgCl}_2$ , 1 mM DTT, 20 mM  $\text{Na}_2\text{MoO}_4$ , 0.01% NP-40, and 0.5 mg/mL BGG) was introduced into 96-well plate (black well, black bottom) followed by the desired compound at the indicated final concentrations in DMSO (1% DMSO final concentration). Subsequently, 10 nM Recombinant Hsp90 $\alpha$  or Hsp90 $\beta$  or cGrp94 or Trap-1 and 6 nM FITC-GDA were added in 50  $\mu\text{L}$  and 25  $\mu\text{L}$  assay buffer respectively resulting in a 100  $\mu\text{L}$  final volume. Plates were incubated for 24 h at 4 $^\circ\text{C}$  on a rocker. Fluorescence was determined using excitation and emission filters of 485 and 528 nm, respectively. Percent FITC-GDA bound was determined by assigning the DMSO millipolarization unit (mP) value as the 100% bound value and 0% for FITC-GDA in assay buffer without any protein. Polarization values (in mP units) was measured at 37  $^\circ\text{C}$  with an excitation filter at 485 nm and an emission filter at 528 nm. Polarization values were correlated to % tracer bound and compound concentrations. The concentration of inhibitor at which the 50% displaced tracer was observed, represented apparent  $K_d$ .



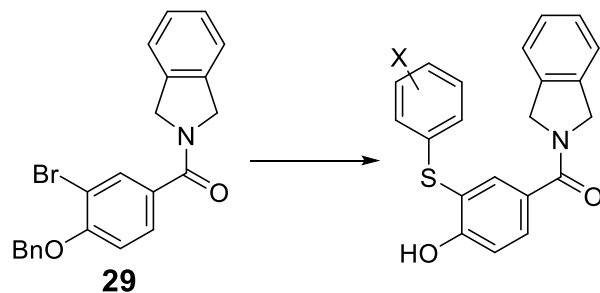
**(3-benzyl-4-hydroxyphenyl)(isoindolin-2-yl)methanone (44)** : (4-(benzyloxy)-3-bromophenyl)(isoindolin-2-yl)methanone (**29**) (100 mg, 0.24 mmol, 1 eq.), palladium acetate (2.6 mg, 0.012 mmol), 2-dicyclohexylphosphino-2',4',6'-triisopropylbiphenyl (XPhos) (11.5 mg, 0.024 mmol), potassium benzyltrifluoroborate (57 mg, 0.29 mmol, 1.2 eq.) and cesium carbonate (156 mg, 0.48 mmol, 2 eq.) were taken in a 15 mL reaction vessel containing THF:water (9:1) (5 mL). Subsequently, reaction mixture was purged with argon for 15 min, vessel was then sealed and heated for 12 h. Upon completion, the vessel was cooled, and solvent volume was reduced under vacuum and extracted with water (30 mL) and ethyl acetate (20 mL X 2). Organic layers were combined, dried over sodium sulfate and concentrated to result in a crude mass. A quick column chromatography was performed and the fractions containing the desired product were concentrated. The obtained crude product was then dissolved in DCM (5 mL) and cooled to 0° C. Boron trichloride (BCl<sub>3</sub>) solution (0.72 mL of 1M DCM solution, 0.72 mmol, 3 eq.) was then added slowly and the reaction was stirred for 30 min, before quenching with water (10 mL). The resulting reaction mixture was then extracted with DCM (20 mL X 2). The collected DCM fractions were washed with water (30 mL) and dried over sodium sulfate. Purification of the residue obtained from evaporating organic fraction afforded **44** (35 mg, 44%) as white solid. <sup>1</sup>H NMR (500 MHz, Chloroform-*d*) δ 7.29 – 7.04 (m, 10H), 6.70 (d, *J* = 8.2 Hz, 1H), 6.27 (s, 1H), 4.92 (s, 2H), 4.67 (s, 2H), 3.94 (s, 2H). <sup>13</sup>C NMR (126 MHz, CDCl<sub>3</sub>) δ 170.5, 155.9, 139.6, 136.5,

136.3, 130.0, 128.8 (2), 128.6 (2), 128.2, 127.8, 127.5, 127.4, 127.1, 126.4, 122.9, 122.3, 115.5, 55.2, 52.6, 36.0. HRMS (ESI)  $m/z$  [M+H] calculated for C<sub>22</sub>H<sub>20</sub>NO<sub>2</sub>, 330.1488, found 330.1493.

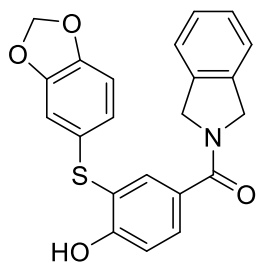


**(6-hydroxy-[1,1'-biphenyl]-3-yl)(isoindolin-2-yl)methanone (45):** (3-bromo-4-hydroxyphenyl)(isoindolin-2-yl)methanone (**8**) (50 mg, 0.158 mmol, 1 eq.) was suspended in water (3 mL). Subsequently, *N,N*-diisopropylethylamine (0.08 mL, 0.48 mmol, 3 eq.) and Pd(OAc)<sub>2</sub> (3 mg, 0.013 mmol) were added, the reaction vessel was sealed and heated to 100° C for 1 h. After cooling to rt, the reaction mixture was extracted with ethyl acetate (20 mL). Organic fraction was dried over sodium sulfate and concentrated to result in a residue that was purified using flash chromatography (SiO<sub>2</sub>, 2:8 ethyl acetate:hexanes) to afford **45** (33 mg, 33%) as white solid. <sup>1</sup>H NMR (400 MHz, Chloroform-*d*) δ 7.58 – 7.51 (m, 6H), 7.49 – 7.40 (m, 1H), 7.39 – 7.29 (m, 3H), 7.20 (d, *J* = 7.3 Hz, 1H), 7.12 – 7.03 (m, 1H), 5.05 (s, 2H), 4.90 (s, 2H). <sup>13</sup>C NMR (101 MHz, CDCl<sub>3</sub>) δ 170.0, 154.1, 136.9, 136.5, 136.4, 136.1, 129.6, 129.4 (2), 129.1, 129.0 (2), 128.4, 128.3, 128.1, 127.5, 122.9, 122.4, 115.8, 55.2, 52.6. HRMS (ESI)  $m/z$  [M+H] calculated for C<sub>21</sub>H<sub>18</sub>NO<sub>2</sub>, 316.1332, found 316.1354.

## General procedure A

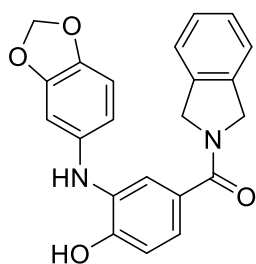


The intermediate **29** (100 mg, 0.24 mmol, 1 eq.) was added to a reaction vessel containing palladium acetate (3 mg, 0.012 mmol) and 1,1'-Bis(diphenylphosphino)ferrocene (dppf) (13 mg, 0.024 mmol), sodium tert-butoxide (95 mg, 1 mmol, 3 eq), and the desired thiol/aniline (0.29 mmol, 1.2 eq.) suspended and/or dissolved in toluene (3 mL). The reaction mixture was purged with argon, sealed and heated to 130° C for 6 h. Subsequently, solvent was removed under vacuum and water (20 mL) was added to the remaining mass and extracted with ethyl acetate (30 mL X 2). Organic fractions were then collected, dried and concentrated to a residue mass that was passed through a pad of silica (3:7 ethyl acetate:hexanes) to result in a crude product which was dissolved in 5 mL DCM, cooled to 0° C, and subjected to BCl<sub>3</sub> (0.72 mL 1M DCM solution, 0.72 mmol, 3 eq.) via slow addition. Upon quenching with water and removal of DCM under vacuum, the remaining reaction mixture was extracted with ethyl acetate (20 mL X 2). Organic fractions were combined, dried and evaporated to a residue which was purified via a flash chromatography (SiO<sub>2</sub>, 3:7 ethyl acetate:hexanes) to furnish the desired products.



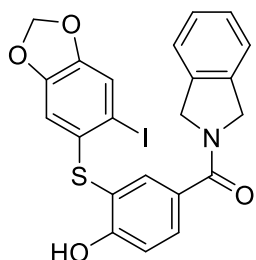
**(3-(benzo[d][1,3]dioxol-5-ylthio)-4-hydroxyphenyl)(isoindolin-2-yl)methanone (46):**

Prepared using general procedure A; 42 mg, Yield 45%, white solid.  $^1\text{H}$  NMR (500 MHz, Chloroform-*d*)  $\delta$  7.74 (d,  $J = 2.1$  Hz, 1H), 7.58 (dd,  $J = 8.4, 2.2$  Hz, 1H), 7.37-7.24 (m, 3H), 7.17 (d,  $J = 7.4$  Hz, 1H), 7.08 (d,  $J = 8.4$  Hz, 1H), 6.81 (dd,  $J = 8.1, 1.9$  Hz, 1H), 6.77 – 6.67 (m, 2H), 5.95 (s, 2H), 5.00 (s, 2H), 4.80 (s, 2H).  $^{13}\text{C}$  NMR (126 MHz,  $\text{CDCl}_3$ )  $\delta$  169.1, 148.5, 147.5, 136.3, 134.6, 130.7, 129.3, 127.8, 127.5, 126.5, 123.3, 122.9, 122.4, 119.3, 115.4, 115.4, 110.1, 109.0, 101.5, 101.4, 55.1, 52.6. HRMS (ESI)  $m/z$   $[\text{M}+\text{H}]$  calculated for  $\text{C}_{22}\text{H}_{18}\text{NO}_4\text{S}$ , 392.0937, found 392.0937.



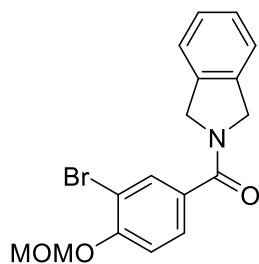
**(3-(benzo[d][1,3]dioxol-5-ylamino)-4-hydroxyphenyl)(isoindolin-2-yl)methanone (47):**

Prepared using general procedure A; 36 mg, Yield 40%, beige solid.  $^1\text{H}$  NMR (500 MHz, Chloroform-*d*)  $\delta$  7.31 – 7.19 (m, 4H), 7.12 (d,  $J = 7.3$  Hz, 1H), 6.94 – 6.87 (m, 1H), 6.81 (dd,  $J = 8.1, 2.3$  Hz, 1H), 6.73 – 6.62 (m, 2H), 6.54 (dt,  $J = 8.2, 2.2$  Hz, 1H), 5.88 (d,  $J = 2.2$  Hz, 2H), 4.92 (s, 2H), 4.76 (s, 2H).  $^{13}\text{C}$  NMR (126 MHz,  $\text{CDCl}_3$ )  $\delta$  171.2, 148.2, 147.5, 142.9, 137.0, 136.4, 136.1, 133.1, 127.7, 127.7, 127.4, 122.8, 122.3, 119.2, 114.2, 113.7, 113.0, 108.5, 102.6, 101.0, 55.2, 52.5. HRMS (ESI)  $m/z$   $[\text{M}+\text{H}]$  calculated for  $\text{C}_{22}\text{H}_{19}\text{N}_2\text{O}_4$ , 375.13339, found 375.1327.



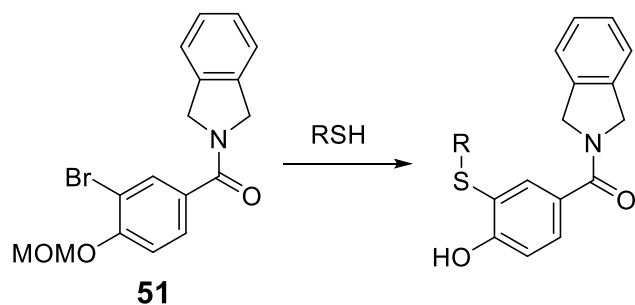
**(4-hydroxy-3-((6-iodobenzo[d][1,3]dioxol-5-yl)thio)phenyl)(isoindolin-2-yl)methanone (48):**

(3-(benzo[d][1,3]dioxol-5-ylthio)-4-(benzyloxy)phenyl)(isoindolin-2-yl)methanone (50 mg, 0.1 mmol, 1 eq.) obtained during the preparation of **46**, was dissolved in trifluoroacetic acid (TFA): acetonitrile (1:9) (3 mL) along with *N*-iodosuccinimide (25 mg, 0.11 mmol, 1.1 eq.) and the reaction was stirred at rt for 12 h. The reaction was then separated between water (50 mL) and ethyl acetate (50 mL), organic layer was washed with water, dried over sodium sulfate and concentrated to give a crude mass that was quickly passed through a pad of silica (5:5 ethyl acetate: hexanes). The fractions were evaporated to a mass that was dissolved in DCM (3 mL) and cooled to 0° C. BCl<sub>3</sub> was then added slowly to the solution and stirred at 0°C for 1 h. Reaction mixture quenched with water (10 mL) and evaporated under vacuum to remove DCM. After extraction with Ethyl acetate (20 mL X 2), the organic fractions were collected, dried and evaporated to give a crude mass. The resulting mass was purified with flash chromatography to furnish **48** (11 mg, 21%) as off white solid. <sup>1</sup>H NMR (400 MHz, Chloroform-*d*) δ 7.72 (d, *J* = 2.2 Hz, 1H), 7.60 (dd, *J* = 8.4, 2.1 Hz, 1H), 7.32 – 7.21 (m, 3H), 7.17 (s, 1H), 7.09 (dd, *J* = 17.0, 7.9 Hz, 2H), 6.55 (s, 1H), 6.30 (s, 1H), 5.86 (s, 2H), 4.94 (s, 2H), 4.76 (s, 2H). <sup>13</sup>C NMR (101 MHz, CDCl<sub>3</sub>) δ 158.3, 149.4, 147.7, 136.3, 136.3, 135.3, 131.7, 129.8, 127.9, 127.5, 122.9, 122.4, 118.9, 118.4, 115.9, 108.7, 106.8, 102.0, 99.9, 86.5, 55.2, 52.7. HRMS (ESI) *m/z* [M+H] calculated for C<sub>22</sub>H<sub>17</sub>INO<sub>4</sub>S, 517.9917, found 517.9891.



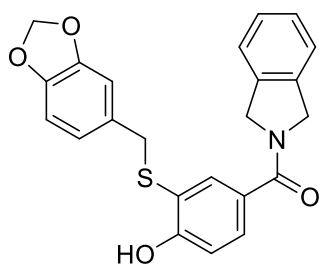
**(3-bromo-4-(methoxymethoxy)phenyl)(isoindolin-2-yl)methanone (51):** To a solution of **8** (2 g, 6.3 mmol, 1 eq.) and *N,N*-diisopropylethylamine (DIPEA)(2.3 mL, 12.6 mmol, 2 eq.) in DCM (30 mL) was introduced chloromethyl methyl ether (1.5 mL 5M solution in THF, 7.56 mmol, 1.2 eq.) at 0°C. After stirring at 0° C for 1 h, the reaction was slowly quenched with sat. sodium bicarbonate solution (10 mL) and extracted with DCM (20 mL X 2). DCM fractions were combined, washed with water, dried over sodium sulfate and evaporated to give a residue that was purified using flash chromatography to afford **51** (2.1 g, 92%) as white solid. <sup>1</sup>H NMR (500 MHz, Chloroform-*d*) δ 7.84 (d, *J* = 2.1 Hz, 1H), 7.53 (dd, *J* = 8.5, 2.1 Hz, 1H), 7.38 – 7.28 (m, 3H), 7.21 (dd, *J* = 17.0, 8.0 Hz, 2H), 5.32 (s, 2H), 5.02 (s, 2H), 4.84 (s, 2H), 3.56 (s, 3H). <sup>13</sup>C NMR (126 MHz, CDCl<sub>3</sub>) δ 168.5, 155.1, 136.3, 136.2, 132.4, 131.2, 127.9, 127.6, 127.6, 122.9, 122.4, 115.3, 112.6, 94.9, 56.5, 55.1, 52.6. HRMS (ESI) *m/z* [M+H] calculated for C<sub>17</sub>H<sub>17</sub>BrNO<sub>3</sub>, 362.0386, found 346.1404.

### General procedure B



In a reaction vessel containing **51** (50 mg, 0.136 mmol, 1 eq), palladium acetate (2 mg, 0.008 mmol) and 1,1'-Bis(diphenylphosphino)ferrocene (dppf) (8 mg, 0.016 mmol), sodium tert-butoxide (48 mg, 0.5 mmol, 3 eq), and the desired thiol (RSH) (0.16 mmol, 1.2 eq.) suspended and/or dissolved in toluene (3 mL). The reaction mixture was purged with argon, sealed and heated to 130° C for 6 h. Subsequently, solvent was removed under vacuum and water (20 mL) was added

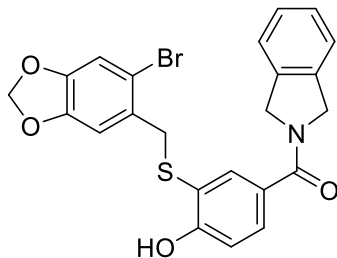
to the remaining mass and extracted with ethyl acetate (30 mL X 2). Organic fractions were then collected, dried and concentrated to a residue mass that was passed through a pad of silica (3:7 ethyl acetate:hexanes) to result in a crude product. The obtained mass was dissolved in methanol (5 mL), the solution was acidified to pH 3 with 2 N HCl solution and stirred for 4 h at 45° C. Upon completion, the methanol was removed under vacuum and the remaining mass was extracted with water (10 mL) and ethyl acetate (20 mL X 2). After combining and drying the organic layer, a flash chromatography (4:6 ethyl acetate: hexanes) was performed to afford the desired monophenols.



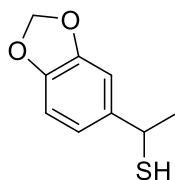
**(3-((benzo[d][1,3]dioxol-5-ylmethyl)thio)-4-hydroxyphenyl)(isoindolin-2-yl)methanone (49):**

Prepared using general procedure B; 39 mg, Yield 72 %, off white solid. <sup>1</sup>H NMR (500 MHz, Chloroform-*d*) δ 7.64 – 7.49 (m, 2H), 7.37 – 7.29 (m, 3H), 7.21 (d, *J* = 7.3 Hz, 1H), 7.03 (d, *J* = 8.4 Hz, 1H), 6.84 (s, 1H), 6.73 – 6.62 (m, 2H), 6.54 (dd, *J* = 7.9, 1.7 Hz, 1H), 5.90 (s, 2H), 5.01 (s, 2H), 4.72 (s, 2H), 3.83 (s, 2H). <sup>13</sup>C NMR (126 MHz, CDCl<sub>3</sub>) δ 169.2, 158.6, 147.8, 147.0, 136.4, 136.3, 135.5, 130.9, 130.8, 129.0, 127.8, 127.5, 122.9, 122.4, 122.2, 118.3, 114.8, 109.0, 108.2, 101.1, 55.0, 52.6, 41.1. HRMS (ESI) *m/z* [M+H] calculated for C<sub>23</sub>H<sub>20</sub>NO<sub>4</sub>S, 406.1107, found 406.1091.



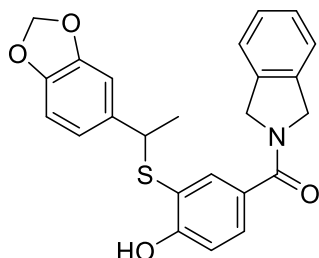


**(3-(((6-bromobenzo[d][1,3]dioxol-5-yl)methyl)thio)-4-hydroxyphenyl)(isoindolin-2-yl)methanone (50):** Prepared using general procedure B; 42 mg, Yield 65 %, off white solid.  $^1\text{H}$  NMR (400 MHz, Chloroform-*d*)  $\delta$  7.64 (d,  $J = 2.2$  Hz, 1H), 7.57 (dd,  $J = 8.4, 2.2$  Hz, 1H), 7.38 – 7.29 (m, 3H), 7.21 (d,  $J = 7.2$  Hz, 1H), 7.06 – 6.97 (m, 3H), 6.49 (s, 1H), 5.92 (s, 2H), 5.02 (s, 2H), 4.78 (s, 2H), 3.97 (s, 2H).  $^{13}\text{C}$  NMR (101 MHz,  $\text{CDCl}_3$ )  $\delta$  169.1, 158.9, 148.0, 147.3, 136.4, 136.3, 135.8, 130.9, 129.2, 129.1, 127.8, 127.5, 122.9, 122.4, 118.0, 115.0, 114.8, 113.0, 110.4, 101.9, 55.1, 52.6, 41.5. HRMS (ESI)  $m/z$   $[\text{M}+\text{H}]$  calculated for  $\text{C}_{23}\text{H}_{19}\text{BrNO}_4\text{S}$ , 486.0194, found 488.0156.



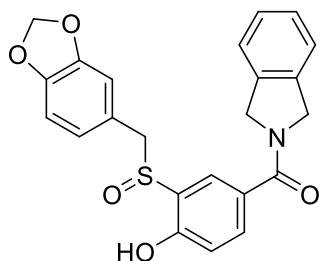
**1-(benzo[d][1,3]dioxol-5-yl)ethane-1-thiol (60):** To solution of 1-(benzo[d][1,3]dioxol-5-yl)ethan-1-ol (**59**) (1 g, 6 mmol, 1 eq.) in toluene (20 mL) was added Lawessons reagent (2.6 g, 6.6 mmol, 1.1 eq.) and the reaction mixture was stirred at 80 °C. Water (10 mL) was added, and the resulting mixture was cooled to room temperature. The organic layer was separated and sequentially washed with saturated sodium bicarbonate solution (10 mL) and brine (100 mL). The organic layer was dried over sodium sulfate and evaporated. The resulting oil was purified by silica gel chromatography ( $\text{SiO}_2$ , 1:9 ethyl acetate:hexanes), which afforded **60** (0.45 g, 44%) as colorless oil.  $^1\text{H}$  NMR (500 MHz, Chloroform-*d*)  $\delta$  6.90 (d,  $J = 1.9$  Hz, 1H), 6.82 – 6.79 (m, 1H),

6.74 (d,  $J = 8.0$  Hz, 1H), 5.95 (s, 2H), 4.19 (qd,  $J = 6.9, 4.8$  Hz, 1H), 1.99 (d,  $J = 4.9$  Hz, 1H), 1.64 (dd,  $J = 6.9, 0.5$  Hz, 3H).  $^{13}\text{C}$  NMR (126 MHz,  $\text{CDCl}_3$ )  $\delta$  147.8, 146.5, 139.8, 119.4, 108.1, 106.9, 101.0, 38.7, 26.3. HRMS (ESI)  $m/z$   $[\text{M}+\text{H}]$  calculated for  $\text{C}_9\text{H}_{11}\text{O}_2\text{S}$ , 183.0474, found 183.0495.



**(3-((1-(benzo[d][1,3]dioxol-5-yl)ethyl)thio)-4-hydroxyphenyl)(isoindolin-2-yl)methanone**

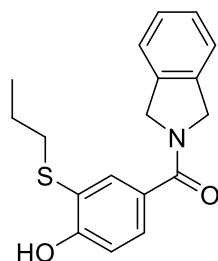
**(54):** Prepared using general procedure B; 38 mg, Yield 68 %, off white solid.  $^1\text{H}$  NMR (500 MHz, Chloroform- $d$ )  $\delta$  7.57 – 7.49 (m, 2H), 7.37 – 7.28 (m, 3H), 7.20 (d,  $J = 7.3$  Hz, 1H), 7.03 – 6.99 (m, 1H), 6.92 (s, 1H), 6.76 (d,  $J = 1.8$  Hz, 1H), 6.69 (d,  $J = 8.0$  Hz, 1H), 6.61 (dd,  $J = 8.0, 1.9$  Hz, 1H), 5.89 (q,  $J = 1.4$  Hz, 2H), 5.05 – 4.96 (m, 2H), 4.71 (s, 2H), 4.10 (q,  $J = 7.0$  Hz, 1H), 1.62 (d,  $J = 7.1$  Hz, 3H).  $^{13}\text{C}$  NMR (126 MHz,  $\text{CDCl}_3$ )  $\delta$  169.2, 158.9, 147.8, 147.0, 136.4, 136.3, 136.1, 135.9, 130.9, 128.8, 127.8, 127.5, 122.9, 122.4, 120.5, 118.2, 114.7, 108.1, 107.2, 101.1, 55.0, 52.6, 49.3, 21.8. HRMS (ESI)  $m/z$   $[\text{M}+\text{H}]$  calculated for  $\text{C}_{24}\text{H}_{22}\text{NO}_4\text{S}$ , 420.1264, found 420.1240.



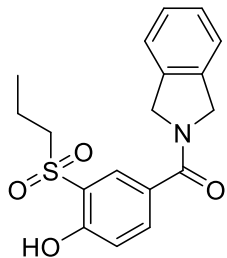
**(3-((benzo[d][1,3]dioxol-5-ylmethyl)sulfinyl)-4-hydroxyphenyl)(isoindolin-2-yl)methanone**

**(55):** To solution of (3-((benzo[d][1,3]dioxol-5-ylmethyl)thio)-4-hydroxyphenyl)(isoindolin-2-yl)methanone (**49**) (25 mg, 0.06 mmol, 1 eq.) in DCM (2 mL) was added *m*-chloroperbenzoic acid

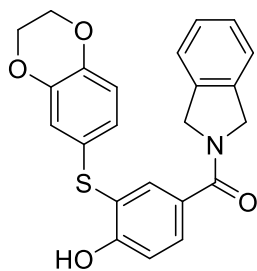
(*m*-CPBA) (32 mg, 0.18 mmol, 3 eq.) at 0°C, allowed to warm to rt and stirred for 1 h. The solvent was removed under vacuum, and water (5 mL) was added. The resulting mixture was extracted with DCM (10 mL X 2) and the combined organic phases were dried over anhydrous sodium sulfate and filtered. Evaporation of the solvent in vacuo followed by flash column chromatography (SiO<sub>2</sub>, 1:3 ethyl acetate:hexanes) afforded **55** (12 mg, 47 %) as off white solid. <sup>1</sup>H NMR (400 MHz, Chloroform-*d*) δ 8.89 (s, 1H), 7.85 – 7.70 (m, 2H), 7.38 – 7.28 (m, 4H), 7.20 (d, *J* = 7.2 Hz, 1H), 7.03 (d, *J* = 8.6 Hz, 1H), 6.73 (d, *J* = 7.9 Hz, 1H), 6.65 (d, *J* = 1.8 Hz, 1H), 6.56 (dd, *J* = 8.0, 1.8 Hz, 1H), 5.95 (s, 2H), 5.01 (s, 2H), 4.73 (s, 2H), 4.31 (s, 2H). <sup>13</sup>C NMR (101 MHz, CDCl<sub>3</sub>) δ 158.1, 150.9, 148.7, 135.9, 132.1, 128.9, 127.9, 127.7, 124.9, 122.9, 122.9, 122.5, 119.9, 118.9, 118.0, 110.8, 108.6, 102.8, 101.5, 99.9, 63.0, 54.9, 52.8. HRMS (ESI) *m/z* [M+H] calculated for C<sub>23</sub>H<sub>20</sub>NO<sub>5</sub>S, 422.1056, found 422.1065.



**(4-hydroxy-3-(propylthio)phenyl)(isoindolin-2-yl)methanone (56):** Prepared using general procedure B ; 23 mg, Yield 54 %, white solid. <sup>1</sup>H NMR (500 MHz, Chloroform-*d*) δ 7.77 (d, *J* = 2.2 Hz, 1H), 7.53 (dd, *J* = 8.4, 2.2 Hz, 1H), 7.38 – 7.27 (m, 3H), 7.19 (s, 1H), 7.06 (d, *J* = 8.4 Hz, 1H), 5.02 (s, 2H), 4.84 (s, 2H), 2.77 – 2.65 (m, 2H), 1.60 (h, *J* = 7.4 Hz, 2H), 1.00 (t, *J* = 7.3 Hz, 3H). <sup>13</sup>C NMR (126 MHz, CDCl<sub>3</sub>) δ 169.4, 158.4, 135.0 (2), 130.1 (2), 129.0, 127.8, 127.5, 122.9, 122.4, 119.6, 114.6, 55.1, 52.7, 38.7, 23.0, 13.2. HRMS (ESI) *m/z* [M+H] calculated for C<sub>18</sub>H<sub>20</sub>NO<sub>2</sub>S, 314.1209, found 314.1218.



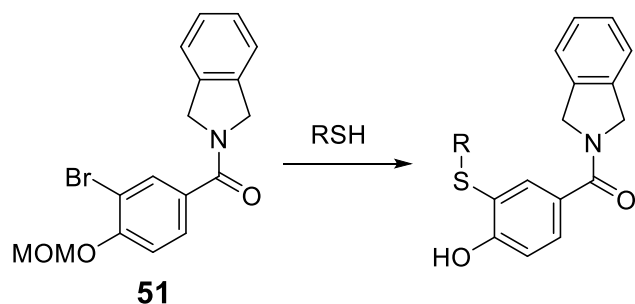
**(4-hydroxy-3-(propylsulfonyl)phenyl)(isoindolin-2-yl)methanone (57):** To solution of (4-hydroxy-3-(propylthio)phenyl)(isoindolin-2-yl)methanone (**56**) (25 mg, 0.08 mmol, 1 eq.) in DCM (2 mL) was added *m*-chloroperbenzoic acid (*m*-CPBA) (41 mg, 0.24 mmol, 3 eq.) at 0° C, allowed to warm to rt and stirred for 1 h. The solvent was removed under vacuum, and water (5 mL) was added. The resulting mixture was extracted with DCM (10 mL X 2) and the combined organic phases were dried over anhydrous sodium sulfate and filtered. Evaporation of the solvent in vacuo followed by flash column chromatography (SiO<sub>2</sub>, 1:3 ethyl acetate:hexanes) afforded **57** (8 mg, 30 %) as off white solid. <sup>1</sup>H NMR (500 MHz, Chloroform-*d*) δ 9.28 (s, 1H), 7.94 (d, *J* = 2.2 Hz, 1H), 7.82 (dd, *J* = 8.6, 2.2 Hz, 1H), 7.38 – 7.28 (m, 3H), 7.20 (d, *J* = 7.4 Hz, 1H), 7.14 (d, *J* = 8.6 Hz, 1H), 5.03 (s, 2H), 4.84 (s, 2H), 3.24 – 3.10 (m, 2H), 1.91 – 1.67 (m, 2H), 1.05 (t, *J* = 7.4 Hz, 3H). <sup>13</sup>C NMR (126 MHz, CDCl<sub>3</sub>) δ 168.0, 157.8, 135.9, 135.5 (2), 128.6 (2), 128.0, 127.7, 122.9, 122.5, 119.4, 119.3, 58.7, 55.1, 52.8, 16.2, 12.8. HRMS (ESI) *m/z* [M+H] calculated for C<sub>18</sub>H<sub>20</sub>NO<sub>4</sub>S, 346.1107, found 346.1116.



**(3-((2,3-dihydrobenzo[b][1,4]dioxin-6-yl)thio)-4-hydroxyphenyl)(isoindolin-2-yl)methanone**

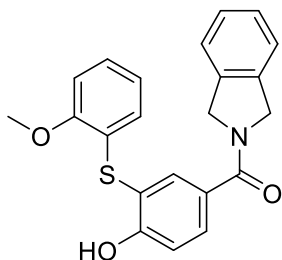
**(58):** Prepared using general procedure B ; 25 mg, Yield 45 %, white solid. <sup>1</sup>H NMR (500 MHz, Chloroform-*d*) δ 7.80 (d, *J* = 2.1 Hz, 1H), 7.62 (dd, *J* = 8.4, 2.2 Hz, 1H), 7.40 – 7.28 (m, 3H), 7.19 (d, *J* = 7.4 Hz, 1H), 7.11 (d, *J* = 8.4 Hz, 1H), 6.82 – 6.72 (m, 4H), 5.02 (s, 2H), 4.83 (s, 2H), 4.24 (s, 4H). <sup>13</sup>C NMR (126 MHz, CDCl<sub>3</sub>) δ 158.1, 143.2, 136.4, 135.2, 130.9, 129.4, 127.8, 127.5, 126.1, 122.9, 122.4, 122.3, 120.7, 118.7, 118.2, 117.9, 117.1, 116.9, 115.5, 64.3 (2), 64.3 (2). HRMS (ESI) *m/z* [M+H] calculated for C<sub>23</sub>H<sub>20</sub>NO<sub>4</sub>S, 406.1107, found 406.1115.

**General procedure C**

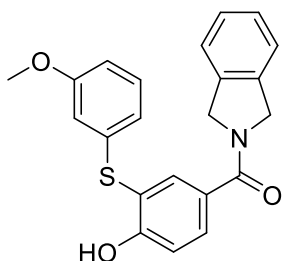


In a reaction vessel containing **51** (50 mg, 0.136 mmol, 1 eq), (dibenzylideneacetone)palladium(0) (Pd(dba)<sub>2</sub>) (5 mg, 0.008 mmol) and 2-dicyclohexylphosphino-2',4',6'-triisopropylbiphenyl (XPhos) (8 mg, 0.016 mmol), sodium tert-butoxide (48 mg, 0.5 mmol, 3 eq), and the desired thiol (RSH) (0.16 mmol, 1.2 eq.) suspended and/or dissolved in toluene (3 mL). The reaction mixture was purged with argon, sealed and heated to 130° C for 6 h. Subsequently, solvent was removed under vacuum and water (20 mL) was added to the remaining mass and extracted with ethyl acetate (30 mL X 2). Organic fractions were then collected, dried and concentrated to a residue mass that was passed through a pad of silica (3:7 ethyl acetate:hexanes) to result in a crude product. The obtained mass was dissolved in methanol (5 mL), the solution was acidified to pH 3 with 2 N HCl solution and stirred for 4 h at 45° C. Upon completion, the methanol was removed under vacuum

and the remaining mass was extracted with water (10 mL) and ethyl acetate (20 mL X 2). After combining and drying the organic layer, a flash chromatography (4:6 ethyl acetate: hexanes) was performed to afford the desired monophenols.

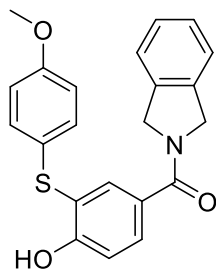


**(4-hydroxy-3-((2-methoxyphenyl)thio)phenyl)(isoindolin-2-yl)methanone (61a):** Prepared using general procedure C; white solid, 19 mg, Yield 37 %.  $^1\text{H}$  NMR (400 MHz, Chloroform-*d*)  $\delta$  7.87 (d,  $J = 2.2$  Hz, 1H), 7.62 (dd,  $J = 8.5, 2.2$  Hz, 1H), 7.38 – 7.24 (m, 4H), 7.18 (d,  $J = 7.2$  Hz, 1H), 7.14 – 7.08 (m, 2H), 6.95 – 6.83 (m, 2H), 5.02 (s, 2H), 4.84 (s, 2H), 3.96 (s, 3H).  $^{13}\text{C}$  NMR (101 MHz,  $\text{CDCl}_3$ )  $\delta$  169.1, 159.1, 157.0, 136.4, 136.3, 135.9, 131.2, 131.2, 129.2, 129.0, 127.8, 127.5, 122.9, 122.8, 122.4, 121.7, 117.7, 115.5, 110.9, 55.9, 55.1, 52.7. HRMS (ESI)  $m/z$  [M+H] calculated for  $\text{C}_{22}\text{H}_{20}\text{NO}_3\text{S}$ , 378.1158, found 378.1165.

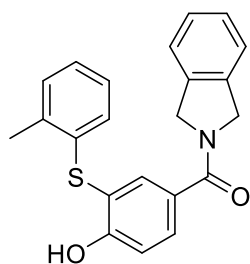


**(4-hydroxy-3-((3-methoxyphenyl)thio)phenyl)(isoindolin-2-yl)methanone (61b):** Prepared using general procedure C; white solid, 22 mg, Yield 44 %.  $^1\text{H}$  NMR (400 MHz, Chloroform-*d*)  $\delta$  7.75 (d,  $J = 2.2$  Hz, 1H), 7.59 (dd,  $J = 8.4, 2.2$  Hz, 1H), 7.30 – 7.20 (m, 4H), 7.13 – 7.04 (m, 2H), 6.70 – 6.57 (m, 3H), 4.93 (s, 2H), 4.75 (s, 2H), 3.68 (s, 3H).  $^{13}\text{C}$  NMR (101 MHz,  $\text{CDCl}_3$ )  $\delta$  200.3,

190.0, 187.1, 187.0, 184.0, 174.9, 174.5, 170.1, 169.7, 168.9, 166.7, 166.5, 164.9, 164.8, 164.7, 162.4, 161.3, 157.7, 132.3, 67.5, 53.1, 52.3. HRMS (ESI)  $m/z$  [M+H] calculated for C<sub>22</sub>H<sub>20</sub>NO<sub>3</sub>S, 378.1158, found 378.1166.

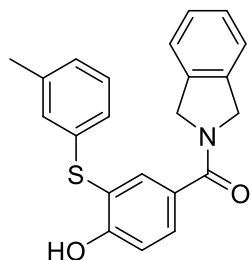


**(4-hydroxy-3-((4-methoxyphenyl)thio)phenyl)(isoindolin-2-yl)methanone (61c):** Prepared using general procedure C; white solid, 20 mg, yield 40 %. <sup>1</sup>H NMR (500 MHz, Chloroform-*d*)  $\delta$  7.53 – 7.44 (m, 2H), 7.35 (dd,  $J$  = 8.4, 2.1 Hz, 1H), 7.32 – 7.28 (m, 3H), 7.26 (dd,  $J$  = 6.4, 2.4 Hz, 1H), 7.14 (t,  $J$  = 8.1 Hz, 2H), 6.99 (d,  $J$  = 2.1 Hz, 1H), 6.96 – 6.90 (m, 2H), 4.93 (s, 2H), 4.60 (d,  $J$  = 1.6 Hz, 2H), 3.81 (s, 3H). <sup>13</sup>C NMR (126 MHz, CDCl<sub>3</sub>)  $\delta$  169.4, 160.3, 154.3, 136.6 (2), 136.5, 136.3, 130.5, 129.3, 127.7, 127.4, 126.4, 125.7, 122.9, 122.2, 115.3 (2), 113.9, 94.8, 56.4, 54.9, 52.5. HRMS (ESI)  $m/z$  [M+H] calculated for C<sub>22</sub>H<sub>20</sub>NO<sub>3</sub>S, 378.1158, found 378.1156.

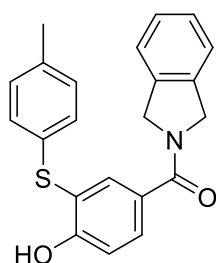


**(4-hydroxy-3-(o-tolylthio)phenyl)(isoindolin-2-yl)methanone (61d) :** Prepared using general procedure B; white solid, 30 mg, Yield 62%. <sup>1</sup>H NMR (500 MHz, Chloroform-*d*)  $\delta$  7.77 (d,  $J$  = 2.1 Hz, 1H), 7.68 (dd,  $J$  = 8.5, 2.2 Hz, 1H), 7.38 – 7.28 (m, 3H), 7.23 – 7.05 (m, 5H), 6.80 (dd,  $J$  = 7.8, 1.3 Hz, 1H), 6.68 (s, 1H), 5.02 (s, 2H), 4.82 (s, 2H), 2.48 (s, 3H). <sup>13</sup>C NMR (126 MHz,

$\text{CDCl}_3$ )  $\delta$  168.9, 158.5, 136.4, 136.2, 136.1, 135.6, 134.0, 131.3, 130.5, 129.7, 127.8, 127.5, 126.9, 126.7, 126.5, 122.9, 122.4, 116.7, 115.6, 55.1, 52.7, 20.2. HRMS (ESI)  $m/z$  [M+H] calculated for  $\text{C}_{22}\text{H}_{20}\text{NO}_2\text{S}$ , 362.1209, found 362.1208.



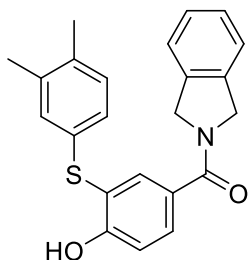
**(4-hydroxy-3-(m-tolylthio)phenyl)(isoindolin-2-yl)methanone (61e):** Prepared using general procedure B; white solid, 28 mg, Yield 58%.  $^1\text{H}$  NMR (500 MHz, Chloroform-*d*)  $\delta$  7.74 (d,  $J$  = 2.1 Hz, 1H), 7.58 (dd,  $J$  = 8.4, 2.2 Hz, 1H), 7.29 – 7.19 (m, 4H), 7.12 – 7.04 (m, 3H), 6.95 – 6.89 (m, 2H), 6.88 – 6.84 (m, 1H), 6.68 (s, 1H), 4.93 (s, 2H), 4.75 (s, 2H), 2.21 (d,  $J$  = 0.7 Hz, 3H).  $^{13}\text{C}$  NMR (126 MHz,  $\text{CDCl}_3$ )  $\delta$  169.0, 158.5, 139.3, 136.4, 136.3, 135.7, 134.6, 131.4, 129.5, 129.2, 128.2, 127.8, 127.6, 127.5, 124.7, 122.9, 122.4, 117.2, 115.6, 55.1, 52.7, 21.4. HRMS (ESI)  $m/z$  [M+H] calculated for  $\text{C}_{22}\text{H}_{20}\text{NO}_2\text{S}$ , 362.1209, found 362.1213.



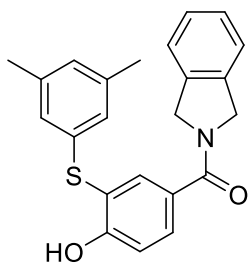
**(4-hydroxy-3-(p-tolylthio)phenyl)(isoindolin-2-yl)methanone (61f):** Prepared using general procedure B; white solid, 31 mg, Yield 63%.  $^1\text{H}$  NMR (500 MHz, Chloroform-*d*)  $\delta$  7.82 (d,  $J$  = 2.1 Hz, 1H), 7.64 (dd,  $J$  = 8.4, 2.2 Hz, 1H), 7.38 – 7.27 (m, 3H), 7.18 (d,  $J$  = 7.4 Hz, 1H), 7.13 (d,  $J$  = 8.4 Hz, 1H), 7.10 (s, 4H), 6.81 (s, 1H), 5.02 (s, 2H), 4.82 (s, 2H), 2.32 (s, 3H).  $^{13}\text{C}$  NMR (126



MHz, CDCl<sub>3</sub>)  $\delta$  169.0, 158.3, 136.9, 136.4, 136.3, 135.4, 131.1, 131.1, 130.1 (2), 129.4, 128.2 (2), 127.8, 127.5, 122.9, 122.4, 118.1, 115.5, 55.1, 52.7, 20.9. HRMS (ESI)  $m/z$  [M+H] calculated for C<sub>22</sub>H<sub>20</sub>NO<sub>2</sub>S, 362.1209, found 362.1223.

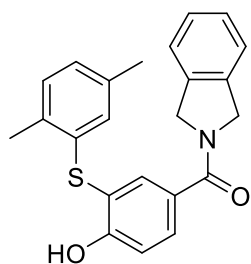


**(3-((3,4-dimethylphenyl)thio)-4-hydroxyphenyl)(isoindolin-2-yl)methanone (61g):** Prepared using general procedure B; white solid, 28 mg, Yield 55%. <sup>1</sup>H NMR (400 MHz, Chloroform-*d*)  $\delta$  7.73 (d,  $J$  = 2.1 Hz, 1H), 7.55 (dd,  $J$  = 8.4, 2.1 Hz, 1H), 7.29 – 7.19 (m, 3H), 7.09 (d,  $J$  = 7.3 Hz, 1H), 7.03 (d,  $J$  = 8.4 Hz, 1H), 6.98 – 6.89 (m, 2H), 6.84 (dd,  $J$  = 7.9, 2.1 Hz, 1H), 6.67 (s, 1H), 4.93 (s, 2H), 4.74 (s, 2H), 2.13 (d,  $J$  = 2.5 Hz, 6H). <sup>13</sup>C NMR (101 MHz, CDCl<sub>3</sub>)  $\delta$  169.1, 158.3, 137.9, 136.4, 136.3, 135.7, 135.3, 131.2, 131.0, 130.6, 129.5, 129.4, 127.8, 127.5, 125.9, 122.9, 122.4, 118.2, 115.5, 55.1, 52.7, 19.8, 19.3. HRMS (ESI)  $m/z$  [M+H] calculated for C<sub>23</sub>H<sub>22</sub>NO<sub>2</sub>S, 376.1365, found 376.1375.

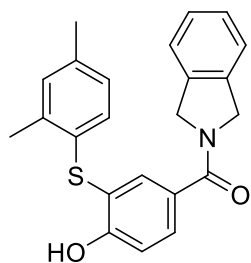


**(3-((3,5-dimethylphenyl)thio)-4-hydroxyphenyl)(isoindolin-2-yl)methanone (61h):** Prepared using general procedure B; white solid, 28 mg, Yield 55%. <sup>1</sup>H NMR (500 MHz, Chloroform-*d*)  $\delta$  7.73 (d,  $J$  = 2.1 Hz, 1H), 7.57 (dd,  $J$  = 8.4, 2.1 Hz, 1H), 7.28 – 7.19 (m, 3H), 7.07 (dd,  $J$  = 18.1,

7.9 Hz, 2H), 6.80 – 6.66 (m, 4H), 4.94 (s, 2H), 4.75 (s, 2H), 2.17 (d,  $J = 0.7$  Hz, 6H).  $^{13}\text{C}$  NMR (126 MHz,  $\text{CDCl}_3$ )  $\delta$  169.1, 158.5, 139.1, 136.4, 136.3, 135.6, 134.3, 131.4, 129.4, 128.7, 127.8, 127.5, 125.5, 125.4 (2), 122.9, 122.4, 117.4, 115.6, 55.1, 52.7, 21.2 (2). HRMS (ESI)  $m/z$  [ $\text{M}+\text{H}$ ] calculated for  $\text{C}_{23}\text{H}_{22}\text{NO}_2\text{S}$ , 376.1365, found 376.1352.

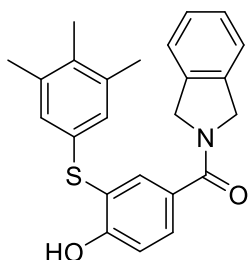


**(3-((2,5-dimethylphenyl)thio)-4-hydroxyphenyl)(isoindolin-2-yl)methanone (61i):** Prepared using general procedure B; white solid, 30 mg, Yield 59%.  $^1\text{H}$  NMR (400 MHz, Chloroform- $d$ )  $\delta$  7.76 (d,  $J = 2.2$  Hz, 1H), 7.68 (dd,  $J = 8.4, 2.1$  Hz, 1H), 7.38 – 7.29 (m, 3H), 7.17 (t,  $J = 7.5$  Hz, 2H), 7.10 (d,  $J = 7.6$  Hz, 1H), 6.99 – 6.88 (m, 1H), 6.63 (d,  $J = 1.9$  Hz, 2H), 5.03 (s, 2H), 4.82 (s, 2H), 2.43 (s, 3H), 2.21 (s, 3H).  $^{13}\text{C}$  NMR (101 MHz,  $\text{CDCl}_3$ )  $\delta$  169.1, 158.4, 136.7, 136.4, 136.3, 135.3, 133.5, 133.3, 131.2, 130.5, 129.6, 127.8, 127.5 (2), 127.5, 122.9, 122.4, 116.9, 115.6, 55.1, 52.7, 21.0, 19.7. HRMS (ESI)  $m/z$  [ $\text{M}+\text{H}$ ] calculated for  $\text{C}_{23}\text{H}_{22}\text{NO}_2\text{S}$ , 376.1365, found 376.1372.



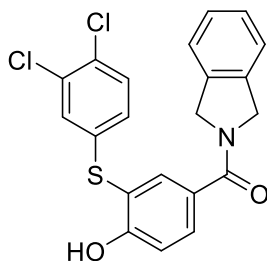
**(3-((2,4-dimethylphenyl)thio)-4-hydroxyphenyl)(isoindolin-2-yl)methanone (61j):** Prepared using general procedure B; white solid, 28 mg, Yield 56%.  $^1\text{H}$  NMR (400 MHz, Chloroform- $d$ )  $\delta$  7.70 (d,  $J = 2.2$  Hz, 1H), 7.62 (dd,  $J = 8.4, 2.2$  Hz, 1H), 7.36 – 7.28 (m, 3H), 7.16 (d,  $J = 7.3$  Hz,

1H), 7.11 (d,  $J = 8.4$  Hz, 1H), 7.05 – 7.01 (m, 1H), 6.89 (dd,  $J = 7.9, 1.9$  Hz, 1H), 6.78 (d,  $J = 8.0$  Hz, 1H), 5.00 (s, 2H), 4.79 (s, 2H), 2.42 (s, 3H), 2.28 (s, 3H).  $^{13}\text{C}$  NMR (101 MHz,  $\text{CDCl}_3$ )  $\delta$  169.0, 158.2, 136.8, 136.6, 136.4, 136.3, 134.9, 131.5, 130.8, 130.2, 129.5, 127.9, 127.8, 127.7, 127.5, 122.9, 122.4, 117.7, 115.5, 55.1, 52.7, 20.8, 20.2. HRMS (ESI)  $m/z$   $[\text{M}+\text{H}]$  calculated for  $\text{C}_{23}\text{H}_{22}\text{NO}_2\text{S}$ , 376.1365, found 376.1352.

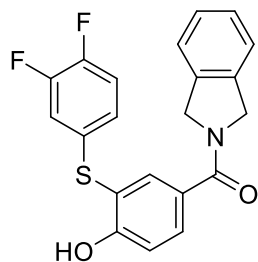


**(4-hydroxy-3-((3,4,5-trimethylphenyl)thio)phenyl)(isoindolin-2-yl)methanone (61k):**

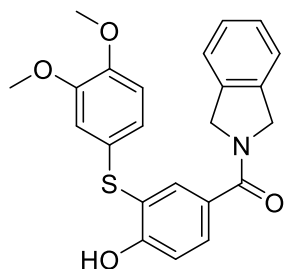
Prepared using general procedure B; white solid, 35 mg, Yield 67%.  $^1\text{H}$  NMR (400 MHz, Chloroform- $d$ )  $\delta$  7.82 (d,  $J = 2.1$  Hz, 1H), 7.63 (dd,  $J = 8.4, 2.1$  Hz, 1H), 7.32 (d,  $J = 25.2$  Hz, 3H), 7.18 (d,  $J = 7.3$  Hz, 1H), 7.12 (d,  $J = 8.4$  Hz, 1H), 6.88 (s, 2H), 6.80 (s, 1H), 5.03 (s, 2H), 4.84 (s, 2H), 2.23 (s, 6H), 2.13 (s, 3H).  $^{13}\text{C}$  NMR (101 MHz,  $\text{CDCl}_3$ )  $\delta$  169.1, 158.3, 137.8 (2), 136.4, 136.3, 135.3, 134.6, 134.4, 131.0, 130.3, 129.3, 127.8, 127.5 (2), 122.9, 122.4, 118.3, 115.5, 55.1, 52.7, 20.6 (2), 15.1. HRMS (ESI)  $m/z$   $[\text{M}+\text{H}]$  calculated for  $\text{C}_{24}\text{H}_{24}\text{NO}_2\text{S}$ , 390.1522, found 390.1529.



**(3-((3,4-dichlorophenyl)thio)-4-hydroxyphenyl)(isoindolin-2-yl)methanone (61l):** Prepared using general procedure B; white solid, 35 mg, Yield 63%. <sup>1</sup>H NMR (500 MHz, Chloroform-*d*) δ 7.72 (d, *J* = 2.0 Hz, 1H), 7.60 (dd, *J* = 8.5, 2.1 Hz, 1H), 7.29 – 7.19 (m, 4H), 7.14 – 7.05 (m, 3H), 6.88 (dd, *J* = 8.5, 2.2 Hz, 1H), 6.82 (s, 1H), 4.93 (s, 2H), 4.75 (s, 2H). <sup>13</sup>C NMR (126 MHz, CDCl<sub>3</sub>) δ 168.8, 158.6, 136.2, 136.1, 135.8, 135.4, 133.5, 131.9, 131.0, 130.8, 129.8, 128.7, 127.9, 127.6, 126.5, 122.9, 122.4, 116.1, 115.9, 55.1, 52.7. HRMS (ESI) *m/z* [M+H] calculated for C<sub>21</sub>H<sub>16</sub>Cl<sub>2</sub>NO<sub>2</sub>S, 416.0273, found 416.0254.

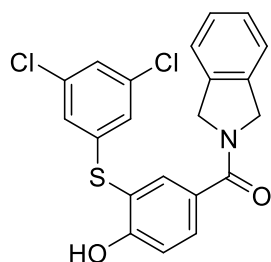


**(3-((3,4-difluorophenyl)thio)-4-hydroxyphenyl)(isoindolin-2-yl)methanone (61m):** Prepared using general procedure B; white solid, 28 mg, Yield 56%. <sup>1</sup>H NMR (500 MHz, Chloroform-*d*) δ 7.74 (d, *J* = 2.1 Hz, 1H), 7.60 (dd, *J* = 8.4, 2.2 Hz, 1H), 7.24 (dt, *J* = 18.2, 8.5 Hz, 3H), 7.09 (dd, *J* = 13.7, 7.9 Hz, 2H), 7.01 (dt, *J* = 9.9, 8.3 Hz, 1H), 6.87 (ddd, *J* = 10.4, 7.1, 2.3 Hz, 1H), 6.82 (dddd, *J* = 8.7, 3.9, 2.3, 1.5 Hz, 1H), 6.60 (s, 1H), 4.94 (s, 2H), 4.75 (s, 2H). <sup>13</sup>C NMR (126 MHz, CDCl<sub>3</sub>) δ 168.7, 158.4, 136.2, 136.2, 135.8, 131.8, 129.9, 127.9, 127.9, 127.6, 123.7 (dd, *J* = 6.4, 3.9 Hz), 122.9, 122.4, 118.3, 118.1, 116.8, 116.6, 116.6, 115.9, 55.1, 52.7. HRMS (ESI) *m/z* [M+H] calculated for C<sub>21</sub>H<sub>16</sub>F<sub>2</sub>NO<sub>2</sub>S, 384.0864, found 384.0871.

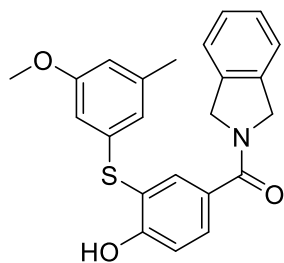


**(3-((3,4-dimethoxyphenyl)thio)-4-hydroxyphenyl)(isoindolin-2-yl)methanone (61n):**

Prepared using general procedure B; white solid, 33 mg, Yield 60%.  $^1\text{H}$  NMR (500 MHz, Chloroform-*d*)  $\delta$  7.68 (d,  $J$  = 2.2 Hz, 1H), 7.51 (dd,  $J$  = 8.4, 2.1 Hz, 1H), 7.28 – 7.17 (m, 3H), 7.08 (d,  $J$  = 7.4 Hz, 1H), 7.01 (d,  $J$  = 8.4 Hz, 1H), 6.79 – 6.66 (m, 3H), 4.92 (s, 2H), 4.71 (s, 2H), 3.76 (d,  $J$  = 12.3 Hz, 6H).  $^{13}\text{C}$  NMR (126 MHz,  $\text{CDCl}_3$ )  $\delta$  169.1, 157.9, 149.6, 148.8, 136.3, 136.2, 134.6, 130.7, 129.3, 127.8, 127.5, 125.2, 122.9, 122.4, 122.2, 119.4, 115.4, 112.8, 111.9, 56.0, 56.0, 55.1, 52.7. HRMS (ESI)  $m/z$   $[\text{M}+\text{H}]$  calculated for  $\text{C}_{23}\text{H}_{22}\text{NO}_4\text{S}$ , 408.1264, found 408.1268.

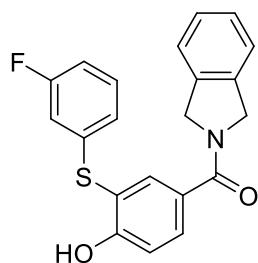


**(3-((3,5-dichlorophenyl)thio)-4-hydroxyphenyl)(isoindolin-2-yl)methanone (61o):** Prepared using general procedure B; white solid, 25 mg, Yield 45%.  $^1\text{H}$  NMR (500 MHz, Chloroform-*d*)  $\delta$  7.74 (d,  $J$  = 2.0 Hz, 1H), 7.64 (dd,  $J$  = 8.5, 2.1 Hz, 1H), 7.24 (dt,  $J$  = 18.3, 8.4 Hz, 3H), 7.15 – 7.07 (m, 3H), 6.88 (t,  $J$  = 1.5 Hz, 2H), 6.62 (s, 1H), 4.94 (s, 2H), 4.76 (s, 2H).  $^{13}\text{C}$  NMR (126 MHz,  $\text{CDCl}_3$ )  $\delta$  168.6, 158.6, 138.9, 136.2, 136.2, 136.1, 136.0, 135.8, 132.3, 130.0, 127.9, 127.6, 126.7, 124.8 (2), 122.9, 122.5, 116.2, 114.8, 55.2, 52.7. HRMS (ESI)  $m/z$   $[\text{M}+\text{H}]$  calculated for  $\text{C}_{21}\text{H}_{16}\text{Cl}_2\text{NO}_2\text{S}$ , 416.0273, found 416.0263.



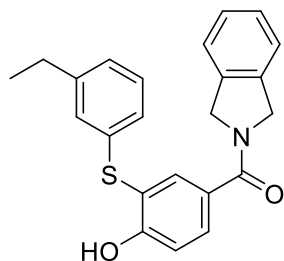
**(4-hydroxy-3-((3-methoxy-5-methylphenyl)thio)phenyl)(isoindolin-2-yl)methanone (61p):**

Prepared using general procedure B; white solid, 34 mg, yield 65%.  $^1\text{H}$  NMR (400 MHz, Chloroform-*d*)  $\delta$  7.74 (d,  $J$  = 2.1 Hz, 1H), 7.58 (dd,  $J$  = 8.4, 2.2 Hz, 1H), 7.30 – 7.19 (m, 3H), 7.07 (dd,  $J$  = 14.2, 7.9 Hz, 2H), 6.54 – 6.35 (m, 3H), 4.94 (s, 2H), 4.75 (s, 2H), 3.65 (s, 3H), 2.18 (s, 3H).  $^{13}\text{C}$  NMR (101 MHz,  $\text{CDCl}_3$ )  $\delta$  169.0, 160.2, 158.5, 140.6, 136.3, 135.8, 131.5, 129.5, 127.8, 127.5, 125.8, 123.3, 122.9, 122.4, 120.4, 116.9, 115.6, 113.1, 110.3, 55.2, 55.2, 52.7, 21.5. HRMS (ESI)  $m/z$  [M+H] calculated for  $\text{C}_{23}\text{H}_{22}\text{NO}_3\text{S}$ , 392.1314, found 392.1319.

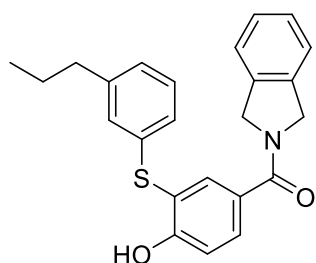


**(3-((3-fluorophenyl)thio)-4-hydroxyphenyl)(isoindolin-2-yl)methanone (61q):** Prepared using general procedure B; white solid, 28 mg, Yield 56%.  $^1\text{H}$  NMR (500 MHz, Chloroform-*d*)  $\delta$  7.76 (d,  $J$  = 2.1 Hz, 1H), 7.61 (dd,  $J$  = 8.4, 2.2 Hz, 1H), 7.29 – 7.20 (m, 2H), 7.16 (td,  $J$  = 8.1, 5.9 Hz, 1H), 7.10 (t,  $J$  = 8.3 Hz, 2H), 6.87 – 6.78 (m, 2H), 6.72 (dt,  $J$  = 9.2, 2.1 Hz, 1H), 6.63 (s, 1H), 4.94 (s, 2H), 4.76 (s, 2H).  $^{13}\text{C}$  NMR (126 MHz,  $\text{CDCl}_3$ )  $\delta$  168.8, 158.6, 137.5, 137.4, 136.3, 136.2, 136.0, 131.9, 130.7 (d,  $J$  = 8.7 Hz), 129.8, 127.9, 127.6, 122.9, 122.6 (d,  $J$  = 3.6 Hz), 122.4, 115.9,

115.8, 114.0 (d,  $J = 24.4$  Hz), 113.6 (d,  $J = 21.4$  Hz), 55.1, 52.7. HRMS (ESI)  $m/z$  [M+H] calculated for  $C_{21}H_{17}FNO_2S$ , 366.0978, found 366.0978.

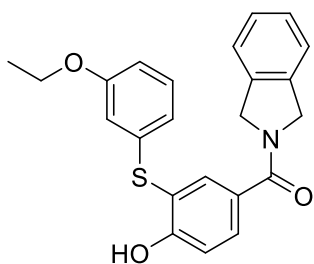


**(3-((3-ethylphenyl)thio)-4-hydroxyphenyl)(isoindolin-2-yl)methanone (61r):** Prepared using general procedure B; white solid, 32 mg, Yield 63%.  $^1H$  NMR (500 MHz, Chloroform- $d$ )  $\delta$  7.74 (d,  $J = 2.1$  Hz, 1H), 7.57 (dd,  $J = 8.4, 2.2$  Hz, 1H), 7.22 (dd,  $J = 18.8, 9.8$  Hz, 4H), 7.13 – 7.03 (m, 3H), 7.00 – 6.91 (m, 2H), 6.86 (dt,  $J = 8.0, 1.4$  Hz, 1H), 4.93 (s, 2H), 4.74 (s, 2H), 2.51 (q,  $J = 7.6$  Hz, 2H), 1.12 (t,  $J = 7.6$  Hz, 3H).  $^{13}C$  NMR (126 MHz,  $CDCl_3$ )  $\delta$  169.0, 158.5, 145.6, 136.3, 136.3, 135.7, 134.6, 131.4, 129.5, 129.3, 127.8, 127.5, 127.1, 126.4, 124.9, 122.9, 122.4, 117.3, 115.6, 55.1, 52.7, 28.7, 15.4. HRMS (ESI)  $m/z$  [M+H] calculated for  $C_{23}H_{22}NO_2S$ , 376.1365, found 376.1346.

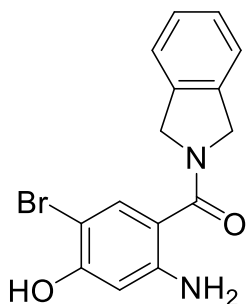


**(4-hydroxy-3-((3-propylphenyl)thio)phenyl)(isoindolin-2-yl)methanone (61s):** Prepared using general procedure B; white solid, 29 mg, Yield 56%.  $^1H$  NMR (400 MHz, Chloroform- $d$ )  $\delta$  7.82 (d,  $J = 2.2$  Hz, 1H), 7.65 (dd,  $J = 8.4, 2.2$  Hz, 1H), 7.36 – 7.25 (m, 3H), 7.21 – 7.11 (m, 3H), 7.04 – 6.99 (m, 2H), 6.96 – 6.92 (m, 1H), 6.88 (s, 1H), 5.01 (s, 2H), 4.82 (s, 2H), 2.52 (dd,  $J = 8.6, 6.8$

Hz, 2H), 1.65 – 1.52 (m, 2H), 0.92 (t,  $J = 7.3$  Hz, 3H).  $^{13}\text{C}$  NMR (101 MHz,  $\text{CDCl}_3$ )  $\delta$  169.1, 158.5, 144.1, 136.4, 136.3, 135.6, 134.5, 131.3, 129.4, 129.2, 127.9, 127.7, 127.5, 127.0, 125.0, 122.9, 122.4, 117.4, 115.6, 55.1, 52.7, 37.8, 24.4, 13.8. HRMS (ESI)  $m/z$   $[\text{M}+\text{H}]$  calculated for  $\text{C}_{24}\text{H}_{24}\text{NO}_2\text{S}$ , 390.1527, found 390.1514.



**(3-((3-ethoxyphenyl)thio)-4-hydroxyphenyl)(isoindolin-2-yl)methanone (61t):** Prepared using general procedure B; white solid, 33 mg, Yield 62%.  $^1\text{H}$  NMR (400 MHz, Chloroform- $d$ )  $\delta$  7.83 (d,  $J = 2.1$  Hz, 1H), 7.67 (dd,  $J = 8.4, 2.2$  Hz, 1H), 7.38 – 7.28 (m, 3H), 7.21 – 7.11 (m, 3H), 6.75 – 6.66 (m, 4H), 5.02 (s, 2H), 4.83 (s, 2H), 3.97 (q,  $J = 7.0$  Hz, 2H), 1.38 (t,  $J = 7.0$  Hz, 3H).  $^{13}\text{C}$  NMR (126 MHz,  $\text{CDCl}_3$ )  $\delta$  168.9, 159.6, 158.6, 136.4, 136.3, 136.1, 135.8, 131.6, 130.2, 129.6, 127.8, 127.5, 122.9, 122.4, 119.5, 116.8, 115.6, 113.7, 112.7, 63.5, 55.1, 52.7, 14.7. HRMS (ESI)  $m/z$   $[\text{M}+\text{H}]$  calculated for  $\text{C}_{23}\text{H}_{22}\text{NO}_3\text{S}$ , 392.1314, found 392.1327.



**(2-amino-5-bromo-4-hydroxyphenyl)(isoindolin-2-yl)methanone (64):** The intermediate **65** (100mg, 0.4 mmol, 1 eq.) was dissolved in DCM (3 mL), to this solution were introduced, N-(3-Dimethylaminopropyl)-N'-ethylcarbodiimide hydrochloride (175 mg, 0.92 mmol, 2.0 eq.),



hydroxybenzotriazole hydrate (124.2 mg, 0.92 mmol, 2 eq.), *N, N*-Diisopropylethylamine (296 mg, 2.3 mmol, 5 eq.) and isoindoline hydrochloride (80 mg, 0.5 mmol, 1.1 eq.) Reaction was stirred overnight at rt, before solvent was removed in vacuo. Subsequently, water (10 mL) was added to the remaining crude mass, acidified with 1N HCl and extracted with ethyl acetate (10 mL x2). The organic fractions were combined, dried over sodium sulfate, filtered and concentrated. The resulting residue was purified by flash chromatography (SiO<sub>2</sub>, 1:3 hexanes/ethyl acetate) to collect (2-amino-5-bromo-4-methoxyphenyl)(isoindolin-2-yl)methanone as brown solid. Obtained product was dissolved in DCM (3 mL), cooled to 0°C and 1M boron tribromide solution in DCM (1.38 mL, 1.38 mmol, 3 eq.) was added slowly. Reaction was quenched with a brine (10 mL), extracted with ethyl acetate (10 X 3), dried over sodium sulfate and purified using flash chromatography (SiO<sub>2</sub>, 1:3 ethyl acetate/hexanes) to produce **64** (51 mg, 38% overall) as beige solid. <sup>1</sup>H NMR (500 MHz, Chloroform-*d*) δ 7.35 (s, 1H), 7.23 (d, *J* = 5.1 Hz, 3H), 7.14 (s, 1H), 6.33 (s, 1H), 5.56 (s, 1H), 4.86 (d, *J* = 38.8 Hz, 4H), 4.62 (s, 2H). <sup>13</sup>C NMR (126 MHz, CDCl<sub>3</sub>) δ 168.8, 154.2, 147.8, 136.3, 131.2 (2), 127.7, 122.7, 114.5 (2), 103.2 (2), 97.2, 53.4 (2). HRMS (ESI) *m/z* [M+H] calculated for C<sub>15</sub>H<sub>14</sub>BrN<sub>2</sub>O<sub>2</sub>, 333.0239, found 333.0256.

#### IV.10 References

1. Chen, B.; Piel, W. H.; Gui, L.; Bruford, E.; Monteiro, A. The HSP90 family of genes in the human genome: insights into their divergence and evolution. *Genomics* **2005**, *86*, 627-37.
2. Li, J.; Soroka, J.; Buchner, J. The Hsp90 chaperone machinery: Conformational dynamics and regulation by co-chaperones. *Biochim. Biophys. Acta, Mol. Cell Res.* **2012**, *1823*, 624-635.
3. Khandelwal, A. Unfolding the Hsp90 Foldasome: Structure-Activity Relationship Studies on EGCG and Development of Isoform-Selective Inhibitors, Ph.D Dissertation, The University of Kansas. **2016**.
4. Gewirth, D. T. Paralog Specific Hsp90 Inhibitors - A Brief History and a Bright Future. *Curr. Top. Med. Chem.* **2016**, *16*, 2779-91.

5. Immormino, R. M.; Kang, Y.; Chiosis, G.; Gewirth, D. T. Structural and quantum chemical studies of 8-aryl-sulfanyl adenine class Hsp90 inhibitors. *J. Med. Chem.* **2006**, *49*, 4953-60.
6. Ernst, J. T.; Liu, M.; Zuccola, H.; Neubert, T.; Beaumont, K.; Turnbull, A.; Kallel, A.; Vought, B.; Stamos, D. Correlation between chemotype-dependent binding conformations of HSP90alpha/beta and isoform selectivity-Implications for the structure-based design of HSP90alpha/beta selective inhibitors for treating neurodegenerative diseases. *Bioorg. Med. Chem. Lett.* **2014**, *24*, 204-8.
7. He, H.; Zatorska, D.; Kim, J.; Aguirre, J.; Llauger, L.; She, Y.; Wu, N.; Immormino, R. M.; Gewirth, D. T.; Chiosis, G. Identification of potent water soluble purine-scaffold inhibitors of the heat shock protein 90. *J. Med. Chem.* **2006**, *49*, 381-90.
8. Hitotsuyanagi, Y.; Kobayashi, M.; Takeya, K.; Itokawa, H. Synthesis of 4-thia-2-azapodophyllotoxin, a new analogue of the antitumour lignan podophyllotoxin. *J. Chem. Soc., Perkin Trans. 1* **1995**, 1387-1390.
9. Llauger, L.; He, H.; Kim, J.; Aguirre, J.; Rosen, N.; Peters, U.; Davies, P.; Chiosis, G. Evaluation of 8-arylsulfanyl, 8-arylsulfoxyl, and 8-arylsulfonyl adenine derivatives as inhibitors of the heat shock protein 90. *J. Med. Chem.* **2005**, *48*, 2892-905.
10. Huang, K. H.; Veal, J. M.; Fadden, R. P.; Rice, J. W.; Eaves, J.; Strachan, J. P.; Barabasz, A. F.; Foley, B. E.; Barta, T. E.; Ma, W.; Silinski, M. A.; Hu, M.; Partridge, J. M.; Scott, A.; DuBois, L. G.; Freed, T.; Steed, P. M.; Ommen, A. J.; Smith, E. D.; Hughes, P. F.; Woodward, A. R.; Hanson, G. J.; McCall, W. S.; Markworth, C. J.; Hinkley, L.; Jenks, M.; Geng, L.; Lewis, M.; Otto, J.; Pronk, B.; Verleysen, K.; Hall, S. E. Discovery of novel 2-aminobenzamide inhibitors of heat shock protein 90 as potent, selective and orally active antitumor agents. *J. Med. Chem.* **2009**, *52*, 4288-305.
11. Heine, N. B.; Studer, A. Radical Difluoromethylation of Thiols with (Difluoromethyl)triphenylphosphonium Bromide. *Org. Lett.* **2017**, *19*, 4150-4153.
12. Alcolea, V.; Plano, D.; Encio, I.; Palop, J. A.; Sharma, A. K.; Sanmartin, C. Chalcogen containing heterocyclic scaffolds: New hybrids with antitumoral activity. *Eur. J. Med. Chem.* **2016**, *123*, 407-418.
13. Moine, E.; Dimier-Poisson, I.; Enguehard-Gueiffier, C.; Loge, C.; Penichon, M.; Moire, N.; Delehouze, C.; Foll-Josselin, B.; Ruchaud, S.; Bach, S.; Gueiffier, A.; Debierre-Grockiego, F.; Denevault-Sabourin, C. Development of new highly potent imidazo[1,2-b]pyridazines targeting *Toxoplasma gondii* calcium-dependent protein kinase 1. *Eur. J. Med. Chem.* **2015**, *105*, 80-105.
14. Tedjamulia, M. L.; Tominaga, Y.; Castle, R. N.; Lee, M. L. The synthesis of all of the dimethyldibenzothiophenes and monoethyldibenzothiophenes. *J. Heterocycl. Chem.* **1983**, *20*, 1485-1495.
15. Mackenzie, L.; Macrury, T.; Harwig, C.; Khlebnikov, V.; Shan, R.; Place, S.; Bird, P.; Pettigrew, J.; Bhatti, N. A. Ship1 modulators and methods related thereto. WO2011069118, Jun 9<sup>th</sup>, **2011**.
16. Stebbins, C. E.; Russo, A. A.; Schneider, C.; Rosen, N.; Hartl, F. U.; Pavletich, N. P. Crystal Structure of an Hsp90-Geldanamycin Complex: Targeting of a Protein Chaperone by an Antitumor Agent. *Cell* **1997**, *89*, 239-250.
17. Li, J.; Sun, L.; Xu, C.; Yu, F.; Zhou, H.; Zhao, Y.; Zhang, J.; Cai, J.; Mao, C.; Tang, L.; Xu, Y.; He, J. Structure insights into mechanisms of ATP hydrolysis and the activation of human heat-shock protein 90. *Acta Biochim. Biophys. Sin.* **2012**, *44*, 300-306.

18. Reynisson, J.; McDonald, E. Tuning of hydrogen bond strength using substituents on phenol and aniline: A possible ligand design strategy. *J. Comput. Aided Mol. Des.* **2004**, *18*, 421-431.
19. Rao, B. D. N.; Venkateswarlu, P.; Murthy, A. S. N.; Rao, C. N. R. HYDROGEN BONDING IN PHENOL, ANILINE, AND THIOPHENOL BY NUCLEAR MAGNETIC RESONANCE SPECTROSCOPY AND CRYOSCOPY. *Can. J. Chem.* **1962**, *40*, 963-965.
20. Hartz, R. A.; Ahuja, V. T.; Macor, J. E.; Bronson, J. J.; Dasgupta, B.; Dzierba, C. D.; NARA, S. J.; KARATHOLUVHU, M. S. Quinazoline-based kinase inhibitors. WO2016053794, Apr 7<sup>th</sup>, **2016**.